

Validation of the Gurney Model for Heterogeneous Systems



Jason Loiseau

Supervisor: Prof. Andrew J. Higgins

Department of Mechanical Engineering

McGill University

A dissertation submitted to McGill University in partial fulfillment of the
requirements for the degree of
Doctor of Philosophy

Acknowledgements

I first and foremost thank my supervisor, Prof. Andrew J. Higgins, for his support above and beyond the call of duty. In my Master's thesis I had written about using up all of my second chance(s); in finishing my PhD I have most certainly burned through many more. This dissertation, and my current career track would not be what they are today without Prof. Higgins.

I would also like to thank Prof. David Frost for his unofficial supervisory role. Prof. Frost was instrumental in completing much the work presented here, as well as motivating the studies involving metallized explosives and the explosive dispersal of granular material. This thesis would be a shell of its present form without his contributions and interpersonal support.

I am also grateful for the support of my fellow graduate students: Justin Huneault and Myles Hildebrand were instrumental in the development of the implosion gun that consumed the early years of my PhD (which sadly didn't make it into this thesis for the sake of coherence). They also provided the all-important social backdrop of bike rides and inebriation that seems to help so many of us make it through graduate school. William Georges was essential in getting the experiments that comprise the first two chapters done, as well as keeping me sane in the lab. Finally, I acknowledge XiaoCheng Mi for consistently drinking the lot of us under the table!

Many of my experiments would not have been possible without the help of some dedicated technical staff. I thank Gary Savard, John Boisvert, Mathieu Beauchesne, and Andreas Hofmann for helping to machine the considerable amount of disposable hardware I needed when it seemed like the Faculty was determined to make sure no one got anything done. I also thank Rick Guilbeault and Lorne McCauley for their help in conducting the many tests done at the Canadian Explosives Research Laboratory.

You can't do anything without money: I appreciate the funding support from NSERC, FQRNT, Fan Zhang at DRDC Suffield, and MITACs along with General Fusion Inc.

Finally, I thank my parents, who have been very understanding while I have not been the most dutiful son over the past few years.

Abstract

Accelerating material to very high speed (up to multiple km/s) is one of the primary uses of high explosives. Thus, the magnitude and mechanisms of energy transfer from a detonating high explosive (HE) to material placed in contact with the charge are critical in engineering applications. When heterogeneous, non-conventional explosives are used to drive material, or when heterogeneous material is driven by explosives, mesoscale multiphase interactions and dissipative mechanisms complicate the analysis and modelling of the explosive-material interaction using both analytic techniques and finite element codes.

Explosives that have been heavily diluted with inert material are of interest in metal driving applications where elimination of a transmitted shock into the metal is desirable: spallation and material ejection can be suppressed in flyer launching, and shock-driven heating and shearing can be reduced in dynamic compaction/compression experiments. Alternatively, the addition of reactive metals can increase the output of an explosive when driving metal, provided the particles react sufficiently quickly. Explosives heavily diluted with dense particles are also of interest for reduced collateral, high-near-field impulse charges. The ancillary casing acceleration capability of these explosives is thus also important to quantify. When explosives are used to drive granular materials, shock compaction of the material bed dissipates explosive energy, resulting in a dispersed material velocity lower than what would be predicted for homogeneous casings. Quantifying the velocity of dispersants is critical for buried blast momentum transfer, impulse/blast mitigation by granular materials, and the performance of certain blast-enhanced charges.

Heterogeneous effects are thus of interest in a number of specialized explosive engineering applications. In the present thesis, the effects of heterogeneities on the explosive acceleration of material was considered in detail through experimentation. Results were analysed in the context of the Gurney model; one of the most ubiquitous analytic tools for estimating the veloc-

ity at which materials are driven by explosives and for comparing the thermochemical output of explosives. Various modifications of the Gurney model were proposed and/or evaluated to account for the heterogeneous effects.

First, a planar flyer plate charge leveraging Photonic Doppler Velocimetry (PDV) was designed to measure the explosive output of heterogeneous HEs. Homogeneous, amine-sensitized liquid nitromethane was used as a benchmark explosive, and the flyer-mass to charge-mass ratio (M/C) was varied from 0.03 to 4.65. These experiments validated that the Gurney model is accurate to within 5%, except for very small values of M/C where the error grows to 10%. Importantly, these experiments also validated flyer launch angle predictions and PDV tilt correction techniques up to very large launch angles.

Second, the validated flyer plate charge was used to measure the metal driving output of explosives loaded with inert additives. Photonic Doppler Velocimetry was again used to measure flyer acceleration. A wide range of formulations and particle additives were tested: packed particle beds saturated with nitromethane, gelled nitromethane with suspended particles, and C-4 admixed with particles. A slapper initiated charge was also used in order to determine the effect of detonation wave incidence angle on flyer acceleration. The Gurney curves for several formulations were also measured. Results were analysed in the context of a modified form of the Gurney equation which included the entrainment of the inert particles in the detonation products with no slip. Agreement was found to be acceptable for an engineering model for all but the very heavily loaded explosives.

Third, a modified, symmetric version of the experimental geometry was used to evaluate the effect of aluminium addition on the propulsive capability of gelled nitromethane. Unlike typical studies of aluminized explosives using the cylinder test, in the present experiments flyer plates of widely varying thickness were used to ascertain if casing expansion timescale influences energy deposition by the aluminium. Time-resolved flyer surface velocity measurements were performed with PDV. Regardless of flyer thickness and aluminium particle size, aluminized explosives drove the flyer plates faster than an equivalent neat explosive within 4–6 μs . This implied prompt reaction and energy delivery by the aluminium to the detonation products.

Finally, the explosive dispersal of a wide variety of granular materials in spherical geometry was performed and various phenomenology related to consolidated shell fracture and particle jet formation were discussed – particularly the segregation and jetting of binary mixtures. The ter-

minal velocity of the jet tips for all experiments were compared to the spherical Gurney model. Experimental terminal velocities were 40–70% lower than what was predicted by the Gurney model, demonstrating that compaction significantly dissipates explosive energy. A modified Gurney model accounting for dissipation as a function of M/C and porosity was compared and shown to accurately predict the dispersant velocity over the full range of M/C and materials considered with a maximum error of 17%.

Conclusively, the amenability and engineering accuracy of the Gurney model was demonstrated for a variety of heterogeneous systems. Because the Gurney model is effectively an energy transfer scaling law, it can be readily modified by changing the conservation equations to account for additions to the system or by adding scaling terms to the M/C ratio and effective explosive energy, E .

Abrégé

L'accélération du matériel à très grande vitesse (jusqu'à plusieurs km/s) est l'une des principales utilisations des explosifs à haute teneur. Ainsi, l'ampleur et les mécanismes du transfert d'énergie de la détonation des explosifs élevés (HE) à des matériaux mis en contact avec la charge sont essentiels dans les applications d'ingénierie. Lorsqu'un explosif hétérogène et non conventionnel est utilisé pour conduire du matériel, ou lorsqu'un matériel hétérogène est entraîné par des explosifs, les interactions multiphasiques à mésoéchelle et les mécanismes dissipatifs sont difficilement modélisés par des codes d'éléments finis et des outils analytiques.

Les explosifs qui ont été fortement dilués avec du matériel inerte intéressent les applications de conduite en métal où l'élimination d'un choc transmis dans le métal est souhaitable: la spallation et l'éjection du matériau peuvent être supprimées et le chauffage et le cisaillement peuvent être réduits. Alternativement, l'ajout de métaux réactifs peut augmenter la performance d'un explosif lors de la conduite de métal, à condition que les particules réagissent suffisamment rapidement. Les explosifs fortement dilués avec des particules denses sont également intéressants pour des charges d'impulsions limitées à longue distance et de haute intensité à courte distance. La capacité de ces explosifs à accélérer l'enveloppe auxiliaire d'une charge est donc importante à quantifier. Lorsque des explosifs sont utilisés pour conduire des matériaux granulaires, le compactage par choc dissipe l'énergie explosive, ce qui entraîne une vitesse de dispersion inférieure à ce que l'on prévoit pour les enveloppes homogènes. La quantification de la vitesse des dispersants est essentielle pour le transfert de moment cinétique d'explosions enterrées, l'atténuation des impulsions/explosions par des matériaux granulaires, et la performance de certaines charges améliorées. Les effets hétérogènes présentent donc un intérêt pour plusieurs applications d'ingénierie explosive spécialisées. Dans la thèse actuelle, les effets des hétérogénéités sur l'accélération du matériau par des explosifs ont été examinés en détail par l'expérimentation. Tout au long, les résultats de la thèse ont été analysés dans le contexte

du modèle Gurney, l'un des outils analytiques les plus omniprésents pour estimer la vitesse à laquelle les matériaux sont entraînés par des explosifs ou pour comparer la production thermo-chimique des explosifs. Diverses modifications du modèle Gurney ont été proposées et / ou évaluées.

Premièrement, on a évalué un concept de lancement de plaque planaire utilisant la Velocimétrie Doppler Photonique (PDV) pour mesurer la performance d'explosifs hétérogènes. Un mélange homogène de nitrométhane sensibilisé avec une amine a été utilisé comme explosif de référence, et le rapport de la masse de plaque à masse de charge (M/C) a été varié de 0,03 à 4,65. Ces expériences ont démontré que le modèle Gurney est précis à mieux de 5%, à l'exception de très petites valeurs de M/C où l'erreur augmente à 8%. Ces expériences ont également validé les prévisions d'angle de lancement et les techniques de correction pour l'inclinaison de l'axe de PDV jusqu'à de très grands angles de lancement.

Deuxièmement, le concept expérimental a été utilisé pour mesurer capacité d'entraînement de métal de plusieurs explosifs lourdement chargés avec des additifs denses et inertes. Le système PDV a de nouveau été utilisé pour mesurer l'accélération de la plaque. On a testé une large gamme de formulations et d'additifs: des couches de particules saturées de nitrométhane, du nitrométhane gélifié avec des particules en suspension, et des particules mélangées à du C4. Une charge initiée lancée par le lancement d'une plaque secondaire a également été utilisée pour déterminer l'effet de l'angle de détonation sur l'accélération de la plaque. Les courbes de Gurney pour plusieurs formulations ont également été mesurées. Les résultats ont été analysés dans le contexte d'une forme modifiée des équations de Gurney qui comprend l'entraînement des particules inertes dans les produits de détonation. L'accord avec les résultats d'expériences a été jugé acceptable pour un modèle d'ingénierie pour tous sauf les explosifs très chargés.

Troisièmement, une version symétrique de la géométrie expérimentale a été utilisée pour évaluer l'effet de l'addition d'aluminium sur la capacité propulsive du nitrométhane gélifié. Contrairement aux études typiques d'explosifs aluminisés à l'aide de charges à cylindre, dans les présentes expériences, des plaques d'épaisseurs très variables ont été utilisées pour déterminer si l'échelle de temps de l'accélération influence le dépôt d'énergie. Peu importe l'épaisseur de la plaque et la taille des particules d'aluminium, les explosifs aluminisés ont conduit les plaques plus rapidement qu'un explosif propre équivalent dans 4–6 μ s. Cela implique une réaction rapide et une livraison d'énergie par l'aluminium dans les produits de détonation.

Enfin, on a discuté de la dispersion explosive d'une grande variété de matériaux granulaires en géométrie sphérique et on a discuté de divers phénomènes liés à la fracture de coquille consolidée et à la formation de jet de particules, en particulier la ségrégation et la projection de mélanges binaires. La vitesse terminale des pointes de jet pour toutes les expériences a été comparée au modèle sphérique de Gurney. Les vitesses terminales expérimentales étaient 40–70% inférieures à ce qui était prédit par le modèle Gurney, démontrant que le compactage dissipe considérablement l'énergie explosive. Un modèle de Gurney modifié tenant compte de la dissipation en fonction de M/C a été comparé aux résultats. Il s'est montré capable de prédire la vitesse des jets sur toute la gamme de M/C et de matériaux considérés avec une erreur maximale de 17%.

En conclusion, la précision et l'utilité du modèle Gurney a été démontrée pour une variété de systèmes hétérogènes. Étant donné que le modèle de Gurney est effectivement une loi d'échelle de transfert d'énergie, il peut être facilement adapté en modifiant les équations de conservation pour tenir compte des ajouts au système ou simplement en ajoutant des termes d'échelle au ratio M/C et à l'énergie explosive efficace, E .

Preface

As this thesis is comprised of manuscripts which are in print (Chapters 1, 2, and 5), accepted for publication (Chapter 4), or being prepared for submission (Chapter 3), my personal contributions are listed below:

Chapter 1: The manuscript was written almost entirely by me. Andrew Higgins provided some text justifying the use of NM as an ideal explosive. Experiments were designed by me and were mostly conducted by me. William Georges assisted in doing the tests and designed a planar impactor slapper that was used for one of the data points. Andrew Higgins provided editorial support and scientific criticism.

Chapter 2: The manuscript was almost entirely written by me. Andrew Higgins contributed small portions of the description of the explosive systems used. Experiments were designed and carried out primarily by me. William Georges helped design the two-stage impactor slapper system and conducted a number of the experiments comprising the Gel with 10% GMB Gurney curve. William also derived the augmented Gurney model using a separate term for the particles, whereas I derived a form by reducing the Gurney energy by the mass fraction of inert. These forms are equivalent and I later discovered that Kennedy had proposed a similar equation [1]. David Frost and Andrew Higgins provided manuscript editing support and scientific criticism.

Chapter 3: The manuscript was entirely written by me. Experiments were designed by me and were conducted by me with the assistance of Samuel Goroshin. Samuel also provided scientific contributions on powder selection. David Frost, Andrew Higgins, and Fan Zhang provided scientific criticism/discussion.

Chapter 4: The manuscript was written by me. The conception of the experiments was previously established by David Frost. I contributed to the selection of many of the configu-

rations tested. Experiments were conducted by me, David Frost, and Samuel Goroshin. Alec Milne developed the analytic Gurney model used. Quentin Pontalier processed the videography data to extract shell velocities.

Chapter 5: The manuscript was written mostly by David Frost. I contributed text and all of the figures. The concept of testing binary mixtures of “jetting” and “non-jetting” material at different volume fractions was developed by me. Experiments were conducted by me, David Frost, and Samuel Goroshin. Bradley Marr processed the videos to extract velocity data.

The author notes the following distinct contributions:

Chapter 1: Although not strictly novel in concept, I presented the experimental measurement of the Gurney curve for a conventional explosive that has notable archival value. The use of orthogonal interferometry probes to directly measure the tilt angle of explosively drive flyers over a wide range of launch conditions in order to verify the Taylor angle equation is a novel contribution.

Chapter 2: I presented the most comprehensive measurement of the accelerating ability of non-conventional explosives heavily loaded with a range of additives with different densities to date. A large number of experiments were conducted to validate a form of the Gurney equation modified to account for the effect of these additives on acceleration ability. I also conducted a number of tests comparing grazing-detonation acceleration to normal-detonation acceleration and demonstrated key differences in the acceleration process between the loading conditions. Finally, I demonstrated that an explosive loaded with a large fraction of dense additive does not obey the scaling in flyer velocity with flyer-to-charge mass ratio that observed for conventional explosives.

Chapter 3: I presented interferometric measurements of flyer acceleration demonstrating that metal particles can promptly react in explosive detonation products regardless of particle size. I further demonstrated that this is a robust phenomenon exhibited by many metals. The reaction of aluminium particles was shown to be sufficiently rapid that acceleration ability did not vary as flyer acceleration timescale was reduced, even for larger, micron-scale particles.

Chapter 4: I presented the most extensive experimental measurement of the terminal velocity of explosively dispersed granular materials and liquids to date. Velocity was demonstrated to correlate well with a modified form of the Gurney equation.

Chapter 5: I demonstrated a unique phenomenon where a thoroughly mixed binary system, comprised of a material resistant to granular compaction and a material that readily compacts, rapidly segregates and forms large scale structures upon explosive dispersal.

Table of contents

List of figures	xxi
List of tables	xxvii
Nomenclature	xxix
Introduction	xxxiii
I Gurney Literature	xxxviii
II Discussion of Photonic Doppler Velocimetry	xliv
1 Validation of the Gurney Model in Planar Geometry for a Conventional Explosive	1
1.1 Abstract	1
1.2 Introduction	2
1.3 Reviewing Gurney’s Model	3
1.4 Extending the Gurney Model	6
1.5 Experimental Setup	9
1.6 Experimental Analysis	14
1.7 Experimental Results and Discussion	16
1.8 Conclusion	20
2 The Propulsive Capability of Explosives Heavily Loaded with Inert Materials	21
2.1 Abstract	21
2.2 Introduction	22
2.3 Effect of Detonation Wave Incidence Angle	25
2.4 Experimental Details	29

Table of contents

2.4.1	Grazing Detonation Charges	30
2.4.2	Normal Detonation Charges	32
2.5	Gurney Analysis	36
2.6	PDV Tilt Correction	40
2.7	Explosives Studied	42
2.7.1	Neat Sensitized Nitromethane	42
2.7.2	Gelled Nitromethane Suspensions of Glass Microballoons and Particles	44
2.7.3	Packed Particle Beds Saturated with Sensitized Nitromethane	46
2.7.4	C-4 with Dispersed Steel or Glass Particles	48
2.8	Experimental Results and Discussion	50
2.8.1	Homogeneous Sensitized Nitromethane Data	51
2.8.2	DETA Dilution of Nitromethane	51
2.8.3	Results with Gelled Nitromethane with Microballoons	55
2.8.4	Results with NM Saturated Packed Beds	66
2.8.5	Results with C-4 Admixtures	74
2.9	Effect of Slapper Energy Transfer and Detonation Wave Incidence	81
2.10	Discussion and Conclusion	85
2.11	Acknowledgements	87
3	Timescale of Aluminium Reaction in Detonation Products Measured via Flyer	
	Plate Experiments	89
3.1	Abstract	89
3.2	Introduction	90
3.3	Charge Design	99
3.4	Mixture Preparation and Properties	102
3.5	Experiments, Results, and Discussion	105
3.5.1	Aluminized Mixtures	106
3.5.2	Other Metallized Mixtures	114
3.6	Conclusion	116
4	Terminal Velocity of Liquids and Granular Materials Accelerated by a High Explosive	119

4.1	Abstract	119
4.2	Introduction	120
4.3	Explosive Dispersal and Jet Formation	121
4.4	Gurney Model and Related Phenomena	125
4.5	Porous Gurney Model	129
4.6	Experimental Setup	130
4.6.1	Materials Tested	132
4.6.2	Velocity Extraction Method	132
4.7	Results and Discussion	133
4.7.1	Particle Dispersal Morphologies	133
4.7.2	Particle Dispersal Velocities	135
4.8	Conclusion	143
4.9	Acknowledgements	144
5	Particle Segregation During Explosive Dispersal of Binary Granular Material Mix- tures	145
5.1	Abstract	145
5.2	Introduction	146
5.3	Experimental Details	148
5.4	Results	149
5.5	Discussion	151
5.6	Conclusion	152
	Conclusion	155
	References	157

List of figures

1	Schematic of a single PDV channel.	xlv
2	The Doppler shifting of laser light by a moving surface, as received by the original source.	xlv
3	Schematic for an angled surface made up of $N(t)$ sub-reflectors covered by a laser spot.	xlvi
4	Validation of PDV measurements using orthogonal probes.	xlix
1.1	Schematic of the Gurney asymmetric sandwich.	4
1.2	Taylor angle analysis for grazing loading.	7
1.3	Rendering of the charge.	11
1.4	Photograph of the charge assembly.	13
1.5	Lateral and longitudinal velocity histories for a 0.8-mm-thick flyer propelled to a total metal velocity of $3598 \text{ m} \cdot \text{s}^{-1}$	15
1.6	Lateral probe PDV traces for all experiments.	18
1.7	Experimental terminal velocities plotted against the tamped and untamped Gurney curves using a Gurney Energy of $2350 \text{ m} \cdot \text{s}^{-1}$	19
2.1	Depiction of the loading conditions depending on detonation wave incidence and detonation velocity	26
2.2	Experimental configurations for both the grazing and normally incident detonation experiments.	29
2.3	Charge assembly used for grazing detonation experiments [9].	31
2.4	Charge assembly used for the normally incident detonation experiments [114].	33
2.5	Normally incident detonation experiment using the 0.25-mm-thick-slapper with the test explosive cavity filled with a mixture of gelled NM and 10% GMBs.	34

List of figures

2.6	Vector decomposition for a flyer being launched via grazing detonation.	40
2.7	Charges loaded with: (a) Gelled nitromethane mixture containing 7.5% GMBs by mass. (b) Packed bed of 725 μm average diameter glass particles saturated with 90/10 NM/DETA. (c) Packed bed of 3 mm diameter steel particles saturated with 90/10 NM/DETA.	47
2.8	Grazing charges loaded with: (a) A mixture of 80/20 Steel/C-4 by mass. (b) A mixture of 60/40 Glass/C-4 by mass.	49
2.9	Experimental terminal velocities plotted against asymmetric sandwich and untamped Gurney curves [9].	52
2.10	Velocity histories of 6.35-mm-thick aluminium flyers propelled by 24-mm-thick layers of nitromethane with various mass fractions of DETA addition.	53
2.11	Normalized 6.35-mm-thick flyer terminal velocities as a function of NM vol. frac. for mixtures containing varying quantities of DETA.	54
2.12	Velocity histories of 6.35-mm-thick aluminium flyers propelled via grazing detonation of a 24-mm-thick charge of gelled NM diluted with varying quantities of GMBs and steel particles.	57
2.13	Terminal velocities of 6.35-mm-thick aluminium flyers propelled by gelled NM containing GMBs and steel particles versus NM vol. fraction.	58
2.14	Velocity histories of aluminium flyers of varying thicknesses propelled by grazing detonation of a 24-mm-thick charge of gelled NM diluted by 10% glass microballoons by mass.	60
2.15	Velocity histories of aluminium flyers of varying thicknesses propelled by normally incident detonation of a 24-mm-thick charge of gelled NM diluted by 10% glass microballoons by mass.	61
2.16	Zoom of the velocity histories of flyer plates propelled via normal detonation of gelled NM with 10% GMB illustrating the wavedynamic response in detail. .	63
2.17	Experimental terminal velocities from the grazing and normal incidence experiments with gelled NM and 10% GMBs plotted against predictions of the Gurney curve using (2.9).	65
2.18	Velocity histories for all 6.35-mm-thick aluminium flyer experiments propelled by NM-saturated, packed particle beds. Charge thickness was 24 mm.	67

2.19	Normalized terminal velocities (symbols) for 6.35-mm-thick aluminium flyers propelled by NM-saturated packed particle beds versus the augmented Gurney model, plotted over the range of explosive-density to diluent-density ratios. . . .	68
2.20	Velocity histories for aluminium flyers of various thicknesses propelled by grazing detonations of 24-mm-thick packed beds of steel particles saturated with sensitized NM.	70
2.21	Velocity histories for aluminium flyers of various thicknesses propelled by normally incident detonations of 24-mm-thick packed beds of steel particles saturated with sensitized NM.	71
2.22	Experimental Gurney curves for the NM-saturated steel packed beds versus the equivalent neat NM experiments	72
2.23	Lateral velocity histories for C-4/steel admixture experiments using 6.35-mm-thick aluminium flyers [113]. Charge thickness was 24 mm.	76
2.24	Lateral velocity histories for C-4/glass admixture experiments using 6.35-mm-thick aluminium flyers. Charge thickness was 24 mm.	77
2.25	Normalized terminal velocity versus M/C as predicted by (2.9) for the steel and glass C-4 admixtures, and by the standard Gurney model for neat C-4. Experimental neat C-4 velocities are included for comparison.	78
2.26	Normalized terminal velocities predicted by the corrected Gurney model (2.20) for the steel and glass C-4 admixtures versus the baseline Gurney model and the experimental results.	79
2.27	Normalized flyer velocities versus explosive volume fraction for the C-4/glass and C-4/steel admixtures.	80
2.28	Velocity histories of 6.35-mm-thick flyers propelled by mixtures of gelled NM with 7.5% GMB by mass when the charge was initiated by the 3.2-mm-thick, 1.6-mm-thick, and 0.25-mm-thick slappers.	81
2.29	Velocity histories of 6.35-mm-thick flyers propelled by packed beds of 280 μ m steel saturated with sensitized NM when the charge was initiated by the 3.2-mm-thick, 1.6-mm-thick, and 0.25-mm-thick slappers.	82

List of figures

2.30	Velocity histories of 6.35-mm-thick flyers propelled by mixtures of gelled NM and varying mass fractions of GMBs for both normal and grazing propulsion using 3.2-mm-thick slappers.	83
2.31	Velocity histories of 6.35-mm-thick flyers propelled by NM-saturated packed beds of various dense media for both grazing detonations and normally incident detonations initiated using 3.2-mm-thick slappers.	84
2.32	Velocity histories of 19-mm-thick flyers propelled by saturated steel packed beds compared to similar experiments.	85
3.1	Depiction of the symmetric charge geometry used.	100
3.2	Charge with twisted pairs and partially filled LWG.	101
3.3	Micrographs of the Viton coated, nano-scale aluminium.	103
3.4	Micrographs of the Valimet H-2, H-10, and H-95 aluminium powders.	104
3.5	Charges being filled with (a) gel mixture containing 15% H-95, (b) gel mixture containing 15% H-10.	105
3.6	PDV traces 12.7 mm flyers propelled by gelled nitromethane aluminized with different sizes of particles at a mass fraction of 15% or 30%.	108
3.7	PDV traces for 6.4 mm flyers propelled by gelled nitromethane aluminized with different sizes of particles at a mass fraction of 15% or 30%.	109
3.8	PDV traces for 0.3 mm flyers propelled by gelled nitromethane aluminized with different sizes of particles at a mass fraction of 15% or 30%.	110
3.9	Detailed comparison of PDV traces for all of the experiments conducted with H-50 aluminization at 15% and 30% mass fractions.	113
3.10	PDV traces for 6.4 mm flyers propelled by gelled nitromethane metallized with magnesium, silicon, and titanium at a mass fraction of 15%.	116
3.11	PDV traces for 0.3 mm flyers propelled by gelled nitromethane metallized with magnesium, silicon, and titanium at a mass fraction of 15%.	117
4.1	Schematic depicting the shock wave compaction, fragmentation and acceleration of a granular material shell by a high explosive charge.	122
4.2	Comparison between the standard Gurney model and the modified power law presented in equation 4.5. Both equations use a Gurney velocity of $2830 \text{ m} \cdot \text{s}^{-1}$	128

4.3	Photographs of explosive dispersal charges	131
4.4	Single video frames taken during the explosive dispersal of SiC particles. . . .	134
4.5	Single video frames taken during the explosive dispersal of S110 steel shot particles.	135
4.6	Single video frames taken during the explosive dispersal of brass particles. . . .	136
4.7	Single video frames taken during the explosive dispersal of a bed of S110 steel shot saturated with water.	137
4.8	Single video frames taken during the explosive dispersal of a bed of SiC particles saturated with water.	138
4.9	Experimental data for liquids, slurries and water-saturated granular materials versus the unmodified spherical Gurney equation (Eq. 4.4—solid black curve) using a Gurney velocity of $2462 \text{ m} \cdot \text{s}^{-1}$	139
4.10	Experimental data for dry granular materials versus the unmodified spherical Gurney equation (Eq. 4.4—solid and dashed black curves) and the modified spherical Gurney equation (Eq. 4.7—red curve) using a Gurney velocity of $2462 \text{ m} \cdot \text{s}^{-1}$	140
4.11	Comparison of terminal velocities for dry, and water saturated powders.	141
4.12	Experimental data for dry granular and icing sugar, S-110 and Vulkan S-30 steels, Fe-114 iron, and BR-102 brass versus material-specific curves constructed using the Milne model. The Gurney velocity was $2462 \text{ m} \cdot \text{s}^{-1}$	142
5.1	Schematic of particle jet formation during explosive dispersal.	146
5.2	Photograph of experimental charge, partially filled with powder. The mass of the ball of C-4 visible in the center of the glass sphere in this case was 75 g. . .	147
5.3	SEM micrographs of the two powders used in present investigation: (a) silicon carbide, and (b) S110 steel shot.	148
5.4	Single frames from high-speed video for trials with mixtures of SiC and steel shot containing: (a) 0% steel, (b) 20% vol. steel, (c) 65% vol. steel, and (d) 80% vol. steel.	150

List of tables

1.1	Summary of experimental conditions for Gurney curve measurements of homogeneous sensitized nitromethane.	17
2.1	Description of the nitromethane-based heterogeneous explosives considered in the present study.	43
2.2	Summary of conditions for DETA dilution experiments. A Gurney velocity of $2310 \text{ m} \cdot \text{s}^{-1}$ was used to fit the augmented model.	52
2.3	Summary of mixtures and test conditions for experiments examining the influence of GMB and steel dilution on the propulsive capability of gelled nitromethane.	56
2.4	Summary of conditions for the gelled nitromethane with 10% GMB Gurney curve measurements.	62
2.5	Summary of conditions for the experiments using packed beds of glass, steel and tungsten particles saturated with liquid nitromethane. A Gurney velocity of $2350 \text{ m} \cdot \text{s}^{-1}$ was used for augmented model predictions.	67
2.6	Summary of experimental conditions for the C-4/glass admixtures.	75
2.7	Summary of experimental conditions for the C-4/steel admixtures.	75
3.1	Summary of conditions for experiments using gelled nitromethane mixed with aluminum	107
3.2	Summary of conditions for experiments using gelled nitromethane mixed with various reactive metals	115

Nomenclature

Acronyms

C-4 Composition-4 High Explosive

EOS Equation of State

LWG Line-Wave Generator

MOC Method of Characteristics

PDV Photonic Doppler Velocimetry

SiC Silicon Carbide

Gurney Parameters

α Mass ratio scaling parameter in porous Gurney model

β Angle the normal to the initial surface of a flyer and the metal velocity vector

$\frac{M}{C'}$ Ratio of mass of accelerated material to the mass of the charge, including inert diluent

$\frac{M}{C}$ Ratio of mass of accelerated material to the mass of the charge

$\frac{N}{C}$ Ratio of mass of tamping material to the mass of the charge

ν Scaling parameter in augmented Gurney model

$\sqrt{2E}$ Gurney velocity of the explosive

τ_c Time when flyer velocity when propelled by a metallized explosive exceeds the baseline velocity

Nomenclature

θ	Taylor angle; angle of deflection of a flyer accelerated via grazing detonation
φ	Porosity of granular material bed
a	Burst radius of casing
b	Extent of expansion of the detonation products
C	Mass of the explosive phase in a charge
C'	Total mass (inc. inert material) of the explosive mixture in a charge
E	Gurney energy (per unit mass) of the explosive
M	Mass of the flyer plate in a charge
m_i	Mass of casing fragment or particle jet
N	Mass of the tamping material in a charge
V_g	Detonation product velocity
V_m	Terminal velocity of a material accelerated by the explosive
V_n	Terminal velocity of tamping material accelerated by the explosive
V_o	Terminal velocity of casing fragments or jets
V_X	Component of flyer velocity in the longitudinal direction for a lab-fixed frame of reference
V_x	Component of flyer velocity in the longitudinal direction for a detonation-fixed frame of reference
V_Y	Component of flyer velocity in the lateral direction for a lab-fixed frame of reference
V_y	Component of flyer velocity in the lateral direction for a detonation-fixed frame of reference
F	Gurney velocity scaling parameter in porous Gurney model
K	Porosity scaling parameter in porous Gurney model

Explosive Parameters

γ	Ratio of specific heats of a gas
ϕ	Volume fraction
ϕ_b	Volume fraction of inert material in an explosive mixture
ϕ_e	Volume fraction of explosive material in an explosive mixture
ρ_b	Solid density of inert material in an explosive mixture
ρ_e	Initial density of the explosive phase
ρ_o	Solid density of granular material
τ_e	Initial thickness of the explosive charge in planar geometry
D	Detonation velocity of the explosive
w_b	Mass fraction of inert material in an explosive mixture

PDV Parameters

$\Phi_n(t)$	Phase difference of electric field of each sub-reflector
$\Phi_R(t)$	Phase of reference signal electric field
ψ	Angle between obliquely observing collimator and the flyer metal velocity vector
$A_n(t)$	Amplitude of sub-reflector electric field
$A_R(t)$	Amplitude of reference signal electric field
c	Speed of light: $299\,792\,458\text{ m} \cdot \text{s}^{-1}$
$E(t)$	Electric field
f_b	Beat frequency created by interference between the source and the Doppler shifted light
f_{las}	Frequency of source laser light
f_p	Frequency of Doppler-shifted laser light returned to optical probe

Nomenclature

f_t Frequency of Doppler-shifted laser light on target surface

$I(t)$ Light intensity at the detector

$N(t)$ Reflectors under laser spot

V_{pdv} Velocity of flyer plate as observed by a laterally oriented probe

V_s Velocity of target surface

Introduction

Condensed-phase high explosives (HEs) are a unique engineering tool. While they have moderate energy densities, ($4.5\text{--}10 \text{ MJ} \cdot \text{kg}^{-1}$), their metastable, self-oxidizing nature permits them to exothermically decompose at phenomenal rates. Typical high explosives detonate with reaction fronts moving at $4\text{--}10 \text{ km} \cdot \text{s}^{-1}$, leading to power densities of $8 \text{ GW} \cdot \text{cm}^{-2}$. The specific power output of HEs thus eclipses the output of all non-nuclear sources: a stick of HE with a diameter of 10 cm approaches the power output of a national electric grid. The output of HEs is also in the form of high pressure gas that is directly useful for doing work. Because of these characteristics, high explosives are indispensable in several sectors: HEs and related propellants form the cornerstone of modern military ordnance. The low cost and controllable destructive power of HEs makes them extremely useful in the mining sector for earthmoving and rock breaking. Explosives also have industrial applications in metal forming, metal cladding, and the shock synthesis of materials. Finally, explosives are a useful tool for the scientific study of materials at high pressure either by directly shocking them or driving metal impactors into them. From an engineering perspective, one of the most important design considerations for explosive charges is the terminal velocity at which a material is driven when placed in contact with the explosive.

The evolution of the personal computer has made finite element codes capable of simulating explosive acceleration accessible to the design engineer. The fidelity of these codes is predicated on accurately fitting parameters to the detonation conditions (CJ pressure and detonation velocity) as well as an equation of state for the isentropic expansion of the detonation products (usually JWL [2]). Consequently, good experiments will always be required for good models. Furthermore, even with low resolution simulations, computational time remains expensive, which slows iterative design. Simple analytic models with engineering accuracy will thus remain highly relevant in explosive engineering for the foreseeable future. The most commonly used analytic tool for estimating the velocity of materials driven by high explosives is the Gurney

model, originally developed by R. W. Gurney in 1943 [3], and used with few embellishments today [4, 5].

I was introduced to the Gurney equations in a manner I suspect is familiar to most explosives engineers: I had to design a charge to accelerate a layer of metal. In my case, I was designing an explosively-imploded, cylindrical liner to operate the gasdynamic cycle of a hypervelocity launcher [6, 7]. While tangling with the nuances of meshing, interface coupling, and equations of state to model the problem in a hydrocode, my advisor handed me copies of Cooper’s “Explosives Engineering” [4], and Walter’s and Zukas’ “Fundamentals of Shaped Charges” [8] to review Gurney’s model. Gurney’s methodology stands in stark contrast to equation-of-state-driven finite element modelling. The physical basis of Gurney’s model hinges simply on the conservation of energy and momentum, and a few elegant simplifying assumptions-concepts familiar to the engineer. The resulting analytic equations are equally simple. Gurney’s model has been one of the most useful tools during my work on high explosives over the last decade. It is consequently of no surprised to me that Gurney’s model is so ingrained in explosives engineering: It has a degree of unabashed simplicity, tractability and predictive accuracy that has guaranteed utility to almost every engineer working with explosives. The concepts developed by Gurney have furthered ingrained themselves into the framework of how we study and quantify the performance of HEs. It is extremely rare to find western literature discussing the propulsive capability of HEs that does not mention Gurney energy/velocity at least in passing. Given the importance of Gurney’s work, and my own personal fondness for this small slice of engineering, I really wanted to frame the core of my PhD around Gurney’s model.

Gurney’s equations are quite simply excellent scaling laws. For a specific geometry, they predict the terminal velocity of a material driven by a high explosive charge based on the ratio of material-mass to charge-mass and the potency of the explosive used. They are also remarkably accurate in doing so, with predictive errors generally much less than 10–20% for typical mass ratios of interest when designing typical explosive devices [9]. A detailed derivation of Gurney’s model is presented in Chapter 1, but some concepts are reviewed here. Gurney’s success hinged on the critical assumption that a given explosive always converts the same fraction of its chemical energy into kinetic energy that is then partitioned between the accelerated material and the expanding gas. To resolve this partition, Gurney assumed that the detonation products follow a linear gas profile with respect to radial or lateral distance from the charge centre/centreline and

that the detonation products have a uniform density. Whether these assumptions were made to elegantly simplify the energy conservation equation, or because of some insight into the physics, or both, remains an open question. Regardless, these assumptions are actually reasonably accurate over the range of mass ratios typically considered in device design, with discrepancies often amounting to cancelling errors [10, 11]. By addressing this partition of energy, The Gurney model implicitly addresses the concept of ballistic efficiency as the product gas must expend energy to accelerate itself in addition to accelerating the driven metal. The model is thus insightful from a phenomenological perspective as well as for engineering estimates. There is a substantial body of work reviewing, experimentally validating, and refining Gurney's model. Many of these references are reviewed in the appropriate manuscripts/chapters comprising this thesis where relevant to the new work discussed. For manuscript conciseness, I did not include every single Gurney reference that I found useful. Thus, I have included a supplemental review section towards the end of the introduction. The present body of work considers the application of Gurney's model to non-ideal, heterogeneous high explosives and then to the dispersal of heterogeneous casings.

The definition and classification of heterogeneous or non-ideal HEs is inherently nebulous and informal. Because of the crystalline nature of most solid explosives, typical melt-cast and plastic-bonded explosive formulations are actually heterogeneous agglomerations of explosive crystals and binder when observed at sufficiently fine scales. The mesoscale structure and composition of these mixtures have important effects on sensitivity and initiation of the bulk explosive, but have limited effects at the engineering scale: bulk samples of these explosives typically exhibit curvature-governed scaling in their detonation velocities and they fully decompose over very short length scales, leading to expansion of a frozen composition of gaseous products slightly behind the detonation sonic surface. Such explosives are typically termed ideal. By contrast, the addition of certain types of heterogeneities, even when very small relative to a sample of bulk explosive, can result in important changes in behaviour at the engineering scale. The detonation velocity, detonation pressure, and sensitivity of a high explosive is highly-dependant on the fraction of voids in the bulk HE. These voids can be introduced either by varying the degree of pressing during manufacture of the charge, entrainment of bubbles during mixing of the explosive, or deliberate seeding using microballoons. For sufficient fractions and sizes of voids, behaviour may transition from ideal to non-ideal. In contrast, the addition of particles with high

density relative to the explosive phase results in a non-ideal detonation because the particle phase and gaseous product phase may not reach equilibrium within the detonation, and fractions of unreacted explosive may exit the sonic surface and burn during product expansion [12]. Such explosives are inherently non-ideal even though the scale of the heterogeneities is much smaller than the typical scale of the charge being tested. This situation is further complicated if the additive can itself decompose exothermically or burn anaerobically in the detonation products. The addition of reactive material is an important optimization consideration for many explosive applications.

Non-ideal explosives have numerous practical applications. The majority of mining explosives are heterogeneous, non-ideal HEs that may have large heterogeneities that are measurable at the charge-scale at critical conditions [13]. Many mining formulations also contain added aluminium to enhance their performance. The base explosive component, ammonium nitrate also has a very long reaction tail and is thus inherently non-ideal [14]. Adding large fractions of inert material to conventional crystalline explosives is useful to reduce the detonation velocity and/or detonation pressure of the mixture; e.g., in the design of two-component explosive lenses [15] or when it is desirable to reduce the shock pressure transmitted into a driven material [16, 17]. Explosives with large metal content are also of interest for air-blast applications, where even inert materials can enhance blast due to later-time deposition of energy via drag and direct impact [18, 19]. Blast enhancement is even more substantial if the metal is reactive in air due to the energy density of most metals and the coupling potential between dispersed burning particles and expanding/reflected blast waves. Smaller fractions of reactive metals can also enhance the metal accelerating capability of high explosives.

Explosive acceleration ability is typically considered in applications involving homogeneous metal shells, e.g., shaped charges, fragmenting munitions, and explosive welding. In these cases, material losses can be well quantified with existing metal equations of state [20]. However, there are a number of applications where the explosive acceleration of heterogeneous materials is relevant: momentum transfer by buried charges or charges surrounded by a granular blast mitigant, sintering of metal powders, and the explosive dispersal of metal powders or reactive composites in order to enhance blast and other target effects. For these systems, dissipative mechanisms during shock loading and high-strain rate deformation alter the partition of explosive energy during acceleration.

The present work explores these non-ideal/heterogeneous effects primarily through experimentation. In the first manuscript (Chapter 1) the propulsive efficiency of neat nitromethane is considered by widely varying the relative explosive loading of aluminium plates and measuring the plate velocity via photonic Doppler velocimetry (PDV). Evaluation of the Gurney curve for an explosive is not novel, but the experiments served to validate the experimental design as well as study the tilt correction of PDV measurements for large flyer angles. Since PDV can only measure the component of metal velocity along the laser beam, total metal velocity must be corrected by a form of the Taylor tubular bomb equations [21]. Traditionally this has been done only for small flyer tilt angles [22, 23], but I validated the method for very large angles using orthogonal PDV probes. In the second manuscript (Chapter 2) the validated experimental methodology is applied to explosive mixtures containing solid additives of varying density and at widely varying mass/volume fractions. Experiments were compared to a Gurney equation modified to account for the expenditure of energy to accelerate the inert material in the detonation product flow. These inert experiments also provide a framework to compare the performance of explosives containing particles that can react with the detonation products on timescales relative to metal acceleration. The third manuscript (Chapter 3) reports PDV measurements of the acceleration of symmetric plate sandwiches propelled by gelled nitromethane mixed with various sizes of aluminium particles as well as other reactive materials. The Gurney model was used to compare changes in propulsive efficiency of the metallized mixtures at different scales of flyer-mass to charge-mass. In the final two manuscripts, the acceleration of heterogeneous shells by a small conventional explosive charge is considered. The heterogeneous shells were composed of dry granular materials, liquids, and wetted granular materials. Velocity of the explosively dispersed material shell was measured via high-speed video. Shell velocities were compared to a Gurney model modified to include energy loss to compaction of the voids in the particle bed. The inclusion of wetted granular shells permitted the direct validation that pore collapse is the primary mechanism of explosive energy dissipation in these systems. Although Chapter 5 appears last, the analysis and writing preceded the writing of Chapter 4.

I Gurney Literature

A number of references exist that review the Gurney model and associated literature. Kennedy provided a derivation of the Gurney model for asymmetric systems as well as equations for several charge geometries [5, 10, 24]. Kennedy's book chapter also tabulates the Gurney energies of many explosives [5] based on the handbook prepared by Dobratz [25]. Experimental validations, extensions or alternatives to the Gurney model, and application of Taylor's model to the launch of a flyer by a grazing detonation are also discussed. Walters also reviewed the Gurney model and alternatives in his review of explosive loading of metals [26]. The present author notes that these works are synthesized in "Fundamentals of Shaped Charges" [8]. Cooper also presents the engineering use of the Gurney equations [4]. Cooper's correction of metal velocity for charge edge effects is particularly useful, and is preceded by a similar analysis by Baum [27], and later by Kennedy [24]. Jones et al. similarly reviewed the Gurney model and demonstrated that it can be extended to estimate the acceleration process of a flyer by assuming a simple polytropic relationship for the detonation products [28]. Dehn presented the history of analytic models for explosively driven casings along with key derivations [29, 30].

Following Dehn's historical summary: Thomas was the first to extend Gurney's model by generalizing it to consider symmetric planar geometries in addition to the cylindrical and spherical cases [31]. He also created his own equation of motion model and developed the technique of dividing a warhead geometry into annular cross sections such that a Gurney analysis can be performed on each slice to determine an overall fragment distribution along the length of a shell or bomb [31, 32]. He also computed the effect of wave dynamics on flyer acceleration and determined their effect on energy transfer was ultimately minimal [31]. This thesis ultimately refutes this assertion by comparing the propulsion of plates driven by normal versus grazing detonations in Chapter 2. Stern further extended the Gurney-Thomas model to include the asymmetric planar case, cylinders and spheres with a solid metal core, and spheres where there is either a free explosive surface or a hollow core [33, 34]. In these cases, energy conservation alone is insufficient to solve for the flyer velocity because of either the free surface velocity of the unconfined explosive or the velocity of the tamper. Stern resolved this issue by introducing the momentum conservation equation. Dehn describes the work of Thomas and Stern in some detail [29]. Since the form of the Gurney model most commonly presented is Stern's extension, it is more accurate

to refer to the Gurney model as the Gurney-Thomas-Stern model. Henry essentially repeated and extended Stern's work and proposed an alternative model to address gradients in detonation product density [35]. Flis noted that Henry's assumptions are not physically consistent and do not provide meaningful improvements over the basic Gurney model [36]. Défourneaux also repeated Stern's work and then considered the efficiency of energy transfer to the flyer as a function of charge parameters [37]. According to Flis, Gurney later attempted to solve for the launch dynamics of the flyer by using a polytropic equation of state for the detonation products but used a value of 1.5 for the ratio of specific heats (γ), which yielded poor agreement with experiment [36]. The present author notes that even when selecting an appropriate value of ≈ 3 for γ Gurney's equation coupled with a simple equation of motion (see Jones et al. [28]) does not yield good agreement over a robust range of flyer-to-charge mass ratios (M/C). Henry also addressed launch dynamics by assuming a linear pressure distribution in slabs, a quadratic distribution in cylinders or a cubic distribution in spheres [35]. This also results in a non-uniform density distribution which can be combined with the system boundary conditions to produce an analytic expression for flyer velocity over time. This model also results in a variable Gurney energy as a function of radial expansion. As pointed out by Flis [38] and Jacobs [39], Henry's model contains several critical errors relating to the conservation of energy and momentum. Flis presented a more tractable solution for the flyer equation of motion by integrating the Lagrangian of the accelerating flyer system [38]. Using the polytropic equation of state and the assumption of a linear velocity gradient in the gas and a uniform gas pressure, Flis derived equations for the kinetic and potential energies of the system that can be integrated analytically with Lagrange's equation. This resulted in a time-dependant solution for the flyer velocity in terms of the final metal velocity.

A number of validations of the Gurney equations as a scaling law exist. Hoskin et al. validated the Gurney equations for plates driven by a grazing or sliding detonation and demonstrated excellent agreement with experiment [40]. They also compared Gurney's model favourably to a method of characteristics solution for predicting flyer velocity. To the author's knowledge they were also the first to address the concept of varying efficiency of energy transfer for different loadings of explosive. Butz et al. similarly experimentally validated the sandwich Gurney equation and showed excellent agreement down to very small ratios of flyer-mass to charge-mass [41]. In contrast, Solem and Singleton conducted tubular bomb tests with aluminium and

steel casings and demonstrated that poor agreement was obtained for small relative masses of casing, with under-predictions of $\approx 20\%$ [42].

A number of authors have attempted to resolve some of the limitations of the Gurney model. Jacobs adjusted the constants within the cylindrical Gurney equation to provide better fits to the Solem and Singleton data, and demonstrated that agreement could be significantly improved [39]. Weinland proposed an alternative but similar scaling law to also fit the Solem and Singleton data [43]. Hirsch attempted to resolve several of the issues related to the departure of Gurney's postulates from the actual gasdynamic expansion process using simple analytic equations [44, 45]. For thin flyers, he observed that only a portion of the explosive can meaningfully contribute to the acceleration. He thus created a correction that replaces some of the centre of the explosive charge with an infinitely stiff, inert core to better represent the actual gas velocity profile. His model is thus a direct extension of Stern's equation with the addition of a rigid-core scaling term that is also a function of M/C . Hirsch also analyzed inconsistencies in the Gurney asymmetric sandwich model when the M/C ratio is small. He mathematically defined an anomalous region where the velocity predicted by the open-face sandwich equation is greater than the velocity predicted by the closed-face sandwich equation. Flis observed that Hirsch's rigid-core model violates the assumptions of a linear velocity gradient and constant density, and proposed alternative forms to render the analytic solution physically consistent [11]. This analytic solution was then validated via hydrocode simulation. Fucke presented similar extensions to the Gurney equations for large values of M/C , rather than the typical corrections for small M/C [46].

Due to the importance of metal acceleration in shaped charge design, a number of improvements have been proposed to specifically treat the implosion of metal liners. Chanteret considered a modified model to treat imploding liners propelled via grazing detonation [47]. Hennequin also developed an implosion-specific model [48]. Both authors coupled an equation of state for the detonation products with the energy equation for the liner and expanding products to produce an expression where the Gurney energy of the explosive varies with the radius of expansion/implosion. Hennequin's model employed empirical fits to data and hydrocode results whereas Chanteret solved the solution completely analytically by portioning the geometry into an exploding part and imploding part using a rigid boundary. This method bypassed the need to consider the radial inertia of the gas beyond a simple scaling parameter. Hirsch also

considered the implosion problem in a similar manner to his other modifications [49]. Chou et al. considered the implosion problem by modifying the Gurney equations to account for the radial component of gas momentum during liner collapse [50]. This required an additional term in the momentum equation, which results in an extra term in the final expression for flyer velocity. This extra term has no explicitly analytic solution and must either be fitted to hydrocode simulations or estimated via an empirical relationship.

The flexibility of Gurney's method allows it to be extended to atypical or unconventional geometries. One configuration of interest is a system comprised of many alternating layers of explosive and metal. These are variously referred to as dagwoods (a stack of plates and explosive layers), jellyrolls (nested tubes of metal and explosive), and onions (nested spherical shells of explosive and metal) [5]. Henry was the first to consider such systems and proposed simple summation formulas to treat the symmetric case with identical layers [35]. Dehn extended these equations to treat the asymmetric case with layers of arbitrary thickness [29]. This model remains incomplete, however, as the number of equations does not allow for a complete solution for the number of unknown velocities. Another example is provided by Kennedy, who corrected the Gurney equations for the case where a plate is accelerated by a very thin explosive layer that does not extend to the plate edges, and where a buffer material was introduced between the flyer and the charge [51]. He reported a different subtraction cone angle and effective M/C ratio compared to conventional configurations. This discrepancy points to significant differences in losses for grazing detonations of thin charges. Fucke also presented corrections for when the explosive fill does not extend to the edge of the flyer sandwich [46]. Voids and buffers can likewise be treated with simple modifications to the basic models. Kennedy suggested that buffers can be adequately considered by treating the interaction as an inelastic collision between buffer and flyer [51]. This method is similar to Jones' approach for multi-layered fragments where some ratio of velocity between fragments is assumed based on wave interactions [52]. Kennedy also reported that certain voids and gaps can be treated simply by lowering the effective explosive density [10].

So far, only Gurney-derived metal propulsion models have been considered. Contemporary to Gurney, G. I. Taylor developed a model for the metal velocity of a cylindrical bomb subjected to an axial detonation by coupling an equation of motion for the expansion of the tube walls with a set of equations governing the detonation and expansion of the explosive products. The model

Introduction

begins with a coordinate transformation from the laboratory reference frame to a detonation-fixed frame. This transforms the complicated problem of flow turning into a steady-state picture of one dimensional expansion away from the detonation wave. Newton's First Law can then be written to describe the axial curvature of the cylinder wall as a function of flow pressure. This equation of motion can also be manipulated to infer the partition of radial-to-axial wall velocity as a function of local wall angle. To solve for the detonation product pressure distribution, Taylor combined the classic Chapman-Jouguet jump conditions across a detonation with the canonical hydrodynamic equations for mass conservation with area change, continuity, and a strong form of the Bernoulli equation. The model is analogous to a De Laval nozzle where the nozzle geometry is dynamically produced by the internal flow itself. In order to simplify the solution, Taylor assumed that in the detonation frame of reference, radial velocity could be neglected as the rate of deflection of the wall is much smaller than the axial post-detonation flow velocity (in the lab frame, radial displacement is greater than longitudinal displacement, however). Even with these assumptions, the final differential equation has no analytical solution and thus the model results are traditionally presented in tabular form.

Taylor's model has evidently not seen the extensive use that Gurney's has, likely due to the restrictive geometry and lack of a closed form solution. However, Taylor's model remains essential as it provides a means of determining the launch angle of the metal and the orientation of the metal velocity vector for situations where the detonation grazes along the flyer. Since most practical devices employ grazing detonations, tilt correction via Taylor's model is ubiquitous and appears in virtually all treatments of axial cylindrical bombs and grazing flyer plates known to the author (see for e.g., Solem [42] and Hoskin [40]). Allison et al. conducted tubular bomb experiments with varying cylinder wall thicknesses and demonstrated excellent agreement with a form of Taylor's model [53, 54]. Butz et al. [41], and Karpp and Predebon [55, 56] have experimentally verified the accuracy of combining Taylor's flyer deflection angle expression with a Gurney velocity estimate to predict the metal projection angle. A number of improved or alternative forms for the collapse angles of imploded liners have been reported in the technical literature; these reports are difficult to obtain but are summarized by Walters and Zukas [8]. A number of analytic models for time-dependant liner tilting also exist. A series of papers by Hirsch, Chou, Flis, Ciccarelli, and Carleone describe a model to address the dynamic rotation or tilting of an imploding liner as it is accelerated using an equation of motion for liner collapse [50,

57, 58]. The derived model was based on the work of Randers-Pehrson [59], as described by Flis [60].

The Taylor model has also received increasing attention as the conceptual basis for analytic fits to detonation product isentropes derived from the cylinder test [61]. Analytic models using a fit to cylinder wall kinematics are advantageous relative to parametric iterative fitting using successive hydrocode simulations using the JWL equation of state. Jackson has presented the development of such an analytic technique [62, 63]. Baker provided extensions to Taylor's model to treat liner thinning, expansion in the reaction zone, and real gas equations of state [64].

A number of alternative gasdynamic solutions for metal acceleration exist. The acceleration of a plate off the end of an explosive charge is effectively similar to the ballistic solution of a projectile accelerated out of a barrel. Lagrange's ballistic problem can thus be used to estimate flyer velocity. In Lagrange's problem, a piston is accelerated by a volume of initially quiescent, pressurized gas. The flow-field is thus governed by a series of plane rarefaction waves without discontinuity. This problem has been rigorously solved by Love and Pidduck for up to three wave reflections but the flow-field can also be approximated as retaining a uniform density that is dependent on the degree of expansion [65]. Setting the value of γ to approximately 3 in a polytropic equation of state adequately represents the average value for most detonation products and is solvable analytically for a number of gasdynamic problems relevant to explosive acceleration of a piston [2, 24, 66, 67]. Aziz solved the expansion of a slug of gas against a rigid piston, which also approximates the present ballistic problem, in a manner similar to Taylor's solution [68]. Thomas showed that for successive simplifications of the Lagrangian equations of motion using a polytropic gas, the Gurney model is recovered as the asymptotic solution when all of the explosives are detonated simultaneously (i.e., if the detonation velocity is set to infinity) [29, 32]. Consequently, these gasdynamic solutions can demonstrate where the Gurney equations will underpredict experiments due to the simplifying gasdynamic assumptions involved.

Many gasdynamic solutions can be obtained via the method of characteristics (MOC) [69]. Fortunately, when $\gamma = 3$ closed form analytic solutions are frequently possible using MOC. A number of works have studied the piston, or flyer plate problem. Lambourn and Hartley solved for the one-dimensional acceleration of a flyer plate including wavedynamics and spall fracture within the plate [70]. Hoskin et al. considered the two-dimensional case to resolve

the acceleration of plates by grazing explosives and then derived Gurney-like expressions for metal velocity [40]. Numerous solutions of a similar type exist in the Russian literature; many of these references are reviewed by Kennedy when closed-form solutions were provided [5, 24]. Numerous other examples exist but lie outside of the scope of the present work.

II Discussion of Photonic Doppler Velocimetry

Photonic Doppler Velocimetry (PDV) is a technique to measure the surface velocity of a moving object by means of indirectly measuring the Doppler shift of laser light reflected by the surface. The technique was initially developed by Strand et al. [71] but has since proliferated throughout the shock physics community owing to the relatively lower cost of the equipment, the high fidelity of measurement, and the ease of integrating measuring probes into experiments.

PDV has emerged as a technique owing to the convergence of infra-red laser technologies for telecommunication and the commercial availability of high-bandwidth (>10 GHz), high-sample rate (>20 Ms/s) digitizers.

The architecture of the velocimeter is comparatively simple and uses a fibre-coupled laser (1-2 W continuous) and a variety of optical components to coherently direct a portion of the laser light onto the moving surface. A schematic of a single PDV channel is depicted in Figure 1. The light reflected by the surface is Doppler-shifted due to surface motion and a portion of the reflected light re-enters the system through the emitting optic. A critical feature is that the returned Doppler-shifted light is blended with a portion of un-shifted light directly from the laser in order to produce a beat frequency at the detector that is much lower than the frequency of either light signal. This is accomplished by using a circulator, splitters, and a retro-reflector to manipulate the light-paths.

The use of a heterodyne scheme is critical if one considers the frequencies involved relative to the bandwidth of the detectors and digitizers. A 1550 nm wavelength corresponds to a frequency of 193.4 THz, or nearly four orders of magnitude greater than the highest bandwidth available in commercial products as of writing. In contrast, the beat frequencies that result from blending the light reflected by a surface moving up to $10 \text{ km} \cdot \text{s}^{-1}$ with the baseline laser signal are in the GHz range, and can thus be resolved with current detectors/digitizers.

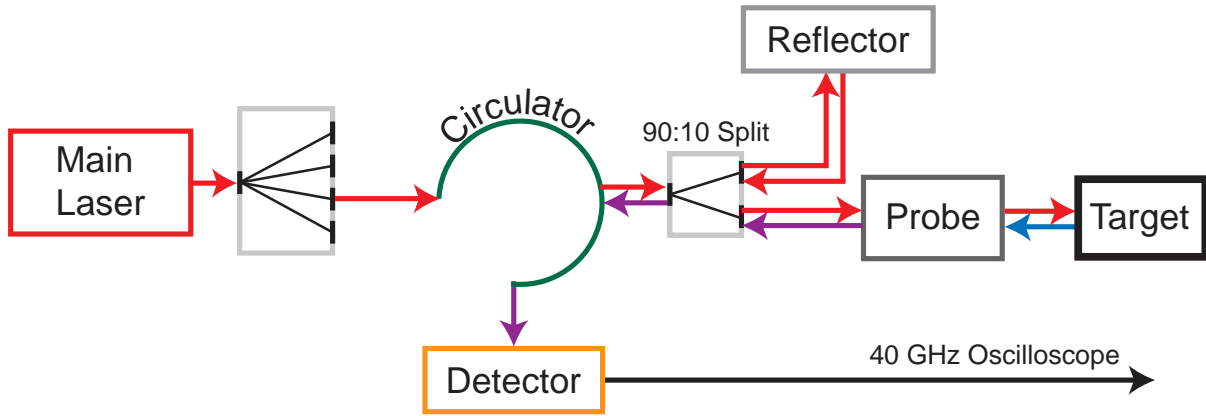


Figure 1: Schematic of a single PDV channel.

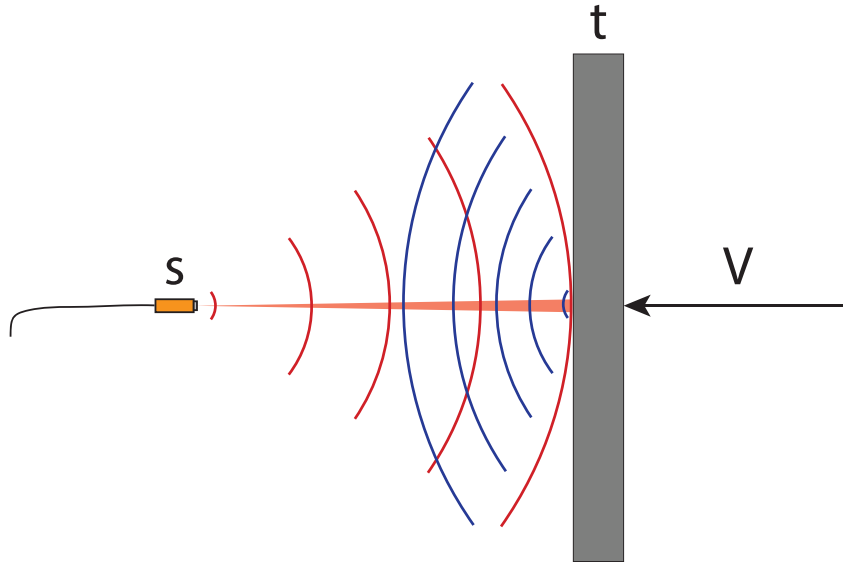


Figure 2: The Doppler shifting of laser light by a moving surface, as received by the original source.

Analysis of the time-resolved beat signal is straightforward in the frequency domain, and yields a time resolved history of the velocity of the moving target surface. Consider the Doppler shift schematic shown in Figure 2. The target surface is moving and receives the laser light from the stationary probe. The frequency of light received by the target is thus:

$$f_t = \frac{c + V_s}{c} f_{\text{las}} \quad (1)$$

Where f_t is the frequency of light perceived at the target, f_{las} is the base frequency of laser light (1550 nm here), V_s is the surface velocity, and c is the speed of light.

Introduction

The target surface then acts as a moving source and the reflected light is returned to the stationary probe, which is now acting as a stationary receiver. Thus:

$$f_p = \frac{c}{c - V_s} f_t \quad (2)$$

Where f_p is the frequency of light returned back to the velocimeter. The beat frequency (f_b), obtained at the detector is defined by:

$$f_b = f_p - f_{\text{las}} = \left(\frac{c}{c - V_s} \right) \left(\frac{c + V_s}{c} \right) f_{\text{las}} - f_{\text{las}} \quad (3)$$

or:

$$f_b = \frac{2V_s}{c - V_s} f_{\text{las}} \approx \frac{2V_s}{c} f_{\text{las}} \quad (4)$$

In order to obtain the time resolved velocity, a Fourier transform is applied over discrete time intervals (windows) along the full data set. The use of a fixed window size imposes a trade-off in the temporal resolution of the velocity history versus accurate calculation of the velocity. For the majority of experiment types this poses no limitations, however accurate resolution of nanosecond-duration events approaches the limitations of the technique.

While the relationship between the frequency of the beat signal and the corresponding velocity is straightforward, the relationship between the measured velocity and the actual velocity of the moving surface can be ambiguous as it relates to the way the time-dependant light intensity is observed by the detector. There is some confusion as to what PDV actually measures, because the core operating principle of the PDV is actually displacement interferometry. The signal returned to the PDV has a phase change corresponding to the displacement of the laser spot away/towards the stationary probe [72]. Specifically, a single beat fringe corresponds to a displacement of 775 nm for a 1550 nm light source. As a result, one might intuitively expect PDV to measure all velocities that correspond to a laser spot displacement.

Based on experiments by Briggs [72, 73] and Dolan [74], it has been demonstrated that PDV only measures the component of the true velocity of the material surface that is directed along the beam path of the probe optic. That is to say, PDV only measures a vector component of the material velocity that generates a Doppler shift, and does not measure any apparent or phase velocities that cause spot displacement. Experimental validations of this operating prin-

ciple include measuring the velocity recorded orthogonally to the trajectory of funny-shaped bullets [72, 73], or observing the angular velocity of eccentrically shaped cams [74]. In the bullet experiments, PDV measurements were taken of a bullet with a ramped nose both in-line with the flight path and at 90° to the muzzle. The in-line probe measured the true projectile muzzle velocity, while the orthogonal probe showed no velocity despite spot displacement up the ramp surface.

Following the discussion from Dolan [74], the reason PDV does not detect spot displacement arising from transverse motion of the surface is because the optical intensity measured by the detector is a function of the cosines of the phase differences returned by each microscopic sub-reflector that make up a single diffuse reflector. Specifically, the intensity observed by the detector, $I(t)$, is proportional to the square of the electric field, $E(t)$:

$$\sqrt{I(t)} \propto E(t) = A_R(t) \cos \Phi_R(t) + \sum_{n=1}^{N(t)} A_n \cos \Phi_n(t) \quad (5)$$

According to Dolan [74], if only the component representing the reflector-reference interference is included:

$$I(t) \propto \sum_{n=1}^{N(t)} A_R A_n \cos \Phi_n(t) \quad (6)$$

This implies that the measured intensity is proportional to the average cosine of the phase differences introduced by each micro-reflector and the reference signal. The reference signal contribution, $A_R(t) \cos \Phi_R(t)$, can be interpreted as a constant baseline intensity as any phase shifts are typically beyond what the detector can measure due to bandwidth limitations.

If we consider an angled surface moving orthogonally to a laser beam spot, as the surface slides through the spot, sub-reflectors at the bottom of the ramped surface will leave the laser spot, while sub-reflectors at the top of the surface will enter the laser spot. This is depicted schematically in Figure 3. While this shift may produce a change in the magnitude of the intensity at the detector due to the continuous component, A_n , the translation of the new reflectors into the spot does not produce a harmonic in the detected intensity since the phase shifts introduced by new reflectors are negligible compared to the constant phase resulting from all of the other detectors residing in the spot from the previous cycle. Consequently, the Fourier transform analysis will report no net surface velocity as the average cosine is not varying each cycle.

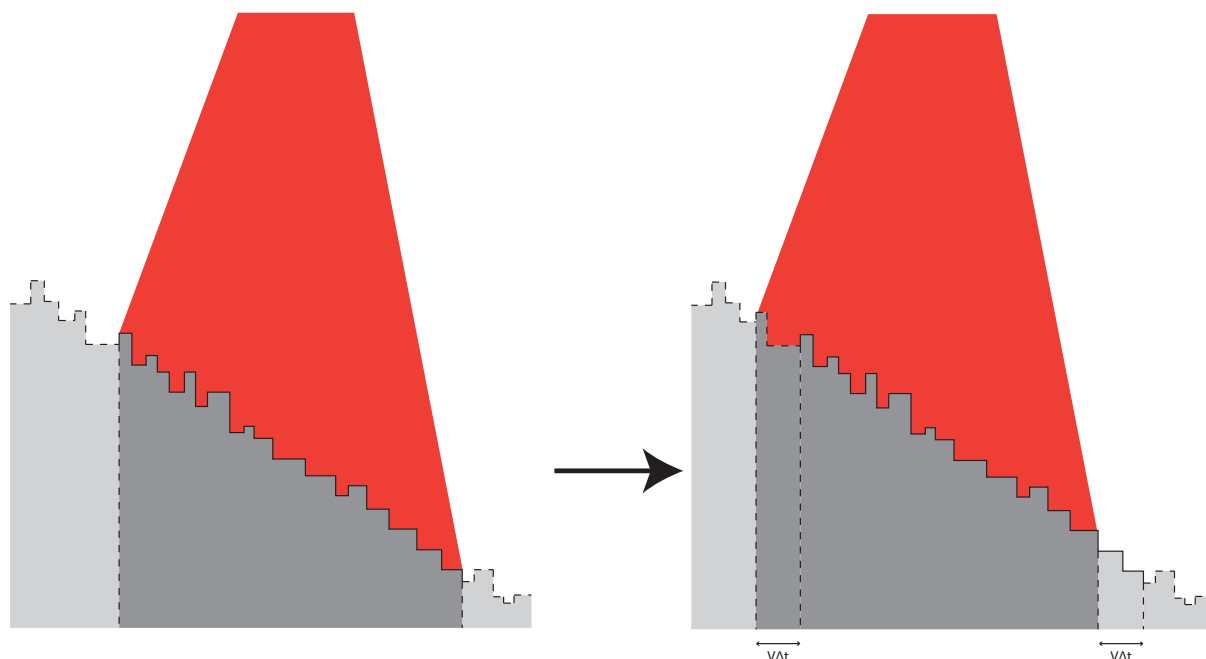


Figure 3: Schematic for an angled surface made up of $N(t)$ sub-reflectors covered by a laser spot (red area). As the surface is ramped into the spot by orthogonal motion of the body, some reflectors leave the spot from the right while others enter the spot from the left. Overall, the average cosine of the phase difference for a given interval is constant since the majority of the sub-reflectors residing in the spot return a constant phase.

This explanation has been verified via simulations using discrete reflectors by Dolan [74], and is consistent with results obtained in the fundamental velocimetry experiments discussed previously [72–74]. In addition to the aforementioned experiments, the present author conducted experiments using orthogonal probes to measure the metal velocity for very thin (< 1 mm) flyer plates where the angle of tilt was substantial. In these experiments, each probe recorded a velocity that was consistent with the component of material velocity along the laser beam, and not a phase velocity due to the detonation wave ramping material into the laser spot. Example PDV data from these experiments is shown in Figure 4, and these results are discussed in detail in Chapter 1. As can be seen, the probe observing parallel to the initial surface of the flyer records a slow, forward flyer motion, instead of the $6 \text{ km} \cdot \text{s}^{-1}$ that would be recorded if the PDV captured phase velocities.

The fact that PDV measures only true material velocity and is incapable of detecting spot displacements arising from a phase velocity or ramping of the surface is advantageous in experiments because there is no ambiguity about what is measured by a given probe. However, for velocimetry measurements of a surface with arbitrary tilt and where the velocity vector is

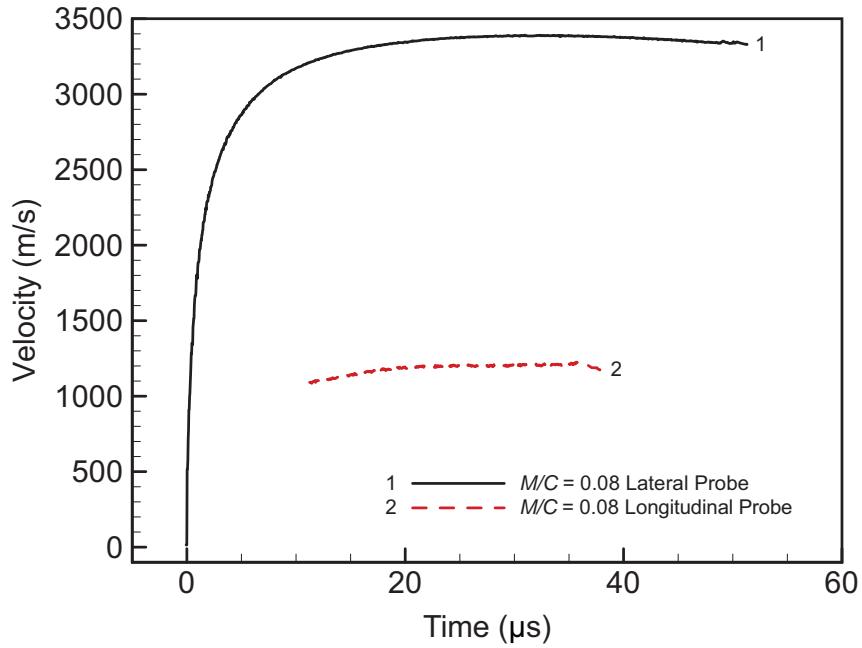


Figure 4: Validation of PDV measurements using orthogonal probes monitoring the acceleration of a 0.8-mm-thick flyer propelled to a total metal velocity of $3598 \text{ m} \cdot \text{s}^{-1}$. Velocity histories are consistent with the true lateral and longitudinal velocities of the flyer.

not aligned along the probe beam, it is necessary to correct measurements to determine the true magnitude of the velocity. In subsequent chapters, a methodology is developed to tilt-correct PDV measurements to determine the terminal velocity of explosively driven flyers.

Chapter 1

Validation of the Gurney Model in Planar Geometry for a Conventional Explosive

Jason Loiseau, William Georges, Andrew J. Higgins

[Published in Propellants, Explosives, Pyrotechnics](#)

1.1 Abstract

Abstract: The analytical model developed by Gurney is a seminal tool for analysing the acceleration of metal flyers driven by detonating high explosives. Despite the continued relevance of this model, relatively few experimental validations over a wide range of flyer-to-charge mass ratios exist in the open literature. The current study presents experimental results for planar aluminium flyers propelled by a conventional explosive over a range of mass ratios varying from 4.65 to 0.03. Flyer velocity was measured via Photonic Doppler Velocimetry (PDV), permitting a continuous measurement of the acceleration process. Measured flyer velocities are compared to terminal velocity estimations from the Gurney model. Experimental terminal velocities are compared to the open face and asymmetric sandwich Gurney models. Excellent agreement is observed for terminal velocity predictions considering the gasdynamic simplifications inherent in the model formulation.

Keywords: Explosive Driven Flyer, Gurney Velocity, PDV, Taylor Angle

1.2 Introduction

The high-velocity projection of materials is one of the primary uses of condensed phase explosives. As such, the efficacy with which a given high explosive accelerates material and the velocity with which material is thrown for a given configuration are essential considerations. A fully rigorous modelling treatment of the acceleration of a metal flyer by a high explosive typically involves the use of a hydrocode with detonation product equation of state data fitted to cylinder test experiments. However, analytical tools are often desirable in engineering design, scaling studies, and as a metric for comparing the efficiency of explosives.

The analytical model developed by Gurney is the seminal method for estimating the terminal velocity of metals accelerated by high explosive [3]. Gurney's method allows for an analytic estimation of terminal material velocity for a large number of charge geometries using a single, empirical parameter representing the energetic yield of a particular explosive. This parameter, termed the Gurney energy, can be extracted from a wide variety of experiments. Because of the elegance, simplicity, and reasonable accuracy of the method, extensions to the Gurney model have been widely used for seventy years. The Gurney energy of an explosive remains an essential metric by which the propulsive capability of an explosive is judged and is ubiquitously referenced in most literature sources studying the explosive acceleration of metals, particularly in the context of cylinder test experiments [23, 75, 76].

While a comprehensive literature review is not possible in the present paper, we would point to some key references: Kennedy [10, 24] and Jones [28] present re-derivations of the extended Gurney model coupled with the momentum equation and provide forms for a variety of geometries. Kennedy further discusses issues of accuracy, applicability, the determination of Gurney energy constants, and the use of the Gurney model to describe the efficiency of explosive launch [5, 10, 24]. Walters, and Walters and Zukas provide a similar treatment as well as a discussion of alternative terminal velocity models [8, 26]. A synthesis of these Gurney model treatments and a review of other analytical modelling of explosively driven flyers can also be found in two books by Walters and Zukas [8, 77]. These texts provide an extended bibliography of alternative analytic formulations and relevant experimental validations. Dehn summarized the history of the development of the extended Gurney models as well as Taylor's model and included derivations of alternative forms [30].

Despite the importance and ubiquity of Gurney-based models, there is a lack of published experimental validations where charge properties are widely varied for a given geometry and the full acceleration history is measured. The Gurney model is described as “nominally 10% uncertain” but this is relatively vague and evidently varies with the charge being analysed [10]. Hoskin et al. conducted untamped flyer plate experiments for a variety of metals and metal-to-explosive mass ratios and showed good agreement (<10% deviation) with experimental terminal velocities [40]. Butz et al. conducted a series of symmetric explosive-metal sandwich tests over a wide range of metal-to-explosive mass ratios and showed good agreement even for thin flyers [41]. Similarly, Allison et al. conducted a series of cylinder experiments varying the wall thickness for a fixed internal diameter [53, 54]. Solem and Singleton widely varied the wall thickness of explosively driven steel and aluminium cylinders and demonstrated dramatic departures from the Gurney model for very thin walls [42]. Jacobs reconsidered the Solem and Singleton data and proposed that very good agreement could be achieved with a modified Gurney model by simply changing the constant value added to the mass ratio term [39].

In the current study we performed a systematic variation of the explosive mass to flyer mass ratio using aluminium flyers in planar geometry. The entire velocity history of the flyer was measured via Photonic Doppler Velocimetry (PDV). Experimental results were compared to Gurney’s model.

1.3 Reviewing Gurney’s Model

The Gurney model was formulated with the aim of explaining a tentative experimental observation: That the velocity of explosively driven fragments is independent of the scale of the charge, but governed by the ratio of metal mass to explosive mass (M/C) and the energetics of the explosive used.

To explore this effect, Gurney considered only a partition of the “work-doing” chemical energy of the explosive (E) into kinetic energy of the detonation product gases and kinetic energy of the metal flyer assuming that the entire charge detonates instantaneously. He wrote energy conservation equations for cylindrical and spherical shells surrounding a high explosive charge using two critical assumptions: First, the detonation product velocity varies linearly from

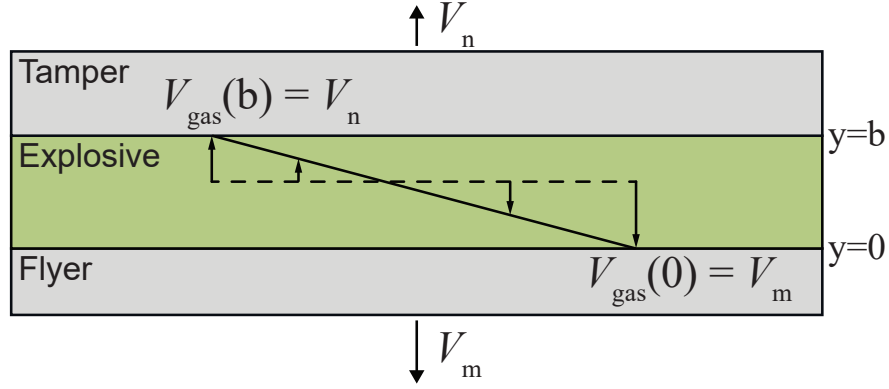


Figure 1.1: Schematic of the Gurney asymmetric sandwich.

zero at the charge centre to the fragment velocity, V_o at the burst radius, a , thus:

$$V_g(r) = \frac{r}{a} V_o \quad (1.1)$$

where V_g is the detonation product velocity as a function of radial position, r . Second, the product density remains spatially uniform and varies inversely proportionally with the expanded volume from the initial explosive density, thus for a cylindrical geometry:

$$\rho_g = \frac{C}{\pi a^2} \quad (1.2)$$

where ρ_g is the detonation product density per unit length at casing burst and C is the mass per length of explosive. Gurney then wrote the conservation of energy:

$$CE = \frac{1}{2} \sum_i m_i V_o^2 + \frac{1}{2} V_o^2 \rho_g \int_0^a 2\pi r \left(\frac{r^2}{a^2} \right) dr \quad (1.3)$$

in cylindrical coordinates, where the kinetic energies of all the fragments with masses, m_i , are summed assuming they have the same average velocity, V_o . Here the term E represents the effective energy per unit mass of explosive. This equation can be straightforwardly integrated to yield the familiar Gurney equation for a cylinder as the unknown burst radius algebraically cancels out after integration:

$$V_o = \sqrt{2E} \left\{ \frac{M}{C} + \frac{1}{2} \right\}^{-\frac{1}{2}} \quad (1.4)$$

This process is readily extendable to most simple geometries with a single degree of freedom and was generalized by Thomas as summarized by Dehn [29, 30]. Stern subsequently extended the model to asymmetric systems where the presence of two unknown velocities requires coupling of the momentum equation to the energy equation [29]. The most common of such systems is the asymmetric sandwich, which also pertains to the experiment in the current study. This geometry is depicted Figure 1.1. A detailed derivation of the model is presented by Jones [28] and Walters [8], but the key equations are reproduced here for completeness. In the sandwich, a plane of zero velocity in the detonation products is assumed, and lateral expansion is neglected, leading to the following form for the gas velocity profile:

$$V_g(y) = \frac{y(V_m + V_n)}{b} - V_m \quad (1.5)$$

Where $V_g(y)$ is the gas velocity as a function of linear position between the flyer and tamper plates, V_m is the velocity of the flyer plate, V_n is the velocity of the tamper plate, and b is an arbitrary bound for the extent of detonation product expansion.

In this system the detonation product density, ρ_g , is defined per unit of flyer plate area as:

$$\rho_g = \frac{C}{b} \quad (1.6)$$

The conservation of energy equation can then be written as:

$$CE = \frac{1}{2}MV_m^2 + \frac{1}{2}NV_n^2 + \frac{1}{2}\rho_g \int_0^b \left\{ \frac{y(V_m + V_n)}{b} - V_m \right\}^2 dy \quad (1.7)$$

And the momentum equation can be written as:

$$0 = -MV_m + NV_n + \rho_g \int_0^b \left\{ \frac{y(V_m + V_n)}{b} - V_m \right\} dy \quad (1.8)$$

where M and N are the masses per unit area of the flyer and tamper, respectively.

These equations can then be integrated and combined. As with the burst radius, the arbitrary expansion thickness, b , cancels out, yielding the following expression for terminal velocity of

the flyer:

$$V_m = \sqrt{2E} \left(\frac{1 + A^3}{3 + 3A} + \frac{N}{C} A^2 + \frac{M}{C} \right)^{-\frac{1}{2}} \quad (1.9)$$

where:

$$A = \frac{1 + 2\frac{M}{C}}{1 + 2\frac{N}{C}} \quad (1.10)$$

In planar geometry the mass ratios can be described in terms of the thicknesses and densities of the flyer, explosive, and tamper.

1.4 Extending the Gurney Model

Because the Gurney model assumes an instantaneous detonation of the entire explosive charge, and as it relies only upon energy conservation, it is incapable of addressing wave dynamic effects during flyer launch or the effect of the direction of propagation of the detonation wave.

If the detonation propagates along a flyer it will necessarily launch the metal at some angle with both lateral and longitudinal velocity components. This situation is depicted in Figure 1.2 for a grazing detonation propagating with velocity, D along the surface of an asymmetrically loaded flyer. At terminal conditions the flyer is assumed to have rotated instantaneously like a hinge with no net deformation and no strength resisting the bending through a total angle, θ , from its original orientation and with a final total velocity vector, V_m , which is inclined by some angle from the lateral (downward) direction. This configuration can be addressed by coupling the expression for the wall deflection angle derived by Taylor [21] in his model of an axially detonating cylindrical bomb, to Gurney's expression for terminal metal velocity [8].

Taylor simplified the picture of a tubular flyer accelerated by an axially propagating detonation by considering a detonation-fixed frame of reference [21]. This reference frame eliminates complexities associated with directional changes in the detonation product flow. Taylor made three further assumptions: First, that the lateral velocity of the flyer and expanding detonation products is small compared to the detonation velocity of the explosive. Second, that wave dynamic reverberations within the flyer can be ignored. Third, that material strength of the flyer can be neglected. This last assumption was never stated explicitly by Taylor but arises from the stated equation of motion for the flyer, which only includes inertial forces resisting the deflection. Given these assumptions, from the perspective of the detonation-fixed observer, the

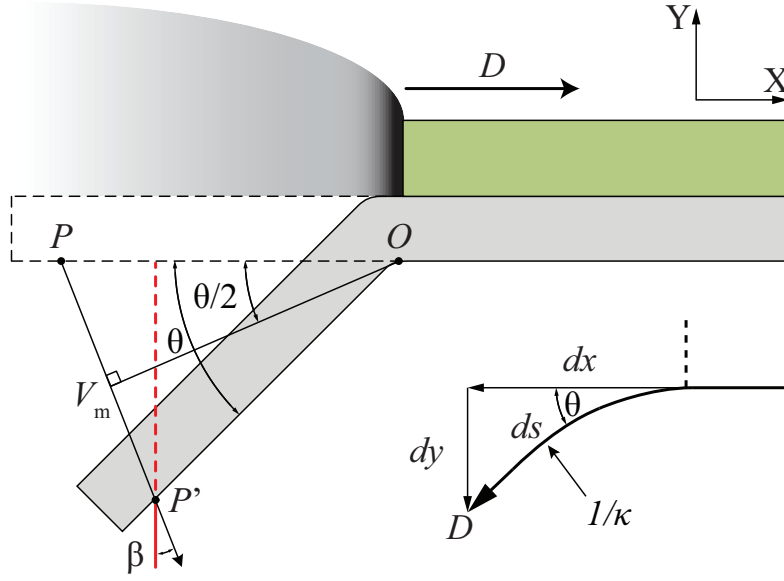


Figure 1.2: Taylor angle analysis for grazing loading.

flyer moves away with a constant velocity, D , with a local radius of curvature, $1/\kappa$, of the arc ds , which is in turn related to the local angle, θ , of the flyer from its original position. This is schematically depicted in the bottom right of Figure 1.2. In the detonation-fixed frame the lateral (vertical) flyer velocity is thus:

$$V_y = D \sin \theta \quad (1.11)$$

While, the longitudinal (horizontal) flyer velocity is:

$$V_x = D \cos \theta \quad (1.12)$$

To determine the relationship between the flyer angle, the detonation velocity, and the flyer velocity for the lab-fixed frame (denoted by X for the longitudinal axis, and Y for the lateral axis) the following Galilean transformation is used:

$$V_Y = V_y = D \sin \theta \quad (1.13)$$

and

$$V_X = D - V_x = D(1 - \cos \theta) \quad (1.14)$$

Validation of the Gurney Model in Planar Geometry for a Conventional Explosive

Consequently the total flyer velocity is:

$$V_m = \sqrt{V_X^2 + V_Y^2} \quad (1.15)$$

or

$$V_m = \sqrt{D^2(\sin \theta)^2 + D^2 - 2D^2 \cos \theta + D^2 (\cos \theta)} \quad (1.16)$$

Applying the identity: $(\sin u)^2 + (\cos u)^2 = 1$ yields:

$$V_m = D\sqrt{2(1 - \cos \theta)} \quad (1.17)$$

Applying the identity: $1 - \cos 2u = 2 \sin u$ one obtains:

$$V_m = 2D \sin \left(\frac{\theta}{2} \right) \quad (1.18)$$

which is the familiar expression for the “Taylor angle” of an explosively driven flyer.

The orientation of the velocity vector relative to the lateral (vertical) direction, Y , can be described by the angle, β , where:

$$\tan \beta = \frac{V_X}{V_Y} = \frac{D(1 - \cos \theta)}{D \sin \theta} = \tan \frac{\theta}{2} \quad (1.19)$$

Consequently:

$$\beta = \frac{\theta}{2} \quad (1.20)$$

The resulting velocity vectors and trigonometry from the simple rotation of the flyer are also depicted in Figure 1.2.

It is not immediately obvious how Taylor’s model for flyer deflection is compatible with Gurney’s model for terminal velocity given the inherently contradictory assumptions involved. Taylor’s model assumes incompressible liner rotation with negligible lateral gas velocity in the detonation fixed frame whereas Gurney’s model assumes that expansion is entirely in the direction of the metal velocity in a coordinate system centred on the plane of zero gas velocity. However, Taylor’s expression for the liner deflection is only a kinematic analysis of the flyer motion that is completely decoupled from the gasdynamic expansion process and instead only

requires that liner motion be approximately strengthless and incompressible. Consequently, any reasonably accurate approximation for the metal velocity can be used. Gurney’s model can thus be applied to the axially/longitudinally grazing case at the terminal flyer angle since product expansion occurs predominantly in the lateral direction regardless of the direction of propagation of the detonation if expansion off the flyer edges can be neglected.

1.5 Experimental Setup

The metal propulsion capability of high explosives is typically studied using the cylinder test where the expansion of products from a detonation propagating along the axis of a cylindrical charge accelerates a tubular copper liner until wall rupture. The standard cylinder test was first developed by Kury et al. and the “full wall” geometry remains the default explosive performance test 50 years later [66]. The success of the cylinder test hinges on the fact that typical high explosives used in military applications asymptotically deliver their maximum energy at similar expansion ratios, independent of charge diameter once the cylinder diameter greatly exceeds the reaction zone length. This allows for a single, scalable test geometry to be used to evaluate the performance of various high explosives as well as provide a test configuration for equation of state calibration [2].

The cylinder test has some limitations however. The requirement to reach a large expansion ratio without bursting generally necessitates using annealed copper for the casing as described by Catanach et al. [78]. Further, for non-ideal explosives it is unclear if they deliver full kinetic energy at expansion ratios that can be reached without wall rupture. For example, in cylinder test (CYLEX) experiments using ammonium nitrate (AN) performed by Davis and Hill, approximately terminal conditions were reached using 102-mm-ID copper cylinders scaled from the CYLEX standard as measured via streak camera [14]. In contrast, PDV measurements of scaled 76-mm-ID copper cylinder experiments with AN reported by Robbins did not always resolve terminal velocity despite probe distancing permitting this in principle [79]. Similar PDV experiments using AN in scaled aluminium cylinders described by Short and Jackson did not reach terminal conditions prior to the end of the PDV signal [80]. The present authors speculate that loss of signal prior to when probe destruction should occur in these studies is caused by detonation products obscuring the laser beam after wall rupture. Wall thinning effects further

complicate the modelling of inner surface measurement versus measured outer surface motion [23, 76]. Finally, it is challenging to machine very thin-walled tubing with representative diameters or using lower density metals, making it impractical to employ a cylindrical test to widely vary M/C .

An alternative to the cylinder test is to launch planar flyer plates via grazing detonation within a rectangular slab of explosive. This permits mass ratio variations to extreme values by simply varying plate and/or slab thicknesses. Hoskin et al. represents one example where shorting pins were used to record only terminal velocity for flyers over a large range of M/C [40]. Similarly Butz et al. used symmetric sandwiches to validate the Gurney equation down to small values of M/C [41]. Souletis and Mala [81] investigated the effective energy transfer of explosive slabs to symmetric flyer plates for different charge and plate thicknesses, and for varying plate/charge widths following the method proposed by Défourneaux. More recent interest in planar explosively driven flyers has arisen with the invention of interferometric techniques to measure material velocity, thereby bypassing the challenges of using streak or framing cameras with planar geometry. Gimenez et al. reported the use of thin plates sandwiching an explosive slab to successfully calibrate equation of state parameters [82]. A similar test was devised by Hill to resolve the high pressure, early-time acceleration of material using tantalum flyer plates [83].

A challenge of planar geometry is ensuring that sufficient product expansion occurs normal to the flyer and that terminal velocity is reached before lateral expansion from the charge edges influence the experiment. One solution is to simply make the charge very long and wide such that measurements at the centre remain undisturbed. Gimenez evaluated that a modest charge width of 90 mm when using thin, low density metal flyers is sufficient to reach expansion ratios similar to what is obtained in the cylinder test [82]. An alternative is to laterally confine the sides of the charge with thick steel plates as described by [83]. A drawback of heavy lateral confinement is that products can jet around the moving flyer and be guided into the path of optical probes by the heavy walls for large flyer travel distances.

In the current study, we have opted to use a slightly different design, which is depicted via a rendering and a photograph in Figure 1.3 and Figure 1.4, respectively. The explosive slab was made 95 mm wide and 175 mm long and was typically 24 mm thick. To further mitigate against non-uniformity in explosive loading due to lateral expansion, the flyer was surrounded

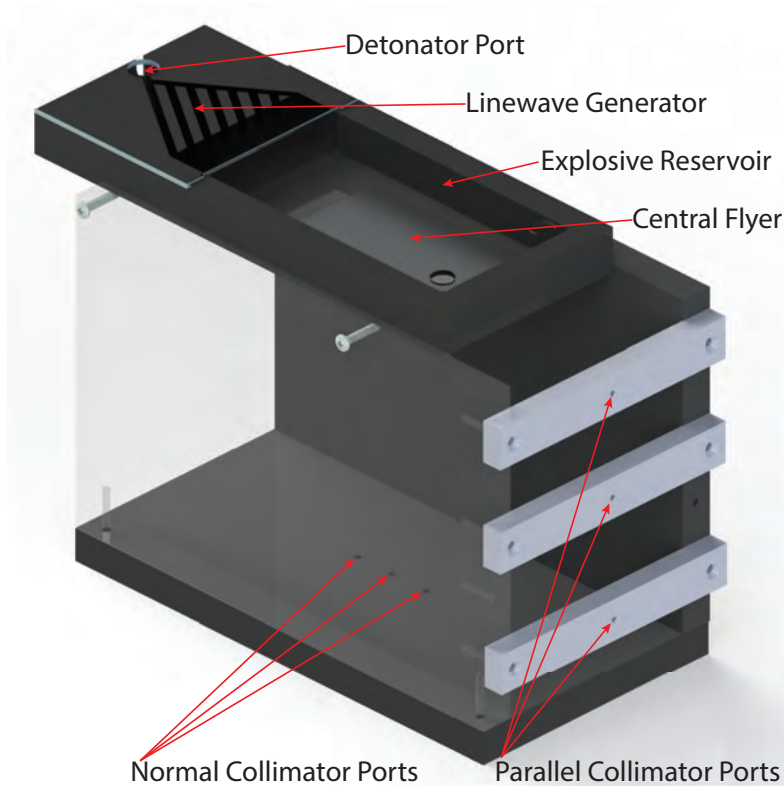


Figure 1.3: Rendering of the charge.

by a square ring of material of equal thickness to the flyer. The width of the ring was designed such that the portion of explosive subtracted via the “trapezoid method” did not encompass any of the explosive directly above the flyer. The trapezoid method is a simple geometric technique for estimating the effective mass of explosive in systems with significant edge effects for use with the Gurney equations [4, 5, 27]. It assumes that any mass of explosive outside a cone or trapezoid with a 60° base angle does not participate in the acceleration of the flyer and can be neglected. In principle, this allows for the central flyer to be more uniformly accelerated while the mechanically decoupled ring lags behind. Since we are concerned primarily with the “forward” problem of flyer acceleration, the combination of charge width and addition of the ring were deemed sufficient to provide quasi-2D motion at the flyer centre where measurements are made. The flyer and ring are assembled via bonding to a 0.2-mm-thick Mylar sheet with a very thin layer of epoxy that buffers the flyer from the explosive. In the case of the 0.3-mm-thick and 0.8-mm-thick flyers, the Mylar and ring were omitted and a single-piece flyer was used.

The explosive used was nitromethane (NM) sensitized by 10% diethylenetriamine (DETA) by weight. While nitromethane, being a homogeneous liquid, is typically not considered a

Validation of the Gurney Model in Planar Geometry for a Conventional Explosive

conventional explosive, it was selected for this study for several reasons. Although nitromethane possesses some non-usual features its detonation behaviour can still be approximated as a “gamma-law” explosive while its isentrope is similar to conventional explosives and its behaviour can be described within the JWL EOS framework [66, 67, 84, 85]. This makes it analogous to more traditional/conventional HEs for the purpose of metal acceleration. The Gurney energy of nitromethane is comparable to solid explosive compositions formulated with PETN, RDX, etc. While it has a lower CJ pressure (13 GPa vs. 20–30 GPa) and detonation velocity ($6 \text{ km} \cdot \text{s}^{-1}$ vs. $7\text{--}8 \text{ km} \cdot \text{s}^{-1}$) these can mostly be attributed to its lower density [25, 86]. On an energy-per-mass basis, it is relatively comparable to conventional solid explosives. The relatively high Gurney Energy but lower detonation pressure and detonation velocity is attractive because it permits the acceleration of flyers with reduced shock ring-up during initial motion; a situation that is more tractable for analytic acceleration models. Further, being a liquid, it can easily be poured into a container of any geometry with perfect coupling. NM does not exhibit a velocity deficit of more than 1% from its infinite charge diameter detonation velocity, unless the charge diameter or thickness is very near the critical value, a condition which was avoided in this study. Finally, dilution with other liquids permits an entirely incompressible acceleration of metals. Homogeneous nitromethane also serves as an excellent control case for follow-on studies that examine inclusions of inert or reactive materials. Indeed, nitromethane has been the base-explosive for a wide ranging study of non-ideal explosive effects for the last two decades [87–93].

The nitromethane slab was contained by a rectangular PVC reservoir. The flyer assembly was glued into a shallow recess in the reservoir while the top surface was sealed with a 3-mm-thick clear PVC plate to permit visual observation of the filling process. Consequently only an unsymmetrical geometry was considered. The grazing detonation was initiated via a line wave generator that was also filled with sensitized nitromethane. The waveshaper was initiated via a strip of rubberized explosive to ensure planarity through the thickness. The explosive assembly was supported over a base by two PVC slabs with screw tabs that easily break away upon plate launch.

Heterodyne laser interferometry (PDV) was used to measure the ballistic trajectory of the flyer. In most experiments the optical collimator for the laser beam was mounted within the support base, perpendicular to the initial position of the flyer surface, 115 mm downstream

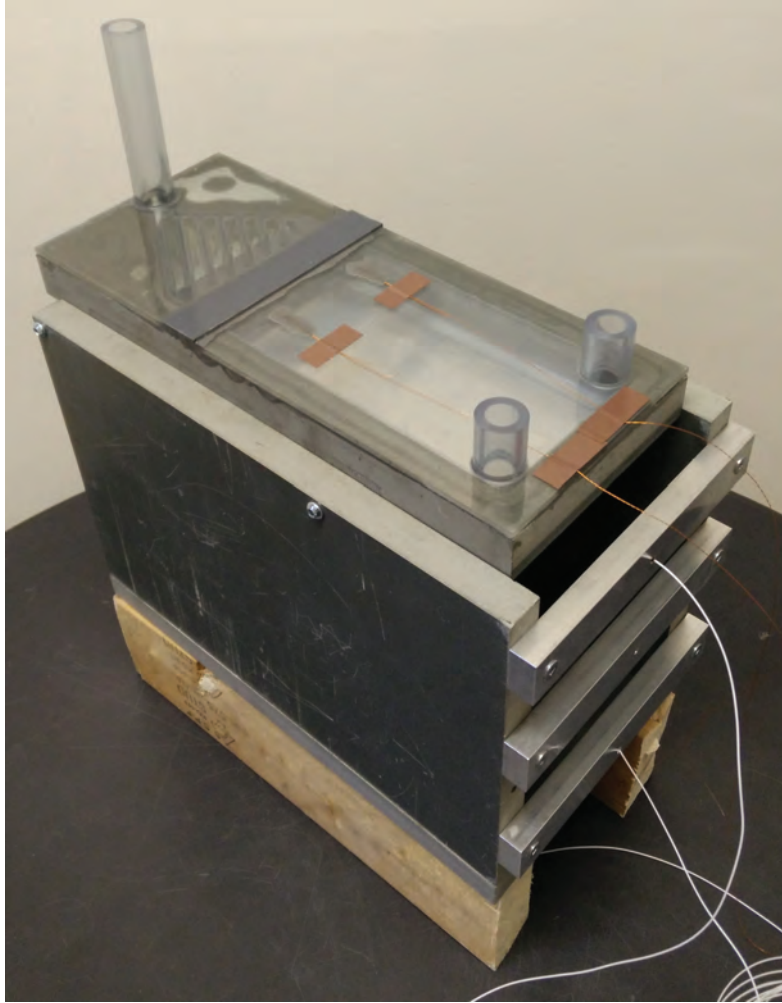


Figure 1.4: Photograph of the charge assembly.

from the end of the line wave generator to ensure steady detonation propagation conditions. For select experiments where the launch angle of flyer was substantial, additional collimators were mounted parallel to the initial position of the flyer surface and parallel to the estimated launch vector to properly resolve the absolute flyer velocity.

The flyer mass to charge mass ratio (M/C) was varied from 0.03 to 4.65 by changing the reservoir and/or flyer thickness over nine experiments. At the extremes, these ratios represent a 0.3-mm-thick flyer loaded by 24 mm of explosive and a 19-mm-thick flyer loaded by 10 mm of explosive, respectively. The flyers were 6061-T6 aluminium in all cases.

1.6 Experimental Analysis

Generally, Photonic Doppler Velocimetry only measures the component of material velocity along the laser beam path [73, 74]. Because the total metal velocity vector is inclined by half of the Taylor angle, as described in Section 2, a probe directed along the lateral direction (vertically in the charge, or normal to the initial position of the flyer) will only measure this velocity component rather than the total velocity. The laser beam path for a laterally observing probe is indicated by the red line in Figure 1.2, which subtends the angle, β , with the total metal velocity vector per the geometric argument presented in Section 1.4. Consequently, the total metal velocity can be related to the measured lateral velocity, V_{pdv} , via:

$$V_m = \frac{V_{\text{pdv}}}{\cos\left(\frac{\theta}{2}\right)} \quad (1.21)$$

since $\beta = \theta/2$, as described previously. Souers validated this analysis via hydrocode and experiment for full-wall cylinder tests where the Taylor angle is less than 15° [22, 23]. In the present study flyer deflections exceeding 30° were observed, necessitating direct validation of the assumptions inherent in calculating these angles. For large flyer deflections a second, orthogonal PDV probe was mounted to measure the longitudinal (forward/horizontal) velocity as the large deflection angle permits a clear signal return. Combined with simultaneous measurement of the longitudinal (downward/vertical) velocity, this permits direct measurement of the direction and magnitude of the total metal velocity vector. Figure 1.5 shows the lateral and longitudinal velocity histories of a 0.8-mm-thick flyer accelerated to a total velocity of $3598 \text{ m} \cdot \text{s}^{-1}$ as calculated based on vector addition of the measured orthogonal components.

Detonation velocity was measured via an array of four self-shortening twisted pairs aligned along the explosive slab to be an average of $6067 \text{ m} \cdot \text{s}^{-1}$ over all six experiments. From this value, the Taylor angle can be calculated and used to correct lateral PDV velocity measurements to yield the total metal velocity for each experiment. For the 1.6 mm, 0.8 mm, and 0.3-mm-flyer experiments, the direction of the total metal velocity vector was derived from orthogonal probe measurements and thus the angle β was obtained directly. For the 0.03 mm and 1.6 mm experiments the Taylor angle was under-predicted by approximately one degree. Similarly, for a 3.2-mm-thick flyer launched to $2052 \text{ m} \cdot \text{s}^{-1}$ (corresponding to the $2023 \text{ m} \cdot \text{s}^{-1}$ normal ve-

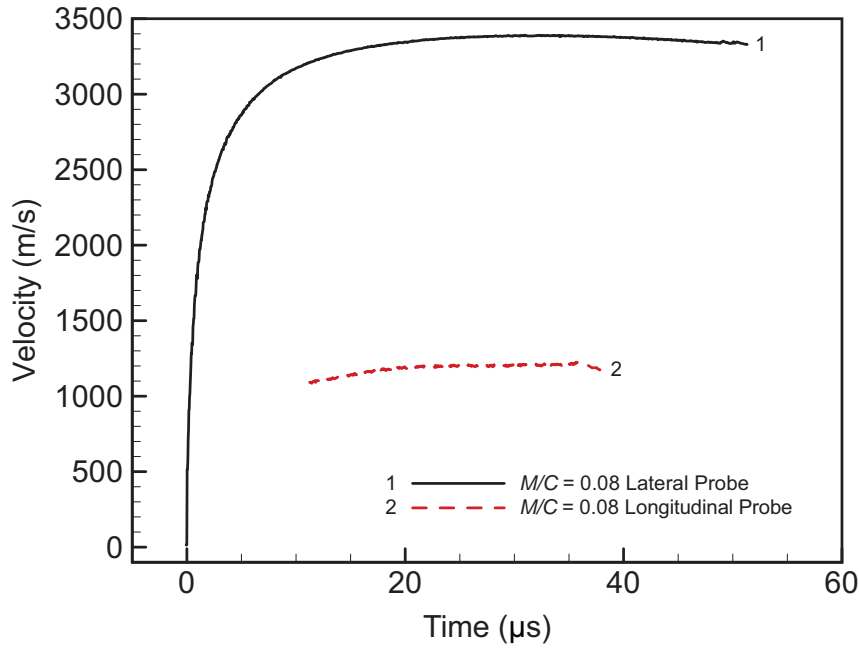


Figure 1.5: Lateral and longitudinal velocity histories for a 0.8-mm-thick flyer propelled to a total metal velocity of $3598 \text{ m} \cdot \text{s}^{-1}$.

locity measured via PDV), the Taylor angle was measured directly via piezoelectric pins to be 19.4° compared to an estimated value of 18.7° using Equation 1.18, representing only a 0.7° (3.6%) underestimation. In contrast, in the 0.08 mm experiment orthogonal measurements gave an estimate of 39.1° for the experimental value of the Taylor angle. A theoretical value for this Taylor angle can be estimated directly from the measured absolute metal velocity and the detonation velocity to be 34.5° via Equation 1.18. This represents a 4.6° (12%) underestimation of the angle. Consequently, it can be concluded that the Taylor angle approximation is quite accurate for loadings of $M/C > 0.5$. Further, as the Taylor angle decreases, the forward velocity component becomes negligible and the magnitude of the correction for probe angle drops below 1%.

Analysis of the PDV traces is also complicated by the fact that a probe not aligned along the total metal velocity vector is constantly seeing “new metal” pass through the laser spot. For a longitudinal (horizontal) probe this means that flyer velocity is only measured at a fixed detonation product expansion ratio. Consequently, the longitudinal probe must be mounted sufficiently below the initial flyer position such that the flyer is at terminal velocity as it crosses the laser beam. For a lateral velocity probe, longitudinal flyer motion feeds metal launched at an earlier time through the laser spot, causing premature measurements at a higher product expan-

sion ratio. These complications do not pose a problem for the measurement of flyer terminal velocity but introduce errors when fitting models to flyer acceleration, necessitating corrections for tilt and longitudinal motion.

1.7 Experimental Results and Discussion

The velocity histories for all nine experiments as recorded by the laterally observing probes are depicted in Figure 1.6. In all experiments, terminal velocity was obtained. Deceleration in the 0.3 mm and 0.8-mm-thick flyer experiments ($M/C < 0.08$) can be attributed to aerodynamic drag due to the low flyer mass and high velocity. In the 0.3-mm-thick flyer experiment, aerodynamic drag was of sufficient magnitude and abruptness that it may have negatively impacted the terminal velocity of the flyer. Ideally such an experiment would be repeated in vacuum or with a scaled-up geometry using a flyer with greater inertia. Also, in the 6.4-mm-thick-flyer experiment ($M/C = 0.63$), a strong elastic precursor wave was observed prior to shock breakout. In all the other experiments, the elastic precursor was either very weak or entirely absent.

The corresponding flyer thicknesses, explosive layer thicknesses, and charge to flyer and charge to tamper mass ratios are summarized in Table 1.1. Table 1.1 also summarizes the predicted Gurney velocity based on Equation 1.9, including the tamping effect of the PVC lid for all cases, the maximum velocity recorded by the probe, the total metal velocity, and the predicted and measured Taylor angles. Figure 1.7 shows the experimental data compared to two Gurney curves constructed using a Gurney energy of $2.35 \text{ km} \cdot \text{s}^{-1}$. The Gurney energy was determined by down-scaling the published value of $2.41 \text{ km} \cdot \text{s}^{-1}$ to account for the small energetic decrement due to the addition of the 10% DETA by mass [25]. The tamped Gurney curve was constructed using the experimental values for N/C , leading to a pronounced kink in the curve due to the experimental detail of thinning the explosive reservoir while the top PVC lid thickness was fixed, resulting in a step-like increase in the tamper-to-mass ratio (N/C) as the M/C ratio was increased through a value near unity. The untamped Gurney curve was constructed by simply setting the value of N/C to zero over the range of M/C values considered experimentally.

As can be ascertained from both Figure 1.7 and Table 1.1, the accuracy of the Gurney model predictions is quite good, with an average error of less than 5% over the full range of mass ratios

1.7 Experimental Results and Discussion

Table 1.1: Summary of experimental conditions for Gurney curve measurements of homogeneous sensitized nitromethane (flyer/reservoir geometries and mass ratios) and predicted and measured velocities and deflection angles of the flyer. A Gurney Energy of $2350 \text{ m} \cdot \text{s}^{-1}$ was used for the sensitized NM.

Flyer	Reservoir	$\frac{M}{C}$	$\frac{N}{C}$	V_{Gur} (m/s)	V_{pdv} (m/s)	θ (°)	θ_{exp} (°)	V_{m} (m/s)	Error (%)
19.1 mm	9.9 mm	4.65	0.4	451	438	4.3	-	438	2.9%
12.7 mm	9.4 mm	3.27	0.4	608	597	5.7	-	598	1.7%
6.4 mm	10.4 mm	1.47	0.4	1093	1067	10.3	-	1071	2.1%
6.4 mm	24.1 mm	0.63	0.2	1727	1622	16.3	-	1639	5.4%
3.2 mm	15.4 mm	0.50	0.3	1972	2023	18.7	19.4 ^a	2052	3.9%
3.2 mm	24.1 mm	0.32	0.2	2357	2387	22.4	-	2433	3.1%
1.6 mm	23.9 mm	0.16	0.2	2957	2873 ^b	28.2	29.2 ^d	2969	0.4%
0.8 mm	24.1 mm	0.08	0.2	3311	3389 ^b	34.5 ^c	39.1 ^d	3598	8.0%
0.3 mm	24.1 mm	0.03	0.2	3830	3837 ^b	39.7 ^c	41.2 ^d	4130	7.3%

^a Measured via a planarity test using shock pins.

^b Calculated using the “open face” Gurney equation (setting $N/C = 0$ in Eq. 1.9) in anomalous region. All other values calculated with experimental value of N/C .

^c Calculated using the experimental value for metal velocity, all other values calculated based on the Gurney/Taylor estimate.

^d Calculated using orthogonal velocity components as shown in Fig. 1.5.

considered. In the present experiments, excellent agreement between the Gurney model and experiment was maintained until an M/C ratio of 0.16. For the experiments with M/C ratios of 0.08 and 0.3 a more substantial deviation of 7-8% was observed. These results are broadly consistent with criteria for good agreement cited in the literature. Kennedy [10] suggests good agreement for $M/C > 0.2$ based on the work of Henry, and later, good agreement for $M/C > 0.1$ [24] based on comparison to simple analytic gasdynamic models and the experimental results of Hoskin for open face sandwiches driven by a grazing detonation [40]. Finally Kennedy [5] suggests good agreement for $M/C > 1/3$ based on comparison between the Gurney model and the gasdynamic solution for the normal detonation of an open-faced sandwich from Aziz et al. [68], but noted that for symmetric sandwich experiments conducted by Butz et al. [41] good agreement was observed down to an M/C value of 0.05. Evidently, these findings do not correlate directly with the present experimental configuration, but qualitative similarities are expected. The present results for lightly tamped asymmetric sandwiches are most similar to the results presented by Hoskin, with similar errors at the extremes of M/C .

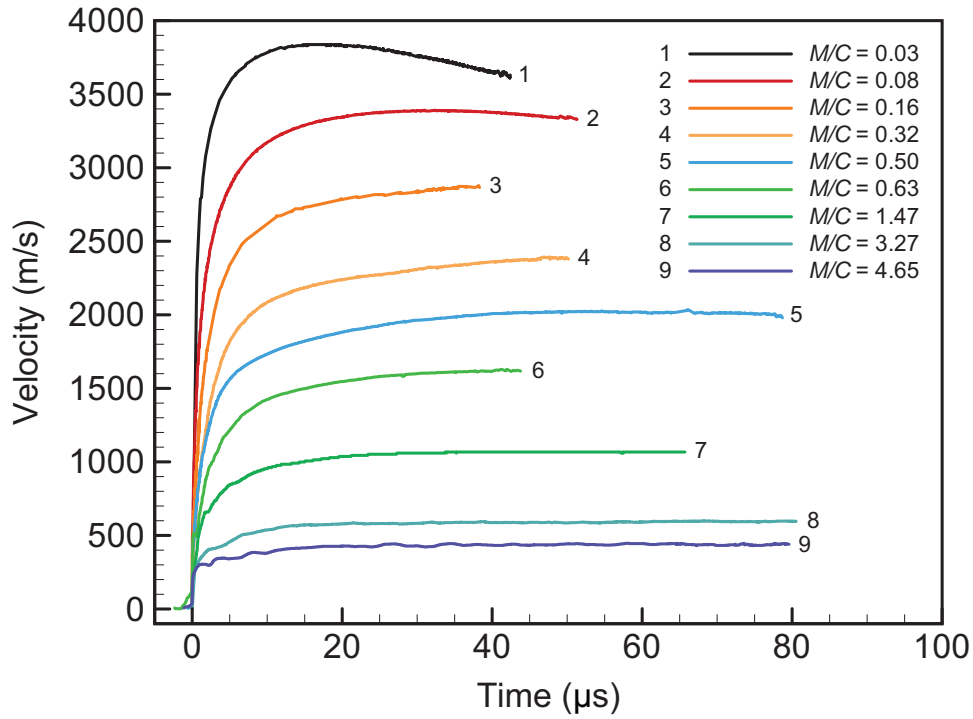


Figure 1.6: Lateral probe PDV traces for all experiments.

Several explanations have been proposed throughout the evolution of the literature to explain the remarkable predictive behaviour of such a simple model applied to what is a highly dynamic, wave-governed process. A most probable explanation is simply that the assumptions of a linear velocity profile and uniform density are relatively close to reality for large detonation product expansion ratios, with discrepancies amounting to cancelling errors. It has been previously noted that the symmetric sandwich geometry is the best case for good agreement owing to the inherent similarity between the actual expansion process and the model assumptions, whereas in the case of geometries with radial symmetry more drastic departures are expected [41, 44].

Two effects can explain the larger underprediction for small values of M/C in the current study. First, as the flyer gets thin relative to the explosive, Gurney's model fails to represent the actual expansion of the detonation products. In the case of a thin flyer, terminal velocity can be reached while a non-linear gradient in gas velocity exists. Consequently, the assumption of a linear gas profile leads to overestimating the energy partitioned into expanding the detonation products and underestimating the energy delivered to the flyer for these cases. This effect is discussed by Hirsch for spheres, cylinders and sandwiches [44, 45]. Second, Hirsch noted that the asymmetric (tamped) Gurney equation begins to underpredict the open-faced Gurney equation

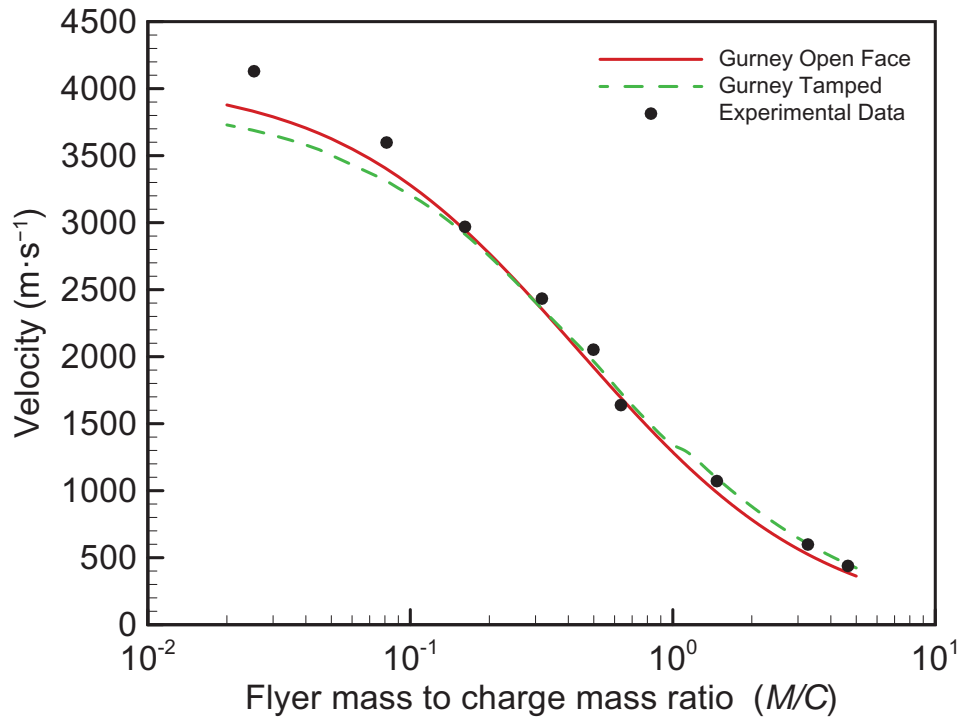


Figure 1.7: Experimental terminal velocities plotted against the tamped and untamped Gurney curves using a Gurney Energy of $2350 \text{ m} \cdot \text{s}^{-1}$.

for a given value of M/C for certain relative values of M/C vs N/C if both ratios are sufficiently small. This can be described as the “Hirsch criterion” defined by the following expression:

$$\frac{M}{C} \left(4 \frac{N}{C} + 1 \right) < \frac{1}{2} \quad (1.22)$$

In Figure 1.7, this anomalous behaviour of the asymmetric sandwich theory curve is noted where it begins to underpredict as compared to the untamped theory curve—a non-physical result. Consequently, for certain combinations of M/C and N/C , the Gurney model is discarding the effect of a tamper. In the present study the criterion is met experimentally for the 1.6 mm, 0.8 mm, and 0.3-mm-thick flyer experiments. However, only the 0.8 mm and 0.3 mm experiments show significant departure between experiment and theory and between the tamped and untamped theory curves. This can be attributed to the relatively low absolute mass of the tamping material, and thus the correspondingly small tamping effect.

In the current study, the relative failure of the Gurney model in predicting terminal metal velocity for small experimental values of M/C can thus be attributed to a combination of incor-

rectly modelling gasdynamic expansion at these loadings and the anomalous discarding of the tamping effect where the Hirsch criterion is met.

A secondary consideration is that the initial flyer velocity imparted by the transmitted oblique shock following the detonation increases slightly as the flyer gets thinner. Since the Gurney model only considers the effect of gasdynamic expansion, it is incapable of dealing with variability in shock effects which could otherwise be “built-in” to the value of the Gurney energy. This variability in shock acceleration can be observed in the experimental traces. The 0.8-mm-thick flyer was initially shock accelerated to $512 \text{ m} \cdot \text{s}^{-1}$ whereas the 6.4-mm-thick flyer loaded with an equal explosive thickness was initially accelerated to only $300 \text{ m} \cdot \text{s}^{-1}$ by the initial shock. The ratio of energy transferred by the shock versus the gasdynamic expansion of the detonation products also varies significantly with the flyer to charge mass ratio. For $M/C = 0.08$ the contribution of the shock is only approximately 15%, whereas it represents almost 50% of the total velocity for $M/C = 4.65$. These considerations suggest that superior agreement for small values of M/C can be obtained by correcting the Gurney equations by separately accounting for the contributions of gasdynamic expansion and initial shock loading. This methodology was proposed and elaborated upon by Backofen et al. [94, 95].

1.8 Conclusion

In the present study, we have experimentally measured the acceleration history and terminal velocity of aluminium flyers over a wide range of metal to charge mass ratios using Photonic Doppler Velocimetry. Predictions of flyer launch angle compare relatively favourably to experimental observations. These angles were then used to correct normal PDV probe data to determine the total metal velocity. These velocities were very well predicted by a combination of the asymmetric sandwich and untamped Gurney models. The average error from the model was less than 5%, a result superior to the nominal 10% accuracy ascribed to Gurney in the literature [10]. These results reinforce the exceptional usefulness of the Gurney methodology for engineering calculations involving explosive-metal interactions providing the launch process is not heavily influenced by edge effects and the charge under consideration does not correspond to one of the anomalous regions poorly covered by the model assumptions.

Chapter 2

The Propulsive Capability of Explosives Heavily Loaded with Inert Materials

Jason Loiseau, William Georges, David L. Frost, and Andrew J. Higgins

[Accepted in Shock Waves](#)

2.1 Abstract

The effect of inert dilution on the accelerating ability of high explosives for both grazing and normal detonations was studied. The explosives considered were: 1) neat, amine-sensitized nitromethane (NM), 2) packed beds of glass, steel, or tungsten particles saturated with amine-sensitized NM, 3) NM gelled with PMMA containing dispersed glass microballoons, 4) NM gelled with PMMA containing glass microballoons and steel particles, and 5) C-4 containing varying mass fractions of glass or steel particles. Flyer velocity was measured via Photonic Doppler Velocimetry (PDV) and the results were analysed using a Gurney model augmented to include the influence of the diluent. Reduction in accelerating ability with increasing dilution for the amine-sensitized NM, gelled NM, and C-4 was measured experimentally. Variation of flyer terminal velocity with the ratio of flyer-mass to charge-mass (M/C) was measured for both grazing and normally incident detonations in gelled NM containing 10% microballoons by mass and for steel beads saturated with amine-sensitized NM. Finally, flyer velocity was measured in grazing versus normal loading for a number of explosive admixtures. The augmented Gurney

model predicted the effect of dilution on accelerating ability and the scaling of flyer velocity with M/C for mixtures containing low-density diluents. The augmented Gurney model failed to predict the scaling of flyer velocity with M/C for mixtures heavily loaded with dense diluents. In all cases, normally incident detonations propelled flyers to higher velocity than the equivalent grazing detonations because of material velocity imparted by the incident shock wave and momentum/energy transfer from the slapper used to uniformly initiate the charge.

2.2 Introduction

The acceleration of materials to high velocity is one of the primary uses of high explosives (HEs). Projection of warhead fragments, imploding the liner of a shaped charge, and shock compression of material are typically performed using conventional HEs. The loading by conventional HEs is quite violent (detonation pressures of 10–50 GPa), leading to wavedynamic reverberation within the accelerated materials, which may generate spall or microstructural changes. In some applications, it is desirable to accelerate materials “shocklessly” to intermediate velocities; for example in explosive welding/cladding [96], dynamic compaction and shear experiments [16], or to minimize ejecta launched from surface asperities [97, 98]. Softer loading is typically accomplished by using weak explosives that have low detonation pressures and detonation velocities that are subsonic relative to the driven material, or by introducing gaps between the HE and the driven material.

Conventional HEs typically display behaviour that approximates theoretical behaviour during detonation and then during the subsequent expansion from the Chapman-Jouguet state down to ambient conditions. The chemical decomposition in ideal HEs occurs over very short times prior to substantial gasdynamic expansion, and thus over very small spatial distances relative to the size of typical charges. Despite a typically polycrystalline and/or multi-phase nature, ideal explosives can be modelled as the decomposition of a homogeneous material using continuum models because the heterogeneities are much smaller than the scale of the charges being modelled [93]. Heterogeneities for these explosives only enter via the selection of source-terms in continuum reaction models, for example when HE grain size influences bulk explosive sensitivity by changing hot spot formation. Consequently, conventional HE detonation wave structure is broadly described by classic ZND theory and the propagation of detonation waves through a

bulk explosive sample is well characterized by front curvature theory. Conventional/ideal explosives decompose promptly within the detonation reaction zone, leading to little or no additional chemical energy release during the early-time expansion of the detonation products. Materials in contact with the HE are thus driven via isentropic (adiabatic) expansion of the detonation products. Product expansion can be approximated as a polytropic process with a constant value of γ unique to the explosive [67]. A constant value of γ rarely leads to good agreement in detail, however. Accurate engineering calculations for ideal explosives can typically be made using an equation of state like the Jones-Wilkins-Lee (JWL) formulation, which corrects for variations in the value of γ at high and intermediate pressures before ideal gas behaviour is recovered. Ultimately, two regimes of ideality can be defined: ideal detonation-scale dynamics (order of $\approx 1 \mu\text{s}$) and ideal expansion scale dynamics (order of $\approx 10\text{--}100 \mu\text{s}$).

Low detonation velocity explosives are typically formulated using an intrinsically weaker explosive such as ammonium nitrate (AN) or admixing solid, inert materials into a conventional crystalline HE (TNT, RDX, HMX, etc.) or a neat liquid explosive. AN formulations are inherently non-ideal due to detonation dynamics of the heterogeneous prills, substantial scaling of detonation energy release with charge diameter, and chemical energy release that extends well into the expansion of the detonation products [14]. The addition of inert particles to an ideal high explosive generates non-ideal behaviour because of momentum and thermal transport between the explosive phase and the particles. Depending on the size and dispersion of the added particles, the detonation wave must either transmit through or diffract around them, leading to detonation-scale heterogeneities. For sufficiently high loadings of inert particles, detonation wavelets may fail, causing the reaction zone to lengthen as undetonated explosive burns behind the detonation front [12, 86]. At larger volumes of product expansion, aerodynamic drag and heat transfer between detonation products and particles results in a non-ideal gasdynamic expansion. HE/dense particle mixtures are thus an interesting class of non-ideal explosive in that very fine scale heterogeneities ($<100 \mu\text{m}$ particles) significantly influence the bulk (or engineering scale) detonation and expansion behaviour of the explosive.

Detonics studies of explosive/inert admixtures date back to the earliest development of multiple-component explosive lenses using trinitrotoluene (TNT) diluted with various salts [99, 100]. Previous studies on the effect of dense particle diluents in HEs have typically focused on detonation properties such as detonation velocity, detonation pressure, and reaction zone

length [12, 86, 101–104]. The theoretical framework describing such detonations has evolved, starting with the assumption of equilibrium between the phases such that only the density and volume fraction of the inert diluent influences the detonation velocity and pressure of the explosive. Further evolutions included compression and heating of the diluent while equilibrium in flow velocities of the two phases is assumed. The most rigorous treatments of explosive admixtures include slip between the explosive and particle diluent phases, such that the particles experience drag in addition to thermal non-equilibrium. Finally, modelling of a fully-reactive flow allowed for local detonation failure, re-initiation, and later-time burning due to wavelet interactions around the particles in order to fully resolve detonation pressure and velocity.

Other work has focused on the blast output and momentum transfer from HE/dense particle admixtures [19, 105–107]. Such explosives are capable of either increasing the total blast impulse if reactive particles are used, or increasing blast impulse in the near-field while reducing blast impulse farther from the charge if inert particles are used.

Comparatively little work has been done on examining early-time gasdynamic expansion and energy transfer relevant to metal-driving by these heterogeneous explosive/inert-particle admixtures. Voskoboinikov experimentally examined the decrement in flyer velocity obtained by mixing a wide variety of solid diluents into crystalline explosive blends for both grazing and normally incident detonations; however, results were only analysed in the context of the additive approximation for estimating flyer initial free surface velocity and only thin flyer plates ($\approx 1\text{--}1.5\text{ mm}$) were used [108]. HE/tungsten admixtures over-driven by an outer cladding of conventional HE were studied by Kato for use in imploding a shaped-charge liner [109, 110].

The behaviour of explosives with dense particle inclusions is also useful to benchmark the performance of explosives mixed with reactive particles. Heavily aluminized explosive formulations ($\approx 30\%$ mass fraction) are often employed to increase the specific blast output of a charge but typically have lower Gurney energies than pure explosive formulations. However, depending on the base high explosive, binder (if present), and fineness of the aluminium, the aluminium particles may react sufficiently quickly to contribute to acceleration ability. Quantifying the metal accelerating ability of mixtures with unambiguously non-reactive additives is thus useful for determining the energetic contribution of particle reaction to the metal-driving performance of composite explosives [111]. In particular, it permits the direct determination

if particles are reacting exothermically over timescales relevant to metal-driving, even if the reaction does not provide absolute performance enhancement over the baseline explosive.

In the current study, we present measurements of the acceleration and terminal velocity of flyers propelled by various explosive/particle admixtures. Heterodyne laser interferometry (i.e., Photonic Doppler Velocimetry, or PDV) was used to measure the velocity history of each flyer. Data from prior works is also included [9, 112–114]. A number of explosives were used as the base energetic material: amine-sensitized nitromethane (NM), poly(methyl methacrylate)-gelled NM, and C-4, an RDX-based plastic explosive. A wide range of particle sizes and densities were considered: fine glass microballoons, various sizes of glass beads, fine tungsten powder, and steel particles of various sizes. For select admixtures, we measured the differences in flyer acceleration and terminal velocity between grazing detonations and normally incident detonations. We also considered scaling of flyer velocity with the ratio of flyer-mass to charge-mass (M/C), diluent mass/volume fraction, and diluent density. Results were compared to predictions of an augmented Gurney model.

2.3 Effect of Detonation Wave Incidence Angle

The effect of detonation wave orientation on metal acceleration by a high explosive is generally not considered. The Gurney model assumes that a flyer reaches the same terminal velocity regardless of how the detonation wave interacts with the surface of the flyer. Rather, If the detonation grazes along the surface of the flyer, it is launched to the same terminal velocity but inclined at some angle that is a function of the terminal metal velocity and the detonation velocity of the explosive [5]. We postulate that the acceleration and terminal velocity of an explosively driven flyer can vary due to differences in the wavedynamic loading that arises as the detonation wave is tilted relative to the flyer.

In the case where a conventional explosive is detonated such that the wave grazes along the surface of the flyer at supersonic velocity relative to the flyer material sound speed, an oblique shock is driven into the flyer that remains attached to the detonation wave. This situation is depicted in Fig. 2.1a. The shock breaks out at the exposed flyer surface, leading to a jump in material velocity. The magnitude of this velocity is determined by the detonation pressure, relative impedances of the flyer and detonation products, and shock attenuation through the

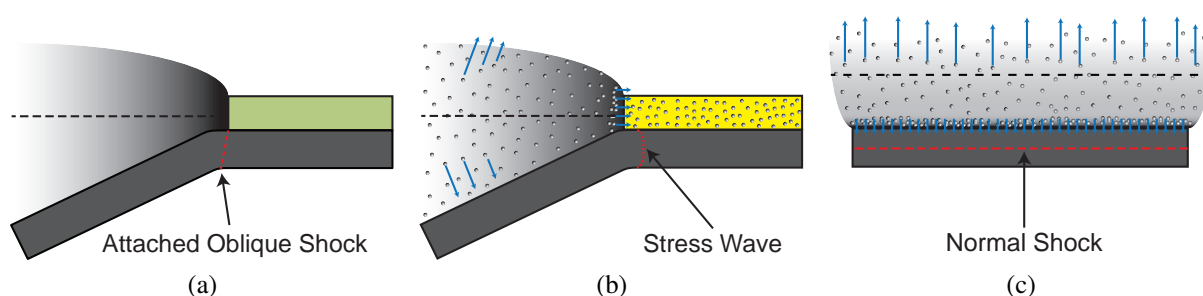


Figure 2.1: Depiction of the loading conditions for **(a)** a grazing detonation in a conventional explosive with a detonation velocity supersonic relative to the flyer material sound speed, **(b)** a grazing detonation in a non-ideal explosive loaded with particles with a detonation velocity slower than the flyer material sound speed, and **(c)** a normal detonation in a non-ideal explosive loaded with particles [114].

flyer thickness. Subsequent reflections of this wave then alternate between rarefactions and compressions as they travel through the thickness of the flyer and interact with the interfaces and the Taylor wave from the detonation [40]. This results in an oscillatory compressive-tensile loading that manifests as an initial sharp jump in metal free-surface velocity, followed by ringing of the free-surface velocity as the flyer accelerates. The explosively driven acceleration can be seen as a coupling between wavedynamic loading and a ballistic acceleration from the expanding detonation product gases [94, 95, 115]. If the angle of interaction of the detonation wave is tilted towards the flyer surface, the total material velocity imparted by the shock wave loading will increase relative to the grazing case, and this may slightly increase the terminal velocity of the flyer. These increases are offset by the reflection of shocks into the detonation products, which temporarily slow the gas expanding against the flyer. In terms of gasdynamic analogies, the acceleration of a flyer via a grazing detonation is similar to isentropic nozzle flow where the nozzle profile is determined by kinematic acceleration of the nozzle walls by action of the flow pressure, as described by Taylor [21]. The acceleration of a flyer via a normal detonation is analogous to the acceleration of a piston by an expanding gas, except where the first interaction is a transmitted shock into the piston and a reflected shock into the gas, rather than the reflection of a rarefaction at the gas/piston interface as in the solution of Lagrange's ballistic problem [65]. In order to distinguish between material velocity imparted by the transmission of a strong shock wave into the material, and material velocity that is caused by expansion of the detonation products against the flyer, the terms *wavedynamic* and *gasdynamic* (or *ballistic*) are respectively used.

2.3 Effect of Detonation Wave Incidence Angle

This conceptual picture changes somewhat if the explosive has a detonation velocity that is subsonic relative to the flyer sound speed and if the explosive contains dense diluents. For a subsonic detonation grazing along the surface of the flyer, no oblique shock is generated and instead a weak compressive precursor wave is driven in the flyer ahead of the detonation, as depicted in Fig. 2.1b [80, 116]. If the explosive contains a dense inert diluent, the layer of particles closest to the surface of the flyer will impinge against the flyer due to the pressure differential between the detonation and the confining flyer. However, the majority of the initial velocity of the particles is in the direction of the detonation wave, and solid particle motion normal to the initial flyer position only occurs at later times when the detonation products expand laterally and aerodynamically drag the particles up to speed. The particles thus have limited interactions with the flyer plate and can only influence flyer motion by changing the expansion of the detonation products. In contrast, if the detonation is normally incident, a shock wave will be transmitted into the flyer regardless of the explosive detonation velocity and particles will first impinge against the flyer due to imparted material velocity from the passage of the detonation wave. This is followed by aerodynamic acceleration of the particles as the detonation product expands against the flyer. This situation is depicted in Fig. 2.1c. Consequently, diluent properties such as particle size and density may have larger effects than what has been previously observed in grazing experiments [112, 113]. Note that the dashed black lines depicted in Fig. 2.1 correspond to the idealized plane of zero detonation product flow velocity, while the blue arrows indicate the idealized velocity vectors of solid diluent particles.

The effect of detonation wave incidence angle on the acceleration of metal flyers is rarely discussed in the literature despite its importance in the design of a variety of explosive devices. This is likely due to complications arising from the violent loading generated by conventional explosives and the experimental initiation of planar, normally incident detonation waves.

Normally incident detonation of a conventional explosive charge in contact with a flyer will typically produce spall unless the flyer is sufficiently thin that fast wave transit times limit the maximum tensile loading arising from rarefaction interactions. Spallation can also be suppressed by the introduction of a vacuum or air gap between the charge and the flyer surface, but this necessarily complicates charge design [17]. Initiation of a planar, normal detonation also requires the use of a detonation-wave shaping device. If a two-component explosive lens is used, the width of the receptor and the ratio of detonation velocities governs the total size of the

lens and thus the minimum explosive loading of the flyer. If a flyer plate initiator (slapper) is used, the detonation may be over-driven and the slapper will contribute momentum and energy to the system.

In a series of papers, Backofen proposed that flyer acceleration can be modelled by a two-step process of coupled wavedynamic acceleration from shock transmission and ballistic acceleration from product expansion [94, 95, 115]. In this framework, energy transferred to the flyer by the shock is a function of M/C , detonation wave interaction angle, and shock impedances while the energy transferred to the flyer from detonation product expansion remains a function of only M/C .

Similarly, impedance matching and simple wavedynamic models can be used to estimate the oscillatory free surface velocity of a shocked flyer during its acceleration [62]. The absence of further explicit treatments of wavedynamic and incidence effects may be explained by the ubiquity of hydrocode simulations, which implicitly capture wavedynamic and gasdynamic acceleration with sufficient accuracy to model device behaviour.

A limited discussion of incidence effects also arises in the literature covering certain specialized devices. Explosive flyer cascades, wherein a series of progressively thinner flyer plates are explosively accelerated via impact initiation of their respective charges by the preceding flyer, have been investigated to achieve impactor velocities in excess of $10 \text{ km} \cdot \text{s}^{-1}$ [117–121]. These cascades incorporate features addressing many of the above issues. Air gaps or lower-density solid buffers are used to attenuate the transmitted shock in the thicker flyers [118, 119]. Velocity enhancement of the final flyer results from a combination of energy and momentum transfer from the preceding flyer, dynamic tamping from the preceding flyer, and the generation of an overdriven detonation in the final explosive charge.

For shaped charge design, the introduction of a wave shaping device to tilt the detonation wave normal to the liner has been shown to increase jet velocity and penetration ability by reducing the liner collapse angle and eliminating variability in the collapse process when a sweeping wave implodes a liner [100]. By contrast, the explosive welding literature emphasises the use of grazing detonations of low-detonation-velocity, low-brisance explosives to eliminate the compression-rarefaction pulses which may fail the weld in tension and to provide an oblique impact between the target materials, thereby forming a scouring jet [96, 122].

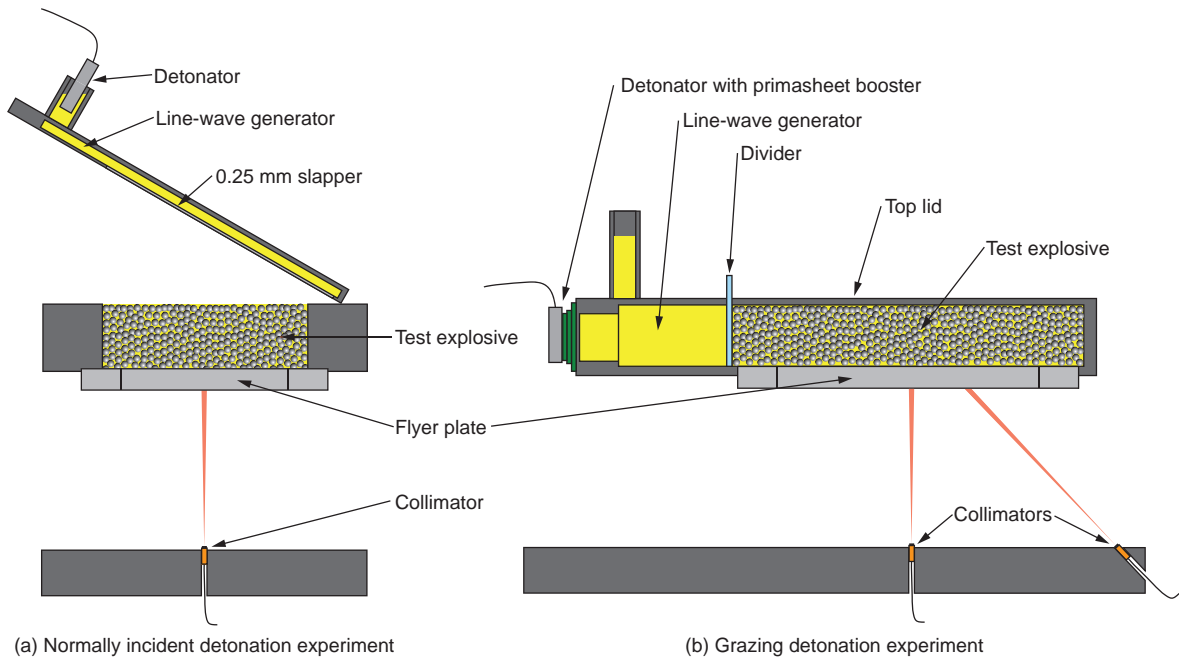


Figure 2.2: Experimental configurations for both the grazing and normally incident detonation experiments.

In the present study, the use of low detonation pressure, low impedance explosives permitted the direct experimental evaluation of wavedynamic contributions to flyer acceleration and to directly measure the scaling of flyer velocity with flyer-to-charge mass ratio (M/C) for both grazing and normal incidence.

2.4 Experimental Details

The metal accelerating ability of high explosives is typically studied using the cylinder expansion test (CYLEX), wherein an axially propagating detonation is used to accelerate a cylindrical metal liner [22, 23, 66, 76, 78]. The standard-scale CYLEX test possesses numerous advantages: amenability to streak camera monitoring of wall motion, symmetric expansion of the detonation products, amenability to analytic modelling, and the ability to probe most of the detonation product pressure range of interest for driving metal prior to wall rupture (< 20 relative volumes). Several disadvantages exist as well: The cylinder is difficult to load with heterogeneous mixtures which need to be packed, it is challenging to widely vary cylinder wall thickness, and wall rupture may occur when driven by non-ideal explosives prior to reaching terminal velocity, obscuring measurement. Furthermore, material wall thinning during expansion must be

accounted for when measuring the energy delivered by the detonation, and this will necessarily vary if the initial wall thickness is varied [23]. It is also technically challenging to initiate a cylindrically expanding detonation for the purposes of loading the cylindrical wall normally. Consequently, cylindrical charges are less amenable to compare detonation wave incidence effects.

With the advent of modern interferometric velocimetry techniques, it is no longer necessary to rely on casing radial symmetry to prevent measurement obscuration by detonation products. Planar metal acceleration experiments can thus be used, with the major limitation that product expansion off the edges of charge must be considered [9, 82, 83]. In the present experiments, two charge configurations for launching planar flyer plates were used to compare loading via grazing and normally incident detonation waves. A detailed description of the charge designs is subsequently presented and schematics of the two charge configurations are shown in Fig. 2.2.

Measurement of the velocity histories of both the grazing-detonation-propelled flyers and normal-detonation-propelled primary flyers was done with Heterodyne Laser Interferometry (PDV), developed by Strand et al. [71]. Collimators with a listed working distance of 200 mm and a 3.2-mm-diameter lens were used to direct the PDV laser on the flyer plates. The collimators were 1550 nm single mode, single SM-28e fibre, FC/ACP coupled. A sliding window Fourier Transform analysis was used to convert time-resolved blended laser beat frequency into time-resolved flyer free-surface velocity.

2.4.1 Grazing Detonation Charges

The grazing experiments were conducted using a charge design validated by measuring the Gurney curve for neat amine-sensitized nitromethane in a previous study [9]. The charge is shown in Fig. 2.3. The explosive slab was 95 mm wide, 175 mm long, and nominally 24 mm thick and was contained by a rectangular PVC reservoir. The flyer assembly was glued into a shallow recess in the bottom of the reservoir while the top surface was sealed with a 3-mm-thick clear PVC plate to permit visual observation of the filling process. Consequently, only an asymmetric sandwich geometry was considered.

One end of the reservoir was machined with a line-wave generator (LWG) to initiate a planar, grazing detonation in the test explosive. The LWG was filled with liquid nitromethane (NM) sensitized with 10% diethylenetriamine (DETA) by weight (90/10 NM/DETA). The NM was

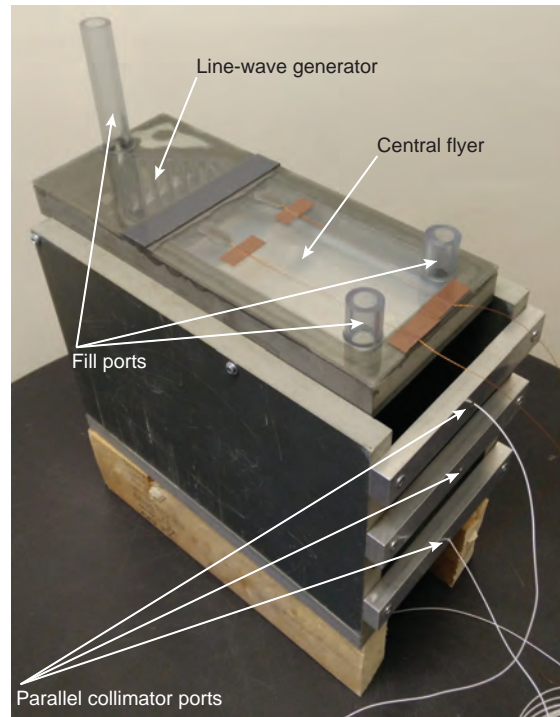


Figure 2.3: Charge assembly used for grazing detonation experiments [9].

segregated from the test explosive by a 2-mm-thick clear PVC barrier, allowing transmission of the detonation. The LWG was initiated via a strip of rubberised explosive placed on a sealed slit at the top vertex to ensure wave planarity through the thickness. Orica Excel MS detonators were used to initiate the rubberised explosive.

The reservoir/flyer/LWG assembly was supported over a base by two PVC slabs with screw tabs that did not interfere with the path of the flyer. In most experiments, the optical collimator for the laser beam was mounted within the support base, perpendicular to the initial position of the flyer surface, 115 mm downstream from the end of the LWG to ensure steady detonation propagation conditions. For select experiments where the flyer launch angle was substantial, additional collimators were mounted parallel to the initial position of the flyer surface and/or inclined nominally at 45° from the horizontal. Detonation velocity was measured for all tests using a set of 4 or 5 twisted wire pairs distributed along the length of one side of the charge. This was necessary to help characterize the explosive, ensure consistent detonation of the charge for heavily diluted explosives, and provide a means of correcting for tilt of the flyer plate during launch, as described in Section 2.6.

To mitigate non-uniformities in explosive loading resulting from product expansion off of the charge edges, the flyer was surrounded by a square ring of material of equal thickness to the flyer. The width of the ring was designed such that the portion of explosive subtracted via the trapezoid method did not encompass any of the explosive slab above the central flyer. The trapezoid method is a simple geometric technique for estimating the effective mass of explosive in systems with significant edge effects [4, 27]. It assumes that any mass of explosive outside a cone or trapezoid with a 60° base angle does not participate in the acceleration of the flyer and can be neglected.

In principle, the use of a segregated ring of material permits the central flyer to be accelerated uniformly while the mechanically decoupled ring lags behind and curves due to the uneven pressure loading. The flyer and ring were assembled via bonding all parts to a 0.25-mm-thick Mylar sheet with a very thin layer of epoxy. The Mylar sheet buffered the flyer plate from the explosive to prevent leakage through the joints. For very thin flyers (< 0.8 -mm-thick) the Mylar and metal ring were omitted and a single-piece flyer was used due to the parasitical mass of the adhesive and difficulties in assembling a flat flyer from very thin sheet segments. On the basis of experimental agreement for Gurney curve measurements using neat nitromethane, edge effect mitigation in the charge design was sufficient for the purposes of evaluating scaling effects.

2.4.2 Normal Detonation Charges

In order to initiate a planar detonation wave normally incident to the flyer plate, a slapper initiation system was used. A thinner flyer plate (referred to subsequently as the *slapper*) was explosively accelerated via grazing detonation and then used to impact-initiate a slab of heterogeneous test explosive. Detonation and expansion of the test explosive accelerated a primary flyer, whose acceleration and terminal velocity was measured with the PDV. An assembled test apparatus is shown in Fig. 2.4.

The slapper was epoxied into the bottom of a rectangular PVC frame that was machined with a 109 mm by 109 mm wide cavity for the explosive. One end of the frame was machined with a LWG in order to generate a planar, grazing detonation to launch the slapper. 90/10 NM/DETA was used to fill this LWG and propel the slapper. A 3.2-mm-thick clear PVC lid was cemented into place over the frame to confine the NM within the slapper frame. The slapper LWG was initiated by inserting the detonator through the fill tube into direct contact with the

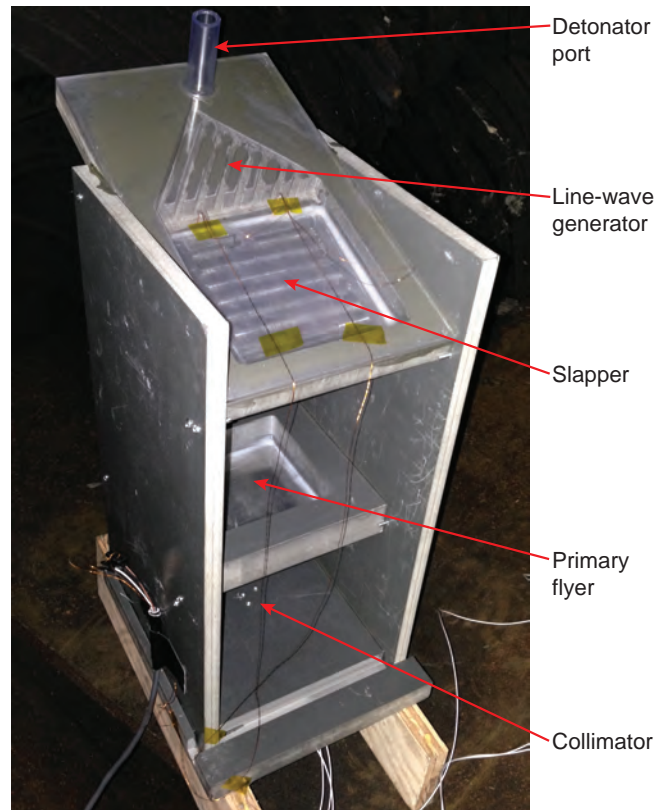


Figure 2.4: Charge assembly used for the normally incident detonation experiments [114].

NM. A shallow cylindrical pocket was machined into the LWG frame to centre the detonator once inserted.

The primary flyer was epoxied into the bottom of a second, 25-mm-deep square PVC frame containing a 95 mm by 95 mm pocket for the test explosive. The pocket was 24.1 mm deep after gluing in the flyer due to a presence of a small lip to center the primary flyer in the frame. The pocket was left uncovered and was filled to a uniform thickness by levelling the charge prior to an experiment.

The flyer cascade was formed by supporting the two frame assemblies on top of each other with screw tabs inserted into lateral PVC slabs that were then connected to a PVC support base. The slapper assembly was angled relative to the primary flyer assembly by the experimental Taylor angle of the particular slapper plate, based on results from a prior study [9]. The slapper assembly was also placed slightly forward relative to the centre of the test explosive reservoir to account for the non-normal orientation of the metal velocity vector during grazing launch of the slapper. Horizontal spacing between the two PVC frames was set to the minimum distance required for the slapper plate to reach terminal velocity based on velocimetry measurements of



Figure 2.5: Normally incident detonation experiment using the 0.25-mm-thick-slapper with the test explosive cavity filled with a mixture of gelled NM and 10% GMBs.

grazing detonation accelerations [9]. The PVC support base was drilled to house up to three optical collimators for redundant measurement of the primary flyer velocity.

Several configurations were used for the slapper. As the shock initiation behaviour of highly diluted nitromethane explosives has not been extensively studied [123], we initially opted for a very conservative design using a relatively thick, high-velocity slapper; a square, 3.2-mm-thick 6061-T6 aluminium plate with an edge length of 82.6 mm. It was surrounded by a set of aluminium strips of equal thickness with widths of 16 mm to reduce velocity deficits and plate bowing from expansion off the sides of the charge. Epoxy and a Mylar sheet were also used to assemble the strips around the flyer. Explosive loading of the slapper was designed such that the terminal slapper velocity resulted in a shock pressure equivalent to 80% of nitromethane's Chapman-Jouguet detonation pressure when striking neat nitromethane. This slapper was propelled to a terminal velocity of $2023 \text{ m} \cdot \text{s}^{-1}$ with a Taylor angle of 19.4° using a 15.4-mm-thick layer of sensitized NM [9]. Impact planarity of the 3.2-mm-thick slapper was $\lesssim 400 \text{ ns}$ as measured via shock pins [9, 114]. We thus initially opted for a very conservative design where

the slapper generated a relatively long pulse-width shock with a pressure sufficient to initiate detonation in neat NM with negligible shock-run distance.

While primary flyer velocity enhancement due to over-driving the detonation is likely limited, impact by the thick slapper still transfers significant momentum and energy to the system, and the slapper plate itself also acts as a tamper during expansion of the products. These velocity enhancement effects must be separated from the influence of the dense diluents and wave incidence angle effects.

Based on the successful initiation of all of the explosive mixtures using the thick 3.2 mm slapper, a subset of additional experiments were conducted where the thickness of the slapper plate and its explosive loading were halved. Preservation of the M/C ratio of the slapper system yielded a similar terminal velocity and Taylor angle, but slapper momentum was halved. This permitted a quantification of the velocity imparted to the primary flyer by the slapper, while still meeting a conservative initiation criteria. The momentum/energy contribution of this 1.6-mm-thick slapper was still deemed excessive for use in a series of experiments to measure the scaling of primary flyer velocity with the ratio M/C for two heterogeneous explosives. Momentum and energy transfer would be especially problematic for cases where the slapper mass greatly exceeds the primary flyer mass; leading to cascade-like velocity enhancement. For the purposes of scaling experiments, a very thin slapper system based around a 0.25-mm-thick aluminium plate was adapted from a previous study [17]. This slapper reservoir was 3.8 mm thick. The Mylar buffer and metal edge strips were omitted when assembling the 0.25 mm slapper into its reservoir.

The 0.25 mm slapper was propelled to a velocity of $3096 \text{ m} \cdot \text{s}^{-1}$ according to PDV measurements. Slapper impact planarity was measured to be $\lesssim 200 \text{ ns}$ by self-shorting twisted pair wires placed in a test explosive when inclined 30° from the horizontal [17]. In principle, an even thinner explosive layer could have been used (1–2 mm) to propel the slapper based on critical diameter considerations [124], however corner turning through the LWG, as well as the stiffness of the slapper frame were concerns. A charge configured with the 0.25-mm-thick slapper is shown in Figure 2.5.

2.5 Gurney Analysis

The Gurney model is a widely used set of analytic equations to predict the terminal velocity of material accelerated by explosives for a variety of simple charge geometries [3]. The model hinges on the assumptions that explosive energy is instantly converted into kinetic energy of the detonation products and that the detonation products expand with a linear velocity gradient and a uniform density. These assumptions permit closed-form integration of the conservation of energy and momentum equations for the system of detonation products and confining material. Integration yields equations that are a function of the ratio of confining material mass to explosive mass (M/C , N/C), the charge geometry, and an empirical fitting constant that defines the amount of thermochemical energy that is converted into kinetic energy for a specific mass of explosive.

Although Gurney initially derived metal velocity equations only for filled cylindrical and spherical bombs, subsequent work by Stern [33, 34], Thomas [32], and Henry [35] expanded the model to planar geometry and more complex cylindrical/spherical configurations. The Gurney equations are also well described in more accessible preceding literature, e.g., Kennedy [5, 10] and Jones [28]. In a prior paper, the authors validated the Gurney model for the planar, open-face sandwich geometry, and demonstrated that it is quite accurate (maximum error of <10%) [9]. A number of other validations exist, e.g., Hoskin [40], Butz [41], and Jacobs [39]. The Gurney equations are thus suitable for engineering estimates of flyer propulsion.

In the present context, we are considering how adding an inert diluent to a high explosive changes its ability to accelerate a confining material. The effect can be estimated by the Gurney model by including straightforward modifications detailed subsequently. Since the experiments considered an asymmetric sandwich geometry, the model is formulated for the case where the two confining layers move at independent velocities.

The conservation of momentum and energy equations can be modified to account for the participation of the diluent in partitioning these quantities as the detonation products expand and the two confining plates are accelerated. We follow the Lagrangian (material fixed) coordinate formulation described by Kennedy [10] to define the integration bounds. With the inclusion of

the inert diluent, the conservation of energy equation becomes:

$$CE = \frac{1}{2}MV_m^2 + \frac{1}{2}NV_n^2 + \frac{1}{2} \int_0^{\tau_e} V_g(y)^2 \rho_g \phi_g dy + \frac{1}{2} \int_0^{\tau_e} V_b(y)^2 \rho_b \phi_b dy \quad (2.1)$$

and the momentum equation becomes:

$$0 = -MV_m + NV_n + \int_0^{\tau_e} V_g(y) \rho_g \phi_g dy + \int_0^{\tau_e} V_b(y) \rho_b \phi_b dy \quad (2.2)$$

The linear gas velocity profile can be expressed in terms of the flyer and tamper velocities as:

$$V_g = \frac{y(V_m + V_n)}{\tau_e} - V_m \quad (2.3)$$

Here ρ_b is the solid density of the diluent, ρ_g is the density of the detonation products, ϕ_g is the volume fraction of detonation products, and ϕ_b is the volume fraction of diluent. C , M , and N are the masses of the high explosive phase, flyer plate, and tamper plate, respectively. Masses can be expressed either on an absolute basis or per unit area of the sandwich. E is the effective energy per unit mass of explosive. V_m is the terminal velocity of the flyer, and V_n is the terminal velocity of the tamper. V_g and V_b the velocities of the detonation product and diluent, respectively. τ_e is the thickness of the explosive charge, and is used as the upper integration bound for the Lagrangian coordinate, y .

The introduction of another set of unknowns, namely the velocity and the volume fraction/dispersion of the diluent in the detonation products at terminal conditions, requires additional assumptions to generate a closed-form solution. To remain consistent with the standard Gurney model, we assume that the diluent remains uniformly dispersed throughout the detonation products as they expand and that it does not slip relative to the detonation products. That is, the products and the diluent have the same velocities for a given Lagrangian position, or that $V_g = V_b$.

In this formulation, the density of the detonation products can be considered to be a constant because:

$$\rho_g \phi_g = \rho_e \phi_e = \frac{C}{\tau_e} \quad (2.4)$$

The Propulsive Capability of Explosives Heavily Loaded with Inert Materials

Here C is defined per unit area and ρ_e and ϕ_e are the density and initial volume fraction of the base explosive, respectively. Similarly, the density of the diluent and its volume fraction are constant when integrating from 0 to τ_e . These density/volume fraction terms can thus be moved outside of the integral and the energy and momentum equations then become:

$$2CE = MV_m^2 + NV_n^2 + \{\rho_e\phi_e + \rho_b(1 - \phi_e)\} \int_0^{\tau_e} \left(\frac{y(V_m + V_n)}{\tau_e} - V_m \right)^2 dy \quad (2.5)$$

and:

$$0 = -MV_m + NV_n + \{\rho_e\phi_e + \rho_b(1 - \phi_e)\} \int_0^{\tau_e} \left(\frac{y(V_m + V_n)}{\tau_e} - V_m \right) dy \quad (2.6)$$

The terms in the curly brackets can be simplified to:

$$\kappa\rho_e\phi_e = \kappa\frac{C}{\tau_e} \quad (2.7)$$

where:

$$\kappa = 1 + \frac{\rho_b}{\rho_e} \left(\frac{1 - \phi_e}{\phi_e} \right) \quad (2.8)$$

Integration and combination of the energy and momentum equations yields the following equation for the terminal velocity of the flyer:

$$\frac{V_m}{\sqrt{2E}} = \left\{ \left(\frac{N}{C} + \frac{\kappa}{3} \right) A^2 + \frac{\kappa}{3} (1 - A) + \frac{M}{C} \right\}^{-1/2} \quad (2.9)$$

where:

$$A = \frac{\kappa + 2\frac{M}{C}}{\kappa + 2\frac{N}{C}} \quad (2.10)$$

and:

$$V_n = AV_m \quad (2.11)$$

According to Rumchik, Kennedy proposed an alternative form of the Gurney equation to account for a mass of inert diluent by scaling the Gurney energy of the explosive [1], thus:

$$\frac{V_m}{\sqrt{2E(1-w_b)}} = f\left(\frac{M}{C'}, \frac{N}{C'}\right) \quad (2.12)$$

where f is a scaling function for the geometry in question, w_b is the mass fraction of diluent, and C' is the total mass of the mixture, including both the high explosive and the diluent. For the asymmetric explosive sandwich, the flyer velocity can be estimated by:

$$V_m = \sqrt{2E(1-w_b)} \left\{ \frac{1+A'^3}{3+3A'} + \frac{N}{C'} A'^2 + \frac{M}{C'} \right\}^{-1/2} \quad (2.13)$$

with:

$$A' = \frac{1 + 2\frac{M}{C'}}{1 + 2\frac{N}{C'}} \quad (2.14)$$

Notably, (2.9) and (2.13) are equivalent for a given explosive/inert admixture provided that the correct mass is used: either the mass of just the explosive phase for (2.9), or the total mixture mass for (2.13). These equations are referred to as the *augmented Gurney model* throughout the rest of the paper.

In modifying the Gurney model, it was assumed that the diluent retains the same velocity profile as the detonation products throughout the expansion process. If the base explosive and diluent are miscible liquids of similar densities this is likely a very good assumption since mixing occurs at the molecular level and both components will decompose into gasses. Similarly, fine, low-density solid particulate will rapidly get dragged to near the velocity of the detonation products. However, if the particles are heavy due to their size and/or solid density, they will slip and experience drag not only through the detonation process but also as the detonation products expand. A priori, the assumption of equivalent velocity distributions in the derived model, even at large product expansions, is not fully rigorous. Similarly, the degree of slip is likely to be influenced by particle size for a given material density.

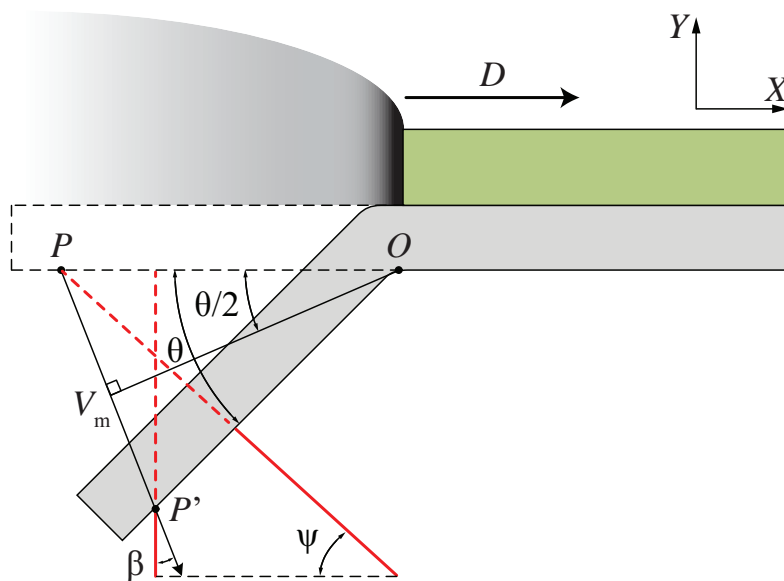


Figure 2.6: Vector decomposition for a flyer being launched via grazing detonation. The orientation of the PDV probe beams are indicated in red lines relative to the rotation of the flyer and the inclination of the metal velocity vector.

2.6 PDV Tilt Correction

When a flyer is launched via a detonation that grazes along its surface, it is flung at an angle, θ , from its initial position. The terminal metal velocity vector, V_m , contains components that are downwards (lateral) and forwards (longitudinal) relative to the flyer's initial position.

In all experiments the primary, PDV collimator was oriented initially normal to the initial surface of the flyer. Since PDV measures only the material velocity oriented along the path of the laser beam, a collimator viewing the flyer normally only measured the downward component of the total metal velocity of the flyer [72–74]. For flyers with large tilt angles, a secondary collimator was mounted inclined at some angle, ψ , from the horizontal of the charge base. This collimator also measured only a component of the total metal velocity vector as the beam was never aligned with the velocity vector. Consequently, the PDV velocities had to be tilt-corrected in order to extract the true terminal velocity as calculated by the Gurney model.

Tilt correction was accomplished by using the Taylor model for relating the inclination angle of the flyer to the total terminal velocity of the flyer [5, 21]. Figure 2.6 depicts the launch of a flyer by a grazing detonation propagating at velocity, D , with a terminal inclination (Taylor) angle, θ , relative to two PDV laser beams. The Taylor model establishes that the metal velocity vector is inclined forward relative to the normal of the stationary flyer surface by half of the

flyer inclination angle. The angle θ is related to the detonation velocity and the metal velocity via the well-established equation:

$$V_m = 2D \sin\left(\frac{\theta}{2}\right) \quad (2.15)$$

Although Taylor's original paper can be difficult to obtain [21] re-derivation of (2.15) has been presented by several sources, including Dehn [29] and Kennedy [5]. The present authors also derived Taylor's expression in a preceding paper [9], and evaluated the relationship between the velocity measured by the normal PDV probe, V_{pdv} , and the total metal vector based on the cylinder test analysis presented by Souers [22]:

$$V_{\text{PDV}} = V_m \cos \beta \quad (2.16)$$

Where $\beta = \theta/2$. In a similar manner, the relationship between the velocity measured by the inclined probe, V_{ang} , can be related to the total metal velocity vector by:

$$V_{\text{ang}} = V_m \sin(\psi + \beta) \quad (2.17)$$

In the prior study, both the Taylor formula and the relationship between the normal PDV velocity and the total metal velocity were validated in flyer plate experiments with sensitized nitromethane [9]. Orthogonal PDV probe measurements were used to determine the total metal velocity magnitude and direction independent of any assumptions of the Taylor model. Agreement between the Taylor model and orthogonal measurements was within 5° , with typical errors of no more than 2° .

Consequently, direct use of the Taylor model in the present context is sufficiently accurate to tilt-correct the collected PDV data. For experiments with small Taylor angles, the normal PDV probe terminal velocity was corrected via simultaneous solution of (2.15) and (2.16) since the detonation velocity was measured in all experiments. For flyers with large Taylor angles, an angled probe was included and the total metal velocity was determined by simultaneous solution of (2.16) and (2.17). We note that the velocity correction is small to the point of being almost negligible unless the Taylor angle is very large because the correction factor is cosine of the half-angle. For a Taylor angle of 30° the true metal velocity is only 4% greater.

A more problematic consequence of the way PDV measures flyer velocity is that if a flyer has an appreciable forward velocity, new metal that was launched at an earlier time enters the collimator beam spot as the flyer moves forward. By consequence, a probe observing normally relative to the initial flyer position will measure an acceleration that is faster than the true acceleration of a metal element at a fixed longitudinal position along the flyer. This complicates hydrocode simulation of the full acceleration process but poses no issue for a Gurney analysis of the terminal flyer velocity since flyer motion is steady state at this point.

This effect is rarely discussed in detonation product equation of state modelling since CYLEX experiments typically involve shallow wall angles ($< 15^\circ$), and thus inclining the laterally observing probe by $\approx 7^\circ$ measures nearly the true metal acceleration/velocity with sufficient accuracy compared to other experimental errors. Alternatively, Jackson added a ramp-velocity term to account for forward cylinder motion past a normally-observing PDV probe [62, 63]. For the purposes of modelling thin flyers with large tilt angles, either the probe data must be corrected for translation of the flyer past the probe spot, or model data must be extracted at a lab-fixed position where the laser spot interacts with the flyer surface.

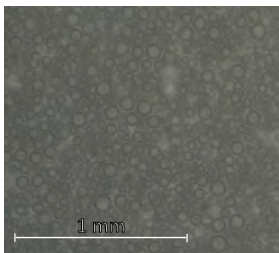
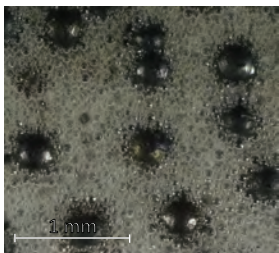
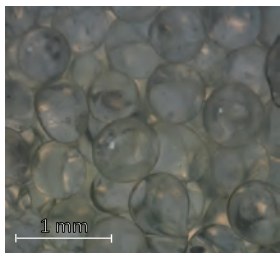
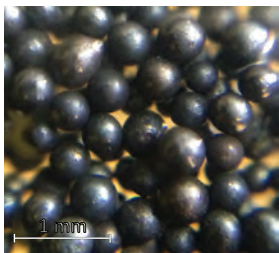
2.7 Explosives Studied

The present study considered four different heterogeneous explosive admixtures containing inert particle inclusions, along with a control consisting of a neat liquid explosive described in a prior study [9]. The heterogeneous systems consisted of: 1) packed beds of solid particles saturated with liquid nitromethane, 2) poly(methyl methacrylate)-gelled nitromethane with suspended glass microballoons, 3) gelled nitromethane with microballoons and steel particles, and 4) C-4 mixed with varying fractions of steel or glass particles. The preparatory techniques and compositions of the explosive admixtures are detailed in this section. Table 2.1 shows micrographs of the nitromethane-based explosives considered in the present study and lists the achievable range of mass/volume fractions for each mixture type.

2.7.1 Neat Sensitized Nitromethane

As a control explosive without particulate inclusions, nitromethane (NM, Sigma Aldrich 108170, reagent grade, 96%) sensitized with 10% by mass of the amine diethylenetriamine

Table 2.1: Description of the nitromethane-based heterogeneous explosives considered in the present study.

Gelled NM with GMBs	Gelled NM with GMBs + Steel Beads	Liquid NM with Glass Beads	Liquid NM with Steel Beads
 <ul style="list-style-type: none"> • suspension of particles • 18.3–55.5% particle vol. frac. • 2.5–12.5% particle mass frac. 	 <ul style="list-style-type: none"> • particle suspension with contact • 56.2–72.8% particle vol. frac. • 30.0–91.3% particle mass frac. 	 <ul style="list-style-type: none"> • bed of close-packed particles • 61% particle vol. frac. • 78% particle mass frac. 	 <ul style="list-style-type: none"> • bed of close-packed particles • 60% particle vol. frac. • 91% particle mass frac.

(DETA, Sigma Aldrich, D93856, 99%) was used. The flyer plate launching capability of 90/10 NM/DETA was previously characterized by the authors [9] and the results are reviewed subsequently in Section 2.8.1. The addition of an amine to NM sensitizes the mixture via an auto-catalytic reaction leading to intermediate NM anions [125]. Amine sensitization also reduces the influence of characteristic failure waves emanating from casing expansion compared to equivalent neat NM experiments [126].

Nitromethane with excess DETA addition (27.5% and 45% by mass) was also used in the present study to examine the effect of inert dilution in a uniform explosive. The sensitizing effect of DETA reaches a maximum at approximately 10% by mass [124]. On the basis of an increase in explosive critical diameter for detonation failure and a reduction in the mixture oxygen balance for mixtures containing greater than 10% DETA, it can be inferred that a portion of this excess DETA is behaving as an inert diluent. However, the extent of thermochemical involvement of the excess DETA is not obvious a priori since the amine will also decompose and may recombine with the decomposed NM.

The use of DETA as a diluent is attractive compared to other alternatives (alcohols, acetone) because the initial sensitization keeps the critical diameter reasonably low and the two liquids

are readily miscible. The effect on flyer launch capability of the DETA-diluted explosive will be compared to the same equivalent charge of NM (without excess DETA) in this study.

2.7.2 Gelled Nitromethane Suspensions of Glass Microballoons and Particles

In order to suspend particles such that particle loading could be varied independently, which was not possible with the packed beds subsequently discussed in 2.7.3, NM gelled with poly(methyl methacrylate) (PMMA) was used for the neat explosive component in a subset of experiments. The NM (Sigma Aldrich 108170 or 360554) was gelled via the addition of 4% mass fraction of large (1 cm^3) chunks of PMMA (cast, optically-clear acrylic, McMaster-Carr P/N 8560K266, Series 8560K999). The mixture was then gently tumbled on a roller mill for several weeks while the PMMA dissolved. The resulting 96/4 NM/PMMA gel has a consistency similar to syrup or honey. DETA was not used in these mixtures. We emphasize that the use of large pieces of cast (not extruded) PMMA is essential to obtain a high viscosity gel; use of PMMA powder (as obtained from a chemical supplier, for example) gels more quickly but does not result in as great a final viscosity.

The PMMA gelling permits glass microballoons (GMBs, 3M K1) to be held in suspension in the nitromethane for a period of many hours. The K1 GMBs have a true density of $0.125\text{ g} \cdot \text{cm}^{-3}$ and a mean diameter of $65\text{ }\mu\text{m}$. The GMBs physically sensitize the gelled nitromethane to detonation. However, the addition of large volume fractions of GMBs heavily dilutes the explosive, greatly reducing the fraction of energetic material in the mixture and its density. This decreases the detonation energy, velocity, and pressure of the explosive as more GMBs are added. Consequently, while the explosive mixture remains sensitive, it becomes less energetic.

Sensitization via GMB addition is mechanistically different than sensitization via amine addition. Amines make the NM decompose more readily via the autocatalytic formation of intermediate anions [126]. GMBs sensitize the nitromethane by introducing hot spot sites, as the collapse of a balloon under shock wave loading generates intense, localized heating. These hot spots lead to thermal initiation of the NM. Detonation behaviour and critical diameter scaling of GMB-sensitized, gelled nitromethane has been extensively studied by Presles, Gois, and co-

workers [87–89, 127–132]. Highly dispersed GMBs result in a non-ideal detonation governed by failure wave propagation and hot spot driven re-initiation. Experimental evidence of wave propagation on witness plates and non-hydrodynamic scaling of critical-diameter to critical-thickness has been presented in the preceding literature [93, 133]. These non-idealities are not expected to influence flyer plate launching behaviour as detonation-scale heterogeneous effects do not directly influence adiabatic expansion of the detonation products unless the reaction tail is substantially extended.

This low-density explosive enables shockless loading of the flyer plate in the case of grazing detonation as GMB dilution typically reduces the detonation velocity to well below the sound speed of most metals. When the detonation front arrived normal to the flyer surface, the low-density and low detonation pressure of the explosive permitted flyer launch without complete spallation. Note that normally incident detonations of neat liquid nitromethane or typical military explosives in contact with the flyer will cause the spallation of a complete free surface, making it difficult to define the flyer velocity. Thus, a series of flyer plate tests with both normal and grazing detonations were conducted wherein the mass fraction of GMBs was varied to 2.5%, 7.5%, 10%, and 12.5%.

Mixtures were prepared by adding the required mass of GMBs to a known mass of gel and then gently mixing via a slow roller mill overnight to ensure uniform dispersion of the GMBs. While the 2.5% and 7.5% mixtures retain reasonable viscosity, and the 10% mixture is pourable with some difficulty, the 12.5% mixture is quite thick, with a texture similar to melted marshmallow. Consequently, for the grazing experiments this mixture was loaded into an open charge casing with the aid of utensils and then the PVC lid was affixed. A grazing charge filled with a gelled NM mixture containing 7.5% GMBs by mass is depicted in Fig. 2.7a.

Gelled Nitromethane with Glass Microballoons and Steel Particles

Because of the thickening effect of substantial GMB addition, the NM-PMMA/GMB admixture can suspend dispersed, high-density particles. Increasing mass fractions of 280 μm diameter steel particles (SAE J444/J827 standard S-110 steel shot) were added to a mixture of 87.5/12.5 NM-PMMA/GMBs by mass. The mixture was prepared by first adding the 12.5% mass fraction of GMBs to the gel and then roller milling until the balloons were fully dispersed. Next, the steel particles were added and thoroughly mixed in by hand with a mixing paddle until complete

dispersion was visually ascertained. Experiments were conducted with mixtures containing 20%, 50%, and 90% mass fraction of steel, relative to the total mixture mass.

2.7.3 Packed Particle Beds Saturated with Sensitized Nitromethane

A packed bed with particles in direct, jamming contact with each other results in an approximately constant volume fraction of particles as the particle size and material is varied. Packed beds of various materials were saturated with 90/10 NM/DETA (the same mixture as in 2.7.1), prepared immediately prior to the experiment. NM has a low surface tension ($36.53 \text{ mN} \cdot \text{m}^{-1}$ at 25°C) and low viscosity ($0.630 \text{ mPa} \cdot \text{s}$ at 25°C), and thus easily filled the interstitial spaces of the pack bed [134]. The resulting saturated packed bed mixtures were thus mostly inert material by volume ($\approx 60\%$) and overwhelmingly inert material by mass ($>70\%$). The detonation properties of packed particle beds saturated with sensitized NM have been extensively studied [90, 91, 135], as have the dispersal of particles in the detonation product flow and resulting blast loading [18, 105].

Detonation behaviour of these mixtures is determined by the net deficit in available energy due to volumetric replacement of the high explosive by particles, non-equilibrium energy transfer to the particles during detonation, and the possibility of local detonation failure between particles as described in prior literature [12, 86, 101–104]. Despite the reduction in detonation energy, nitromethane-particle admixtures typically have lower critical diameters than neat nitromethane due to hot spot formation as the shock interacts with the particles. Further, Lee identified two propagation regimes depending on whether the detonation is transmitted through small particles or if the detonation percolates through the particle bed via detonation wavelet diffraction around large particles [90, 91]. In the present study, we examine how non-equilibrium between the detonation product and diluent phases extends to the intermediate expansion of the detonation products.

For the packed bed experiments, the charge was loaded with explosive mixture by initially filling a portion of the charge with sensitized NM and then adding particles that settled into the liquid until a slurry-like state was reached. The addition of more liquid or particles was alternated until the charge volume was completely filled. Any excess liquid was then siphoned off before the experiment. This was done to ensure that no air was trapped in the packed bed. A consistent explosive loading was maintained by agitating the particle bed during settling,

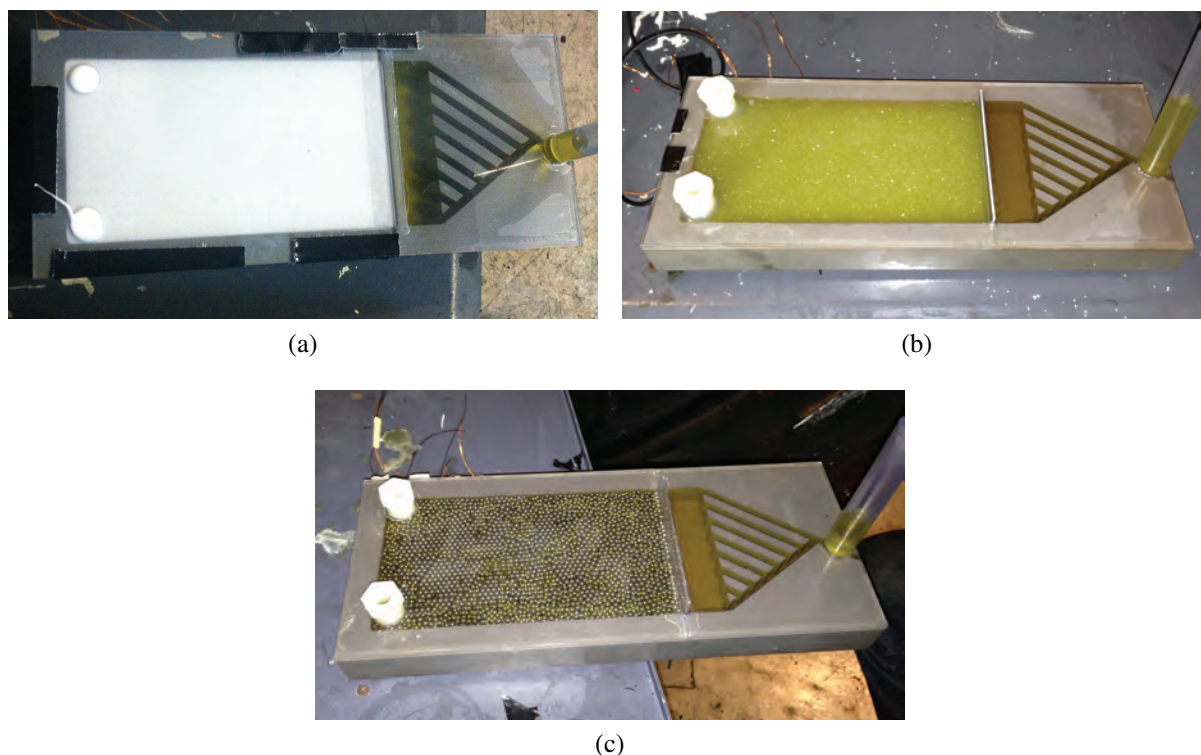


Figure 2.7: Charges loaded with: **(a)** Gelled nitromethane mixture containing 7.5% GMBs by mass. **(b)** Packed bed of 725 μm average diameter glass particles saturated with 90/10 NM/DETA. **(c)** Packed bed of 3 mm diameter steel particles saturated with 90/10 NM/DETA.

thereby ensuring the particle bed approached the packing limit. For the grazing experiments, the fully enclosed nature of the charge allowed precise control of the charge volume. For the normal detonation experiments, the test explosive cavity was levelled via bubble level and then slowly filled with mixture until a meniscus was formed at the top surface of the mixture.

Three particle materials were considered: glass ($\rho = 2.5 \text{ g} \cdot \text{cm}^{-3}$), steel ($\rho = 7.9 \text{ g} \cdot \text{cm}^{-3}$), and tungsten ($\rho = 18.5 \text{ g} \cdot \text{cm}^{-3}$). The solid density of the packed bed material was thus varied by nearly an order of magnitude. Three different particle sizes were considered for steel (280 μm , 432 μm , and 3 mm diameters) and two for glass (120 μm and 725 μm diameters). Thus, particle size was also varied by an order of magnitude. The 3 mm steel particles were 010–1020 grade steel balls (McMaster-Carr P/N 96455K49). The smaller glass and steel particles were standard blasting/peening media. The 280 μm and 432 μm steel particles were SAE J444 standard, S-110 and S-170 cast steel shot. MIL-PRF-9954C standard, Potters Ballotini Beads were used for the glass particles. The 725 μm glass particles were Potters #3 beads (US sieve 20–30, 850 μm max. diameter, 600 μm min. diameter). The 120 μm glass particles were Potters #10 beads (US sieve

The Propulsive Capability of Explosives Heavily Loaded with Inert Materials

100-170, 150 μm max. diameter, 90 μm min. diameter). The tungsten powder used had a wide size distribution and included a large population of $< 10 \mu\text{m}$ particles that prevented complete settling, resulting in a lower packing fraction and larger explosive mass for the fixed charge volume compared to the other particles used. A charge filled with the sensitized-NM-saturated 725 μm glass beads is shown in Fig. 2.7b. A charge filled with 3 mm steel beads and sensitized NM is shown in Fig. 2.7c.

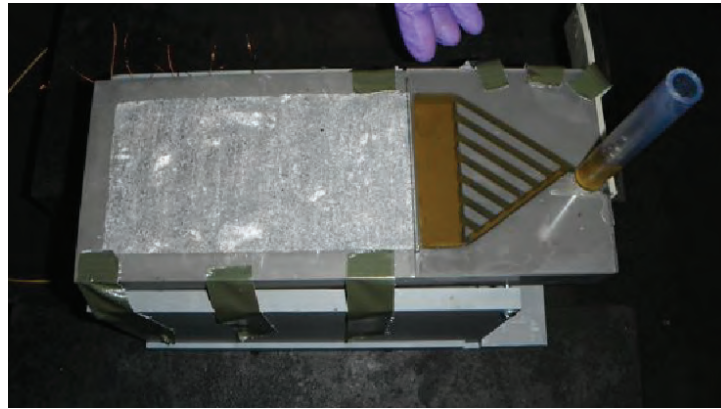
The properties of the packed bed explosives used in the experiments are reported along with the experimental results in Table 2.5 of Section 2.8.4. Most beds using the blasting media had similar packing fractions, generating a typical variation in explosive mass of no more than 10 g with an average of 180 g in grazing experiments using the 24.1 mm reservoir. However, the particle morphology of the Tungsten powder resulted in a low particle loading (55% vol. frac. versus 60% vol. frac.) compared to the blasting media. Similar reproducibility and packing fractions were observed for the normal detonation experiments conducted with saturated blasting media.

2.7.4 C-4 with Dispersed Steel or Glass Particles

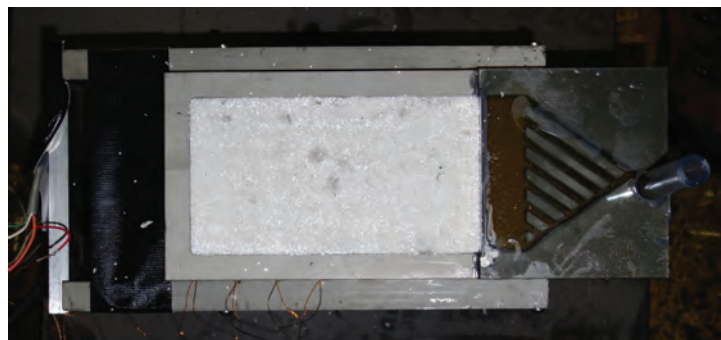
Experiments were also conducted with mixtures of C-4 with varying mass fractions of dispersed steel or glass particles. C-4 is an RDX (cyclotrimethylenetrinitramine)-based explosive with approximately 90% mass of RDX and the balance being plasticizer, binder, and some form of oil. The exact composition is usually not available from the supplier, and this was the case with the current study. C-4 is also known to have batch-to-batch variations in formulation and properties, but all C-4 used in the present study came from the same batch. C-4 has a relatively high Gurney energy, and is a high detonation pressure explosive, in contrast to the nitromethane-based explosives used throughout the rest of this study.

The use of a plastic explosive permitted the dispersion of a wide range of particle loadings, irrespective of particle solid density, without having to add non-energetic material to thicken the mixture. The dilution of a standard, crystalline-explosive based composition is also interesting for comparison to the liquid and gel systems studied in parallel.

Starting with the C-4 base explosive, 280 μm mean size steel particles (SAE J444/J827 standard S-110 steel shot), or 725 μm mean size glass particles (MIL-PRF-9954C standard Potters Ballotini #3 glass beads), were mixed in to a maximum of 80% mass fraction of steel or 60%



(a)



(b)

Figure 2.8: Grazing charges loaded with: **(a)** A mixture of 80/20 Steel/C-4 by mass. **(b)** A mixture of 60/40 Glass/C-4 by mass.

mass fraction of glass. In order to disperse the particles uniformly throughout the explosive, the C-4 was finely divided and placed into zipper storage bags along with a portion of the requisite mass of particles. The particles were then worked into the C-4 by hand against a flat surface. After mixing, the divided explosive mixture was recombined and pressed into the charge casing using a plastic putty knife and a wooden roller. Although the dispersion was relatively uniform, portions of unmixed explosive remained for the largest particle loadings; this is especially visible for the C-4/steel admixtures due to the colouration of the steel particles. However, the unmixed explosive represented a small fraction of the overall mixture and thus did not significantly alter the results. Standardized BAM (Bundesanstalt für Materialforschung und-prüfung) friction tests on mixtures with intermediate loadings were conducted and the explosive was not sensitized to a dangerous degree by the particle inclusions.

Photographs of charges loaded with 80/20 steel/C-4 admixture and 60/40 glass/C-4 admixture by mass are shown in Figs. 2.8a and 2.8b respectively after the wave-shapers were filled

with sensitized nitromethane. Note the small portions of unmixed explosive that are visible on the surface of the C-4/steel mixture. The PVC lid was omitted in all C-4 experiments and levelling of the free surface of the charge was accomplished via careful packing of the explosive up to the lip of the PVC casing with the roller.

Several challenges arose during the mixing and testing of these admixtures. The addition of particles at varying loadings had a non-monotonic effect on the packing density of the explosive phase despite careful pressing of the admixture into the charge. Likewise, large loadings of particles caused some breakdown of the binder, further modifying the consistency of the explosive phase. The texture of the admixture changed from the familiar sticky dough texture of neat C-4 to a texture akin to wet sand when the volume fraction of particle additive exceeded 30%. It was not possible to reach packed bed conditions as the explosive became too crumbly to effectively pack and there were concerns about the ability to detonate the admixture. The experimental effects of these non-idealities are subsequently discussed in Section [2.8.5](#).

2.8 Experimental Results and Discussion

In this section we compare experimental terminal velocities with predictions of the standard and augmented Gurney models. We were interested in studying four primary variations: 1) how acceleration ability (AA) changes as larger volume fractions of diluent are added to the explosive, 2) how AA varies as the density of the diluent is increased for a given diluent volume fraction, 3) the scaling of AA with flyer-mass to charge-mass for a diluted explosive versus the neat explosive, and 4) differences in AA for grazing detonation versus normal detonation loading.

Variations in flyer velocity with increasing dilution were plotted using the volume fraction of the high explosive phase in the mixture (ϕ_e). This permits a direct comparison of the effect of diluent density on the change in AA for a given degree of dilution. That is to say, comparing on a volume-fraction basis demonstrates the effect of changing the density of the diluent while the mass of high explosive in the charge remains fixed.

To analyse the scaling of flyer velocity with the ratio of flyer mass to charge mass, results were always plotted in terms of the mass of high explosive, C , contained in the mixture relative to the mass, M , of the flyer. This was done so that scaling results for the diluted explosive

could be directly compared with equivalent experiments at the same M/C ratios using the neat explosive. For some mixtures it was more convenient to use (2.13) to estimate flyer velocity; for example if multiple diluents with different densities are present. In this case, the total mass of the mixture (C') is used in calculating the flyer velocity as a function of M/C' . To compare these results with an equivalent loading of the neat explosive we need only calculate the value of M/C since $C = C'(1 - w_b)$.

2.8.1 Homogeneous Sensitized Nitromethane Data

The Gurney curves for neat 90/10 NM/DETA were determined from PDV measurements over multiple experiments and are reported in detail in a prior study by the authors [9]. The tamped and untamped curves (solid green and solid red lines respectively) and experimental data are replotted in Fig. 2.9 as they are useful to compare with the experimental measurements of the Gurney curve for packed beds of steel particles saturated with 90/10 NM/DETA (Section 2.8.4).

As the flyer-to-explosive mass ratio was varied from $M/C = 4.65$ to $M/C = 0.03$ (more than two orders of magnitude), the observed flyer velocity was found to match the predictions of the standard Gurney model extremely well, in most cases within 5% of the predicted value. Increasing deviations away from the Gurney prediction were only observed when the flyer became extremely thin (0.3 mm) in comparison to the explosive charge (24.1 mm thick). Even under these conditions, however, the agreement with the standard Gurney model was within 10%.

2.8.2 DETA Dilution of Nitromethane

A set of three experiments were conducted to measure the effect of DETA addition on the propulsive capability of liquid nitromethane. In all three experiments, a flyer thickness of 6.35 mm was used. Mixtures with mass fractions of 10%, 27.5%, and 45% DETA were tested. While DETA participates chemically in the decomposition of NM during detonation, and will decompose into gaseous products itself, it remains a net energetic sink relative to the explosive phase. The normally oriented PDV velocity histories for all three experiments are shown in Fig. 2.10.

A monotonic decrement in flyer velocity and detonation velocity was observed with increasing quantities of DETA, as expected. For the flyer propelled by the mixture containing 10% of

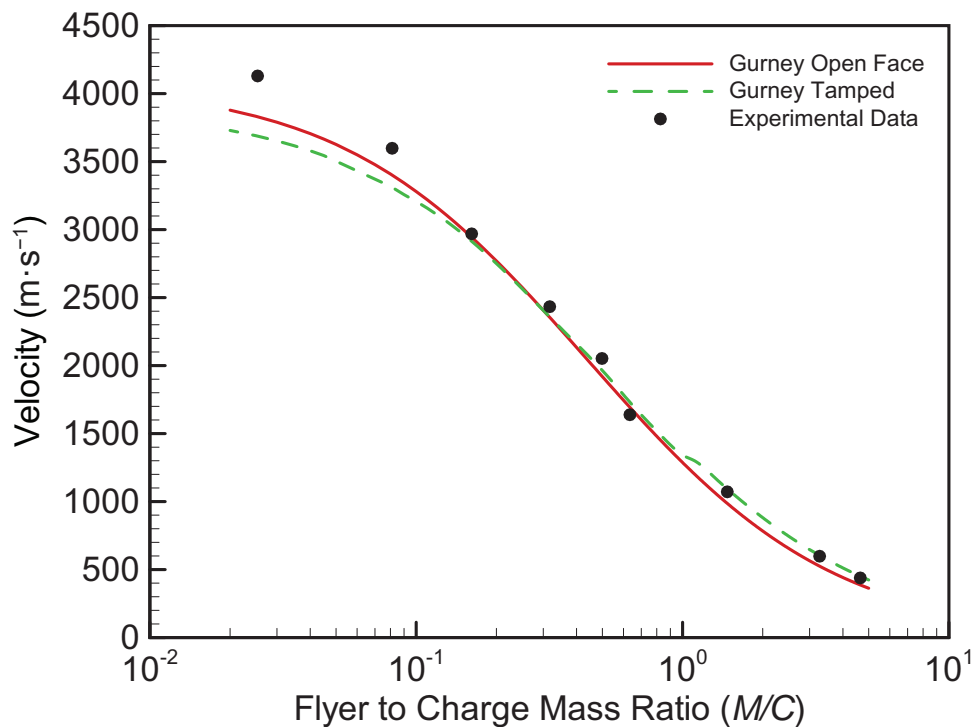


Figure 2.9: Experimental terminal velocities plotted against asymmetric sandwich and untamped Gurney curves [9].

Table 2.2: Summary of conditions for DETA dilution experiments. A Gurney velocity of $2310 \text{ m} \cdot \text{s}^{-1}$ was used to fit the augmented model.

w_{DETA} (%)	ϕ_e	ρ_{mix} ($\text{g} \cdot \text{cm}^{-3}$)	D ($\text{m} \cdot \text{s}^{-1}$)	θ (°)	$\frac{M}{C'}$	V_m ($\text{m} \cdot \text{s}^{-1}$)	V_{Gur} ($\text{m} \cdot \text{s}^{-1}$)	V_{Cooper} ($\text{m} \cdot \text{s}^{-1}$)	V_{Koch} ($\text{m} \cdot \text{s}^{-1}$)	Error: V_m vs. V_{Gur} (%)
10.0	0.88	1.14	6145	15.32	0.63	1638	1622	1532	1476	0.99
27.5	0.68	1.10	5693	14.60	0.65	1447	1429	1394	1343	1.20
45.0	0.50	1.06	5201	13.16	0.67	1192	1223	1252	1206	2.66

DETA, a shock breakout of $\approx 512 \text{ m} \cdot \text{s}^{-1}$ and a small rarefaction pullback were observed at the flyer free surface. For the experiment containing 27.5% DETA a small breakout of $\approx 283 \text{ m} \cdot \text{s}^{-1}$ was observed and rarefaction pull-back was suppressed. No shock breakout was obtained for the 45% DETA mixture.

Table 2.2 reports the densities, detonation velocities, experimental Taylor angles, flyer-mass to mixture-mass ratios (M/C'), and the terminal velocities obtained in the experiments versus predictions of the augmented Gurney model. Mixture densities were obtained using the Cheetah 2.0 thermochemical code. To generate an adequate fit to the data, a value of $2310 \text{ m} \cdot \text{s}^{-1}$ was used for the Gurney velocity ($\sqrt{2E}$) of neat nitromethane, a value lower than reported by Dobratz [25] ($2410 \text{ m} \cdot \text{s}^{-1}$) and by the authors for the Gurney curve for 90/10 NM/DETA

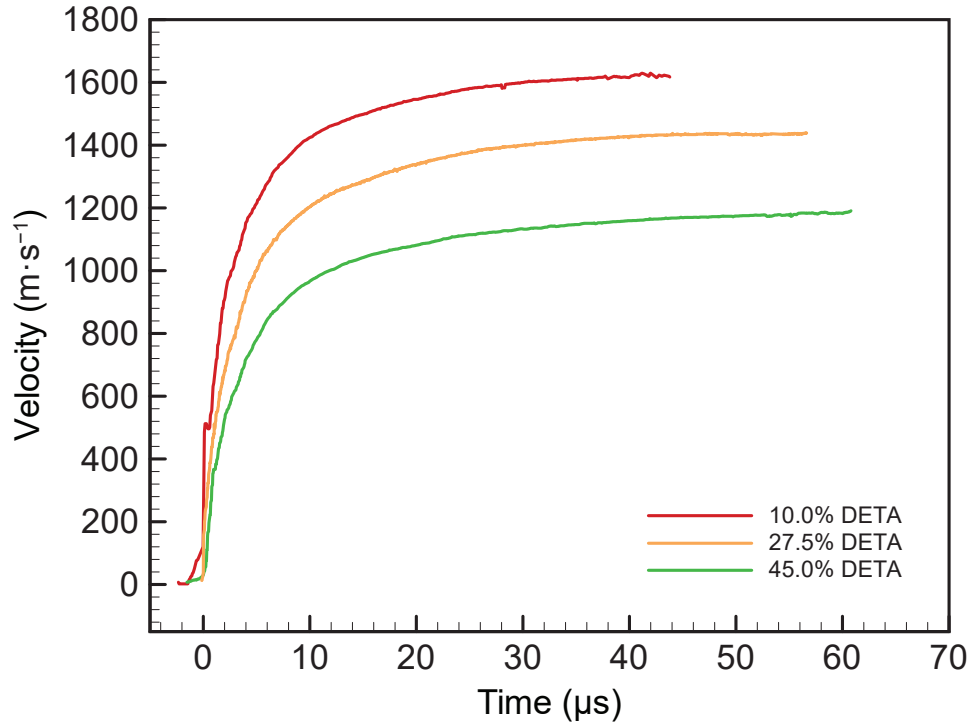


Figure 2.10: Velocity histories of 6.35-mm-thick aluminium flyers propelled by 24-mm-thick layers of nitromethane with various mass fractions of DETA addition.

($2477 \text{ m} \cdot \text{s}^{-1}$ neat, $2350 \text{ m} \cdot \text{s}^{-1}$ with sensitization) [9]. Overall error is quite low (<5%) using this lower Gurney velocity; errors between the experiments and the augmented Gurney model are listed in far right column of Table 2.2.

Flyer velocities normalized by the selected Gurney energy for the three experiments are plotted as solid symbols in Fig. 2.11 as a function of NM volume fraction (ϕ_e); the augmented model is plotted as a solid line. One explanation for the lower effective NM Gurney energy is that decomposition of the DETA diverts additional energy from the detonation products compared to a solid or chemically inert diluent, which is only heated and dragged aerodynamically.

Alternatively since these mixtures are approximately homogeneous liquids, mixture Gurney velocity can be estimated from mixture detonation velocity via one of several proposed empirical fits. For example, Cooper suggests the simple relation [4]:

$$\sqrt{2E} = 0.337D \quad (2.18)$$

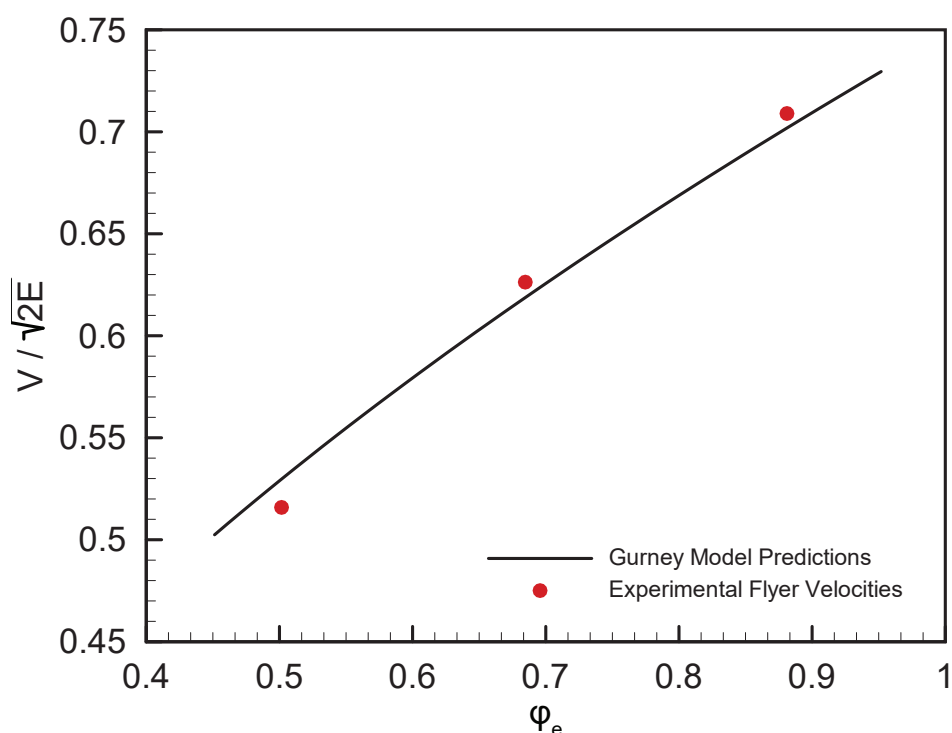


Figure 2.11: Normalized 6.35-mm-thick flyer terminal velocities as a function of NM vol. frac. for mixtures containing varying quantities of DETA. Data points (symbols) are compared to the augmented Gurney model (2.9) using a Gurney velocity of $2310 \text{ m} \cdot \text{s}^{-1}$ for NM.

Similarly, Koch proposed the following linear fit based on the detonation energy of the high explosive and an adiabatic expansion of the detonation products [136]:

$$\sqrt{2E} = \frac{D}{3.08} \quad (2.19)$$

Table 2.2 lists the predictions for flyer terminal velocity using these two correlations for Gurney velocity, based on the measured detonation velocities of the mixtures. Agreement is quite good for the heavily diluted mixture using either fit, however they under-predict flyer velocity for experiments with lower mass fractions of DETA. Effectively both linear fits fail to match the slope of the nearly linear variation of flyer velocity with explosive dilution. In the present context, decrementing a known Gurney energy for the base explosive by the degree of dilution is thus a better method for engineering estimates of flyer velocity than fitting based on detonation velocity.

A third approach is to estimate the Gurney velocity of the mixtures via JWL parameters determined by Cheetah 2.0, following the method proposed by Miller and Alexander [75]. In

principle, an accurate thermochemical calculation of the detonation energy as well as an accurate approximation of the detonation product adiabat would provide an accurate estimate of flyer propulsion, including losses to decomposition of the DETA. However, Cheetah 2.0 poorly predicted the JWL parameters for neat NM relative to other literature sources (e.g., Dobratz [25]), resulting in over-predicted flyer velocities in hydrocode simulations. For calculations of mixtures with large fractions of DETA, Cheetah 2.0 substantially over-predicted the mixture detonation velocities and erroneously predicted an increase in D for the mixture containing 45% DETA relative to the mixture containing 27.5% DETA. Similarly, Cheetah 2.0 JWL parameters result in anomalously high estimates of mixture Gurney velocity, as well as a non-monotonic propulsive capability.

Given predictive accuracy of the diluent approximation, the assumption that additional DETA beyond the point of maximum sensitization acts as an inert material is validated. Likewise, since there is only a small overprediction in velocity for the extreme of dilution tested, it is unlikely that decomposition of the DETA is a significant factor affecting flyer terminal velocity. Liquid explosive mixtures are also a best-case for the augmented model. In the case of a uniform liquid mixture, the entire mixture will decompose into largely gaseous products with some solid carbon phases, resulting in an effectively uniform flow without slip between heterogeneous phases.

2.8.3 Results with Gelled Nitromethane with Microballoons

In this subset of experiments, three effects were studied. First, we considered how increasing the mass fraction of low-density inclusions influenced the AA of gelled nitromethane. Second, we added increasing mass fractions of steel inclusions to a fixed composition of gelled NM/GMBs and examined how flyer velocity was decremented. Finally, we examined the scaling of flyer velocity with the M/C ratio for both grazing and normally incident detonations for a fixed mass fraction of GMBs.

Effect of Microballoon and Dense Inert Additive Dilution on Gelled Nitromethane

Figure 2.12 shows the velocity histories for all gel dilution experiments: mixtures containing 2.5% (18% vol. frac.), 7.5% (41% vol. frac.), and 12.5% (55% vol. frac.) mass fraction of

The Propulsive Capability of Explosives Heavily Loaded with Inert Materials

Table 2.3: Summary of mixtures and test conditions for experiments examining the influence of GMB and steel dilution on the propulsive capability of gelled nitromethane. A Gurney velocity of $1925 \text{ m} \cdot \text{s}^{-1}$ was used for the explosive phase of the steel and GMB mixture, while a Gurney velocity of $2300 \text{ m} \cdot \text{s}^{-1}$ was used for the explosive phase of the GMB-only mixture.

w (%) (gel / GMB / steel)	ϕ (%) (gel / GMB / steel)	ρ_{mix} ($\text{g} \cdot \text{cm}^{-3}$)	D ($\text{m} \cdot \text{s}^{-1}$)	θ ($^{\circ}$)	$\frac{M}{C'}$	V_m ($\text{m} \cdot \text{s}^{-1}$)	V_{Gur} ($\text{m} \cdot \text{s}^{-1}$)	Error (%)
97.5 / 2.50 / 0.00	81.7 / 18.3 / 0.00	0.91	5616	15.47	0.78	1512	1473	2.56
92.5 / 7.50 / 0.00	58.6 / 41.4 / 0.00	0.69	4496	15.19	1.03	1188	1233	3.76
87.5 / 12.5 / 0.00	44.5 / 55.5 / 0.00	0.55	3871	15.01	1.28	1011	1060	4.85
70.0 / 10.0 / 20.0	43.8 / 54.5 / 1.70	0.68	3605	14.41	1.04	904	891	1.41
43.8 / 6.30 / 50.0	41.6 / 51.8 / 6.60	1.04	3521	14.13	0.69	866	882	1.76
8.70 / 1.20 / 90.0	27.2 / 33.9 / 38.9	3.39	2668	13.90	0.21	645	643	0.31

GMBs, and mixtures of gel plus 12.5% GMBs by mass further diluted by S110 steel particles comprising 20%, 50%, and 90% of the total mixture mass. All experiments in this subsection used a grazing detonation loading. Since the detonation velocity was subsonic for all mixtures relative to the flyer sound speed, and because the detonation pressure is quite low due to the substantial volumetric dilution, no shock was transmitted into the flyers and their acceleration was smooth and ballistic.

As expected, increasing the quantity of diluent reduced flyer terminal velocity regardless of the diluent density. Further, we note that initial flyer acceleration diminished with decreasing terminal velocity. This is characteristically different than the initial acceleration from high detonation pressure, high detonation velocity explosives, as described in Section 2.3. Notably, the addition of 50% by mass of steel caused little reduction in flyer velocity relative to 20% addition. While there was substantially more steel by mass, the total quantity of explosive, as quantified by the explosive volume fraction, only changed by 1%. By consequence, only a small decrement in propulsive capability was expected.

Table 2.3 lists the conditions for all experiments including mass fractions, volume fractions, mixture densities, detonation velocities, experimental Taylor angles, flyer-mass to mixture-mass ratios (M/C'), and terminal flyer velocities versus predictions of (2.13). The experimental results (solid symbols) compared to augmented Gurney model predictions are plotted as a function of the volume fraction of the explosive phase (ϕ_e) in Fig. 2.13. We note that at the extreme particle loading, only 27% of the mixture volume is explosive and the detonation velocity is reduced to $2.7 \text{ km} \cdot \text{s}^{-1}$, less than half of the detonation velocity of neat nitromethane. The mixture remained detonable despite the highly dispersed explosive phase due to the hot spot sensitization

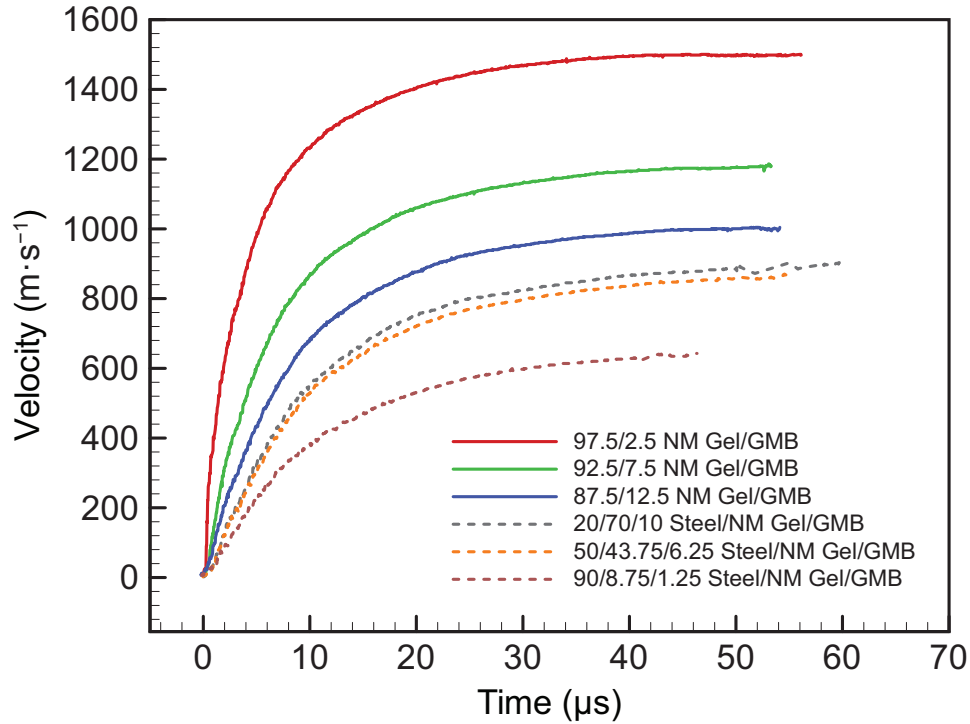


Figure 2.12: Velocity histories of 6.35-mm-thick aluminium flyers propelled via grazing detonation of a 24-mm-thick charge of gelled NM diluted with varying quantities of GMBs and steel particles.

of the microballoons. Detonation velocity was consistent along the length of the charge for all mixtures based on the resolution of measurement of the twisted pairs.

In keeping with the notion that Gurney energy is an experimental fitting parameter, good agreement between experimental terminal velocities and predictions of the augmented Gurney model were obtained by selecting different Gurney energies for the base NM component depending on if the mixture contained steel particles. The terminal velocity of the flyer was estimated by scaling the Gurney energy according to the combined mass fractions of both diluents in (2.13).

A Gurney velocity of $2300 \text{ m} \cdot \text{s}^{-1}$ was used to fit the curve for the mixtures containing only microballoons. This value is nearly equal (difference of only $10 \text{ m} \cdot \text{s}^{-1}$) to what was obtained for the DETA dilution experiments. A maximum error of 5% was encountered when predicting velocities for the GMB-only admixtures. Good agreement is expected because the microballoons are effectively introducing voids into the explosive and the mass of relatively dense material shell (borosilicate glass, $\rho \approx 2.2 \text{ g} \cdot \text{cm}^{-3}$) is negligible. Consequently, the additive will quickly accelerate to the velocity of the detonation product flow.

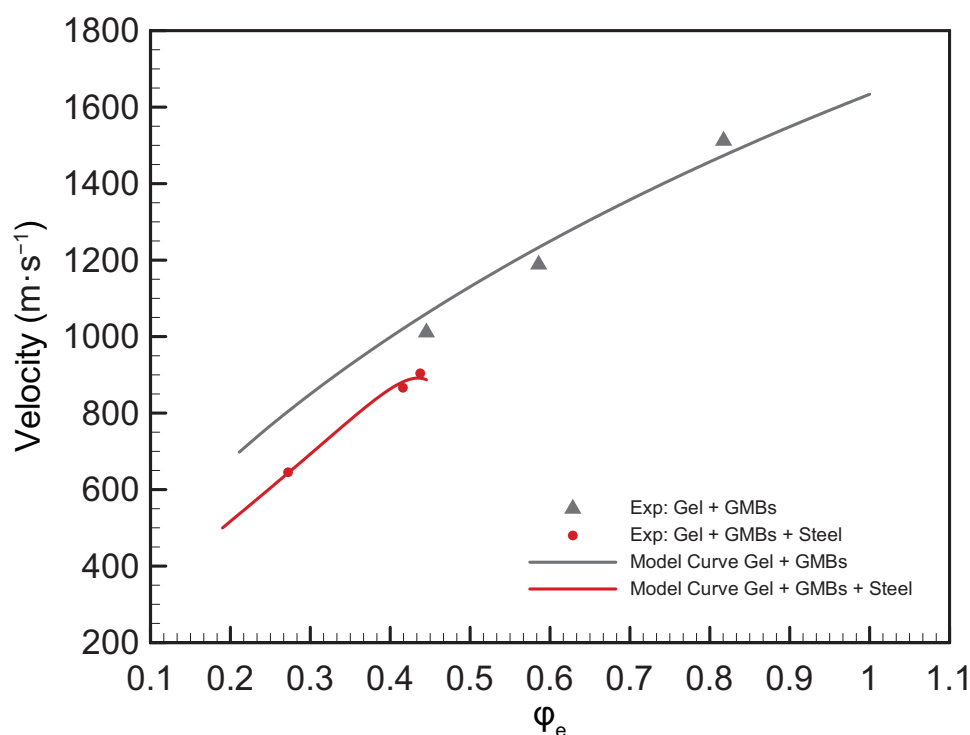


Figure 2.13: Terminal velocities of 6.35-mm-thick aluminium flyers propelled by gelled NM containing GMBs and steel particles versus NM vol. fraction. Data points (symbols) are compared to the augmented Gurney model (2.13) using a Gurney velocity of $2300 \text{ m} \cdot \text{s}^{-1}$ for NM in the GMB mixtures, and $1925 \text{ m} \cdot \text{s}^{-1}$ for NM in the GMB plus steel mixtures.

In contrast, use of this Gurney velocity with the gelled-NM/GMB/steel admixture substantially over-predicted the flyer velocity compared to the experimentally measured terminal velocities. A lower Gurney velocity was fit to this data: $1925 \text{ m} \cdot \text{s}^{-1}$. With this lower value, the model accurately predicted the decrement in flyer velocity for the three mass fractions of steel considered to within less than 5% error. The discontinuity in flyer velocity and Gurney velocity due to the addition of the steel particles is clearly visible in Fig. 2.13 at 45% volume fraction of explosive. The model curves for each Gurney velocity are plotted independently as a result.

A change in Gurney energy is not rigorous given that the same batch of nitromethane (Aldrich 108170 –96% reagent grade NM) was used in all six experiments and PMMA mass fraction was controlled to within 0.1 g per 2000 g of gel. One factor that contributed to the lower effective Gurney energy is the extended flyer acceleration timescale relative to the GMB-only admixtures. From the velocity histories it can be observed that the flyers propelled by the steel/GMB/gel were still slightly accelerating when the signals were lost; consequently the Gurney velocity is underestimated. The addition of steel thus measurably reduced the

effective driving pressure pushing the flyer even when there was a similar quantity of explosive in the mixture (44% vs 45% of the charge volume). This suggests that there is a secondary effect of diluent density that is not captured by the Gurney model assumptions, wherein both the GMBs and steel are considered equivalent on a mass fraction basis. The most likely cause for the discrepancy is more slip between the detonation products and the steel particles, compared to between the products and the collapsed GMBs. It is interesting that the discrepancies in propulsive efficiency when steel is added to the system can be modelled as a reduction in the effective energy of the explosive phase for diluent fractions and M/C values considered in this experimental subset. Departures in Gurney scaling due to the presence of large fractions of dense diluent are further considered in Section 2.8.4.

Gurney Curve for Gelled NM with 10% GMBs

Gelled nitromethane admixed with GMBs is an attractive system to evaluate the scaling of flyer terminal velocity with M/C because the resulting heterogeneous detonation product flow will most closely approximate the assumptions of the augmented Gurney model. Further, because of the low detonation pressure of the explosive, the gelled-NM/GMB admixture is useful to evaluate this scaling under normal detonation loading since it is less likely to completely spall the flyer.

A mixture containing 10% GMBs by mass was selected as a compromise between ease of loading the charge casings and avoiding spallation. In total, 17 trials were performed; 8 at normal incidence and 8 at grazing incidence with 1 repeat. The flyer-mass to charge-mass ratio was varied from 0.04 to 4.56 for both incidences by changing the thickness of the flyer plate while maintaining the reservoir thickness constant. The 0.25-mm-thick slapper was used to initiate all normal-incidence experiments. The charge lid was omitted in all grazing experiments and the charge casings were levelled via bubble level prior to filling. This eliminated any additional complications introduced by having one range of experiments tamped since the normal experiments could not incorporate an equivalent tamper by design. For all configurations, charges were filled until the formation of a meniscus. Mixture viscosity prevented spillage in all experiments. The velocity histories for the grazing experiments are shown in Fig. 2.14 and the velocity histories of the normal incidence experiments are shown in Fig. 2.15. Note that the

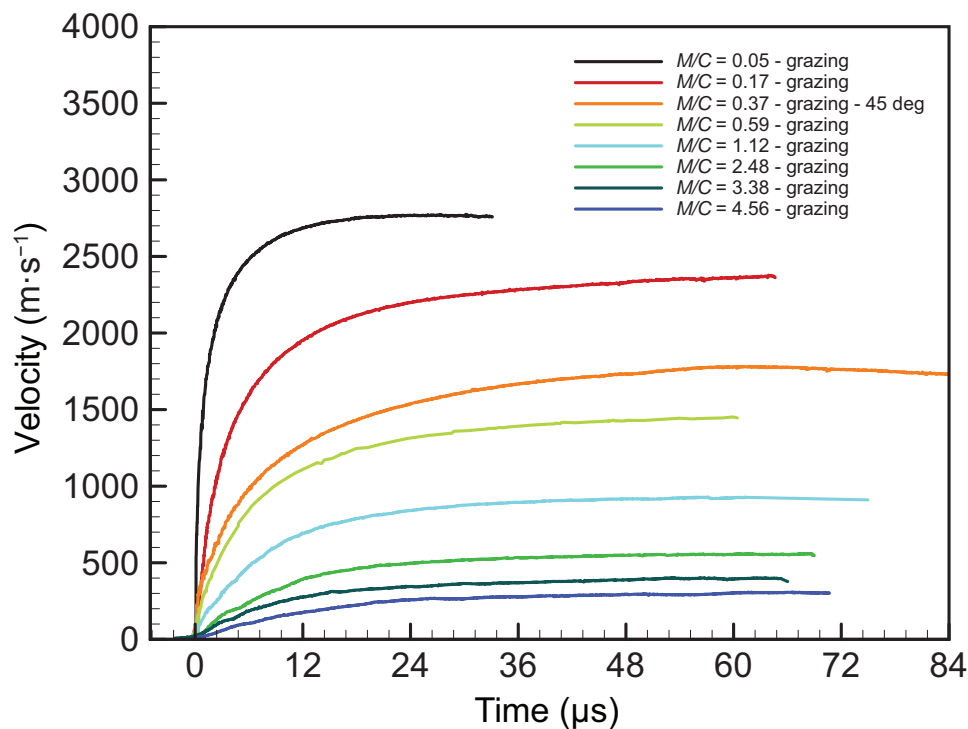


Figure 2.14: Velocity histories of aluminium flyers of varying thicknesses propelled by grazing detonation of a 24-mm-thick charge of gelled NM diluted by 10% glass microballoons by mass.

deceleration observed for the thinnest flyer is caused by aerodynamic drag because of the very high speed and large cross-sectional area relative to the areal density.

All grazing experiments had smooth, shockless flyer accelerations because of the subsonic detonation velocity relative to the flyer sound speed and the low detonation pressure of the explosive. Note that for the $M/C = 0.37$ experiment, the angled probe data was scaled and plotted instead of the normally oriented probe data because the signal quality was poor for this probe. As expected, flyer terminal velocity decreased with increasing flyer thickness. It is notable that the very thick, high mass flyers ($M/C > 2.4$) reached terminal velocity faster than flyers with intermediate explosive loadings ($0.17 \leq M/C \leq 0.59$), despite the much slower initial accelerations. This is consistent with observations using neat liquid explosive described in a preceding paper, where it was observed that thick flyers reached terminal velocity promptly after shock breakout at the flyer free surface [9]. In the present experiments, acceleration is extended and ballistic in nature because the oblique shock transmitted by the detonation is absent.

In contrast, a strong shock breakout was observed at the free surface for all flyers propelled via normally incident detonations. For the 0.25 mm and 0.95 mm flyers there was little oscil-

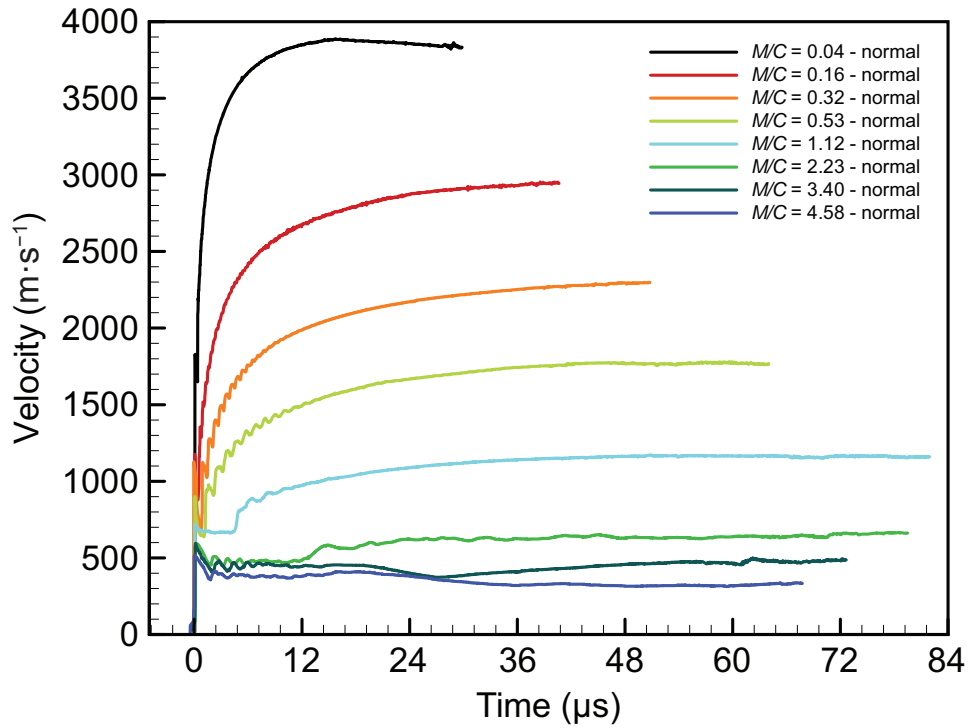


Figure 2.15: Velocity histories of aluminium flyers of varying thicknesses propelled by normally incident detonation of a 24-mm-thick charge of gelled NM diluted by 10% glass microballoons by mass.

lation in the free surface velocity since the shock reverberation timescale was fast and thus the flyer equilibrated quickly. For the 1.95 mm and 3.17 mm flyers a continuous ring-up in surface velocity was observed throughout most of the flyer acceleration. For the 6.35 mm flyer a shock breakout followed by a pullback and a velocity plateau 4 μs in duration was obtained. After this plateau the flyer free surface ballistically accelerated to the flyer terminal velocity. The plateau is associated with spallation within the flyer, however the flyer was recovered intact post experiment and sectioning revealed no large void growth. Consequently, spallation remained incipient and no large free surface was generated. For the thicker flyers, the duration of the spall plateau was extended and the strength of the shock breakout was attenuated by the greater thickness of material. For the 12.7 mm flyer, only a very small ballistic acceleration was observed after the spall plateau and the terminal velocity of the flyer did not exceed the initial free surface velocity imparted by the shock. For the 19 mm flyer only a small, late time acceleration was observed after a further drop in flyer velocity, while the 25 mm flyer did not accelerate at all after the spall plateau. We note that in all cases the flyers were recovered intact with no material spallation off of the free surface. The terminal velocity recorded by the PDV thus represented the true flyer

The Propulsive Capability of Explosives Heavily Loaded with Inert Materials

Table 2.4: Summary of conditions for the gelled nitromethane with 10% GMB Gurney curve measurements. A Gurney velocity of $1975 \text{ m} \cdot \text{s}^{-1}$ was used for augmented model predictions.

Flyer thickness (mm)	Mixture mass (g)	$\frac{M}{C}$	θ ($^\circ$)	V_m ($\text{m} \cdot \text{s}^{-1}$)	V_{Gur} ($\text{m} \cdot \text{s}^{-1}$)	Error (%)
0.25	282.8	0.04	52.05	3038	2892	4.8
0.25	269.2	0.05	51.29	3069	2879	6.2
0.25	160.5	0.04	0.0	3885	2903	25.3
0.95	282.2	0.17	29.94	2452	2337	4.7
0.95	165.3	0.16	0.0	2951	2381	19.3
1.95	262.4	0.37	28.72	1875	1800	4.0
1.95	164.5	0.32	0.0	2295	1905	17.0
3.17	271.3	0.59	22.59	1473	1459	0.9
3.17	163.2	0.53	0.0	1774	1535	13.5
6.35	283.0	1.12	13.92	933	998	7.0
6.35	155.0	1.12	0.0	1168	1003	14.1
12.70	256.9	2.48	8.46	556	562	1.0
12.70	155.0	2.23	0.0	664	610	8.1
19.05	282.1	3.38	5.88	398	436	9.6
19.05	152.6	3.40	0.0	487	434	10.9
25.40	278.7	4.56	4.56	305	337	10.4
25.40	151.0	4.58	0.0	333	336	1.1

velocity. These thick flyer experiments are a unique situation where gasdynamic expansion of the detonation products is not providing meaningful flyer acceleration but merely counteracting wavedynamic deceleration due to rarefactions after the passage of the incident shock.

Figure 2.16 shows a detailed view of the wavedynamic features of the normal incidence experiments at early times (0–5 μs). For all experiments, the interaction between the Taylor wave and the first rarefaction emanating from the flyer free-surface generated a strong initial pull-back in the free surface velocity after the initial jump in velocity from the shock. Subsequently, either the free surface began to oscillate from alternating reflections of rarefaction and compression waves or it spalled in the case of the thicker flyers ($>3 \text{ mm}$) [40]. Notably, the flyers with spall plateaus had initial free surface velocities of about $580 \text{ m} \cdot \text{s}^{-1}$, with some attenuation with greater thickness. Similarly, the flyers without a spall plateau had initial free surface velocities of about $1000 \text{ m} \cdot \text{s}^{-1}$. By contrast the thinnest, 0.25-mm-thick flyer had an initial free surface velocity of $1830 \text{ m} \cdot \text{s}^{-1}$; a discrepancy that cannot be attributed to reduced attenuation. Rather,

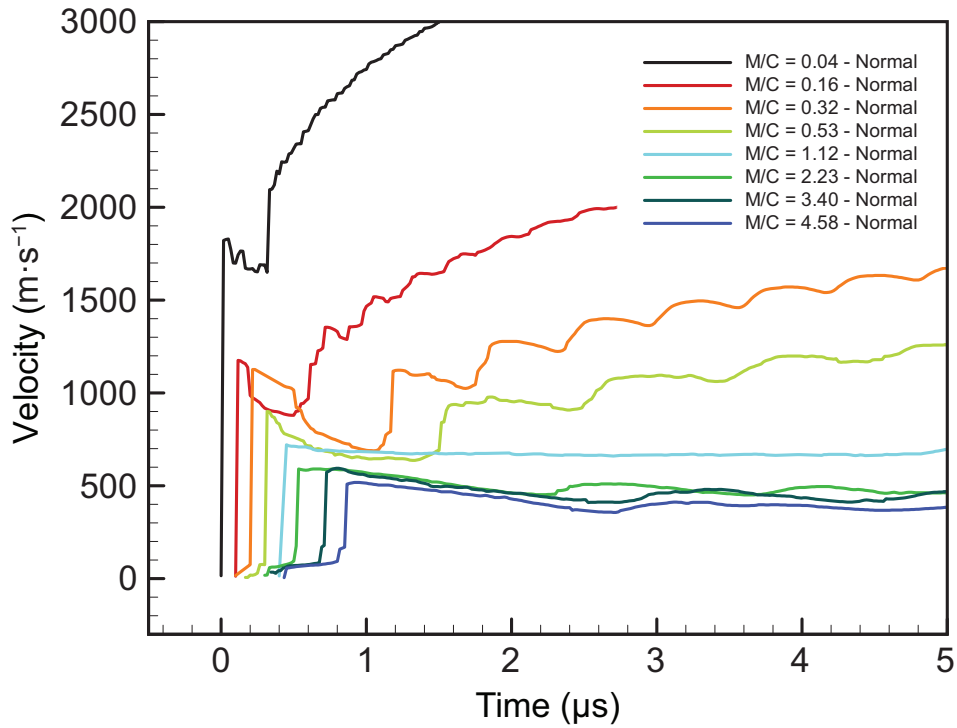


Figure 2.16: Zoom of the velocity histories for flyer plates propelled via normal detonation of gelled NM with 10% GMB illustrating the wavedynamic response in detail. Note the large initial free surface velocity for the 0.25-mm-thick flyer; corresponding to transmission of von Neumann spike pressure rather than detonation pressure.

this increase resulted from the transmission of the von Neumann spike shock pressure, rather than the lower Chapman-Jouguet detonation pressure. This is postulated to occur when the flyer is thinner than the length of the explosive reaction zone [117]. Under these conditions, a thin flyer may be launched to higher velocity than a thicker flyer even if both are loaded to an equivalent M/C ; this is a critical design consideration for hypervelocity explosive cascades [117]. These discrepancies illustrate that the wavedynamic effects scale not only with the mass ratio of the charge, but also the absolute size. This is in contrast to the charge-size invariance postulated in the Gurney model.

The experimental conditions, velocities and Taylor angles for all trials are listed in Table 2.4. In order to permit direct comparison of the normal and grazing incidence experiments, the grazing detonation PDV data was tilt-corrected to obtain the magnitude of the total metal velocity using the detonation velocity measured in each individual experiment. The average detonation velocity was $3.79 \text{ km} \cdot \text{s}^{-1}$ with a maximum deviation of $0.12 \text{ km} \cdot \text{s}^{-1}$. For thick flyers with small Taylor angles, only a normally observing probe was used. For thinner flyers with Tay-

for angles greater than 25° , an angled probe nominally observing at 45° from the vertical was added so that the true metal velocity could be explicitly calculated. We note the exceptionally large tilt angle of 51° observed for the 0.25-mm-thick flyer. The normally-incident-detonation experiments are denoted by a Taylor angle of 0° . Note that the experiments are tabulated and plotted based on the ratio of flyer-mass to mass of the explosive phase (M/C) for this sub-set of data.

Figure 2.17 plots the experimental data points for both loading conditions against the predictions of the augmented Gurney model (solid curve) tabulated previously, and against the standard Gurney model (dashed curve) for homogeneous 90/10 NM/DETA. The augmented Gurney model was fitted to the grazing data set using a Gurney velocity of $1975 \text{ m} \cdot \text{s}^{-1}$. We note that this is lower than the value used to fit the GMB dilution experiments, and is in fact closer to the value used to decrement the model predictions when steel was added. The flyer velocity obtained with the 10% GMB mixture propelling a 6.35-mm-thick flyer was also anomalously low relative to the GMB dilution experiments for a similar flyer thickness. This lower velocity cannot be explained solely by the elimination of the tamper in this subset of experiments as the contribution of the tamper was included in calculating the Gurney velocity for the dilution experiments and the 90/10 NM/DETA experiments. Rather it is likely that there was variation in the batch of gelled-NM used for this series compared to the dilution experiments. As with the gel dilution experiments, a single chemical batch was used for all 17 tests. For these experiments a $\geq 95\%$, reagent grade NM was used (Sigma Aldrich 360554). Based on the two experiments conducted with 0.25-mm-thick flyers, the experimental results are at least reproducible within the subset of experiments conducted with the same batch of explosive.

Despite this discrepancy, agreement between the grazing experiments and predictions of the augmented Gurney model are quite good using a lower value for the Gurney velocity/energy: an average error of 5.4% and a maximum error of 10.4%, occurring at the largest value of M/C considered. We note that agreement is not quite as good as for the neat nitromethane case. Even with a low average error, the augmented model over-predicts the terminal velocity for large values of M/C (> 3) and then under-predicts the terminal velocity for small values of M/C (< 0.2). By contrast, for the neat explosive experiments, consistent agreement is obtained over a wide range of M/C values, with systematic underprediction accruing as a result of departures from Gurney's gasdynamic assumptions for very small values of M/C . Similarly, the scaling of

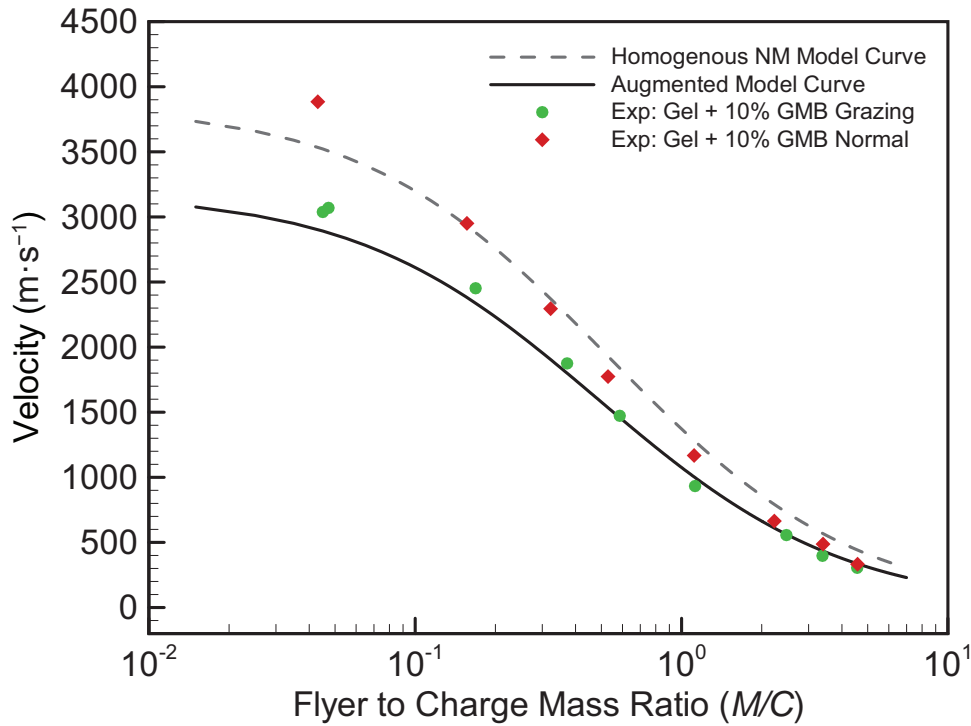


Figure 2.17: Experimental terminal velocities from the grazing and normal incidence experiments with gelled NM and 10% GMBs plotted against predictions of the augmented Gurney model using (2.9). A Gurney velocity of $1975 \text{ m} \cdot \text{s}^{-1}$ was used for the NM. The tamped Gurney equation for an equivalent mass of neat liquid NM with a Gurney velocity of $2350 \text{ m} \cdot \text{s}^{-1}$ is included for comparison.

flyer velocity for the normal experiments deviated from model predictions for values of $M/C > 1$. In all cases the normally incident detonations propelled the flyer to a faster terminal velocity relative to the equivalent grazing loading. The deviation between the two loading conditions increased as the flyer thickness was reduced. For small M/C , the terminal velocities obtained with normal detonation loading of gelled-NM/GMBs ($\sqrt{2E} = 1975 \text{ m} \cdot \text{s}^{-1}$) eventually exceeded velocities obtained using grazing loadings of NM/DETA ($\sqrt{2E} = 2350 \text{ m} \cdot \text{s}^{-1}$). This is visible in Fig. 2.17 by comparing the dashed curve to normal data. The extent of overshoot of the normal experiments from the standard model predictions is similar in magnitude to what was observed for the neat liquid grazing experiments due to gasdynamic departures, and those experiments contained no diluent.

Ultimately, it is not possible to quantify the precise contributions leading to the non-Gurney scaling in the normal experiments, as several phenomena are contributing as the value of M/C is reduced: departures from the gasdynamic assumptions in the Gurney model, material ve-

locity imparted by the reverberating detonation shock or von Neumann spike shock, and momentum/energy transfer from the slapper plate. Although the amount of energy transferred to the system is small due to the low mass of the slapper, its relative importance increases as the primary flyer is thinned. In the extreme case, the two flyers were of equal thickness, and thus slapper contribution is significant simply due to tamping of the explosive in addition to depositing energy via impact. Consequently, while the amount of energy deposited via impact remains the same as M/C is varied, the relative degree of tamping increases as M/C is reduced. The contribution from gasdynamic departures can be estimated from departures in the grazing case which are on the order of $200 \text{ m} \cdot \text{s}^{-1}$, or 25% of the total increase above the augmented Gurney model obtained for the smallest value of M/C considered under normal loading. The large initial material velocity imparted by the VN spike instead of the CJ detonation is also a major contributor to the large jump in terminal velocity observed for the 0.25-mm-thick flyer relative to the 1-mm-thick flyer.

2.8.4 Results with NM Saturated Packed Beds

In this subset of experiments we considered the propulsion of 6.35-mm-thick aluminium flyers by packed particle beds saturated with 90/10 NM/DETA. These explosive mixtures represent a practical upper limit of explosive dilution with inert solids because the explosive fills only the voids between jammed particles. For the different steel and glass media considered, the particles were nearly mono-sized and thus the packed beds approached the random close packing limit. Consequently, a very consistent volume fraction of explosive was maintained in these experiments: 38%–40%. For the tungsten packed bed, a large fraction of ultra-fine particles prevented bed settling and the charge was 45% explosive by volume. The glass and steel experiments thus had nearly identical M/C ratios while the tungsten experiment had a slightly smaller ratio. The velocity histories for the five packed bed experiments are shown in Fig. 2.18 while the experimental conditions are listed in Table 2.5, including mixture mass and volume fractions, mixture density, detonation velocity, tilt-corrected terminal flyer velocity, and prediction error of the augmented Gurney model.

As with the previous sets of experiments, because the detonation velocity is subsonic relative to the flyer sound speed, no shock is driven into the flyer and accelerations are again smooth and ballistic. For the glass and steel experiments, the initial flyer acceleration is very similar

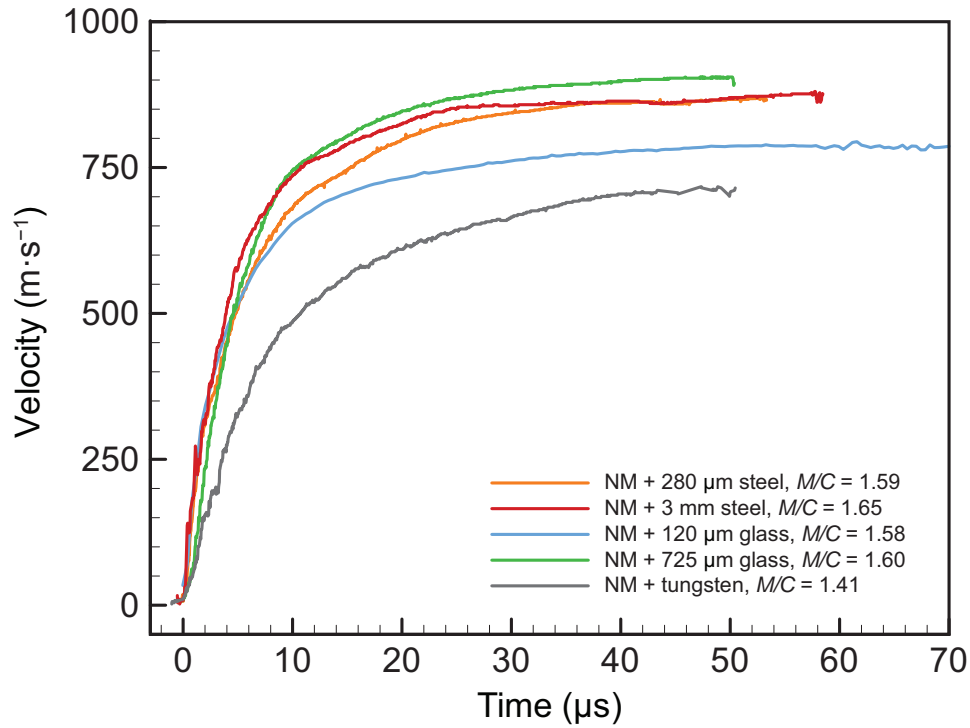


Figure 2.18: Velocity histories for all 6.35-mm-thick aluminium flyer experiments propelled by NM-saturated, packed particle beds. Charge thickness was 24 mm.

regardless of diluent density and particle size. Deviations to different terminal velocities only occurred due to variations in the decay of flyer acceleration. Interestingly, the same terminal velocity was reached for both the 3 mm steel particles and the 280 μm steel particles, despite the order-of-magnitude difference in particle size. The flyer propelled by the explosive containing 3 mm particles overshoot relative to the flyer propelled by the mixture with 280 μm particles but then asymptoted more quickly, resulting in a terminal velocity that was effectively identical to within experimental error. By contrast, the flyer propelled by explosive containing fine glass

Table 2.5: Summary of conditions for the experiments using packed beds of glass, steel and tungsten particles saturated with liquid nitromethane. A Gurney velocity of $2350 \text{ m} \cdot \text{s}^{-1}$ was used for augmented model predictions.

Material	w_b	ϕ_e	ρ_{mix} ($\text{g} \cdot \text{cm}^{-3}$)	D ($\text{m} \cdot \text{s}^{-1}$)	θ ($^\circ$)	$\frac{M}{C}$	V_m ($\text{m} \cdot \text{s}^{-1}$)	V_{Gur} ($\text{m} \cdot \text{s}^{-1}$)	Error (%)
Glass - 120 μm	0.78	0.38	1.97	4248	10.69	1.58	791	1061	34.12
Glass - 725 μm	0.78	0.39	1.96	3523	14.89	1.60	913	1059	16.02
Steel - 280 μm	0.91	0.40	5.16	4740	10.49	1.59	867	895	3.33
Steel - 3 mm	0.92	0.38	5.30	5840	8.63	1.65	878	869	1.02
Tungsten	0.95	0.45	10.68	2658	15.51	1.41	718	756	5.34

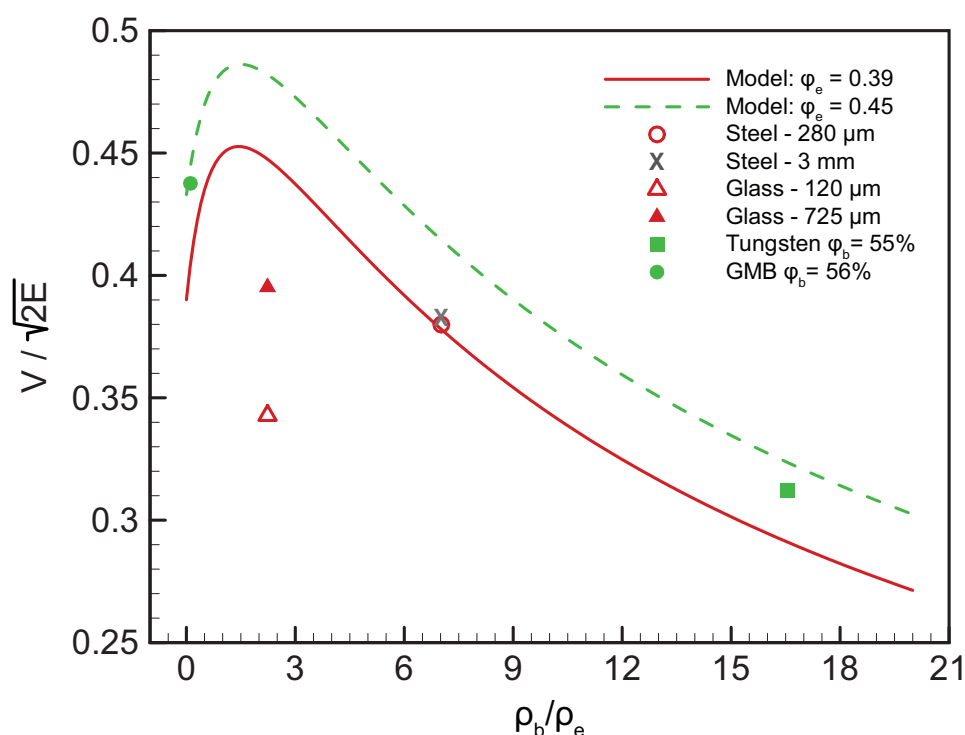


Figure 2.19: Normalized terminal velocities (symbols) for 6.35-mm-thick aluminium flyers propelled by NM-saturated packed particle beds versus the augmented Gurney model, plotted over the range of explosive-density to diluent-density ratios.

particles (120 μm) asymptoted to a lower terminal velocity compared to the flyer propelled by the larger particles (725 μm). For dilution with the tungsten powder, the initial acceleration was slower than for explosives containing less dense diluents and the terminal velocity is lower on an absolute basis, despite the presence of more explosive. Consequently, increasing diluent density introduces a modest but measurable reduction in flyer terminal velocity when the increase in density is substantial. Particle size effects are unclear given the differing behaviour between the glass and steel particles, however these results suggest that the assumption that the diluting particles match velocities with the detonation products is not completely unfounded for the purposes of estimating flyer velocity. Similar terminal velocities for both sizes of steel particles particularly emphasises that the degree of slip between the detonation products and solid particles is not the sole determining factor in the terminal acceleration ability of the explosive mixture.

Augmented Gurney model predictions of flyer velocity for experiments using the denser diluents are accurate for the values of M/C considered here, with a maximum error of around 5% using a Gurney velocity of $2350 \text{ m} \cdot \text{s}^{-1}$. However, the model substantially overpredicts the

terminal velocities obtained with the glass admixtures. This effect is plotted in Fig. 2.19, which depicts the model-predicted and experimentally obtained variations of normalized flyer velocity versus the ratio of diluent density to explosive density. Two lines are included, one that corresponds to the explosive volume fraction in the steel and glass beds, and one that corresponds to the volume fraction obtained in the tungsten experiment. The gelled NM experiment containing 12.5% GMBs by mass is also included in the plot since it had a similar explosive volume fraction to the tungsten experiment. The augmented model predicted a peak in velocity at a density ratio of 1.4. The normalized velocity at this point is effectively equal to the value obtained if an equivalent mass of the neat explosive was instead used to propel the flyer. This may arise simply from anomalous mathematical behaviour due to the addition of the energy and momentum terms for the beads, similar to how the tamped Gurney model underpredicts flyer velocity compared to the untamped model for certain mass ratios. Or, it may demonstrate that the addition of large fractions of dense diluents changes the manner in which flyer velocity scales with explosive loading. These effects are explored in the subsequent series of experiments.

Gurney Curve for NM-Saturated Steel Particle Bed

The Gurney curve for the steel particle bed saturated with NM was measured to determine if flyer velocity scales anomalously as the relative explosive loading is varied when a large fraction of dense diluent is present in the explosive. The M/C ratio was varied by using different aluminium flyer plate thicknesses while the explosive reservoir was held at a constant thickness of 24.1 mm. The flyers used were 0.8 mm, 3.2 mm, 6.4 mm, 12.7 mm, and 19.1 mm thick for the grazing experiments and 0.25 mm, 1.0 mm, 2.0 mm, 3.2 mm, 6.4 mm, 12.7 mm, and 19.0 mm thick for the normally incident experiments.

Explosive packing was quite reproducible between experiments, with an average of 180.1 ± 5 g of sensitized NM and an average of 1893 ± 55 g of steel placed in the reservoirs for the grazing experiments. An average of 1028 ± 150 g of steel and 103 ± 8 g was placed in the normal experiments. For most of normal incidence experiments, the 280 μm steel particles were substituted for larger, 432 μm (S-170) particles. Similar mass and volume fractions were obtained for both particle sizes.

The lateral PDV velocity histories for all grazing experiments are shown in Fig. 2.20 and the PDV velocity histories for all normal experiments are shown in Fig. 2.21. To construct the

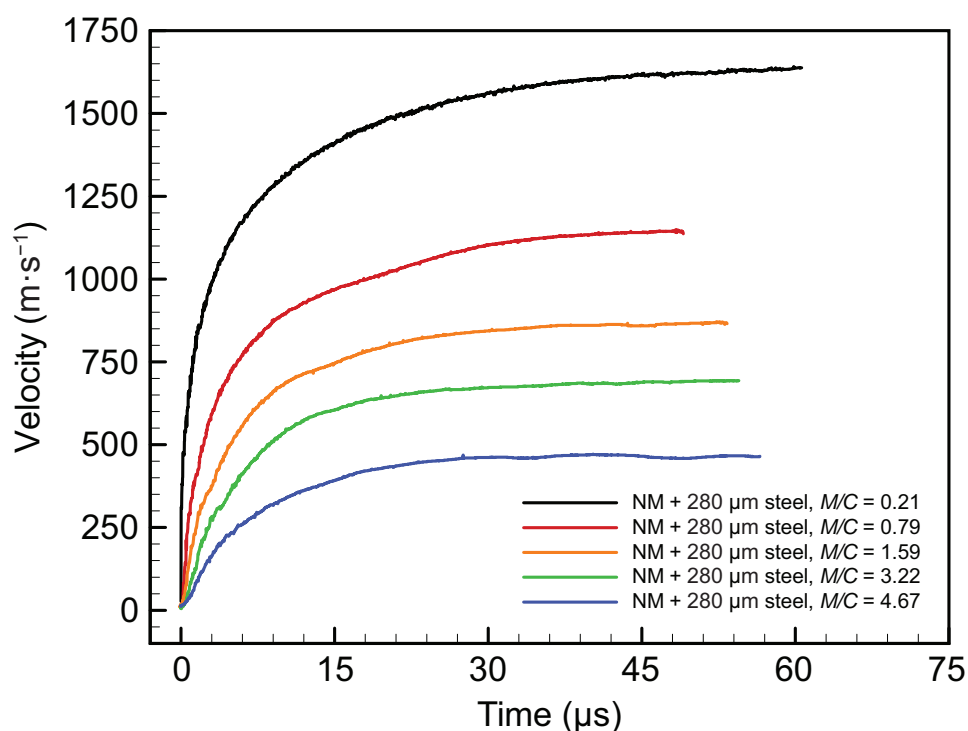


Figure 2.20: Velocity histories for aluminium flyers of various thicknesses propelled by grazing detonations of 24-mm-thick packed beds of steel particles saturated with sensitized NM.

grazing Gurney curve, experimental terminal velocities were tilt-corrected using the detonation velocity measured for each experiment. The average detonation velocity of the packed-bed explosive was $4.74 \text{ km} \cdot \text{s}^{-1}$ with a maximum deviation of $0.11 \text{ km} \cdot \text{s}^{-1}$.

The Gurney curves based on the grazing and normally incident experiments are shown in Fig. 2.22; the grazing terminal velocities (green squares) and normal-incidence terminal velocities (red diamonds) are plotted against predictions of the standard Gurney model (black curve) and the augmented Gurney model (red curve) over the range of flyer-mass to NM-mass ratios (M/C) considered experimentally. A constant tamper-mass to NM-mass ratio (N/C) of 0.39 was used to account for the tamping effect of the PVC lid in the calculation of both theory curves. The tilt-corrected, neat sensitized nitromethane data points (from [9]) at equivalent values of M/C are plotted as black circles and closely follow the standard Gurney model as described previously.

A key result demonstrated by Fig. 2.22 is that the NM-saturated packed bed system does not follow typical Gurney model scaling in either incidence case. For values of $M/C > 2.2$ the experimental terminal velocities converged with or exceeded the velocities obtained with an equiv-

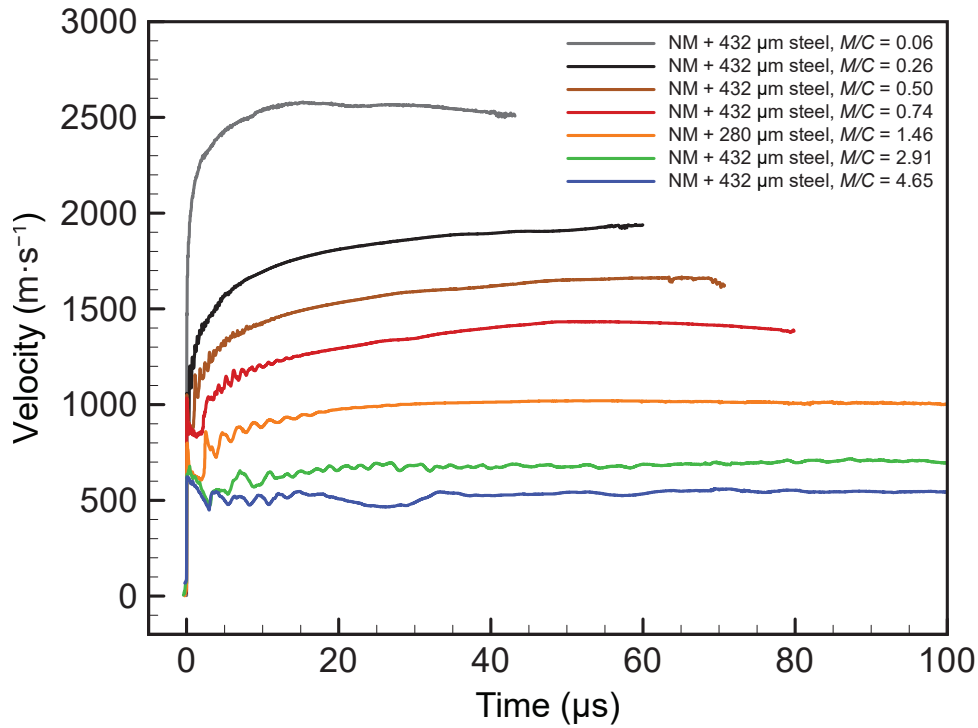


Figure 2.21: Velocity histories for aluminium flyers of various thicknesses propelled by normally incident detonations of 24-mm-thick packed beds of steel particles saturated with sensitized NM.

alent ratio of just the neat explosive in grazing geometry. In this range of M/C the augmented Gurney model over-predicted the experimental terminal velocities by up to $\approx 200 \text{ m} \cdot \text{s}^{-1}$. For values of $M/C < 2.2$, the augmented Gurney model systematically under-predicted experimental terminal velocities and the degree of under-prediction increased with decreasing M/C ratio. As with the experiments with gelled NM and 10% GMBs, the normal incidence experiments with the saturated beds yielded terminal velocities that were greater than the equivalent grazing experiments to a degree that increased as M/C was decreased. This resulted in augmented model under-predictions in excess of $1000 \text{ m} \cdot \text{s}^{-1}$ for small values of M/C .

Poor agreement at small values of M/C can be explained by the fact that the augmented model is effectively reducing the Gurney velocity of the explosive mixture. For a sandwich, the limit velocity as the ratio of metal mass to explosive mass tends to zero is $\sqrt{6E}$ [5]. Because the mass fraction of inert in these experiments is so large, the reduction in Gurney energy in $\sqrt{2E(1 - w_b)}$ is dramatic, resulting in a much lower metal velocity limit relative to the neat explosive, as depicted by the left-most portion of the two curves in Fig. 2.22. The experimental results instead display a growing deficit relative to the equivalent neat explosive, indicating a

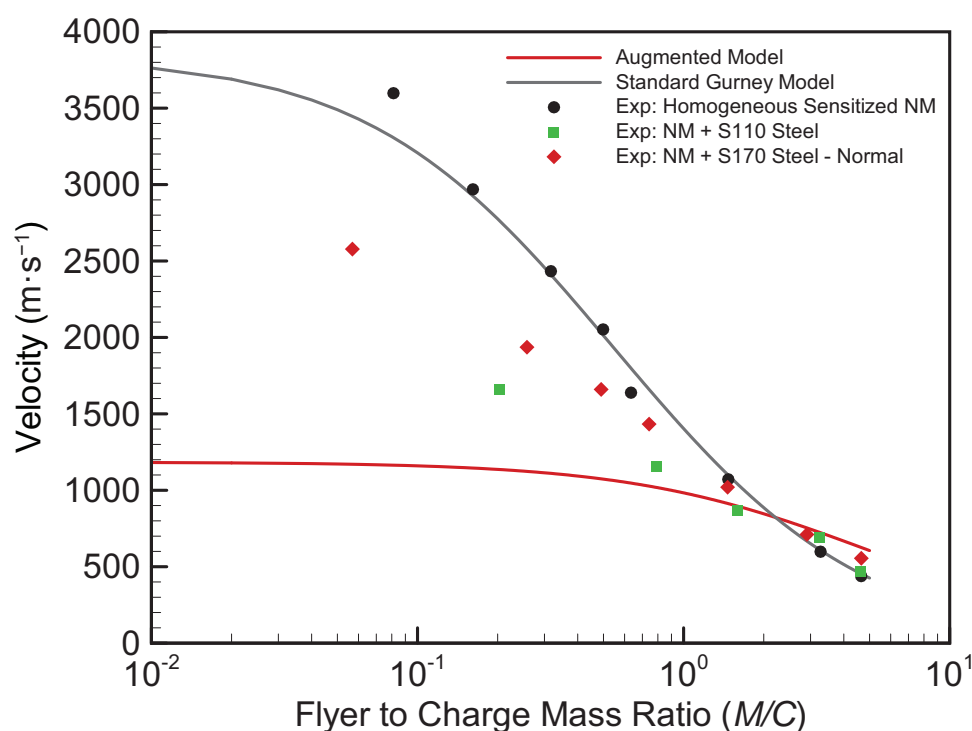


Figure 2.22: Gurney curves of the experimental terminal velocities of the neat NM experiments and the NM-saturated steel packed-bed experiments versus predictions of the standard asymmetric sandwich model and (2.9), respectively. A Gurney velocity of $2350 \text{ m} \cdot \text{s}^{-1}$ was used for both curves.

physical metal velocity limit that is intermediate between the two models. Due to poor agreement with the models, the degree of departure due to gasdynamic factors at small M/C cannot be determined. Further, no material velocity increase due to action of the von Neumann spike was observed for the 0.25-mm-thick flyer propelled normally. This was attributed to the scale of the heterogeneous inclusions relative to the NM reaction zone length.

For large values of M/C , we emphasize that the experimental velocities for the grazing packed bed systems exceed the equivalent experimental velocities for the neat explosive when the same mass ratio (M/C) of explosive component was used. Note that the same thickness of tamping lid was used throughout the neat liquid and packed bed experiments and the same flyer thicknesses were used for the large ($M/C > 2.5$) mass ratio experiments: 12.7 mm and 19.1 mm thick. In the case of the neat liquid experiments, the large mass ratios were obtained by thinning the explosive reservoir.

The propulsive efficiency of the packed bed system thus increased relative to the equivalent neat liquid explosive system for large M/C or larger flyer inertias. We posit that this is due to

self-tamping within the explosive. Assuming that the linear velocity profile in the detonation products is reasonably realistic, as the velocity of the flyer diminishes relative to the velocity of a light tamper or the free expansion velocity of the products, the plane of zero gas velocity moves closer to the surface of the flyer and consequently more kinetic energy is partitioned to expand products away from the flyer. This is demonstrated by Hoskin et al., where the efficiency of energy transfer was shown to reach a maximum at an M/C value of around 0.5, and subsequently diminishes as the explosive loading is further reduced [40]. For a packed bed saturated with explosive, this larger fraction of detonation products expanding away from the flyer must initially push against and around the dense particles, thereby accelerating them. This impediment to product expansion is similar to the effect of a solid tamping plate. This tamping effect offsets losses to accelerating and heating of the particles, resulting in a similar or greater propulsive efficiency than if the neat explosive was detonated alone. By contrast, if the flyer has little inertia, the plane of zero velocity moves towards the centre of the charge and a larger fraction of particles are accelerated in the direction of the flyer. Further, at the limit of very low inertia flyers, terminal velocity is limited by acoustic decoupling from the detonation products. In these configurations, acceleration and heating of the particles are a net sink that reduces the efficiency of the explosive. The dynamic tamping effect is also likely unique to untamped or weakly tamped asymmetric geometries since a symmetric system is self-tamping as the explosive is surrounded by material, however symmetric sandwich or cylindrical experiments are required to verify this postulate.

While the augmented Gurney model poorly predicts the experimental velocities quantitatively, it qualitatively predicts the mass ratio where the packed bed mixture exceeds the performance of the neat explosive and it approximates the degree of performance enhancement. The augmented model can also be used in conjunction with the standard Gurney model to bound the expected flyer terminal velocity for M/C values much greater than the crossover point of the two Gurney curves. This set of experiments also represents an extreme case of inert dilution as a high-density diluent with the maximum possible diluent volume fraction was used. Based on the results from Section 2.8.3, superior agreement is anticipated as diluent density and volume fraction are lowered.

2.8.5 Results with C-4 Admixtures

The effect of diluent volume fraction and density on the propulsive efficiency of a heterogeneous high explosive was further considered using solid explosives in order to address the anomalous results obtained with glass versus steel particles as described in Section 2.8.4. The use of C-4 as the baseline energetic material permitted the dispersion of the dense particles without the complications of a second, low-density diluent phase, as was the case with the gelled NM experiments.

This series consisted of 3 tests with neat C-4, 7 tests with 725 μm glass particles where the mass fraction was varied from 5% to 60%, and 4 tests with 280 μm steel particles where the mass fraction was varied from 15% to 80%. In all experiments, 6.35-mm-thick aluminium flyers were used. For all but one experiment, the 24.1-mm-thick PVC charge mold was filled completely with admixture and then levelled with a dowel roller. For the experiment with only 306 g of neat C-4, the requisite mass of explosive was added and rolled with the wooden dowel until level. Uniform thickness of explosive in this case was ensured by measuring the surface with a level and vernier calliper. A nominal density of $1.623 \text{ g} \cdot \text{cm}^{-3}$ was used when modelling the C-4 as this was the highest packing density obtained with the neat explosive. A Gurney velocity of $2680 \text{ m} \cdot \text{s}^{-1}$ was selected to best match the neat C-4 experiments.

The lateral PDV velocity histories for the steel admixture experiments are shown in Fig. 2.23, while the lateral PDV velocity histories for the glass admixture experiments are shown in Fig. 2.24. The velocity histories for the two neat C-4 experiments where the casing was entirely filled with C-4 are included with the glass experiments as dashed lines. Neat C-4 velocity histories corresponding to an approximately equivalent explosive mass as the 15% steel and 80% steel admixtures are included with the steel experiments as dashed lines. The detailed conditions and explosive properties for the glass and steel experiments are listed in Tables 2.6 and 2.7, respectively. The three neat C-4 experiments are repeated in both tables to facilitate comparison. Each table lists the explosive volume fraction, achieved explosive density, flyer-mass to explosive-mass ratio (M/C), detonation velocity (D), and flyer terminal velocity.

The known quantities for each experiment were the masses of added particles, masses of the included C-4, and the charge volume. Based on the solid density and mass of particles, the volume fraction of the charge occupied by inert material was calculated. This also directly

2.8 Experimental Results and Discussion

Table 2.6: Summary of experimental conditions for the C-4/glass admixtures.

w_b (%)	ϕ_e (%)	Mass C-4 (g)	ρ_e (g · cm ⁻³)	$\frac{M}{C}$	D (m · s ⁻¹)	V_m (m · s ⁻¹)
0.0	100.00	653.0	1.62	0.44	7881	2366
0.0	100.00	629.1	1.56	0.45	7964	2241
5.0	96.58	653.6	1.68	0.44	7711	2327
10.0	92.96	637.2	1.70	0.45	7775	2296
16.2	88.50	598.3	1.68	0.48	7504	2181
28.0	79.68	525.6	1.64	0.54	7161	2029
44.0	66.80	425.0	1.58	0.67	6524	1748
50.0	62.62	376.0	1.49	0.76	5968	1617
60.0	55.26	300.0	1.35	0.95	5054	1370
0.0	100.00	306.0	1.56	0.94	7792	1558

Table 2.7: Summary of experimental conditions for the C-4/steel admixtures.

w_b (%)	ϕ_e (%)	Mass C-4 (g)	ρ_e (g · cm ⁻³)	$\frac{M}{C}$	D (m · s ⁻¹)	V_m (m · s ⁻¹)
0.0	100.00	653.0	1.62	0.44	7881	2366
0.0	100.00	629.1	1.56	0.45	7964	2241
15.0	96.69	592.2	1.52	0.48	7878	2149
50.0	82.60	549.5	1.65	0.52	7396	2078
66.0	71.28	467.2	1.63	0.61	6520	1818
80.0	61.14	306.8	1.25	0.93	5114	1349
0.0	100.00	306.0	1.56	0.94	7792	1558

yielded the charge volume occupied by the explosive (ϕ_e), and thus the achieved packing density of the explosive phase (ρ_e) since the mass of C-4 in the charge casing was also known. The mass ratio was calculated by dividing the areal density of the flyer: $\tau_m \rho_m$ by the areal density of the included explosive: $\tau_e \rho_e \phi_e$, where the variable τ represents the thickness of the layer in question. This value for the ratio is nearly identical to the one calculated based on ratio of the actual mass of the flyer divided by the charge planar surface area (charge-width times charge-length) to the actual mass of explosive divided by the same surface area.

Non-monotonic variation in the density of the explosive phase was observed throughout the experiments, likely due to interaction between the particles and the binder. The addition of small volume fractions of glass (<15%) increased the explosive packing density by 5%. The addition of large volume fractions of glass (>35%) substantially reduced the packing density by 17%

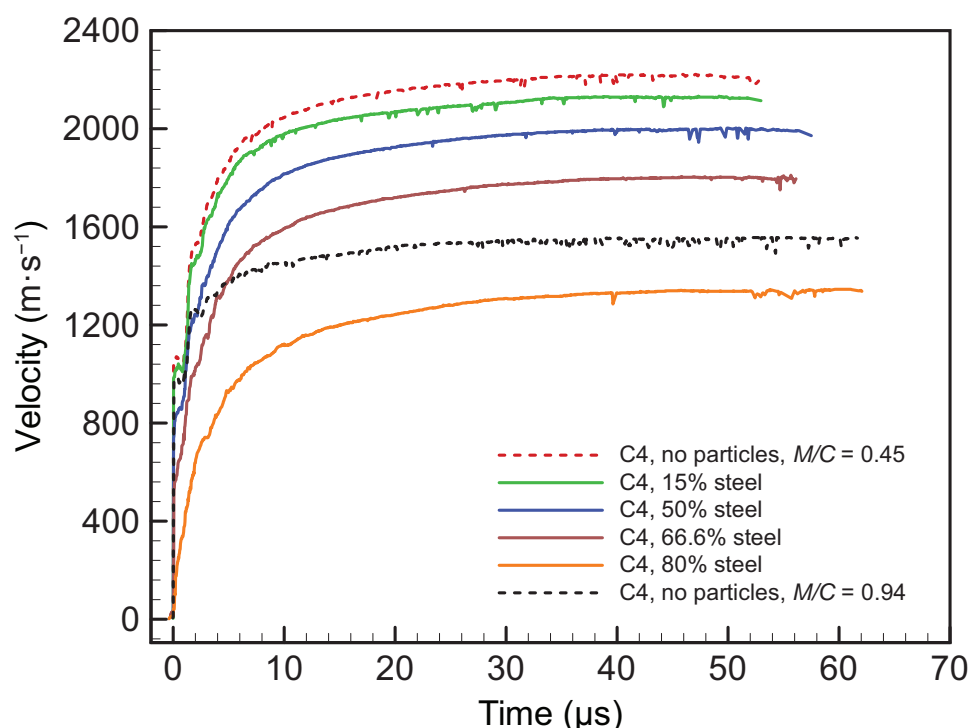


Figure 2.23: Lateral velocity histories for C-4/steel admixture experiments using 6.35-mm-thick aluminium flyers [113]. Charge thickness was 24 mm.

of the nominal value. In the steel admixtures, little density variation was observed until 80% loading, where the density of the explosive phase was reduced by 23% of the nominal value.

For both the steel and glass admixtures, a progressive decrement in flyer velocity was observed when particle loading of the admixture was increased. For the neat C-4 experiments, a sharp shock breakout with an $1100 \text{ m} \cdot \text{s}^{-1}$ material velocity was observed. With progressive increases in particle volume fraction, the magnitude of this shock breakout was reduced. This corresponds with a reduction in the detonation pressure of the explosive and a reduction in the speed of the dragged oblique shock wave. For the highest loading of glass (60%), the shock breakout was nearly eliminated and the detonation was subsonic relative to the flyer sound speed. For the 80% loading with steel, the detonation velocity was also subsonic relative to the flyer sound speed and the shock breakout was entirely suppressed. This resulted in a nearly smooth acceleration similar to what was observed in the diluted nitromethane experiments.

To analyse the metal driving capability of these admixtures, the terminal flyer velocities for all experiments were plotted against the augmented Gurney model (2.9). Because of variations in explosive density throughout the experiments, it was necessary to use spline fits in order

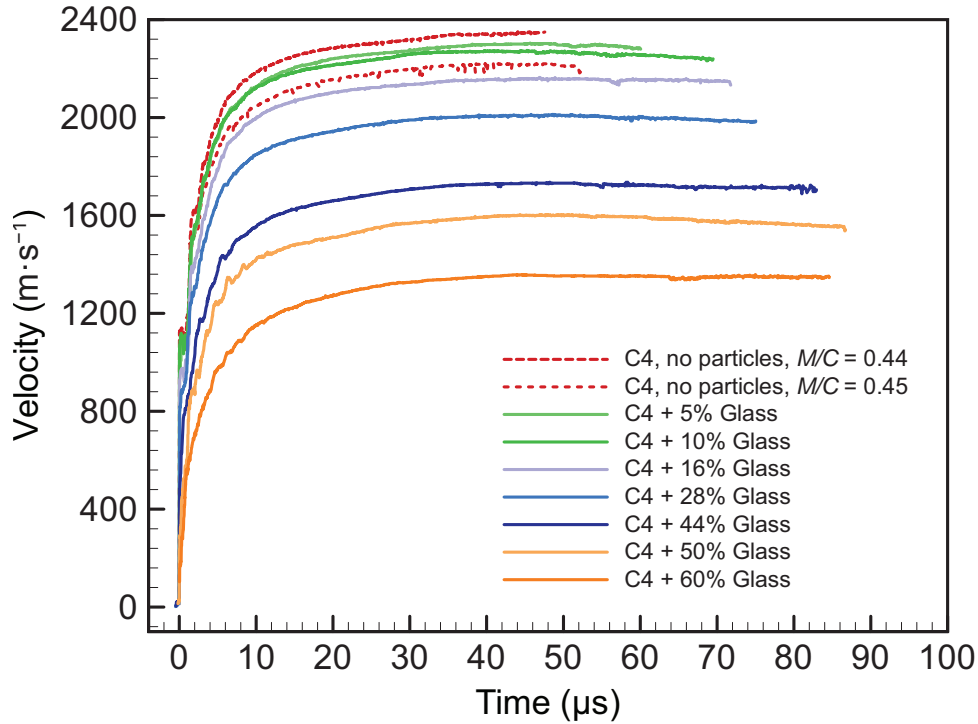


Figure 2.24: Lateral velocity histories for C-4/glass admixture experiments using 6.35-mm-thick aluminium flyers. Charge thickness was 24 mm.

to generate smooth model curves. Splines were fit to the explosive density and variation in explosive mass as a function of M/C as the degree of dilution was increased. These splines were then used to construct the model curves over the range of explosive volume fractions and M/C ratios considered experimentally. Either form of the augmented model (2.9) or (2.13) can be used interchangeably. If (2.13) is used instead, the Gurney energy must be scaled by a spline fit to the experimental mass fraction of particles versus M/C while M/C' is calculated using the entire mass of mixture divided by the charge surface area. This curve is functionally identical to the curve generated using (2.9) when converted and plotted in terms of M/C .

Figure 2.25 shows the augmented model prediction for the steel ($\rho_b = 7.85 \text{ g} \cdot \text{cm}^{-3}$, dashed blue curve) and glass ($\rho_b = 2.5 \text{ g} \cdot \text{cm}^{-3}$, dashed red curve) admixtures versus prediction of the standard Gurney model (black curve) and the experimental neat C-4 data over the charge mass ratios considered. Velocities were normalized by the C-4 Gurney velocity. A critical inconsistency is observed between these curves, particularly for the glass curve. The augmented model curves converge with and then surpass both the standard model and the experimental velocities obtained with C-4 that did not include particles. At these mass ratios, this is clearly

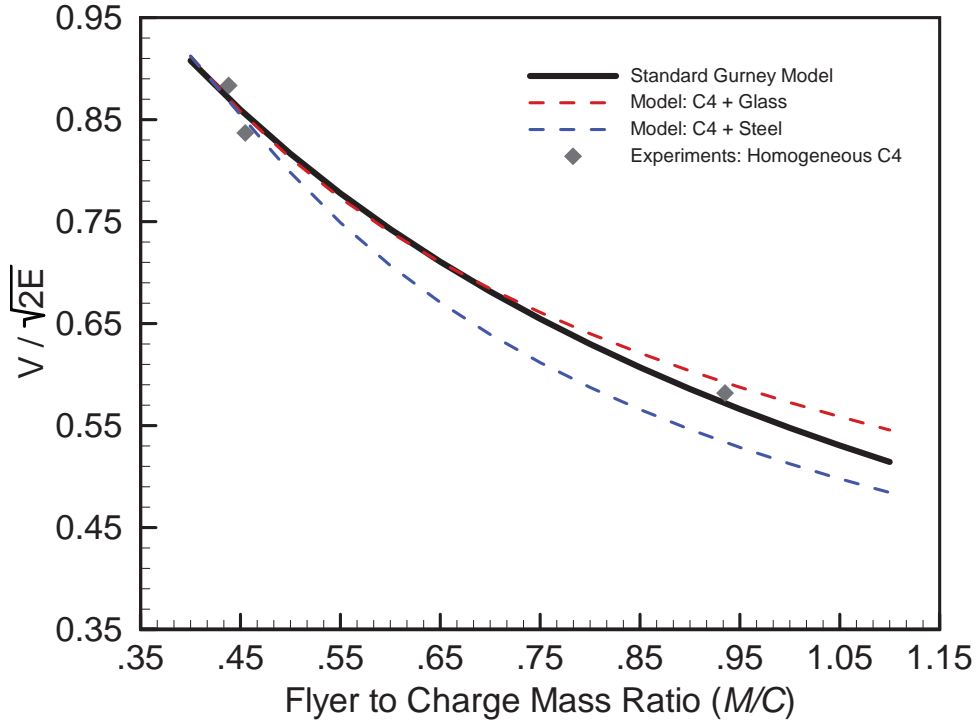


Figure 2.25: Normalized terminal velocity versus M/C as predicted by (2.9) for the steel and glass C-4 admixtures, and by the standard Gurney model for neat C-4. Experimental neat C-4 velocities are included for comparison.

non-physical, as was the case with the glass packed bed results in Section 2.8.4. Since scaling the Gurney energy by diluent mass fraction does not already account for this inconsistency, we postulate that this is another example of a mathematical artefact analogous to the tamped Gurney equation predicting a lower velocity than the untamped equation for certain mass ratios. A second modification to the Gurney model was proposed, where the charge mass ratio was scaled. Since all experiments were un-tamped, N/C can be set to zero, yielding the following Gurney equation:

$$\frac{V_m}{\sqrt{2E}} = \left[\frac{1}{3} \left\{ \frac{1}{\kappa} \left(2\nu \frac{M}{C} \right)^2 + 5\nu \frac{M}{C} + \kappa \right\} \right]^{-\frac{1}{2}} \quad (2.20)$$

We have added the empirical scaling parameter, ν . We subsequently refer to this equation as the *corrected Gurney model*. Reasonable agreement over the range of diluent mass fractions and charge mass ratios was obtained when:

$$\nu = \phi_e \frac{C_{\text{nom}}}{C_e} \quad (2.21)$$

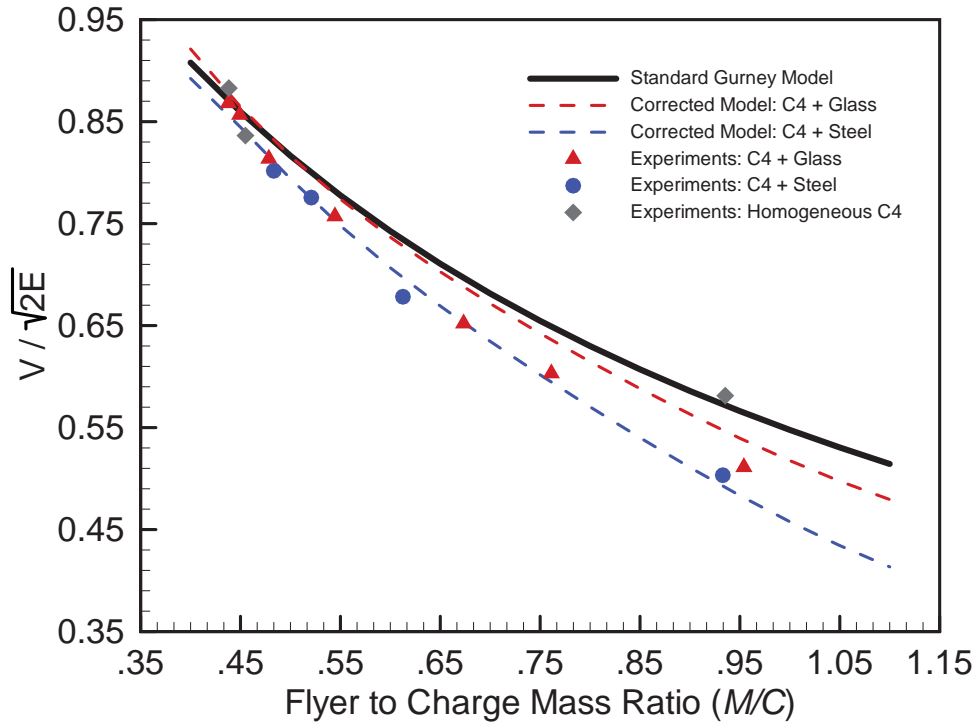


Figure 2.26: Normalized terminal velocities predicted by the corrected Gurney model (2.20) for the steel and glass C-4 admixtures versus the baseline Gurney model and the experimental results.

where C_{nom} is the nominal charge mass at full density and C_e is the actual mass of explosive for a given experiment. C_{nom} represents the mass of explosive that would be contained in the charge if no particles were present and the explosive was packed to maximum density.

Smooth curves were constructed using this newly corrected equation (2.20) and are plotted versus the full experimental data set and the standard, untamped Gurney model in Fig. 2.26. All flyer velocities were normalized by the C-4 Gurney velocity. The corrected model curves now reasonably predict terminal velocities lower than the standard Gurney model, with velocities converging to the baseline as diluent mass fraction is reduced to zero. Agreement for the steel admixtures is quite good, however the corrected glass model over-predicts the glass experiments over the full range of data. The glass data instead follows the steel corrected model. Experimental velocities obtained experimentally for the glass are overall only slightly higher than the velocities obtained with a similar mass of explosive mixed with steel. The model prediction that more explosive energy is lost in having to accelerate a similar volume of heavier material is not fully realized experimentally. This is consistent with the results obtained for packed beds of glass and steel particles saturated with 90/10 NM/DETA (Section 2.8.4). This is postulated

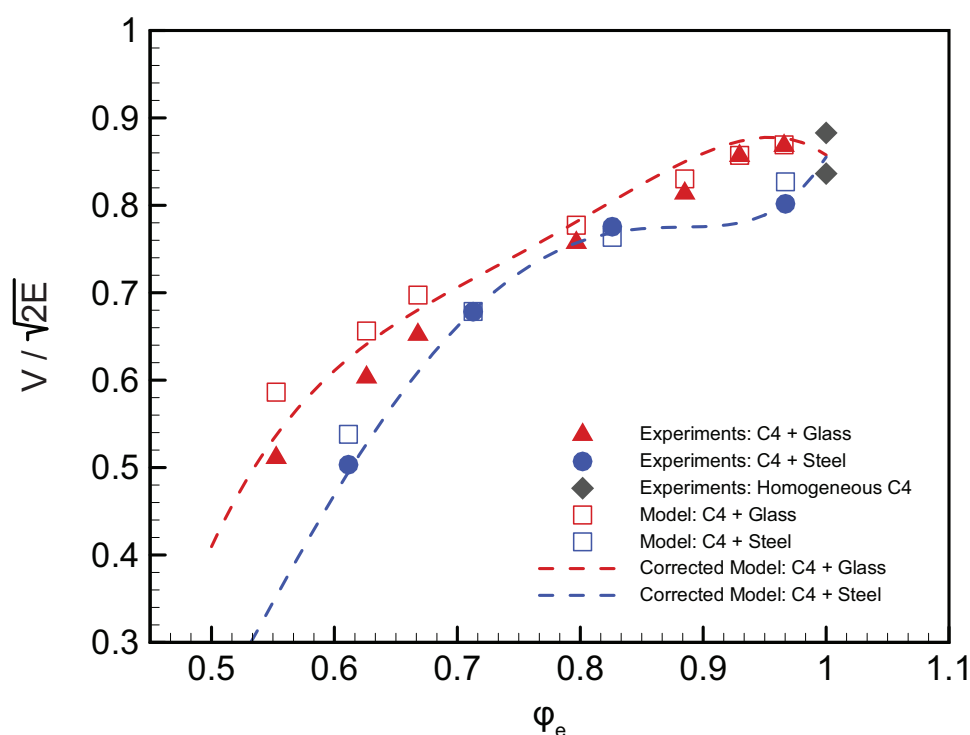


Figure 2.27: Normalized flyer velocities versus explosive volume fraction for the C-4/glass and C-4/steel admixtures. Experimental results are plotted as solid symbols, predictions from the corrected model (2.20) are plotted as dashed lines and predictions from the augmented model (2.9) are plotted as hollow squares.

to occur either from variations in slip between the detonation products and the particles due to their differing areal densities, or because the augmented Gurney model is over-predicting velocities because it crosses over the baseline curve for an equivalent mass of neat explosive at smaller M/C ratios.

Alternatively, the data may be compared against the corrected model by plotting the normalized velocities versus the experimental volume fractions of explosive. This is shown in Fig. 2.27, which plots the normalized flyer terminal velocities versus explosive volume fraction for both the steel and glass experiments. Predictions of the corrected model (2.20) are plotted as dashed lines, experimental data points are plotted as solid symbols and predictions of the augmented model (2.9) are shown as hollow symbols. Oscillations in the curves are due to variations in the explosive density and thus explosive mass. The slightly faster terminal velocities for a given amount of volumetric glass dilution versus steel dilution is more apparent in this format and the corrected model overall reasonably follows the experimental results when plotted on a volume fraction basis.

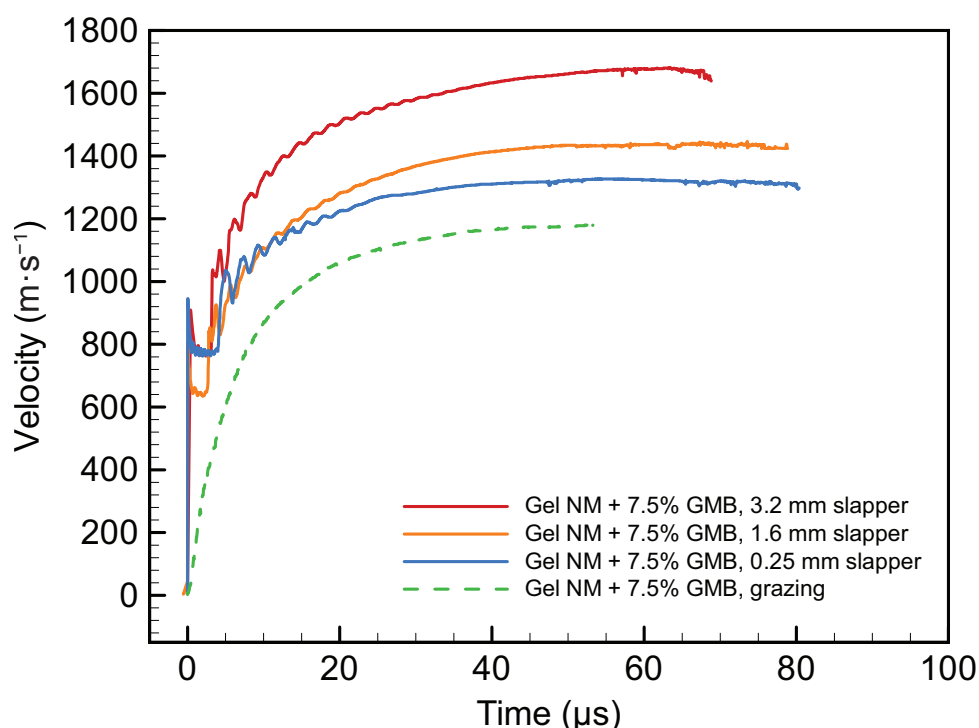


Figure 2.28: Velocity histories of 6.35-mm-thick flyers propelled by mixtures of gelled NM with 7.5% GMB by mass when the charge was initiated by the 3.2-mm-thick, 1.6-mm-thick, and 0.25-mm-thick slappers.

2.9 Effect of Slapper Energy Transfer and Detonation Wave Incidence

Incidence

In this section we consider the effect of slapper energy transfer and detonation wave incidence on the accelerating ability of various explosive/particle admixtures. In Sections 2.8.3 and 2.8.4 it was experimentally shown that flyer terminal velocity when propelled by normally incident detonations is greater than when propelled by grazing detonations for both high and low-density diluents. Further, the degree of increase varied as M/C was changed. In the present section, the effect of varying slapper momentum for different diluent permutations was studied explicitly.

In a set of six experiments, we examined variation in flyer terminal velocity when mixtures of gelled NM with 7.5% GMBs by mass or packed beds of 280 μm steel particles saturated with sensitized NM were impact-initiated with slapper plates of different thicknesses. Slappers with thicknesses of 3.2 mm, 1.6 mm, and 0.25 mm were tested with each mixture. The properties of these slappers are described in Section 2.4.2. The resulting velocity histories for the gel and steel

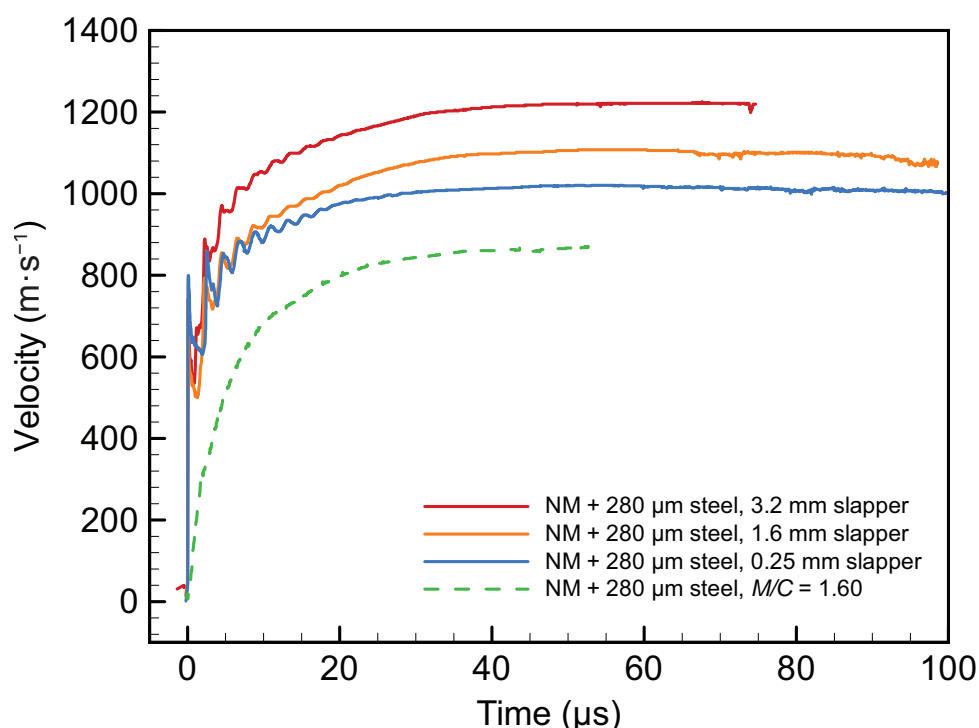


Figure 2.29: Velocity histories of 6.35-mm-thick flyers propelled by packed beds of 280 μm steel saturated with sensitized NM when the charge was initiated by the 3.2-mm-thick, 1.6-mm-thick, and 0.25-mm-thick slappers.

packed beds are shown in Figs. 2.28 and 2.29 respectively. The equivalent grazing experiments are represented by dashed lines in these figures.

For the gel experiments, an initial free surface velocity of $940 \text{ m} \cdot \text{s}^{-1}$ was obtained for all three trials, suggesting that the detonation pressure was consistent and not over-driven in all cases. A small spall plateau was observed in all cases, followed by re-acceleration of the flyers. Compared to the grazing case, the velocity augmentations were 41% at $1679 \text{ m} \cdot \text{s}^{-1}$, 21% at $1437 \text{ m} \cdot \text{s}^{-1}$, and 12% at $1328 \text{ m} \cdot \text{s}^{-1}$ for the 3.2 mm, 1.6 mm, and 0.25 mm slappers, respectively.

For the steel experiments, an initial free surface velocity of $797 \text{ m} \cdot \text{s}^{-1}$, followed by a very short pull-back rather than a distinct spall plateau, was observed. We attribute these effects to a lower relative detonation pressure and the high impedance of the explosive/steel mixture. Again, a similar free surface velocity was obtained throughout the experiments although there are differences in the shape of the pull-back. Compared to the grazing case, the augmentations in velocity were 40% at $1220 \text{ m} \cdot \text{s}^{-1}$, 27% at $1109 \text{ m} \cdot \text{s}^{-1}$, and 17% at $1019 \text{ m} \cdot \text{s}^{-1}$ for the 3.2 mm, 1.6 mm, and 0.25 mm slappers respectively.

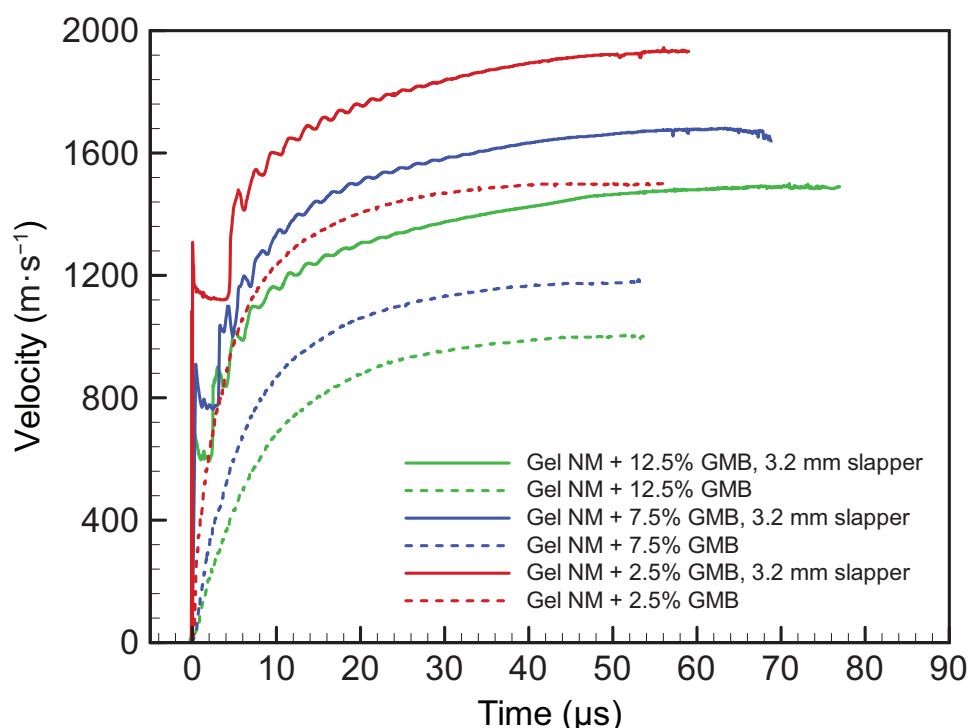


Figure 2.30: Velocity histories of 6.35-mm-thick flyers propelled by mixtures of gelled NM and varying mass fractions of GMBs for both normal and grazing propulsion using 3.2-mm-thick slappers.

Notably, the relative increases for both sets of experiments for each slapper thickness are quite similar. It can be concluded that if heavily overdriven conditions are avoided, and if the flyer is too thick to be partially accelerated by the von Neumann spike, the slapper is effectively acting like a dynamic tamping plate that has some residual momentum that must be overcome when the products expand after impact initiation. Further, based on similar augmentation for both the low-density and high-density diluents, it can be concluded that interactions between the flyer and the solid particles are not a source of energy transfer in the heterogeneous system.

In subsequent experiments initiated with the 3.2-mm-thick slapper, the degree of GMB dilution of the gelled NM was varied, and the particles were changed for the NM-saturated packed beds. Figure 2.30 shows the velocity histories for 6.35-mm-thick flyers propelled by normally incident detonations in gelled NM containing 2.5%, 7.5%, and 12% GMBs by mass compared to the equivalent grazing experiments. The augmentations in velocity were 28% at $1935 \text{ m} \cdot \text{s}^{-1}$, 41% at $1679 \text{ m} \cdot \text{s}^{-1}$, and 47% at $1489 \text{ m} \cdot \text{s}^{-1}$ for the 2.5%, 7.5%, and 12.5% mixtures respectively. Figure 2.31 shows the velocity histories for 6.35-mm-thick flyers propelled by packed beds of steel and glass particles saturated with amine-sensitized NM under both grazing and

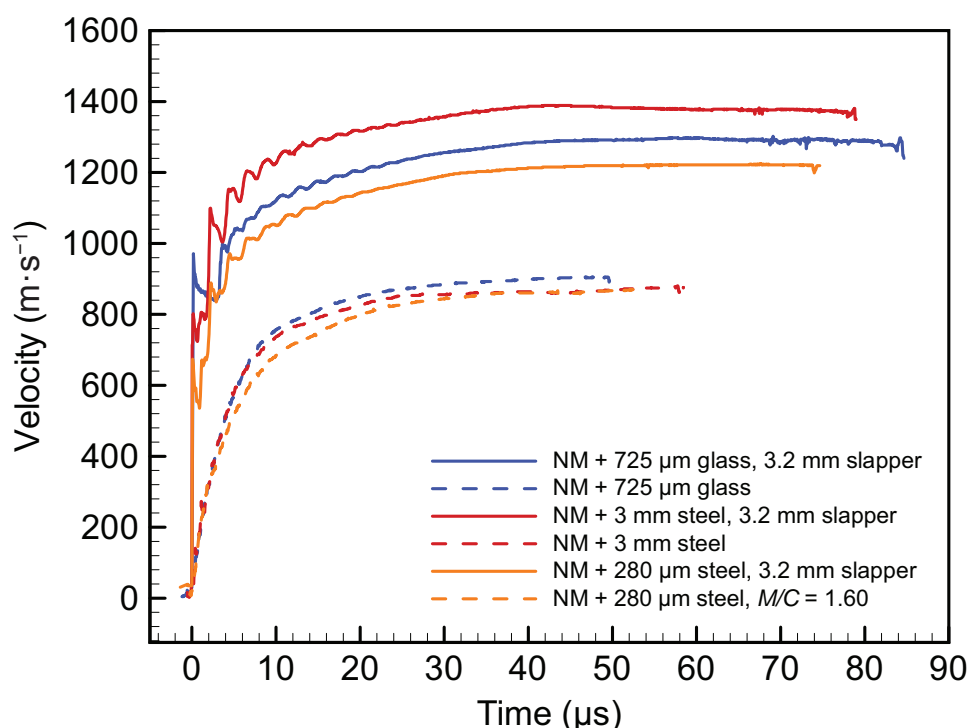


Figure 2.31: Velocity histories of 6.35-mm-thick flyers propelled by NM-saturated packed beds of various dense media for both grazing detonations and normally incident detonations initiated using 3.2-mm-thick slappers.

normal loading. Flyer velocity augmentations were 42% at $1296.5 \text{ m} \cdot \text{s}^{-1}$, 41% at $1221 \text{ m} \cdot \text{s}^{-1}$, and 58% at $1390 \text{ m} \cdot \text{s}^{-1}$ for the $725 \mu\text{m}$ glass, $280 \mu\text{m}$ steel, and the 3 mm steel, respectively.

The increase in flyer velocity augmentation with increasing GMB dilution can be explained by the increase in effective tamping ratio (N/C) as the amount of explosive is reduced via dilution. The anomalous increase in the velocity for the large steel beads can be explained by wavedynamic effects. The very large particle experiment had a high initial shock breakout compared to the smaller particle experiment ($800 \text{ m} \cdot \text{s}^{-1}$ vs. $670 \text{ m} \cdot \text{s}^{-1}$) as well as a much weaker pull-back ($74 \text{ m} \cdot \text{s}^{-1}$ vs. $133 \text{ m} \cdot \text{s}^{-1}$). This likely explains much of the discrepancy in terminal velocity. The clustering of velocity augmentation ratios around 40% for most of the mixtures again suggests that momentum/energy transfer from the particles are not responsible for the majority of the velocity increase relative to the grazing case.

In a final pair of experiments, 19-mm-thick aluminium flyers were propelled via normally incident detonations in saturated packed beds of the $280 \mu\text{m}$ steel and the 3 mm steel using the 3.2-mm-thick slapper for initiation. Here the 3 mm steel system again reached a higher terminal velocity than the $280 \mu\text{m}$ steel system. Augmentations were 44% and 35% for the large particle

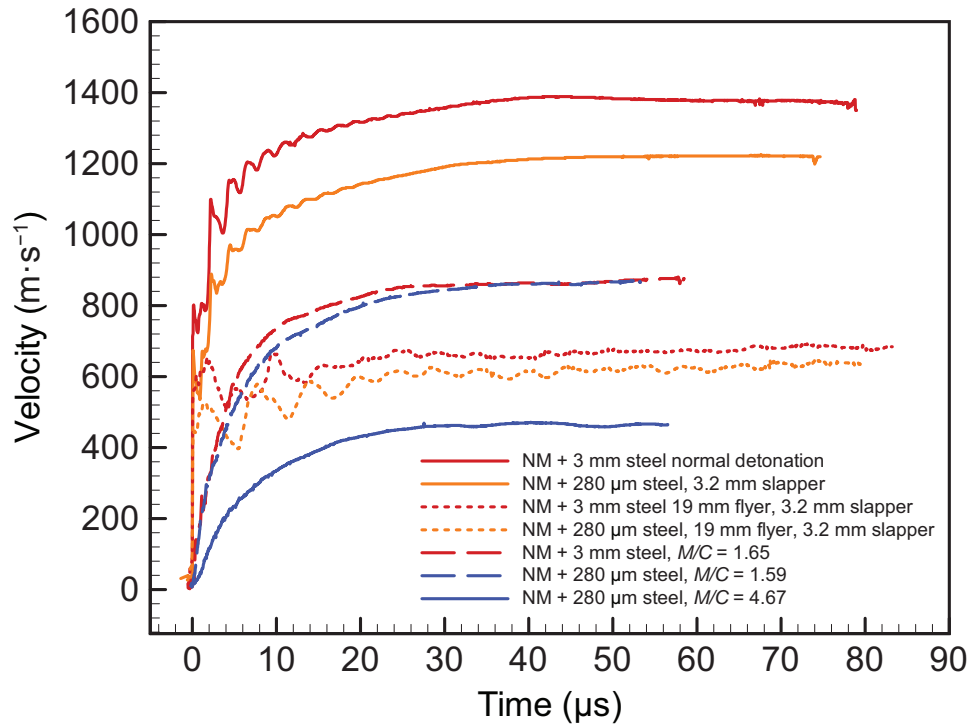


Figure 2.32: Velocity histories of 19-mm-thick flyers propelled by saturated steel packed beds compared to similar experiments.

and small particle, normally initiated experiments over the small particle grazing experiment with a 19-mm-thick flyer.

2.10 Discussion and Conclusion

Throughout the data presented here, four explosive propulsion considerations were examined. First, we measured the decrement in flyer velocity resulting from the progressive addition of diluents to explosives. As the flyer mass was also held fixed, this resulted in a modest variation in M/C as explosive was substituted for inert material. Second, we determined how flyer terminal velocity scaled with M/C for two heterogeneous explosives. Third, we considered the impact of diluent solid density on the reduction in flyer velocity for a given volume fraction of diluent. Finally, we considered how the interaction of a normal detonation wave with a flyer changes how the flyer velocity scales with diluent material properties and M/C .

These variations were generally considered in the context of an augmented Gurney equation that accounts for the presence of a given fraction of inert diluent. The augmented Gurney model has limiting characteristics which explain why it only agrees well within a certain range of

The Propulsive Capability of Explosives Heavily Loaded with Inert Materials

M/C and density ratio of the diluent and explosive. The implemented modifications reduce the effective Gurney energy of the baseline explosive but also increase the effective mass ratio of the explosive (M/C'). As a consequence, the augmented equation predicts a different scaling of flyer velocity with the mass ratio of just the explosive phase (M/C) compared to the baseline Gurney equation. At the asymptotic limit where M/C tends to zero, it predicts a much lower ultimate velocity. At larger values of M/C , it predicts that the heterogeneous mixture will achieve a higher terminal velocity than if the explosive contained in the mixture was used alone to propel the flyer.

A consequence of this model behaviour is that the goodness of the agreement with experiment is conditional on where the experiments fall relative to these two extremes. For very low-density diluents, model predictions are quite good for all ranges of M/C and fraction of diluent because the asymptotic/final metal velocity is not tremendously decremented at small ratio values, and the curve will not cross over the baseline Gurney curve for meaningful large values of M/C . This explains why the model is accurate for the GMB and DETA dilution experiments. Similarly, the model is also quite good at predicting the effect of dilution by dense particulates like steel over a narrow range of intermediate values of M/C .

The model encounters the most problems when it is applied to a material like glass because of how the density ratio of glass to typical explosive densities changes the scaling of the Gurney equation. This problem can be somewhat mitigated by applying an additional correction factor for the ratio of M/C in the augmented model. Similarly, the augmented model fails to predict flyer terminal velocity scaling with M/C for explosives heavily diluted with dense material. This is further complicated by the fact that their experimental propulsive capability scales very differently from a conventional explosive. It was demonstrated that propulsive efficiency of saturated packed bed explosives increases with M/C and can match or slightly exceed the terminal velocity achieved by an equivalent neat quantity of the base explosive. The onset of this phenomenon is well predicted by comparing the augmented Gurney model to the classic Gurney model for the packed-bed system considered experimentally. In general, care must be taken to ensure that predictions of improved accelerating ability are physical as opposed to a model artefact as both situations can be encountered experimentally, as demonstrated by the experimental data in the present study.

Finally, it was demonstrated that normally incident detonations cause departures from classic Gurney scaling due to wavedynamic effects that scale with the physical thickness of the charge and not only M/C . These departures from any form of the Gurney model occur regardless of the type of heterogeneous explosive. In particular, the transmission of von Neumann spike pressure instead of detonation pressure results in a substantial increase in flyer terminal velocity. Effect of the diluent material on terminal velocity was consistent between the normal and grazing experiments as well, indicating that transfer of momentum and energy from the particles to the flyer is negligible for propulsion.

Ultimately, the augmented Gurney model is relatively useful to analyse flyer propulsion for heterogeneous explosive systems. It is particularly well suited to estimating the diluting effect of various binders and reactive additives that may remain inert on metal acceleration timescales in the context of the cylinder test or similar metal propulsion experiments. In such cases, the mass fractions of diluent are typically no greater than 30% and the value of M/C is intermediate.

2.11 Acknowledgements

We would like to thank the personnel who have contributed to the present work: Oren Petel built the PDV system used throughout this study and helped conduct the initial packed bed experiments. Justin Huneault wrote the final iteration of the scripts used to process the raw PDV detector data. A number of undergraduate students helped conduct the experiments: Andrew Milne, David Waknin, Asal Kaveh, Thomas Lee, Fredric Lam, Abtin Ameri, and Marc-Antoine Lavoie. We also thank Rick Guilbeault and Lorne McCauley at the Canadian Explosives Research Laboratory (Natural Resources Canada) for assisting with the C-4 explosive tests.

Chapter 3

Timescale of Aluminium Reaction in Detonation Products Measured via Flyer Plate Experiments

Jason Loiseau, Samuel Goroshin, David L. Frost, Andrew J. Higgins, and Fan Zhang

3.1 Abstract

Explosive acceleration of a symmetric sandwich of metal flyers was used to study the propulsive capability (AA) of gelled nitromethane mixed with atomized aluminium (Al) with various particle sizes. The addition of other reactive metals such as silicon, magnesium, and titanium at 15% mass fraction was also studied. Three flyer plate thicknesses were considered to examine the influence of metal acceleration timescale and charge-mass-scaling on propulsive efficiency. Aluminium was added at 15% mass fraction for particles with diameters of 2 μm , 10 μm , 50 μm , and 95 μm . Additionally, the 50 μm particles were added at 30% mass fraction. Viton-coated nanometric aluminium particles were also tested, but these resulted in poor AA performance. AA was increased for all mixtures containing 15% aluminium, with the 10 μm and 50 μm particles resulting in the best performance. The prompt increase in flyer velocity over the baseline explosive indicated that aluminium reaction begins very close to the detonation sonic plane and

Timescale of Aluminium Reaction in Detonation Products Measured via Flyer Plate Experiments

the concept of ignition delay cannot be defined. Prompt reaction was also observed for the other metals, although AA was poor relative to aluminium.

3.2 Introduction

The addition of reactive metal powders to high explosive (HE) formulations in order to increase the energetic output of the explosion is a well-established practice. Aluminized explosives were first proposed and patented at the turn of the 20th century. Use in military explosives became more common throughout the Second World War in high performance applications such as naval torpedoes and aerial bombs as the cost of atomized aluminium became comparable to other bomb components. In the modern context, aluminized explosive formulations are widely used in military ordnance to maximize air blast impulse or to optimize lethality through a combination of fragment acceleration and enhanced blast output. Aluminium is also used to optimize detonation behaviour and increase the earth-moving capability of blasting explosives.

Despite the extensive history of incorporating reactive metals to increase the performance of explosives, the kinetics/reaction mechanisms, timescale of metal particle reaction, and total energetic output at different timescales remain unresolved from first principles. Formulations are typically developed using a thermochemical code or prior experience as a starting point and then refined based on experimental evaluations to meet particular performance requirements. In principle, metal particles may react on three distinct timescales: within the reaction zone of the base energetic material, thereby contributing to the detonation energy of the explosive; within the detonation products in the first $\sim 100\mu\text{s}$ of expansion, thereby increasing the energy of the detonation products as they expand and increasing the propulsive capability of the explosive; with the detonation products and the ambient air once they exit the product fireball over a period of ms, enhancing the blast output.

The ability to enhance the blast output of explosives by adding large mass fractions ($\sim 20\text{--}50\%$) of aluminium or other reactive metals has been robustly demonstrated. Critical conditions where reactive augmentation fails only exist in the limit where the charge becomes very small and/or very heavily loaded with material such that the particles are insufficiently heated to continue burning once they interact with ambient air. Such conditions are easily avoided for practical formulations. However, the optimization of such mixtures is quite complex, with an

interplay of factors including particle size, particle concentration, interactions with obstacles, jetting and material-dependant combustion dynamics. Such topics are outside of the scope of the present work. Overall, exothermic reaction of a significant portion of the metal content of metallized HEs is a robust phenomenon at ms timescales.

By contrast, there is no well accepted empirical evidence that aluminium particles react sufficiently quickly to influence the detonation energy in ideal explosives. Reaction progress in a condensed phase detonation is extremely fast, such that flow rapidly exits the sonic surface of the detonation wave and can no longer influence the shock front leading the detonation. This timescale is generally considered too short for overcoming the passivating oxide layer and substantial reaction of the metal. That is to say, the aluminium behaves as a chemically inert material from the perspective of influencing detonation pressure and detonation velocity. Decrements in detonation velocity (VOD) and detonation pressure (brisance) with increased fractions of aluminium certainly must have been observed during very early characterisation of TNT-aluminium formulations for military applications. Initially the cause of the VOD deficits was controversial, with disagreement over whether they arose due to compression, heating, and drag on the particles, as with a conventional additive or due to some very-fast endothermic reaction. For instance, Wise observed detonation velocity deficits in TNT-aluminium and postulated it was an inert thermalization effect in 1945 [137]. Similarly, in 1947 Copp reported VOD deficits for TNT-aluminium admixtures and modelled these deficits by considering mechanical compression and heat transfer to the aluminium particles [99]. By contrast Cook reported VOD deficits and shaped charge driving deficits for aluminized TNT and attributed these deficits to endothermicity a decade later [138]. More extensive experimental study of the VOD and detonation pressure of TNT-aluminium admixtures and the availability of computational thermochemical codes ultimately demonstrated that aluminium typically behaves inertly rather than endothermically in the detonation. A summary of this issue as well as experimental detonics results are presented by Price [139]; where an attempt at quantifying VOD deficits with various analytic corrections and thermochemical calculations was made. Extensive study of the effects of aluminium mass fraction, particle size and morphology, and process control on the detonation behaviour of HE-aluminium admixtures has been presented in the literature. A complete review of the detonics references is challenging and outside of the scope of the present study but a summary of some references is included for completeness. Unambiguously, detonation

Timescale of Aluminium Reaction in Detonation Products Measured via Flyer Plate Experiments

velocity is reduced with increasing the mass fraction of aluminium for various explosives (up to 60%) [137, 139, 140]. Decreasing the particle size has been shown to reduce the mixture detonation velocity for TNT compositions by Wise [137] and Price [139]. Trzcinski et al. showed a limited effect of aluminium particle size on the detonation velocity of RDX-Al mixtures [141]. The literature also emphasizes the importance of process control, as a reduction in density of the explosive can dominate the detonation performance of the explosive. For example, Trzcinski et al. demonstrated that flake aluminium results in lower detonation velocities than quasi-spherical particles due to the degree of porosity introduced with the flakes [140]. Similarly high-porosity in alumina inclusions resulted in lower detonation velocities compared to low-porosity mixtures containing aluminium or LiF [141].

It has frequently been anticipated that the large available surface area of nanometre-scale particles ($<1\text{ }\mu\text{m}$) would increase the aluminium reaction rate sufficiently to achieve performance-enhancing exothermicity within the detonation reaction zone. In general, this effect has not been observed experimentally. Brousseau and Anderson reviewed existing literature on explosive formulations containing nanometric aluminium and conducted experiments with TNT, RDX, and ANFO [142]. They observed that the use of nanometric aluminium did not increase the detonation velocity for RDX or ANFO, but measurably increased the detonation velocity for TNT compared to mixtures containing micron-scale aluminium particles. TNT/nano-Al still demonstrated lower detonation velocities relative to homogeneous TNT. By contrast Baudin et al. observed a reduction in detonation velocity for TNT mixtures with their candidate nano-scale particles compared to $5\text{ }\mu\text{m}$ particles during cylinder test experiments [143]. Similarly, Lefrancois et al. reported that reducing particle size to the nanometric scale did not increase the detonation velocity or reduce the reaction zone thickness based on detonation time of arrival and front curvature measurements [144]. Gogulya et al. also demonstrated that nanometric aluminium particles resulted in lower detonation velocities than micron-scale particles, particularly for HMX formulations [145]. This decrease was quite precipitous relative to the modest effect of particle size beyond $20\text{ }\mu\text{m}$. However, they did observe that for positive oxygen balance explosives (BTNEN) the decrement was smaller than for negative oxygen balance explosives. Davydov and Gubin have argued that some nanometric aluminium reacts in the detonation reaction zone in order to explain the decrease in detonation velocity of mixtures containing nanometric aluminium compared to micron-scale aluminium; reaction of some aluminium would

produce oxides that would then thermalize in the reaction zone, thereby reducing detonation energy [146]. Exothermic aluminium reaction does not therefore imply a net increase in the energetics on detonation timescales. Miller et al. studied the effect of varying aluminium particle size from 60 μm to 3 μm and then to 150 nm and 50 nm on the detonation of velocity of Ammonium dinitramide (ADN) containing 20% aluminium by mass [147]. They observed no effect or a slight reduction ($\approx 300 \text{ m} \cdot \text{s}^{-1}$) of detonation velocity for the micron-scale particles but observed an increase from $\approx 4 \text{ km} \cdot \text{s}^{-1}$ to $\approx 5 \text{ km} \cdot \text{s}^{-1}$ for the 150 nm particles and then to 6.0–6.6 $\text{km} \cdot \text{s}^{-1}$ with the 50 nm particles. They observed no effect on detonation when various sizes of aluminium were mixed with HMX or CL-20. Overall, it should be concluded that aluminium produced by current powder metallurgy, regardless of particle size, does not display sufficient or prompt exothermicity to positively contribute to the detonation of typical high explosives with thin reaction zones and high detonation velocities ($> 6 \text{ km} \cdot \text{s}^{-1}$). Lack of robust increases in detonation velocity with nano-scale particles in ANFO further support the lack of net-exothermicity within the detonation reaction zone. VOD enhancements using nano-particles in TNT mixtures reported by Brousseau [142] and ADN mixtures reported by Miller [147] are thus important outliers.

Ultimately, it is the anaerobic reaction of aluminium with the detonation products during early expansion (7–10 relative volumes) that has generated the most debate. The relative performance of aluminized explosives in this regime is generally characterized by their ability to accelerate metal. The reaction of the aluminium at this stage is also phenomenologically complex, involving a mechanism for very rapidly by-passing the passivating oxide or engineering coating, and whether the particle burns with a diffusion-limited radial flame profile or kinetically with a film layer being continuously stripped off by high-speed flow. The degree of exothermicity is also heavily dependant on the thermochemistry of each individual composition with explosive-phase oxygen balance and interactions with energetic or inert binders playing important roles. The reaction of aluminium may also modify the total number of moles of gas produced and thereby diminish metal-pushing capability despite reacting exothermically. There are thus two primary considerations: can the aluminium react with the detonation products in a sufficiently short timescale to increase the anaerobic work-doing capability of the explosive, and is the overall reaction sufficiently exothermic and sufficiently complete to more than compensate for the

Timescale of Aluminium Reaction in Detonation Products Measured via Flyer Plate Experiments

reduction in mass of explosive component, potential reductions in gaseous product generation, and energetic losses to accelerating and heating the particles?

There is a breadth of early experimental evidence suggesting that micron-scale or smaller aluminium particles will begin to react anaerobically in the detonation products close behind the sonic plane of the detonation reaction zone. These studies included both metal-driving experiments as well as detonics experiments. The first metal-driving study was conducted by Kury et al. using the copper cylinder tests for a wide variety of HMX/Viton-based formulations containing 5 μm aluminium particles, and optionally ammonium perchlorate or potassium perchlorate [111]. Results were compared to RUBY thermochemical code predictions of cylinder velocity versus relative product expansion. Based on the velocity history of the cylinder walls, they ascertained that sufficiently small aluminium particles can begin to react within $\lesssim 4 \mu\text{s}$ after the passage of the detonation. They also estimated that approximately 50% of the aluminium reacted within the first 20 μs of production expansion. Larger particles of the other perchlorate fuels/oxidisers displayed slower reaction rates, although complete reaction over the timescale of the cylinder expansion was achieved with small potassium perchlorate particles. Kury et al. ultimately concluded that reactive materials could react sufficiently quickly to positively increase the work done by detonation products driving closely-coupled metal, but that the overall performance was not measurably increased over the base explosive. They also observed a form of critical condition, where initial wall acceleration was slower than for the base explosive but similar terminal velocities were reached due to the later-time energy release from the additives. Finally, they showed that experimental results can be bracketed by thermochemical calculations assuming 100% additive reaction and 0% additive reaction.

More recent works considering metal acceleration have largely presented similar findings and have focused on binder optimization, particle size and novel explosives. As with detonation performance, nanometric particles have been anticipated to increase metal accelerating performance. Makhov et. al. studied the effect of aluminium particle size on the metal driving capability of HMX, nitroguanidine (NG), and Bis(trinitroethyl)nitroamine (BTNEN) using both flyer plates accelerated by normally incident detonations (end-on) and grazing detonations in copper cylinders [148]. They observed a net increase in the terminal velocity of the driven metal over the base explosive for all configurations and explosives studied for aluminium particle sizes below 150 μm ; larger particles only broken even or resulted in lower terminal metal

velocities. For all formulations, reducing particle size increased terminal flyer velocity through the range of micron-scale particles considered, however, the use of ultra-fine sub-micrometer particles did not result in higher metal velocities compared to small, micron-scale particles. These observations were explained by the postulate that reducing particle size through the micron range increased reactivity due to an increase in surface area but that these increases were offset at the sub-micron scale by substantial increases in the relative fraction of passivating oxide content. The maximum augmentations in metal velocity were quite small ($\approx 5\%$) and were obtained with BTNEN. Notably, oxygen balance was a poor indicator of relative performance increase from aluminium addition as both NG and HMX displayed similar increases despite the poorer balance of NG. Similarly, Davydov and Gubin argued that metal acceleration ability is determined by the atomicity of the detonation products, advantaging hydrogen-free, oxygen deficient explosives relative to CHNO explosives [149]. They demonstrated a maximum 4% increase in the metal driving capability by aluminizing HMX, and a maximum of 8% for BTNEN. In a separate paper, Davydov and Gubin measured the effect of activating alloying elements on the propulsive effectiveness of HMX and BTNEN [146]. They found that activation and ultra-fine particles did not increase the propulsive efficiency compared to the base explosive despite increasing the calorimetric output. Miller et al. also tested the propulsion efficiency of their ADN/aluminium/viton mixtures (74/23/3) as well as HMX/aluminium/viton (75/20/5) mixtures using plates propelled off the end of a short cylindrical charge. They observed a peak flyer velocity enhancement of 15% with 3 μm particles, 9% with 150 nm particles, and no enhancement with the 60 μm particles. They observed no propulsive enhancement for the HMX mixtures regardless of the size or type of particle used. Baudin et al. did not observe an improvement in the propulsive capability of TNT mixed with nano-particles over mixtures containing 5 μm particles [143]. However, Lefrancois et al. did observe modest metal pushing enhancement for RDX mixed with 5 μm particles and no benefit of using nano-scale particles due to the quantity of oxide present in the powder [144]. Similarly, Manner et al. conducted cylinder test experiments for cast HMX containing Valimet H-2 aluminium or LiF (69% HMX, 15% additive, 15% binder) and demonstrated a robust increase in wall velocity of approximately 13% for the aluminized experiment compared to the experiment with LiF within 2 μs of the passage of the detonation; wall velocity further increased at later times [150]. By contrast, Rumchik observed a net decrease in explosive Gurney energy for all tested aluminized RDX mixtures [1].

Timescale of Aluminium Reaction in Detonation Products Measured via Flyer Plate Experiments

This suggests that powder metallurgy, binder formulation, and explosive processing are critical factors governing propulsive efficiency of aluminized explosives. Anderson et al. concluded for instance that binder selection was the primary factor determining promptness of aluminium reaction [151]. Tappan et al. conducted sub-scale cylinder tests with benzotrifuroxane (BTF) and hydrazinium nitrate/hydrazine (HzMN/Hz) mixed with 15% aluminium and 15% LiF. BTF is hydrogen free, leading to CO_2 being the only detonation product that can meaningfully oxidize the aluminium. By contrast HzMN/Hz is carbon free, such that H_2O becomes the primary oxidizer of the metal for those mixtures. In both cases, cylinder wall velocity exceeded the inert LiF mixture after 1 μs . Superior performance increase was observed in the BTF experiments, with aluminium reaction going approximately to completion prior to wall rupture. It was further claimed that the aluminium reacted within the BFT detonation zone owing to the prompt net exothermicity, front curvature, and rapid formation of CO at the expense of CO_2 from thermochemical calculations; the authors thus argued that detonation velocity is insufficient to quantify aluminium reactivity in the detonation. This is similar to what was argued by Davydov and Gubin [146]. By contrast reaction of aluminium was deemed much slower with water in the case of HzMN/Hz and did not go to completion prior to wall rupture.

Detonics experiments have similarly demonstrated prompt reaction of aluminium particles. Gogulya et al. used optical pyrometry and a material with pressure-dependent opacity to measure the reaction timescale and approximate detonation temperature and pressure profiles for HMX mixed with varying sizes and mass fractions of aluminium [152]. They observed that detonation pressure was lower than the HMX baseline for all mixtures regardless of mass fraction but that the pressure decayed slower than the HMX baseline. Similarly, they observed that temperature was similar to the baseline HMX and measurably higher than an equivalent inert admixture containing similar fractions of LiF. These results were interpreted to indicate that onset of particle reaction occurs at the detonation sonic plane, but that the small extent of reaction only offsets detonation energy losses from heating and accelerating the particles. Enhanced reaction, manifesting as a double peak in the pressure profile, was noted for ultra-fine (500 nm) particles. Similarly, Lubyatinsky and Loboiko used the same optical window technique to demonstrate that RDX containing up to 19% by weight of aluminium displays very prompt reactivity, comparable to TNT when mixed with RDX [153]. Finally, Lefrancois et al. studied the detonation structure of AN emulsion explosive using pyrometry and carbon

film gauges and observed aluminium reaction within 5 μs of detonation as well as a two-peak luminance-temperature structure associate with initial heat transfer to “cold” particles followed by energy release due to surface reaction of the particles [154].

A number of studies have been conducted using nitromethane or gelled nitromethane admixed with reactive particles as opposed to more conventional solid crystalline explosives. Liquid/gelled nitromethane is an attractive model system since heterogeneous mixtures containing dispersed solid particles can be prepared via simple mixing techniques, thereby limiting many of the processing challenges involved with preparing binder-based or melt-cast solid explosives. Unlike with casting or pressing, the porosity and uniformity of the gelled system can be controlled by varying mixture rheology so that particles disperse easily and entrained air can escape, but the particles then remain in suspension during filling and firing of the charge. Liquid nitromethane can also be loaded to the limits of a packed bed, an extreme loading condition unreachable with castable or pressed explosives. Finally, as a homogeneous liquid explosive, it avoids the possibility of interplay between explosive grain size and reactive particle sizes. Numerous studies have examined the detonation behaviour of nitromethane liquids and gels containing inert and reactive particles [90, 91, 135, 141, 155]. Fewer studies have focused on the propulsive capabilities of aluminized NM. Baudin et al. studied the propulsive effectiveness of nitromethane gelled with 3% poly(methyl methacrylate) (PMMA) and then mixed with 20% and 40% mass fractions of 5 μm and various types of ≈ 100 nm nano-particles using the cylinder test [143]. They observed an increase in propulsive efficiency over the baseline explosive within ≈ 5 μs after the onset of cylinder motion for the 20% admixture for all but one nano-particle mixture. Enhancement was modest and there was no performance increase for the nano-powders relative to the micron-scale powder. Milne et al. conducted copper cylinder tests with nitromethane thickened with 5% polyethylene oxide and mixed with either 5 μm or 10.5 μm aluminium particles with mass fractions varying from 20% to 60% [156]. They observed a net decrease in propulsive capability as more aluminium was added and that the 5 μm particles fully reacted in 50 μs , whereas the 10.5 μm particles reacted over substantially longer timescales and thus demonstrated reduced propulsive efficiency. Milne fitted hydrocode simulations to their CYLEX data to determine a burn time of the particles varying from 50 μs to 220 μs , depending on the size of the particle. By contrast, and more in-line with the Baudin et al results [143], Trzciński et al. observed a net increase in propulsive efficiency with the addition

Timescale of Aluminium Reaction in Detonation Products Measured via Flyer Plate Experiments

of 15% aluminium-magnesium powder to a nitromethane gel containing 4% PMMA in cylinder test experiments. Notably, they also observed a critical behaviour where a 30% addition of Al-Mg powder resulted in an initially slower overall acceleration but ultimately resulted in higher terminal cylinder wall velocities due to particle reaction.

Several nitromethane studies have specifically focused on determining a so-called “ignition delay” between the passage of the detonation front and some form of bulk burning of the aluminium particles. Kato et al. demonstrated a ignition delay time of 2.5 μs after the detonation in cylindrical packed beds of 8 μm aluminium particles saturated with liquid nitromethane [157]. Zhang et al. measured a delay of 13–18 μs for unconfined cylinders of packed beds of 13 μm particles saturated with liquid nitromethane [158]. Frost et al. observed the largest delay of 50 μs for 42–84 μm particles [159]. The existence of such a delay in the onset of reaction for particles larger than $\approx 20 \mu\text{m}$ in nitromethane detonation products would imply an inert, non-enhancing behaviour for all but the smallest particles for many configurations of metal acceleration where the metal is driven to terminal velocity within 20 μs , such as sub-scale CYLEX experiments (see Manner et al. [150] and Tappan et al. [160]).

Given the complexity and often contradictory findings presented in the breadth of the literature, a brief summary to contextualize the motivation of the present study is in order. Overall, it is fairly clear that in the majority of explosive formulations, even nano-scale aluminium particles cannot react with sufficient rate and energetic yield to offset the volumetric loss of energetic material in addition to parasitic losses from accelerating, heating, and deforming particles in the detonation reaction zone. By consequence, aluminium addition is generally a net loss in terms of detonation energy and detonation velocity. We again note the exceptions reported for TNT by Brousseau [142] and for BTF by Tappan [160]. By contrast, based on luminosity, gauge, and metal propulsion experiments it is readily clear that the onset of particle reaction occurs no later than the detonation sonic plane, observations potentially incompatible with the claims of long ignition delays in nitromethane packed beds. Metal-pushing experiments are also a fundamentally indirect means of assessing particle reactivity. Metal velocity will only begin to deviate either from the baseline neat explosive or an explosive containing a representative mass of inert analogue once the particle reaction has delivered sufficient energy to more than compensate for detonation product energy losses incurred from heating and accelerating the reactive particles in the first place. That is to say, the point at which the metal velocity for the reactive case exceeds

the neat or inert case is a break-even point, or reaching net-exothermicity, and necessarily occurs some (brief) time after the particles start to react. In the general case, whether an aluminized formulation exceeds the metal pushing capability of its base explosive depends on whether the particles react at a sufficient rate to approach complete reaction over experimental timescales such that the total energy delivered to the products exceeds the entrainment and heating losses combined with the gas production and energetic deficits from displacing high explosive. These factors are controlled by the fraction and size of the reactive particles. Of equal importance are the oxidation paths (CO_2 , H_2O other) and how these are modified by the thermochemistry of the base explosive and included binder or processing agent (thickening/gelling, emulsifying). The net result is that aluminium contributes either a small propulsive boost ($\approx 15\%$) or none at all depending on the formulation and the selected particles.

Since performance enhancement is determined by the net amount of energy delivered as well as the rate of delivery, we wanted to investigate the role of particle size and mass fraction in an explosive system that has displayed robust performance increases with added metal, namely nitromethane gelled with poly(methyl methacrylate) (PMMA). To further investigate the effect of reaction rate, we considered multiple charge scales using metal confinement of widely varying areal density to determine whether the timescale of product expansion influenced the observed propulsive efficiency of the explosive: Thinner confining metal will reach relative volumes of product expansion where driving pressure exponentially decays much more quickly than thick/massive confinement, and thus less aluminium may have time to react. This scaling variation is especially relevant to ascertain the existence of a particle ignition delay by driving metal over short timescales with explosives containing large, $\approx 100\text{ }\mu\text{m}$ particles. Finally, we wished to examine if rapid metal reaction is a robust phenomenon, not restricted to just aluminium. We thus conducted a subset of experiments adding silicon, magnesium, and titanium particles to gelled nitromethane.

3.3 Charge Design

Metal acceleration by explosives is typically studied using the copper cylinder test, wherein a precision-machined copper cylinder of a scaled thickness-to-diameter ratio is accelerated by a steady-state, axial detonation [66, 78]. The acceleration of a thin steel plate off the end of a

Timescale of Aluminium Reaction in Detonation Products Measured via Flyer Plate Experiments

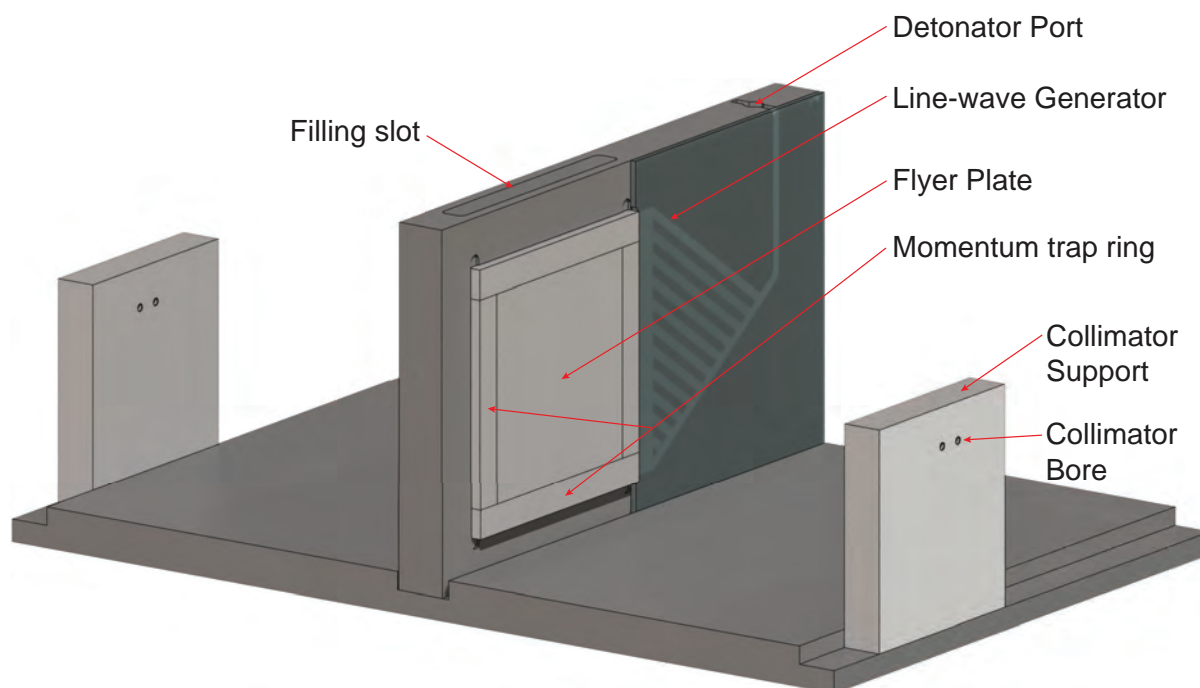


Figure 3.1: Depiction of the symmetric charge geometry used.

charge (M-40 method) has also frequently been used in the previously reviewed Russian literature [149].

In the current study, we have chosen to measure metal acceleration using symmetric sandwiches of aluminium plates propelled by a grazing or sliding detonation. The use of planar flyer plates to measure the propulsive capability of explosives was demonstrated by the authors in previous studies using asymmetric flyer configurations [9, 161]. The use of planar flyer plates is advantageous as it allows for the simple variation of flyer thickness in order to vary the ratio of flyer-plate mass to explosive-charge mass (M/C) compared to cylinders. The grazing detonation configuration also permits the use of thick flyer plates to examine large values of M/C . This variable configuration is thus useful to study if mass-ratio scaling and product expansion timescale influence the propulsive efficiency of aluminized explosives. A symmetric sandwich was used so that a product expansion ratio can be meaningfully defined based on the velocity history of the flyer plates. By contrast, in the case of an asymmetric sandwich, free expansion from the unconfined surface of the charge makes definition of a product expansion ratio unquantifiable from a single velocimetry measurement.

One factor limiting the symmetric slab system is that acceleration of the flyer plates is not fully one-dimensional due to lateral expansion off of the charge edges; the experimental

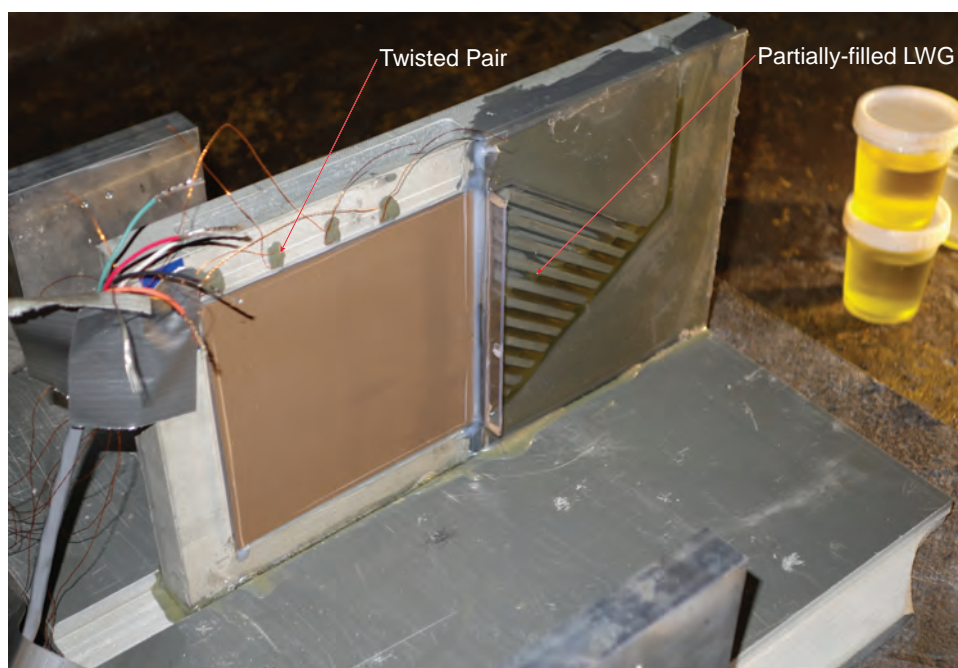


Figure 3.2: Charge with twisted pairs and partially filled LWG.

time over which detonation product expansion at the charge centerline can be considered one-dimensional is thus limited by the propagation of rarefaction waves towards the centre. In preceding papers the authors have demonstrated that representative metal terminal velocities can be reached by using a flyer with sufficient lateral extent combined with a mechanically decoupled ring around the main flyer. These design features have been preserved for the current set of experiments. The flyers were 10.16 cm square in extent and were surrounded by four metal strips of equal thickness and a width of 13 mm. These strips were assembled around the flyer by gluing all five pieces to a 0.2-mm-thick Mylar sheet with a thin layer of epoxy. Flyer thicknesses of 12.7 mm, 6.35 mm, and 0.3 mm were used. In the case of the 0.3-mm-thick flyers, the metal strips and Mylar were omitted.

The charge configuration used for the present study is depicted in Figures 3.1 and 3.2. A rectangular PVC frame was used to hold the two flyer plate assemblies and contain the test explosive. The frame was also machined with a line-wave generator (LWG) to initiate a planar detonation through the width and thickness of the explosive sample. The LWG was covered with a layer of clear PVC, while the two flyer plates retained the test explosive. The LWG was filled with amine-sensitized liquid nitromethane (90% NM, 10% diethylenetriamine). The sensitized NM was segregated from the test explosive with a 1.5 mm PVC buffer that permitted

Timescale of Aluminium Reaction in Detonation Products Measured via Flyer Plate Experiments

transmission of the detonation. The test explosive was poured into the charge cavity via a large slot at the top of the PVC frame. The charge was filled to the top of the slot and an array of twisted wire pairs were inserted into the frame, along the top of one flyer plate, to measure explosive detonation velocity.

A square PVC base with three milled slots was used to hold the explosive frame vertically and align two optical supports that housed collimators in-line with the flyer plates. These collimators were connected to a Photonic Doppler Velocimeter (PDV) to generate time-resolved measurements of flyer velocity. The collimator beams were aligned normal to the initial surface of the flyers and thus only measure the lateral component of metal velocity because of intrinsic properties of the device [74]. Due to the grazing-detonation propulsion, the flyer is propelled at some angle from its initial position and its motion is comprised of both a primary lateral velocity component and a small forward component. The total metal velocity is thus related to the velocity measured by the probe, the launch angle of the flyer, and the detonation velocity of the explosive with the following two equations:

$$V_m = 2D \sin\left(\frac{\theta}{2}\right) \quad (3.1)$$

$$V_{pdv} = V_m \cos\left(\frac{\theta}{2}\right) \quad (3.2)$$

Equation 3.1 is Taylor’s classic equation for the launch angle of a tubular bomb [5, 21]. Equation 3.2 arises from simple trigonometry relating the orientation of the total metal velocity vector from Taylor’s model to the orientation of the normal laser beam. V_{pdv} is the terminal velocity recorded by the normally oriented probe, θ is the terminal flight angle of the flyer (Taylor angle), V_m is the calculated total metal velocity. These relations have been validated by the present authors [9, 161] and Souers et. al. [22].

3.4 Mixture Preparation and Properties

The gelled nitromethane used in the current study was prepared by dissolving 4% poly(methyl methacrylate) (PMMA) by mass into a container of ACS reagent grade nitromethane ($\geq 95\%$, Sigma-Aldrich 360554). We emphasize that using large chunks ($\approx 1 \text{ cm}^3$) of cast PMMA is

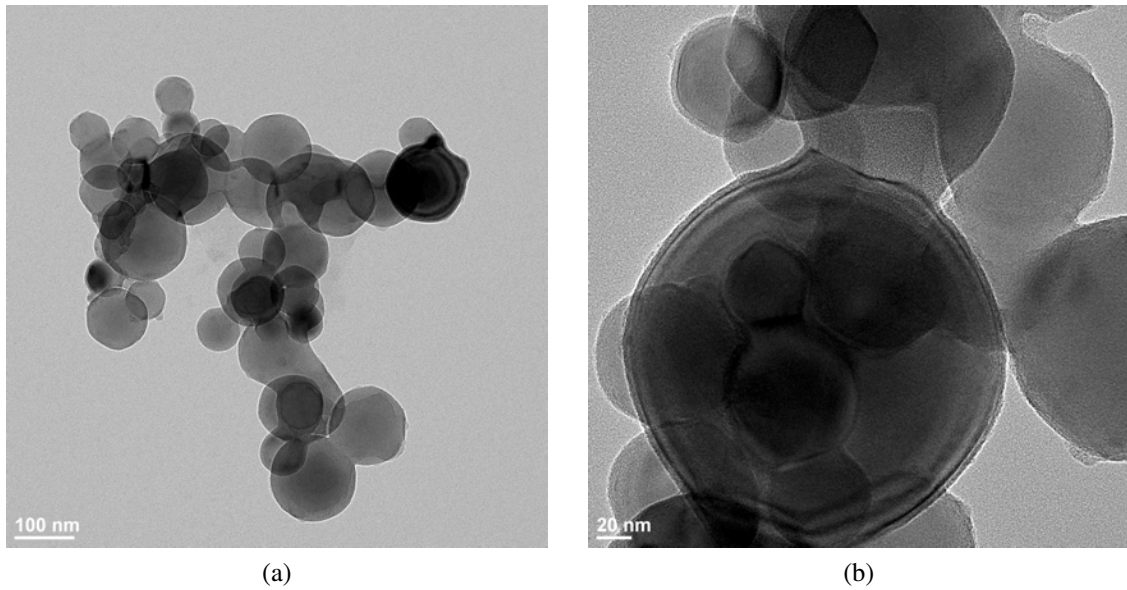


Figure 3.3: Micrographs of the Viton coated, nano-scale aluminium showing the structure of micron-scale agglomerates. TEMs were provided from work done by Trowell et al. [162].

essential in obtaining a high viscosity gel; extruded PMMA or powdered PMMA will not appropriately increase viscosity. Cast, optically-clear acrylic was sourced from McMaster-Carr for the present study: P/N 8560K266, Series 8560K999.

Neat gelled nitromethane is not readily detonable and has a large critical diameter ($d_c \approx 25$ mm), so the baseline explosive was formulated by sensitizing the gel via the addition of a small fraction of 3M K1 glass microballoons, which are chemically inert, but generate hotspots [89, 163]. A mass fraction of 0.5% GMBs was added to the gelled NM, improving sensitivity without eliminating a large volume fraction of explosive in the mixture [89]. Based on the data presented by Presles et al., critical diameter for this mixture is approximately 14 mm, and thus has a critical thickness ($\approx 0.5d_c$) well below the present charge width for metal confinement [89]. The addition of varying mass fractions of dispersed aluminium will further sensitize the mixture, resulting in up to a tenfold decrease in d_c over the base, unsensitized explosive [141, 155, 164].

Various mean sizes of aluminium particles were added to the base explosive mixture at a mass fraction of 15%. Micron-scale powders were sourced from Valimet; tests were conducted using batches of H-95 ($d_{0.5} = 108 \mu\text{m}$), H-50 ($d_{0.5} = 55 \mu\text{m}$), H-10 ($d_{0.5} = 12 \mu\text{m}$), and H-2 ($d_{0.5} = 3.5 \mu\text{m}$) powders. H-50 was also added at a mass fraction of 30% in select experiments. A nano-scale powder (V-ALEX) was also tested at 15% that had a mean diameter ($d_{0.5}$) of

Timescale of Aluminium Reaction in Detonation Products Measured via Flyer Plate Experiments

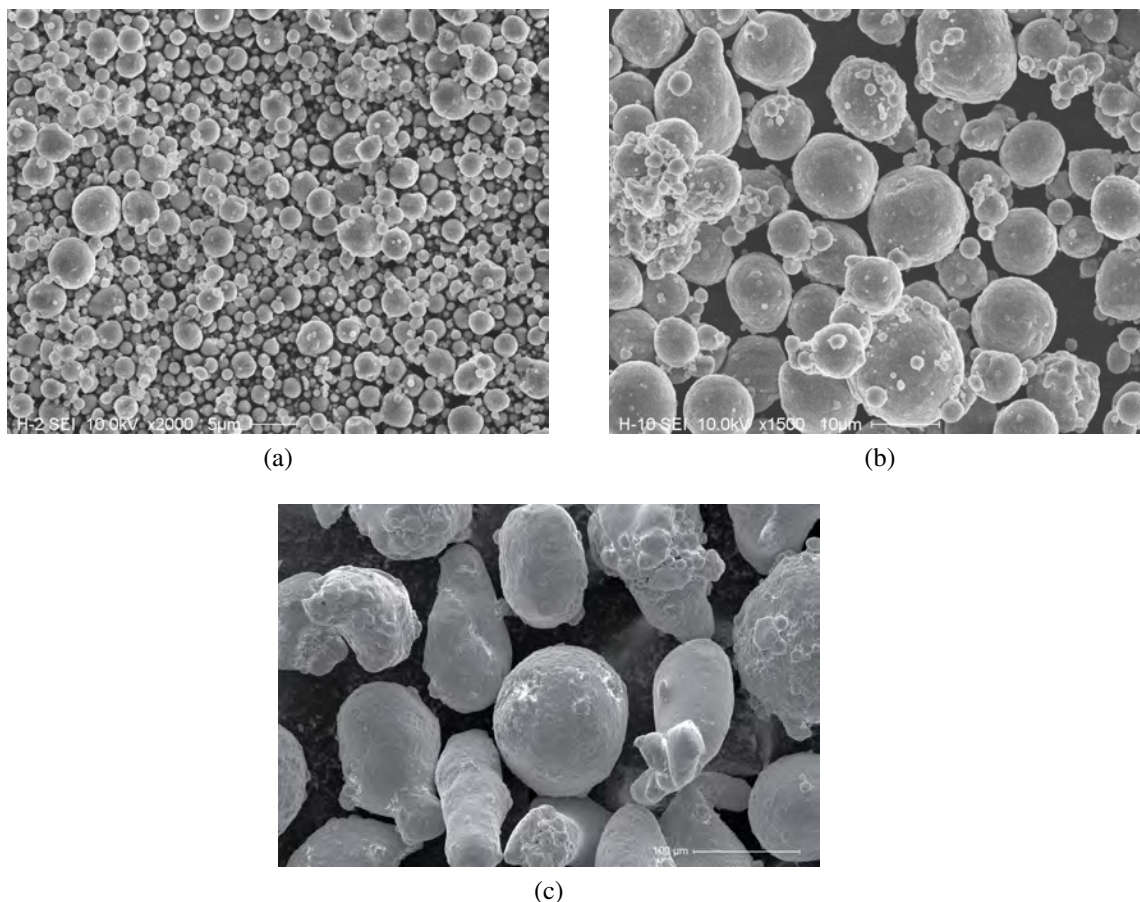


Figure 3.4: Micrographs of the Valimet **(a)** H-2, **(b)** H-10, and **(c)** H-95 aluminium powders.

120 nm and was coated with the fluoroelastomer, Viton during production, eliminating the large fraction of passivating oxide that typically forms on nano-scale aluminium powders. Active aluminium content was 78.2% by mass. In contrast, H-2 has $\approx 99\%$ active metal as measured by TGA [165], but this is likely to decrease as the product further oxidises with age. Micrographs of the V-ALEX and Valimet powders are depicted in Figures 3.3 and 3.4.

Another critical issue arising with the V-ALEX is the formation of large-scale agglomerates that could not be broken up and dispersed during mixing with the gel. Prior composite propellant work with this powder required the use of a surfactant and ultrasonic agitation when mixed with water in order to de-agglomerate the powder during slurry formulation. Ultrasonic mixing was not possible in preparing these experiments due to the high risk inherent in rapidly forming and collapsing bubbles in a liquid high explosive. By contrast, the Valimet powders dispersed with high uniformity. Mixture consistency during pouring is depicted for the H-95, and H-10 powders respectively in Figure 3.5.

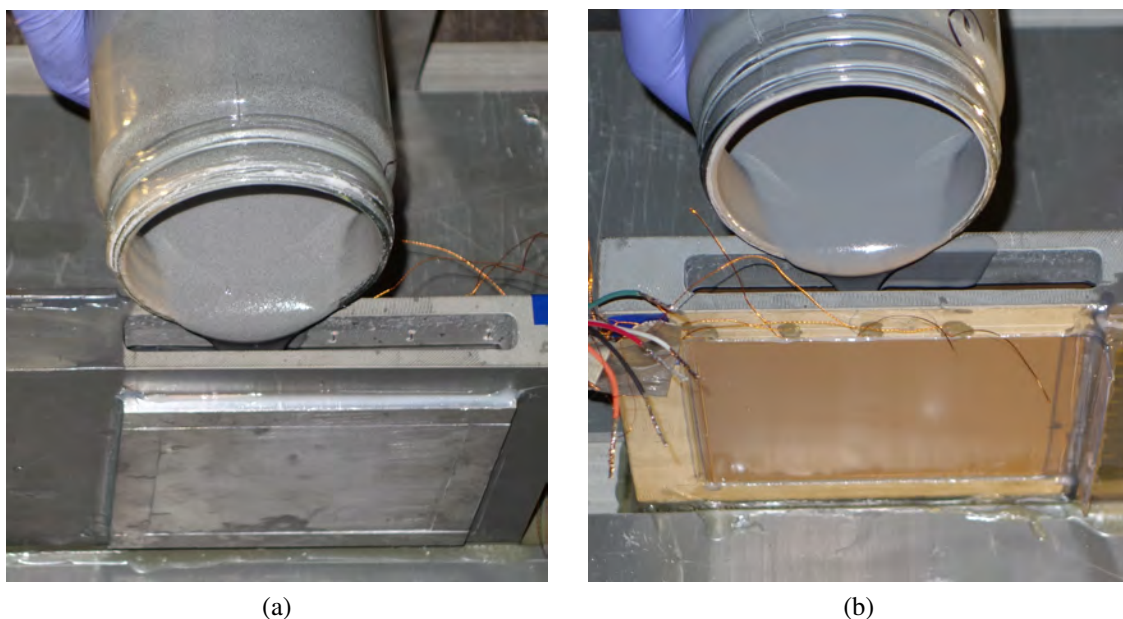


Figure 3.5: Charges being filled with (a) gel mixture containing 15% H-95, (b) gel mixture containing 15% H-10.

In a subset of experiments, other reactive metal powders were added to the base gel explosive. Metals tested included Gran-16 magnesium powder (Reade Manufacturing Co., nearly spherical with some oblate spheroid particles, $d_{0.5} \approx 60 \mu\text{m}$), 99.9% pure titanium (Atlantic Equipment Engineers Ti-101, $d_{0.5} \approx 20 \mu\text{m}$, and silicon. A mixture containing a representative volume fraction of $\approx 30 \mu\text{m}$ diameter alumina was used as the baseline control for an inert particle additive/diluent.

3.5 Experiments, Results, and Discussion

In total, 28 experiments including baseline controls were conducted for the range of aluminium particle sizes and other reactive materials considered. Experiments using the 0.3 mm, 6.4 mm, and 12.7 mm, thick flyer plates were conducted for the range of aluminium powders, whereas only 0.3 mm, and 6.4 mm flyers were used in testing mixtures containing the other metals. Notably, because the detonation velocity of all mixtures was sonic or subsonic relative to the sound speed of the aluminium confinement, all flyer plates were launched without the characteristic shock ringing observed with many explosives. The experimental conditions: mixture properties, charge properties, and terminal velocities, are tabulated for the various aluminium mixtures

Timescale of Aluminium Reaction in Detonation Products Measured via Flyer Plate Experiments

in Table 3.1, and for the other metals in Table 3.2. For the aluminium mixtures a mass fraction of 15% of the total mixture mass was used in the majority of experiments. A subset of experiments containing 30% total mixture mass fraction of H-50 aluminium were also conducted. Mass fractions of 15% were also used when testing the magnesium, titanium and silicon. A mass fraction of 20.5% was used for the control experiments containing alumina to match the volume fraction of particles contained in the 15% mass fraction aluminium experiments.

A summary of all experimental conditions: mass/volume fractions, mixture densities, mass ratios, tilt-corrected terminal velocities, and relative performance are listed in Tables 3.1 and 3.2 for the aluminium tests and other reactive metal tests respectively. The PDV time resolved velocity measurements for all experiments are shown sequentially: Figures 3.6, 3.7, and 3.8 respectively show the velocities for the 15% mass fraction aluminium experiments with 12.7 mm, 6.4 mm, and 0.3 mm flyers relative to the neat baseline and inertly diluted mixtures. Figure 3.9 shows the 15% mass fraction H-50 experiments versus the 30% H-50 experiments and the neat baseline explosive for all three flyer thicknesses. Figures 3.10 and 3.11 respectively show the velocity histories for the Mg, Si, and Ti experiments using 6.4 mm and 0.3 mm flyers in comparison to the H-50, baseline, and inert diluent experiments.

3.5.1 Aluminized Mixtures

The simplest analysis is to merely consider the relative change in flyer terminal velocity on an absolute basis when the fixed charge volume is filled with baseline mixture, inert admixture, or metallized mixture. Based on the velocimetry plots, it is readily evident that flyer terminal velocity was increased over the baseline explosive, and substantially over the same quantity of explosive admixed with inert, for all mixtures containing 15% mass fractions of aluminium. Tilt-corrected terminal velocities using Equations 3.1 and 3.2 are tabulated as V_m in Table 3.1. Flyer velocity increases were obtained regardless of particle size and are tabulated as ΔV_m . In particular, we note that the largest velocity increases were obtained with either H-10 or H-50 aluminium. H-10 at 15% gave the largest velocity increase for the 0.3 mm and 12.7 mm flyers, while H-50 at 15% gave the largest increase for the 6.4 mm flyer. Notably the smaller H-2 particles resulted in lower flyer velocities than the larger H-10 and H-50. The H-95 particles resulted in the overall lowest velocity gains for the Valimet powders. Notably the coated nanometric aluminium (V-ALEX) resulted in the lowest velocity increase of all the aluminium powders. We

3.5 Experiments, Results, and Discussion

Table 3.1: Summary of conditions for experiments using gelled nitromethane mixed with aluminium.

Flyer (mm)	Additive	w_b (%)	φ Gel/GMB/Al	ρ_e (g/cc)	$\frac{M}{C'}$	V_m (m/s)	θ (°)	τ_c (μ s)	ΔV_m (m/s)	$\sqrt{2E}$ inc. (%)
0.3	H-2	15	0.90/0.04/0.06	1.23	0.05	4343	43.2	2.6–3.4	204	4.27
	H-10	15	0.90/0.04/0.06	1.22	0.05	4499	44.7	1.0–1.6	360	8.13
	H-50	15	0.90/0.04/0.06	1.21	0.05	4470	44.5	2.3–2.6	331	7.29
	H-50	30	0.82/0.04/0.14	1.34	0.04	4377	45.5	6.1–6.4	238	4.76
	H-95	15	0.90/0.04/0.06	1.22	0.05	4328	43.2	5.5–6.1	189	3.93
	Baseline	0	0.96/0.04/0.00	1.13	0.05	4139	39.2	n/a	0	0.00
	Alumina	21	0.90/0.04/0.06	1.31	0.04	3632	37.0	n/a	−507	−13.17
6.4	V-ALEX	15	0.90/0.04/0.06	1.21	1.27	1986	20.1	4.9–7.6	83	1.79
	H-2	15	0.90/0.04/0.06	1.23	1.24	2064	20.2	2.3–2.8	160	4.92
	H-10	15	0.90/0.04/0.06	1.22	1.27	2067	20.2	2.4–3.3	163	5.96
	H-50	15	0.90/0.04/0.06	1.21	1.23	2115	20.9	**0.9–1.9	211	7.32
	H-50	30	0.82/0.04/0.14	1.34	1.13	2010	20.4	11.2–12.4	106	−1.63
	H-95	15	0.90/0.04/0.06	1.22	1.26	2035	19.9	4.5–5.6	131	3.98
	Baseline	0	0.96/0.04/0.00	1.13	1.35	1901	17.9	n/a	0	0.00
	Baseline	0	0.96/0.04/0.00	1.13	1.35	1907	22.8	n/a	0	0.00
	Alumina	21	0.90/0.04/0.06	1.31	1.16	1739	17.3	n/a	−165	−13.99
12.7	H-10	15	0.90/0.04/0.06	1.22	2.48	1394	13.5	1.3–1.6	116	4.46
	H-50	15	0.90/0.04/0.06	1.21	2.58	1356	13.0	1.5–7.0	78	3.31
	H-50	30	0.82/0.04/0.14	1.34	2.30	1358	13.8	14.7–15.2	80	−1.61
	H-95	15	0.90/0.04/0.06	1.22	2.51	1361	13.2	**1.7–10.1	83	2.48
	Baseline	0	0.96/0.04/0.00	1.13	2.74	1278	11.7	n/a	0	0.00
	Alumina	21	0.90/0.04/0.06	1.31	2.36	1164	11.7	n/a	−114	−14.58

attributed this poor performance to the relatively high fraction of viton and the presence of both large- and small-scale agglomerates in the mixture. Only one test was conducted with the V-ALEX by consequence.

A more rigorous means of assessing the propulsive performance of the mixtures at terminal conditions is to fit a Gurney velocity for the terminal velocity obtained with each mixture and then derive a percentage difference from the Gurney velocity calculated for the baseline explosive. For a symmetric sandwich, the Gurney velocity ($\sqrt{2E}$) is related to the total metal velocity, V_m , and the ratio of the mass of the flyer to the mass of the explosive charge, $\frac{M}{C'}$ by Equation 3.3:

Timescale of Aluminium Reaction in Detonation Products Measured via Flyer Plate Experiments

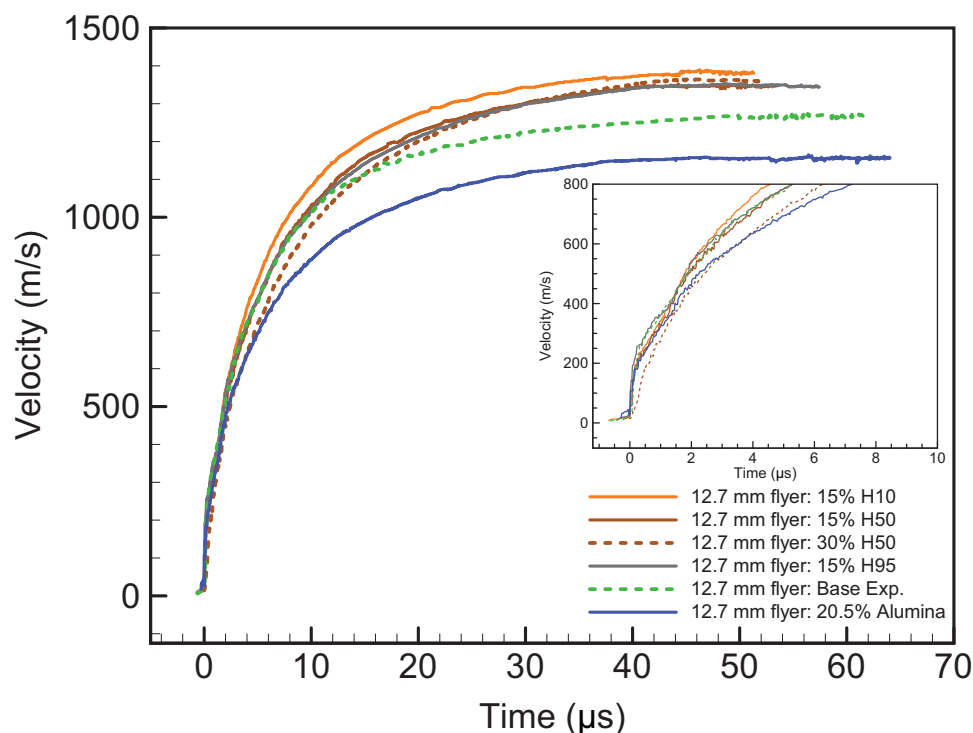


Figure 3.6: PDV traces 12.7 mm flyers propelled by gelled nitromethane aluminized with different sizes of particles at a mass fraction of 15% or 30%. Traces for experiments with the base explosive and explosive diluted with alumina are included for comparison.

$$\sqrt{2E} = V_m \sqrt{\left(\frac{M}{C'} + \frac{1}{3}\right)} \quad (3.3)$$

Note that C' indicates that the total mixture mass is used (including GMBs and metal particles), instead of just the nitromethane component. Using this method, the propulsive efficiency per-gram of mixture is evaluated directly. Values of $\frac{M}{C'}$ were calculated based on the measured mass of mixture poured into the fixed charge volume, allowing for the calculation of the actual mixture density. This value of density was used in combination with the fixed charge width to compute the areal mass of the explosive, and thus the mass ratio of the particular experiment; the areal mass of the flyer was known from its thickness and material density of $2.7 \text{ g} \cdot \text{cm}^{-3}$, with each flyer being $\frac{M}{2}$. Values of $\frac{M}{C'}$ are quite close for each set of experiments at the three flyer thicknesses, with variations typically < 0.02 .

We did not use a single Gurney velocity defined for the full range of baseline $\frac{M}{C'}$ values considered because the 0.3 mm flyer experiments are in the anomalous region of the Gurney curve, where terminal velocities are substantially under-predicted by the Gurney model [9, 24, 45]. In

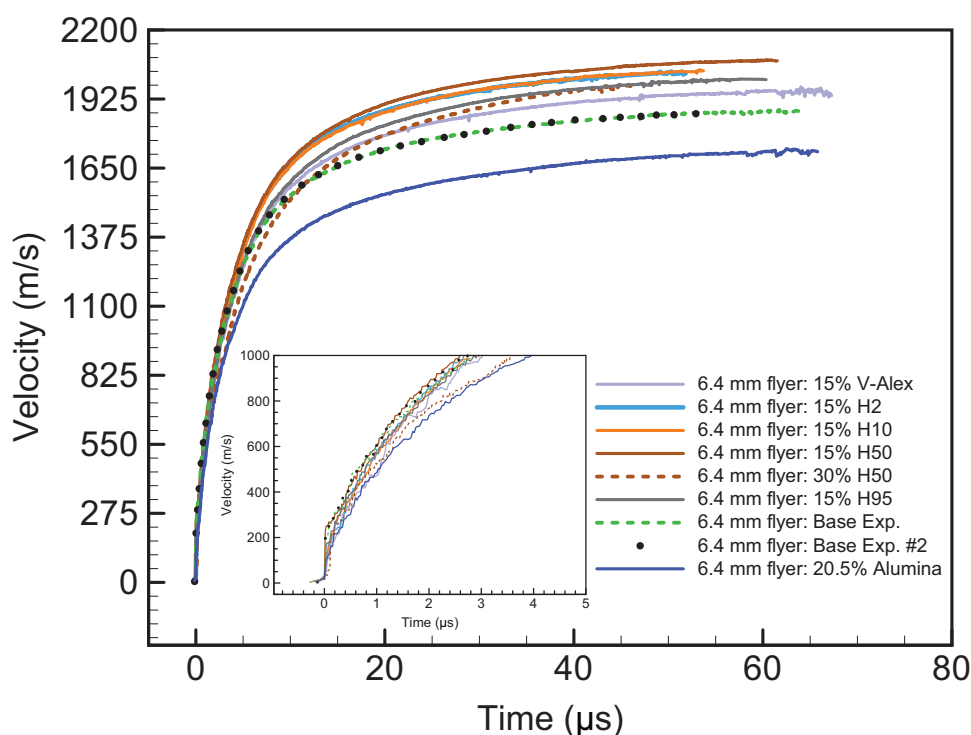


Figure 3.7: PDV traces for 6.4 mm flyers propelled by gelled nitromethane aluminized with different sizes of particles at a mass fraction of 15% or 30%. Traces for experiments with the base explosive and explosive diluted with alumina are included for comparison.

this region, a global baseline Gurney velocity defined to fit all flyer velocities would substantially overpredict the percentage increase in the Gurney velocity for the aluminized mixtures over the baseline gel. The use of a reference Gurney energy fitted to the baseline terminal velocity for each flyer thickness provides a more representative comparison of propulsion capability assuming that Gurney-scaling by the charge mass ratio estimates the partition of energy between the flyer and the detonation products once a representative Gurney velocity/energy has been fitted. It is thereby possible to use a Gurney methodology to compare the higher velocity increases obtained with low mass flyers, with the smaller increases observed for the higher mass flyers. This requires that the values of $\frac{M}{C'}$ do not vary substantially between the metallized mixtures and the baseline mixture for each set of experiments at a given flyer thickness; a condition that was met in the present experiments. The percent-increase in the Gurney energy for the aluminized mixtures is listed in the far-right column in Table 3.1. The variance in mixture Gurney velocities follow the same trends as those observed on a simple ΔV_m basis because the values of $\frac{M}{C'}$ are all very close for each set of experiments at a given flyer thickness. The overall increase in Gurney velocity is quite modest, with values not exceeding 8.5% for the best-performing particle sizes,

Timescale of Aluminium Reaction in Detonation Products Measured via Flyer Plate Experiments

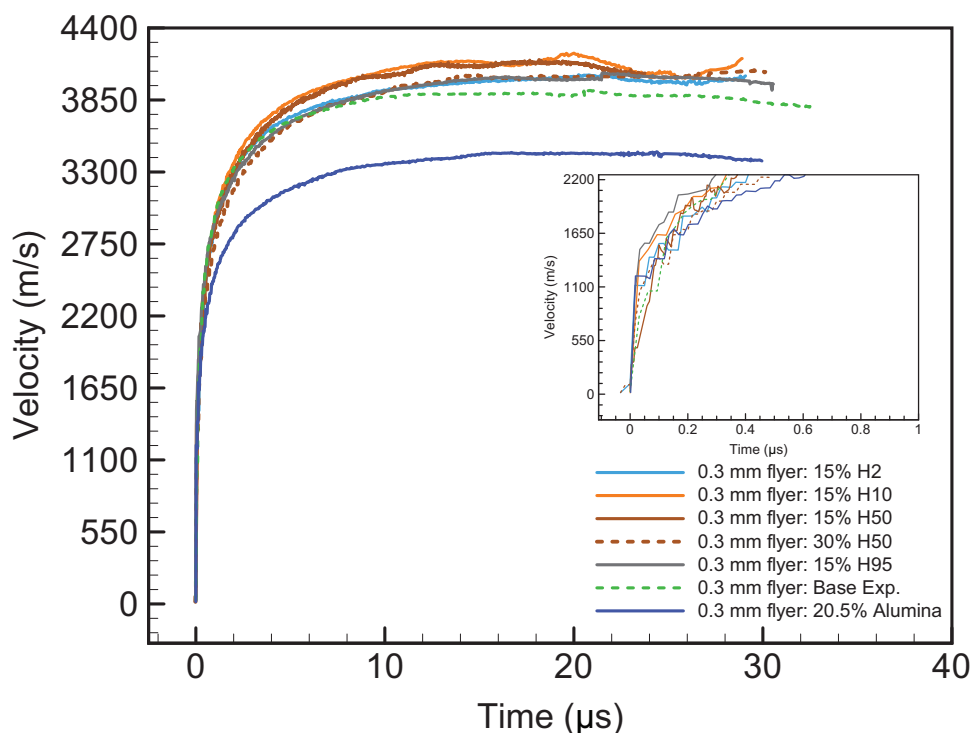


Figure 3.8: PDV traces for 0.3 mm flyers propelled by gelled nitromethane aluminized with different sizes of particles at a mass fraction of 15% or 30%. Traces for experiments with the base explosive and explosive diluted with alumina are included for comparison.

and values as low as 2–3% for the poorly performing particle sizes. These values are consistent with the degree of enhancement observed in prior studies with gelled NM, as well as the general trends reported in the surveyed literature for performance enhancement of C-H-N-O explosives via aluminization. We emphasize that all of the aluminium particles considered exhibited a net contribution of propulsive energy for all flyer configurations, even the large, mean-diameter 95 μm particles.

An important consideration is the relative contribution of particle reaction to propulsive efficiency at the different timescales considered with the three flyer thicknesses; particularly for large particles posited to have low reaction rates due to lesser exposed surface area and potentially large ignition delays due to their relatively large thermal masses. In the present study, the various velocimetry traces show that the 0.3 mm flyers reached terminal velocity in about 15 μs , whereas the 6.4 mm flyers are asymptoting to terminal in about 60 μs , and the 12.7 mm flyers are reaching terminal velocity slightly faster, within about 45 μs . This represents a four-fold variation in acceleration timescale, with the shortest acceleration occurring faster than a proposed ignition delay of the largest particles presently considered. On the basis of the

calculated increases in Gurney velocity we observed no correlation between shorter acceleration times and lower propulsive efficiency due to a reduced window for particles to react. Increases in Gurney velocity derived from the 0.3 mm flyer experiment were as large or larger than the values derived for the experiments with thicker flyers, indicating that added aluminium was equally enhancing propulsive efficiency regardless of the timescale of flyer acceleration. Based on the present results we find no evidence that the energetic contribution of aluminium particles is determined simply by the residence time of an aggregated surface area of aluminium in the detonation products.

The decrements in flyer velocity and Gurney velocity for the mixtures containing the inert alumina are also tabulated and show a consistent decrement of about 13% for all three flyers. The alumina mixture represents an equal volume fraction of explosive but with a larger mass of inert to be accelerated. The inert mixture is thus not perfectly analogous to the aluminium mixture. The authors previously validated a Gurney estimate to account for inert dilution where the flyer velocity can be estimated by simply decrementing the Gurney energy (E) by the mass fraction, w_b , of inert additive according to the following equation:

$$V_m = \sqrt{2E(1 - w_b)} \left[\frac{M}{C'} + \frac{1}{3} \right]^{-\frac{1}{2}} \quad (3.4)$$

With this analytic model, the estimated decrement in Gurney velocity is 11%; reasonably close to the experimental values. By proxy we can infer that a 15% mass fraction of dilution would result in a Gurney velocity decrement of approximately 10%. These deficits highlight part of the reason why aluminization generates such modest overall performance gains: the losses incurred accelerating and heating the particles are substantial and must be more than overcome to generate a performance increase.

To further explore the rapidity of the aluminium reaction for all particles, we extracted the times at which each mixture reached net-exothermicity: the point at which energy delivered by particle reaction exceeds all energy losses to the particles. Net exothermicity was reached very early in the expansion process for all micron-size aluminium particles at mass fractions of 15%, regardless of the relative mass of the flyer plates considered. The times at which net exothermicity were reached for the aluminium experiments are listed as τ_c in Table 3.1, and are defined as the time when the flyer velocity history for the aluminized mixture crosses over the velocity

Timescale of Aluminium Reaction in Detonation Products Measured via Flyer Plate Experiments

history for the baseline explosive. There is some uncertainty in determining these values because the curves often cross with very similar slopes and thus remain coincident for some small interval of time. The values are thus tabulated as a range, with the smallest value indicating the instance where the velocity histories first converge, and the second value indicating the instance where the aluminized velocity history is unambiguously higher than the baseline velocity. For all mixtures with Valimet particle sizes 50 μm and smaller, the baseline flyer velocity was exceeded within around 3.5 μs after the passage of the detonation at the probe location, except for the H-50 experiment with the 12.7 mm flyer. Experiments conducted with the 95 μm particles exhibited longer break-even times than experiments with the smaller powders except for the 12.7 mm experiment, where the flyer velocity exceeded the baseline velocity at breakout but then remained coincident for the longest period of time of the mixtures considered. No robust particle size effect on τ_c was observed for the particles smaller than 50 μm , however. In those experiments, smaller values of τ_c instead correlated with the relative increase in Gurney velocities for experiments with that particular flyer thickness. The V-ALEX experiment also had large value of τ_c relative to even the H-95 experiment; consistent with its poor performance. The particular value of τ_c can thus be considered an approximate indicator of the overall rate of energy deposition of the reacting aluminium into the expanding detonation products. Since the H-2 mixtures displayed prompt exothermicity but overall poorer performance relative to H-10 and H-50 we attribute this deficiency to the presence of a larger mass fraction of inert oxide on the surface of the particles.

In the prior discussion we considered onset of net exothermicity of the reactive particles only relative to a neat baseline mixture. This instance defines the absolute longest delay before reaction onset, but in actuality very early time reaction is masked in part by losses to acceleration and heating the reactive particles through the detonation and early stages of product expansion. The very-early time flyer accelerations are depicted as inlays in Figures 3.6, 3.7, and 3.8. In all cases the initial acceleration is fairly smooth as the detonation is slightly subsonic relative to the sound speed of the flyer material and so the initial jump in wall velocity is small ($\approx 200 \text{ m} \cdot \text{s}^{-1}$) for the two thicker flyers. It is substantially larger for the 0.3 mm flyer. The authors attributed similar increases in initial flyer velocity in very thin flyers to transmission of the von Neumann spike pressure due to the rapid transit time of waves through the thin flyer. Regardless of the initial wavedynamic contribution to flyer motion, the flyer velocity for the aluminized mixtures

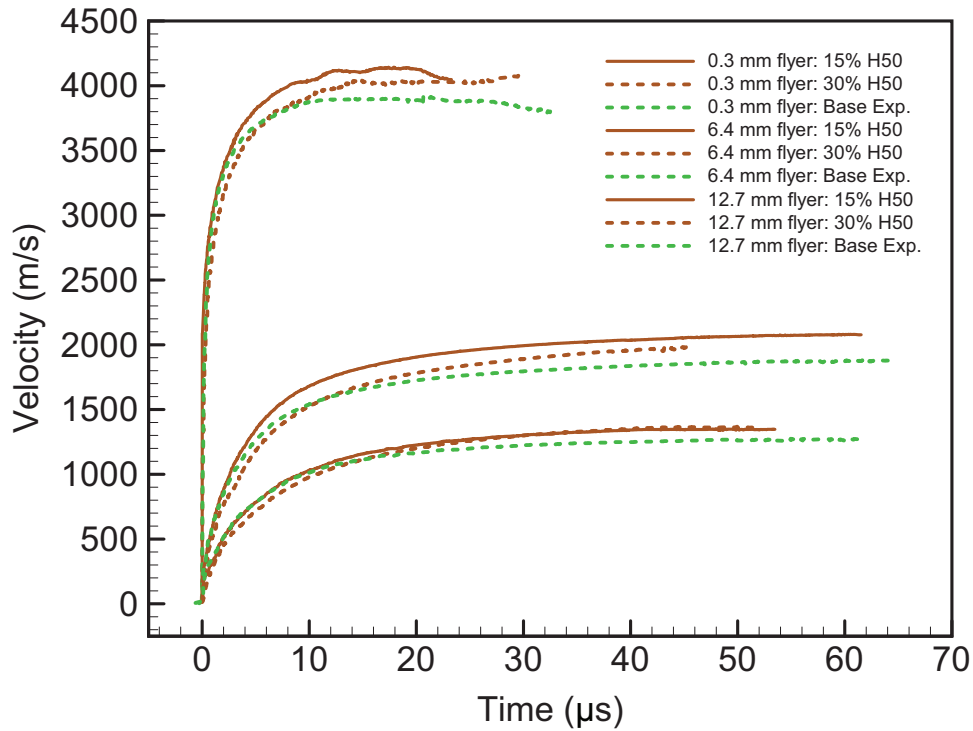


Figure 3.9: Detailed comparison of PDV traces for all of the experiments conducted with H-50 aluminization at 15% and 30% mass fractions. Note the critical behaviour where flyer velocity for the 30% mixture is lower than both the 15% mixture and the base explosive for the first 10 μs but meets or exceeds the performance of the 15% mixture at terminal conditions.

rapidly exceed the velocities for the mixture with alumina. For the 12.7 mm flyer tests, all of the 15% mixtures exceeded the alumina mixture within 1.8 μs . Anomalous, the H-95 mixture exceeded both the baseline and the alumina mixture from the moment of wave breakout at the free surface. For the 6.4 mm flyer tests, all but the H-2 and V-ALEX mixture flyer velocities exceeded the alumina mixture flyer velocity from the moment of initial flyer motion. Finally, for the 0.3 mm flyer tests all aluminized mixture flyer velocities exceeded the alumina flyer velocity within 0.2 μs . While these comparisons are not perfectly ideal owing to the higher density and mass of the inert additive, the authors have previously shown that widely varying additive density did not have a large effect on early-time flyer acceleration providing that the mass of explosive component is the same [161]. Based on these observations we find it impossible to define a particle ignition delay for the NM/Al system. At the resolution of measurement, onset of reaction is practically immediate with some variability between particular tests and plate configurations. Certainly these results indicate that there is no ignition delay, even for $\approx 100 \mu\text{m}$ diameter particles.

Timescale of Aluminium Reaction in Detonation Products Measured via Flyer Plate Experiments

In a final subset of experiments, we considered the addition of 30% H-50 aluminium by mass to the gelled NM. Resulting flyer velocity histories are depicted separately versus the baseline and 15% H-50 experiments in Figure 3.9. This represents a replacement of an additional 8% explosive volume with metal particles and a resulting mixture density increase of about $0.1 \text{ g} \cdot \text{cm}^{-3}$ over the 15% mixtures. The impact on both flyer acceleration and propulsive efficiency is substantial, however. While a modest flyer velocity increase over the baseline mixture was observed for all three flyer configurations, there was a net reduction in Gurney velocity relative to the baseline for the 6.4 mm and 12.7 mm flyer experiments of about 2%. This was due to the larger mixture mass relative to smaller velocity gains than the 15% mixtures. Flyer velocity propelled by the 30% mixture was lower than the baseline for the majority of the acceleration process. The velocities only crossed at late times: $6 \mu\text{s}$ for the 0.3 mm flyers and over double that time, $12 \mu\text{s}$ and $15 \mu\text{s}$ for the 6.4 mm and 12.7 mm flyers respectively. In terms of relative volumes of expansion this corresponds to values of 2.5, 8, and 5 for the 0.3 mm, 6.4 mm, and 12.7 mm flyers respectively. This explains the relatively poor performance of the mixture as detonation products will typically have delivered the majority of their energy to driven metal within 7 relative volumes of expansion. The apparent earlier delivery of energy by the 30% mixture both in terms of timescale and volumes of expansion exhibited in the 0.3 mm flyer experiment is also surprising. Thermochemical equilibrium calculations in Cheetah 2.0 predict the general trend that the 30% mixture should perform similarly to the 15% mixture but overpredicts the performance of the 30% mixture relative to the baseline. Equilibrium calculations are further incapable of addressing the late-time release of energy and uniformly predicts higher velocities than the baseline mixture over all expansion ratios.

3.5.2 Other Metallized Mixtures

The preceding analysis is repeated for mixtures containing the alternative reactive metal powders: Silicon, Gran-16 Magnesium, and Titanium all at 15% mass fractions. Flyer velocity histories for the 0.3 mm and 6.4 mm flyer experiments are shown in Figures 3.11 and 3.10 respectively. Table 3.2 lists all relevant experimental parameters including the times of net-exothermicity, and changes in flyer velocity and calculated Gurney velocity.

For the 6.4 mm flyer experiments, very small increases of less than $100 \text{ m} \cdot \text{s}^{-1}$ were observed for the three different metals. On a Gurney velocity basis, however only the silicon

3.5 Experiments, Results, and Discussion

Table 3.2: Summary of conditions for experiments using gelled nitromethane mixed with reactive metal powders.

Flyer (mm)	Additive	w_b (%)	φ Gel/GMB/Metal	ρ_e (g/cc)	$\frac{M}{C'}$	V_m (m/s)	θ (°)	τ_c (μ s)	ΔV_m (m/s)	$\sqrt{2E}$ inc. (%)
0.3	Gran-16	15	0.87/0.04/0.10	1.18	0.05	4133	41.0	n/a	−6	−0.13
	Silicon	15	0.89/0.04/0.07	1.23	0.05	4225	43.1	12.6	86	1.76
	H-50	15	0.90/0.04/0.06	1.21	0.05	4470	44.5	2.3–2.6	331	7.29
	Titanium	15	0.92/0.04/0.04	1.21	0.05	4188	42.7	n/a	49	0.62
	Baseline	0	0.96/0.04/0.00	1.13	0.05	4139	39.2	n/a	0	0.00
	Alumina	21	0.90/0.04/0.06	1.31	0.04	3632	37.0	n/a	−507	−13.17
6.4	Gran-16	15	0.87/0.04/0.10	1.18	1.29	1931	18.8	24.8–27.9	27	−0.22
	Silicon	15	0.89/0.04/0.07	1.23	1.25	1979	20.0	5.9–6.5	75	0.74
	H-50	15	0.90/0.04/0.06	1.21	1.23	2115	20.9	**0.9–1.9	211	7.32
	Titanium	15	0.92/0.04/0.04	1.21	1.26	1936	19.4	1.6–4.1	32	−1.05
	Baseline	0	0.96/0.04/0.00	1.13	1.35	1901	17.9	n/a	0	0.00
	Alumina	21	0.90/0.04/0.06	1.31	1.16	1739	17.3	n/a	−165	−13.99

mixture displayed an increase in propulsive efficiency of less than 1%. Both the magnesium and titanium mixtures resulted in small net reductions in propulsive efficiency. Examination of the PDV traces yields some distinct phenomenology for the different metals. The 15% magnesium mixture showed similar behaviour to the 30% H-30 mixture, where the flyer velocity was below the baseline mixture for much of the expansion process before finally crossing over near terminal conditions. Due to this similarity in behaviour we postulate that this effect arises for relatively large volume fractions of reactive particles. While the mass fraction of Mg is only 15% its density is low, resulting in a large volume fraction relative to the other 15% mixtures. Mg. volume fraction is 10%, compared to the 14% volume fraction for the 30% H-50 mixture. In contrast, the silicon displays prompt net exothermicity with a similar τ_c to H-95 aluminium, although the net energy deposited is lower than for aluminium. In the case of titanium, net exothermicity was observed very promptly (within $\approx 2 \mu$ s), however the deposition of energy ceased early during the expansion, leading to a flyer velocity that decayed towards the baseline. We speculate this may result from the relatively high density of the titanium as an additive.

For the 3.2 mm flyers, all three metal-laden mixtures fell below the baseline explosive until the very terminal phases of acceleration. The non-tilt-corrected velocities shown in the PDV traces understate the degree of velocity enhancement observed. Because the Taylor angles are

Timescale of Aluminium Reaction in Detonation Products Measured via Flyer Plate Experiments

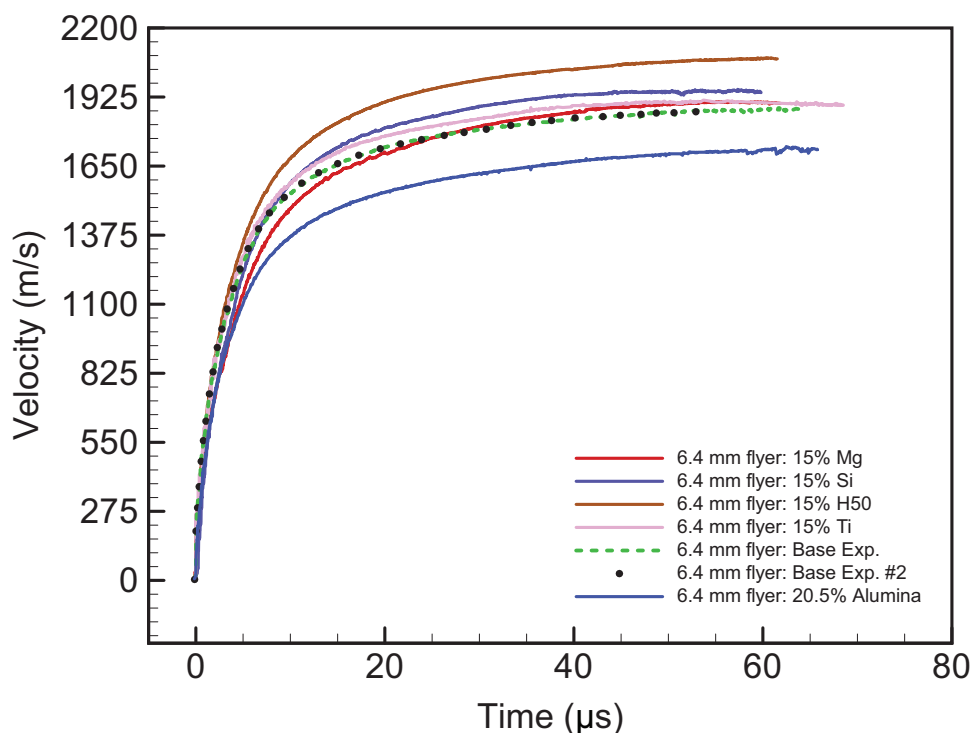


Figure 3.10: PDV traces for 6.4 mm flyers propelled by gelled nitromethane metallized with magnesium, silicon, and titanium at a mass fraction of 15%. Traces for experiments with the base explosive, H-50 aluminization and alumina dilution are included for comparison.

appreciably larger than the baseline case owing to lower VODs, the true metal velocity is actually higher than the baseline. By consequence, even though energy addition occurs just prior to the flyer reaching terminal velocity, the addition is sufficient to result in an increase in the mixture Gurney velocity for this experiments.

Although the magnitude of the overall effect is small, these experiments demonstrate that the rapid exothermic reaction of metal particles in a flow of high explosive detonation products is a generic phenomenon. Prompt energy release is evident relative to the flyer velocity decrement that would be observed for a mixture containing 15% inert particles.

3.6 Conclusion

In the present study, we have considered the acceleration of metal flyers by mixtures containing either 15% or 30% aluminium as well as 15% magnesium, silicon, or titanium. The interplay of particle size and acceleration timescale was evaluated by considering a wide range of micron-scale particles at two distinctly different flyer acceleration timescales by changing the

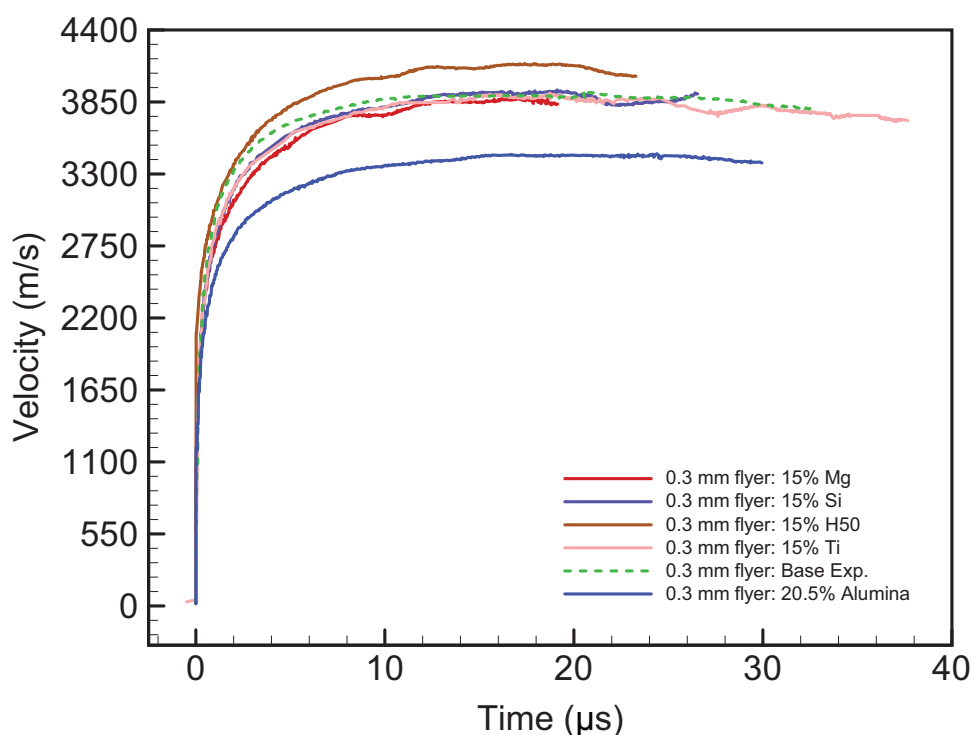


Figure 3.11: PDV traces for 0.3 mm flyers propelled by gelled nitromethane metallized with magnesium, silicon, and titanium at a mass fraction of 15%. Traces for experiments with the base explosive, H-50 aluminization and alumina dilution are included for comparison.

thickness of the flyer plate. We observed a weak effect of particle size on propulsive efficiency, as the largest particle size gave lower flyer velocities than the intermediate particle sizes. The nanometric aluminium considered as well as the smallest micron-scale particles also gave poor metal-driving performance. The poor performance of the nanometric aluminium was attributed to heavy agglomeration and the large mass fraction of coating material. The poor performance of the H-2 aluminium was attributed to a larger fraction of passivating oxide. For all particle sizes, rapid particle reaction was observed, in some cases with no delay after the passage of the detonation wave. Based on these observations we postulate that the concept that metal particles subject to detonation product flow must undergo some thermalization process prior to the onset of bulk combustion to be fundamentally flawed. Instead it is apparent that some sort of surface reaction begins very rapidly after the particles are swept-over by the detonation. It is the competition of the rate and exothermicity of this surface reaction against the losses incurred from heating and accelerating the particles. Based on inert analogues, the degree of detonation product energy lost accelerating and heating particles is substantial, and this in part explains why propulsive enhancement via aluminization is typically so modest. Finally, we

Timescale of Aluminium Reaction in Detonation Products Measured via Flyer Plate Experiments

demonstrated that rapid exothermic reaction of metal particles is not unique to aluminium but observed for the other metals considered here. The impact on propulsive efficiency of these metals is insignificant from an explosive engineering standpoint.

Chapter 4

Terminal Velocity of Liquids and Granular Materials Accelerated by a High Explosive

Jason Loiseau, Quentin Pontalier, Alec Milne, Samuel Goroshin, David L. Frost

[Submitted to Shock Waves](#)

4.1 Abstract

The explosive dispersal of a layer of solid particles or a layer of liquid surrounding a spherical high-explosive charge generates a turbulent, multiphase flow. Shock compression of the material layer during the initial acceleration may partially consolidate the material, leading to the formation of jet-like structures when the layer fragments and sheds particles upon release. Similarly, wavedynamic release of a shock-compressed liquid shell causes the nucleation of cavitation sites, leading to the radial breakup of the shell and the formation of jets upon expansion. In the current study, the maximum terminal jet tip or shell velocity for a wide variety of materials during explosive dispersal was measured using high-speed videography. Charges were constructed using thin-walled glass bulbs of varying diameters and contained a central C-4 burster of varying mass surrounded by the granular material or liquid to be dispersed. This permitted the variation of the ratio of the material mass to the burster charge mass (M/C) from

values between 4 and 300. Results indicate that material velocity broadly correlates with predictions of the Gurney model. For liquids, the terminal velocity is accurately predicted by the Gurney model. For granular materials, Gurney over-predicts the terminal velocity by between 25% and 60%, depending on the M/C ratio of the charge, with larger M/C charges demonstrating larger deficits. These deficits are explained by energy dissipation from the collapse of voids in the dry granular materials. Velocity deficits are insensitive to the degree of jetting and granular material properties. Empirical corrections to the Gurney Model are presented with improved agreement for the dry powder experimental velocities.

4.2 Introduction

High explosive charges are commonly used to explosively disperse fragments from solid casings surrounding the charge. The initial velocities of such fragments can be estimated reasonably accurately with the simple analytical model developed by Gurney [3]. If an explosive is surrounded by a layer of liquid or a bed of granular material rather than a solid metal casing, relatively little information is available regarding the velocity attained by the surrounding material. The velocity at which such non-conventional explosive casings are launched is critical for applications including blast loading analysis from buried or shallow water charges, and the explosive dispersal of aerosols and obscurants.

Milne [166] examined the explosive dissemination of porous particle beds with hydrocode calculations and developed an engineering correction to Gurney theory. The porous Gurney model was compared with the standard Gurney model and validated with experimental data on the explosive dispersal of sand and sugar. In the current study, the terminal velocity of explosively dispersed granular materials, liquids, saturated particle beds, and high-density particle suspensions is examined experimentally.

A common feature of the explosive dispersal of liquids and granular materials is the formation of jet-like structures [167, 168]. It is not known, a priori, whether the presence of jets influences the maximum velocity attained of the dispersed material. The relative importance of the material properties of the liquid or particle layer and layer porosity during the acceleration of the layer material is also poorly understood. While this paper focuses on the velocity attained by the dispersed material, a phenomenological discussion of the dispersal process is important as it

explains the quantities being measured as well as the mechanisms by which energy is dissipated by the material shell. Hence, in the present paper we first review the physical processes that occur during explosive material dispersal, followed by a discussion of the Gurney model and related phenomena. The experimental procedure is then described, followed by a presentation of the experimental results and a comparison of the results with the standard and porous Gurney models.

4.3 Explosive Dispersal and Jet Formation

The explosive dispersal of a shell of particles or liquid surrounding a high-explosive charge generates a high-speed, gas-particle flow. A conceptual model for the explosive acceleration of these types of shells, first articulated by Milne et al. [169], is depicted schematically in Figure 4.1. Detonation of the burster charge generates an outward-travelling shock wave that compresses the particle shell. Sufficiently high shock pressures can induce varying degrees of particle consolidation within the shell. Thin shells comprised of soft/weak materials may be compacted through most of their initial thickness, whereas thick shells of tough/hard materials may only consolidate close to the burster. While this partially-consolidated shell is driven outward by the expanding detonation products, rarefaction waves release the shock pressure. Jet-like structures are then formed as the shell radially expands as the consolidated material fragments due to tensile loading from this rarefaction. These jet-like structures emerge from the detonation product fireball and then shed unconsolidated and weakly consolidated particulate in their wake due to aerodynamic drag. Similarly, tensile loading arising from the wavedynamic release of a shock-compressed liquid shell causes cavitation bubbles to nucleate throughout a liquid layer, leading to the formation of liquid ligaments as the shell breaks up due to growth and coalescence of the bubbles. These ligaments are postulated to form the jet tips upon further expansion and acceleration of the liquid [168]. These jets likewise shed droplets due to aerodynamic drag, with the rate of breakup governed by viscosity, surface tension, and volatility.

Robust phenomenological and quantitative modelling of the formation, number, and velocity of jets formed in dispersed liquids and granular solids remains elusive and alternative mechanisms for jet formation have been proposed. A liquid shell may break up due to strain localization at the tips of Richtmyer-Meshkov instabilities formed at the internal explosive-shell

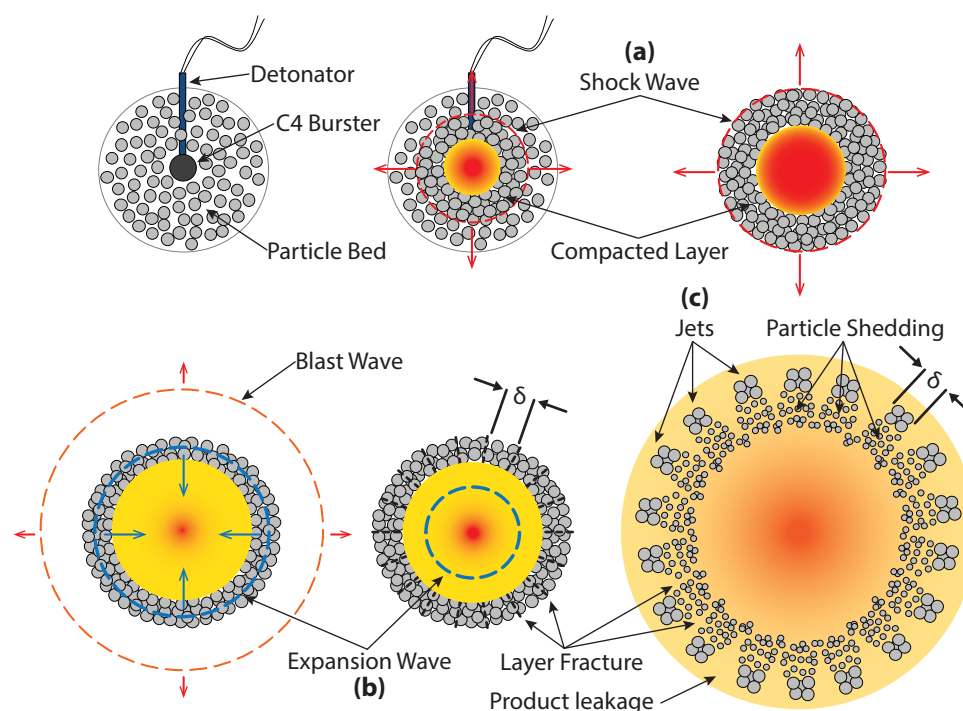


Figure 4.1: Schematic depicting the shock wave compaction, fragmentation and acceleration of a granular material shell by a high explosive charge: (a) Passage of the shock from the detonation compacts a portion of material shell, (b) Once the shock reaches the shell-air interface rarefaction waves propagate back into the shell, causing breakup with fragment sizes on the order of the compacted shell thickness (δ), (c) jets are formed as the fragments shed particulate in their wakes.

interface [170]. Alternatively, the natural fragmentation of the internal charge casing (if present) may perforate and perturb the material shell, leading to the entrainment or growth of jets. Likewise, natural fragmentation of the outer container may lead to the formation of instabilities at the outer layer boundary. While casing fragmentation is likely to play a role in jet formation for experimental configurations where heavy confinement is present, the robustness of the jetting phenomena for a variety of thin-cased and bare charge experiments conducted for the present study suggests that the general phenomena cannot be attributed exclusively to casing effects. Likewise, radiographic results presented by Milne et al. suggested that incipient failure of compressed particle layers or the nucleation of large-scale cavitation bubbles in liquids occurs on the time-scale of the rarefaction fan emanating from the outer surface of the shell having reached the internal detonation product interface [168, 171]. This timescale is too short for hydrodynamic instabilities to grow to the necessary scale to govern the formation of large-scale jets observed experimentally [168, 171]. Consequently, failure or cavitation in the shell upon wavedynamic

release appears to be the most promising mechanism to explain jet formation in both liquids and granular materials.

For explosively dispersed granular material, Milne et al. concluded that the size and thus number of jets correlates well with the thickness of the compacted layer after the initial rarefaction fan had passed through the thickness of the shell [171]. This results in a quasi-monomodal size distribution of terminal fragments/jets. Consequently, the strength, ductility, and toughness of the particle bed will influence the degree of layer compaction and subsequent jet formation. In the present study, it was observed that jetting can be suppressed if sufficiently hard and tough particles are dispersed. Examples will be given in the results section of the different morphologies of the dispersed particle cloud that are observed. For example, during the explosive dispersal of hardened steel shot, the steel shot forms a diffuse layer of largely unconsolidated powder, with little evidence of jet formation. In contrast, a similar mass of a more ductile metallic powder such as pure iron or brass, accelerated by a similar charge mass, exhibited prominent jetting. Therefore, the formation of jets in a granular solid is conditional on the fracture of consolidated material in the shell. Prominent, terminal jetting is thus dependent on the consolidation of an appreciable fraction of the granular shell. This can be further supported by the observation that the saturation of a granular material with a liquid dramatically changes the size and number of jets. This is conjectured to arise because the interstitial fluid suppresses particle compaction, and jet formation becomes governed by liquid cavitation nucleated around particles.

One challenge to the assumption that jetting arises due to the monomodal fragmentation of consolidated material during early wavedynamic release is that consolidated shells of a ductile material should retain some plasticity and undergo natural fragmentation after a degree of expansion. However, in spherical geometry, both brittle ceramic powders (glass, sand, silicon carbide) and ductile metal powders (brass, aluminium, iron) exhibit similar monomodal jetting behaviour, suggesting a similar fracture mechanism. Frost et al. [172] experimentally determined that a cylindrical shell of aluminium powder explosively accelerated by an axial detonation will yield a layer of densified metal that exhibits natural fragmentation. Radiography demonstrated that fragmentation onset occurred promptly after compaction with little plasticity, supporting the assumption of early-time breakup even for ductile materials consolidated from powder. A more fundamental characterization of both the layer material properties after shock compaction, and the early-time propagation of damage in the consolidated material

is thus critical to fully reconcile the jetting behaviour of granular solids, and particularly the resulting monomodal jet distribution.

For liquid dispersal, Milne et al. [168] postulated that jetting is determined by the volumetric distribution of nucleated cavitation sites when the liquid shell is put in tension, assuming a constant and uniform number of nucleation sites per unit of volume. This results in a bimodal behaviour for the number of jets as a function of the ratio of explosive-mass to liquid-mass. As the ratio increases, the total number of sites increases, leading to an increase in the number of ligaments and thus jet population. For a critical ratio, additional nucleation sites merely link up and the number of jets is determined by the number of cavitation sites at the explosive-liquid interface. This leads to a constant number of jets for increasing ratios of liquid mass to explosive mass beyond this “saturation” point.

An important aspect of these systems, given the dissipative and phenomenologically complex nature of the dispersal, is the partition of explosive energy into kinetic energy of the media compared to losses via work done compacting, deforming and damaging particles. Similarly, rapid failure of the shell of media and breakup into jets may reduce the gasdynamic push delivered by the expanding detonation products. The effectiveness of the conversion of explosive chemical energy into kinetic energy of the system is empirically defined by the Gurney energy and the partition of this kinetic energy between the driven material and the detonation products is described by the Gurney equation.

During the explosive acceleration of a metal plate or metal shell, the energy of the explosive is primarily portioned into kinetic energy of the expanding detonation products and kinetic energy of the metal. Souers [20] concluded that for the copper cylinder test, energetic losses amount to around 10% of the Gurney energy due to a combination of material effects including work hardening, irreversible heating, and spall. The effects of pore collapse and particle damage on the terminal velocity of an explosively accelerated and compacted porous shell has seldom been considered [168, 171]. For explosively loaded granular materials, energy dissipation is substantial due to heating and material deformation during pore collapse as the material is compacted. Granular materials are thus good candidates for blast mitigation and prior work has focused on the performance of these systems by directly measuring mitigated overpressure [173–175] or measuring the transmitted shock through a granular bed [176]. A complete review of shock and blast mitigation is beyond the scope of this paper, however a companion

paper presents an analysis of the blast mitigating properties of the materials presently considered. In the current study a Gurney analysis was performed in order to estimate the extent to which explosive energy is dissipated by material effects and other non-idealities in granular and liquid casings.

4.4 Gurney Model and Related Phenomena

The Gurney equations, originally formulated in 1943 by R. W. Gurney to predict the fragment velocities of spherical or cylindrical metal casings driven by a high-explosive core, have been extended to numerous geometries and systems involving the explosive acceleration of material to some terminal velocity [3, 5, 29, 35]. Gurney's methodology continues to be the primary analytic technique to estimate the terminal velocity of explosively accelerated materials, and the Gurney energy remains an important metric of high explosive performance [76].

Detailed derivations and model assumptions are variously described in the literature by Jones [28], Kennedy [5, 10], and Dehn [29, 30]. A basic description of the model is nevertheless included here since model details are relevant to understanding where experimental deviations may occur in the present study. Gurney assumed that the explosive acceleration of a casing could be described by the instantaneous conversion of a portion of explosive chemical energy into gasdynamic potential energy of the detonation products. Product expansion against the casing is simplified by assuming a linear gas velocity profile, V_g , with product radius, r , and the casing burst radius a , thus:

$$V_g = \frac{r}{a} V_o \quad (4.1)$$

Consequently, the conservation of energy can be written as:

$$CE = \frac{1}{2} \sum_i m_i V_o^2 + \frac{1}{2} V_o^2 \rho_g \int_0^a 4\pi r^2 \left(\frac{r^2}{a^2} \right) dr \quad (4.2)$$

Where the effective specific explosive energy (Gurney energy), E , is equal to the kinetic energies of all of the fragments with masses, m_i , assuming they have the same average velocity, V_o , plus the kinetic energy of the detonation products. Here ρ_g is the detonation product density. The detonation products are then assumed to maintain a uniform density during expansion, thus the

Terminal Velocity of Liquids and Granular Materials Accelerated by a High Explosive

density at burst can be related to the mass of explosive, C :

$$\rho_g = \frac{C}{\frac{4}{3}\pi a^3} \quad (4.3)$$

Substitution and integration then yields the familiar Gurney equation for a spherical explosive charge surrounded by a spherical shell accelerated to a terminal velocity, v_o :

$$V_o = \sqrt{2E} \left\{ \frac{M}{C} + \frac{3}{5} \right\}^{-\frac{1}{2}} \quad (4.4)$$

Where $\sqrt{2E}$ is the Gurney velocity, which is unique for each explosive and is determined empirically by fitting its value for a range of experimental terminal velocities at different values of the ratio of casing-mass to charge-mass (M/C). The Gurney energy thus represents a conversion efficiency of the calorimetric or detonation energy of the explosive into energy in the products that subsequently accelerate a casing. The scaling of casing velocity with M/C relies on the assumption that a given mass of charge contributes the same amount of kinetic energy regardless of charge size and geometry. Further, it demonstrates that the efficiency with which kinetic energy is delivered to the casing varies with the relative amount of explosive as varying amounts of energy is partitioned to accelerate the detonation products as they expand. The Gurney equations are thus simple scaling laws which relate the terminal velocity of a casing to the relative amount of explosive driving it and a characteristic propulsive capability of the given explosive.

Despite the simplicity of the Gurney model, it has been shown to be quantitatively accurate for engineering calculations over select ranges of M/C . In planar geometries, where a layer of explosive is sandwiched between flyer plates, accuracy is excellent over several orders of magnitude of M/C [9, 41]. Loiseau et al. demonstrated that the planar Gurney equations are accurate to within 5% for M/C values of 0.2 and greater, and within 10% for M/C values less than 0.2 [9]. The growth of error as the value of M/C becomes small is due to gasdynamic gradients in the detonation products prior to acoustic decoupling of the casing, which represent a significant departure from the assumptions in the model. Overall agreement for geometries with convergence or divergence (i.e., imploding or exploding cylindrical or spherical shells) is poorer. Solem and Singleton conducted tubular bomb experiments with aluminium and steel

casings and showed that under-prediction for thin cases is substantial (up to 40%), whereas over-prediction of approximately 15% occurs for values of M/C around 2.0, the largest values considered [42]. Jacobs reconsidered the Solem data and illustrated that by changing the value of A and selecting a better value for the Gurney energy, accuracy could be improved to within 10% over the experimental range considered [39]. Similarly, Weinland proposed an alternative power scaling-law to better fit the Solem and other ordnance test data [43]. Hirsch corrected the spherical and cylindrical Gurney equations by replacing part of the explosive with an equivalent rigid inert core on the basis that at the limit of an infinite charge of explosive, not all of the geometric forms asymptote to the same terminal velocity [44]. The addition of the inert core increases the predicted velocity for small values of M/C but converges to the basic Gurney equation for larger values. Flis demonstrated that the addition of an inert core invalidates the assumption of a linear velocity gradient coupled with a uniform density and derived new forms for either assumption that are physically consistent [11].

The authors are not aware of any experimental validations of the spherical Gurney equation over a wide range of M/C values; historical modifications have been proposed on the basis of agreement with cylindrical experiments. Since most of these modifications deal with correcting for disagreement at small values of M/C , where the Gurney Model is most problematic, the authors do not recommend any a-priori modifications when considering large ranges of M/C values. In the present study, intermediate to very large values of M/C were considered ($4 > M/C > 300$), a range over which the Gurney equations are seldom used. Further, deviations from the model in the present study are expected to arise due to granular material dynamics and failure rather than gasdynamic and wavedynamic non-idealities. Milne validated the spherical Gurney equation against hydrocode simulations of the explosive acceleration of a steel shell for values of M/C ranging from 1 to 100 using composition A4 explosive (97% RDX, 3% wax). Agreement to within 5% was demonstrated if a fitting form of the Gurney equation was used, where [166]:

$$V_o = \sqrt{2E} \left\{ \frac{M}{C} + A \right\}^B \quad (4.5)$$

Where A and B are treated as fitting constants instead of deriving from integrating the conservation equations for the specified geometry, similar to the method proposed by Jacobs [39].

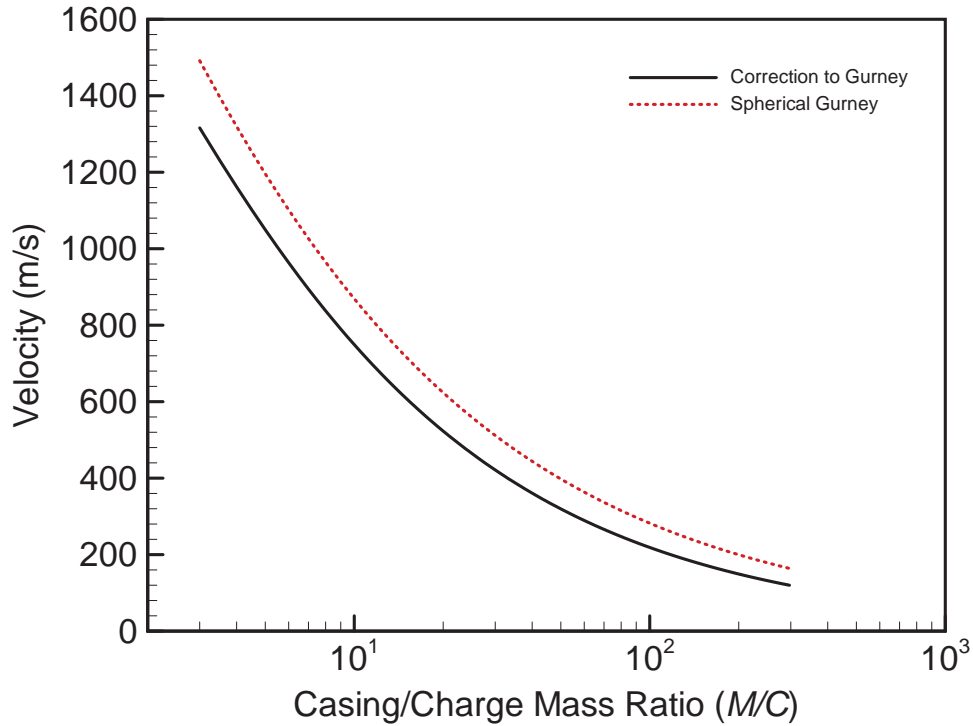


Figure 4.2: Comparison between the standard Gurney model and the modified power law presented in equation 4.5. Both equations use a Gurney velocity of $2830 \text{ m} \cdot \text{s}^{-1}$.

Milne proposed the following values [166]:

$$\sqrt{2E} = 2830, A = 0.97714, B = -0.547239 \quad (4.6)$$

Notably, these modified Gurney fits have provided better agreement by increasing the value of A relative to the geometrically derived value when the range of M/C is large (1–10) [166], or by decreasing the relative value when the range is small (<2) [39]. This suggests a functional dependence of A on the mass ratio of the charge, however no such dependence has been formally proposed in the literature that covers all of the different geometries and the multiple orders of magnitude and ranges of charge mass ratios considered. A comparison of the baseline Gurney model (eq. 4.4) and the corrected power law model (eq. 4.5) is shown in Figure 4.2. As can be seen, the corrected model mostly manifests as a vertical shift of the power law curve. For the purposes of fitting a scattered set of experimental data a simple change of Gurney energy in eq. 4.4 may thus be sufficiently accurate.

The inclusion of a finite casing burst radius in Gurney's original derivation implied an influence of the degree of casing expansion prior to fracture on the terminal velocity of the casing. It

has frequently been postulated that upon fragmentation, casing acceleration largely ceases due to pressure relief from products venting through the cracks, with residual acceleration occurring from the remaining gas and aerodynamic drag induced by the leakage [4]. This had led to the definition of “prompt” and “terminal” Gurney velocities for different explosives, depending if casing fragmentation occurs quickly or if substantial plastic expansion occurs [8]. Similarly, the equivalent Gurney energy can be defined at several scaled expansion ratios for the cylinder test, however this introduces inaccuracies if a constant isentropic expansion factor (γ) is used [23, 76, 177]. However, Hutchinson et al. calculated that cessation of acceleration due to leakage between fragments at expansion ratios typical of brittle metals has been overstated in the literature, with terminal velocity deficits much less than 10% being estimated for representative munition cases [178]. In the present context, with compacted shell fragmentation postulated to occur prior to significant expansion, venting could still be a significant source propulsive loss. Currently, there remains insufficient radiographic measurements of the breakup of consolidated granular shells to permit rigorous estimation of gas escape losses for the present experiments.

4.5 Porous Gurney Model

The dominant difference between a homogeneous shell typically considered in the Gurney model and the heterogeneous, granular systems presently considered is the presence of interstitial pores throughout the particle beds. Under sufficiently strong loading, bed compression and particle deformation can collapse and heat these pores, leading to substantial, entropic dissipation of energy. By consequence, it is expected that the standard Gurney model will poorly predict the initial terminal velocity of the granular material shell, since an appreciable fraction of the explosive energy may be lost as heat during pore collapse.

Using hydrocode simulations, Milne proposed an empirical correction to the Gurney model to account for variable dissipation with different materials over a range of mass ratios. Simulations were conducted comparing the acceleration of homogeneous shells versus heterogeneous granular shells whose compaction is treated with a Hermann P-alpha model [166]. Results of these simulations showed that the amount of energy dissipated during shell compaction was determined by the material solid density and the volume fraction of pores. Greater porosity resulted in greater dissipative losses and thus a lower shell velocity. Material solid density had the

effect of increasing shell velocity for a fixed porosity and M/C ratio. This effect was attributed to a reduction in shell thickness for a specific mass of shell, such that there was a smaller total volume of pores to collapse.

On the basis of these observations and hydrocode results, the Gurney equation was modified to account for variations in scaling due to pore collapse and shell compaction. The corrected equation follows the conventional spherical form with two additional scaling parameters:

$$V_o = F\sqrt{2E} \left\{ \frac{1}{\alpha} \frac{M}{C} + \frac{3}{5} \right\}^{-\frac{1}{2}} \quad (4.7)$$

The scaling parameters α and F are defined as:

$$\alpha = 0.31\rho_o^{0.132} \quad (4.8)$$

and:

$$F = 1 + K \log_{10} \left(\frac{M}{C} \right) \quad (4.9)$$

$$K = 0.168e^{1.09\varphi} - 0.5 \quad (4.10)$$

Where M/C is the shell-mass to explosive-mass ratio, φ is the porosity (bulk density divided by solid density), and ρ_o is the material solid density in kg m^{-3} . K has a negative value.

4.6 Experimental Setup

A spherical charge geometry was created by using thin-walled (1-mm-thick) commercial glass light bulbs with the filaments and neck of the bulb removed via abrasive wet-saw. Two types of bulbs were used: Either G40 (nominal diameter of 12.7 cm) or G25 (nominal diameter of 9.5 cm) bulbs. In select experiments, large 5 l round-bottom laboratory flasks were used to contain very large volumes of granular fill. The thin glass casing was desirable to eliminate any influence of casing mass and casing fragmentation on the jetting and dispersal of the filler materials.

A hand-formed spherical ball of C-4 (28–100 g charge mass) was placed in the middle of the glass sphere with a plastic tube attached to allow the insertion of an electric detonator into the explosive charge prior to the test. For liquid dispersals, the C-4 was placed within a hollow polyethylene sphere (mass 12 g) to isolate it from the liquid. The PE sphere was cut in half,

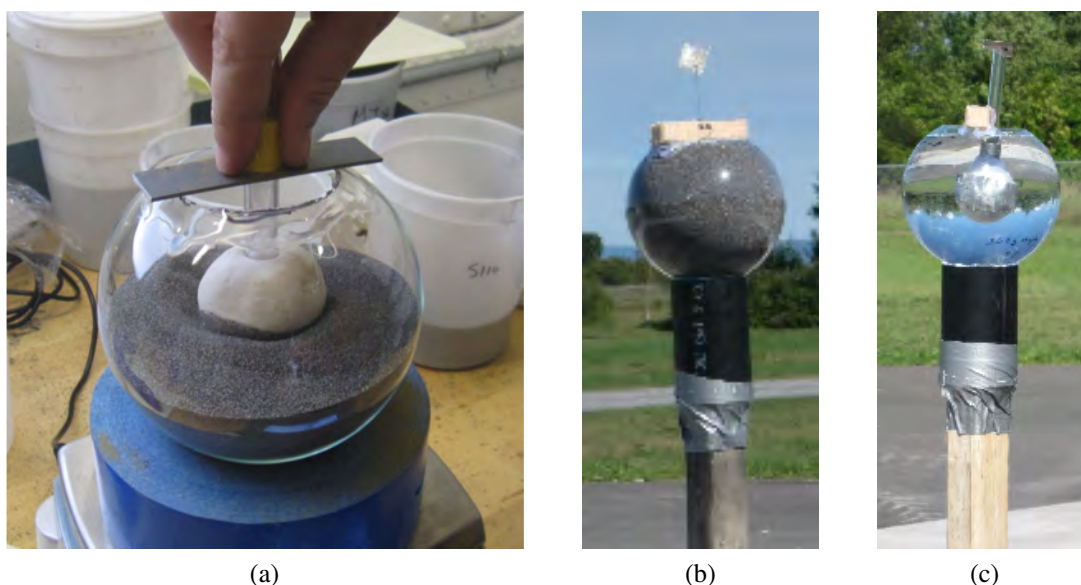


Figure 4.3: Photographs of explosive dispersal charges illustrating (left) filling procedure and burster assembly, (center) filled granular solid charge on stand, (right) filled liquid charge on stand.

drilled with a port for the detonator tube, filled with C-4, and then reassembled with epoxy. The detonator tube was then epoxied into the port and a cross-piece (either PVC strip or a wood block) was used to centre the charge in the bulb via retention of the detonator tube. In the case of solid particles, bare C-4 charges were used. The charge was loaded by filling the sphere half full of powder, then placing the C-4 ball, with attached tube, in the centre of the sphere. The remainder of the powder was then poured in, thereby retaining the charge in place. A vernier calliper was used to centre the burster charge within the bulb and tape, quick-set epoxy, or hot glue were used to affix the burster assembly to the glass casing. The charges were placed on a section of plastic tube attached to the end of a wooden rod, with a height of burst of 1.5 m. A half-filled dry charge with fitted C-4 burster and tube assembly is depicted in Figure 4.3a. Assembled dry powder and neat liquid charges are depicted in Figures 4.3b and 4.3c, respectively.

In total, 63 terminal velocities were collected for charges containing 12 different solid powders, 6 wet powder beds or powder suspensions, and 5 liquids. The fill-mass to charge-mass ratio (M/C) was varied from 4 to 300 by varying the mass of the C-4 charge and using a combination of the different bulb sizes and filler materials with a wide range of masses. High-speed videography was used to capture the dispersal process.

4.6.1 Materials Tested

A large selection of granular materials spanning a wide range of density, hardness, toughness and morphology were explosively dispersed. Dense, high-toughness, and moderate hardness materials were represented by spherical steel blasting media: SAE J444/J827 standard S110 steel shot (280 μm mean size, 45–52 HRC), and stainless steel shot of equivalent standard (Vulkan S-30 Chronital, 280 μm mean size, 30 HRC). Ductile, similar density materials were also used: irregular <150 μm brass (Atlantic Equipment Engineers BR-102, \approx 120 HV), and irregular, \approx 220 μm mean size, 99% pure iron (Atlantic Equipment Engineers FE-114, 47–60 HRB). Ceramic materials studied included spherical, 68 μm mean size, and 120 μm mean size MIL-PRF-9954C standard glass blasting media (Potters Ballotini #13 and #10, respectively, 48 HRC), irregular \approx 60 μm silicon carbide (240 grit), and commercial play sand. Commercial granulated sugar and icing sugar were also dispersed.

Liquids tested included neat water, ethanol, and glycerol. Liquid sodium polytungstate was also dispersed to examine the effect of liquid density. Ultra-fine tungsten carbide powder was suspended in both glycerol and the sodium polytungstate solution to further increase mixture density and to study the effect of solid heterogeneities on the formation of liquid jets. Finally, water was used to saturate and fill the interstitial voids of packed beds of S110 steel, glass media, and a mixture of S110 steel and 240 grit silicon carbide.

4.6.2 Velocity Extraction Method

High-speed videography was used to determine dispersal velocities. The dispersals were recorded with two high-speed cameras: A Photron SA-5 recording at 10,000 fr/s and a NAC GX-8 recording at 5,000 fr/s. The higher spatial and temporal resolution SA-5 videos were used for all velocity measurements. Prior to each test a still image of a chequerboard or graded yard stick was taken to establish an absolute pixel-length scale. Depending on the distance to charge and magnification used between different trials, each pixel corresponded to a physical dimension of 3.1–4.5 mm.

Velocity of the dispersed media was determined by measuring the trajectory of the jet tips or the outer layer of non-jetting materials (S110 steel and S-30 Chronital). To obtain the average position of the jets as a function of time, two circles centred on the bulb were fit on each video

frame. Both circles were drawn so as to fit the tips of the fastest jet at a height corresponding approximately to the height of the charge. One circle fit the fastest jet on the left side of the charge and the second circle fit the fastest jet on the right side. Then the averaged radius between these two circles was extracted to get the mean position of the jet front. The purpose of this method was to account for dispersion asymmetries after detonation of the charge. Due to the detonator tube and truncated bulb at the top, and the tubular stand at the bottom, sections of the dispersed material were perturbed and slowed. Consequently, using the equatorial material position provided the most representative experimental trajectory. To obtain a smooth velocity profile, the position-time curve was fit with a third-order polynomial and differentiated. Because the jets have comparatively low areal density and shed substantial material, the terminal velocity is selected from the curve fit at the instant where the jet tips have visibly emerged from the fireball. An inherent assumption in this analysis is that the velocity of compacted fragment forming the jet tip is representative of the average maximum velocity of the entire material shell before it began to slow and break up under aerodynamic loading.

4.7 Results and Discussion

4.7.1 Particle Dispersal Morphologies

In most cases, the dispersal of liquids and granular materials leads to formation of liquid or particle jet-like structures. As noted earlier, the particle properties influence whether or not jets form and the number and morphology of the jets depends on both the particle properties and M/C ratio. Brittle particles, such as glass, sand, or silicon carbide, particles readily form jets that consist of a parent fragment of partially consolidated material. Each parent fragment sheds fine fragments as it moves radially outwards, generated a billowing wake. An example of this is shown in Figure 4.4, which illustrates the morphology of the jets produced during the dispersal of SiC powder. The jets continue to travel radially outwards until the parent fragment is completely consumed, at which point the jets stop expanding radially but slowly expand in diameter as the fine fragments mix with the surrounding air.

Hard, tough particles, such as hardened steel shot, generally do not form coherent jets during dispersal. An example is shown in Figure 4.5, in which a packed bed of S110 steel shot particles

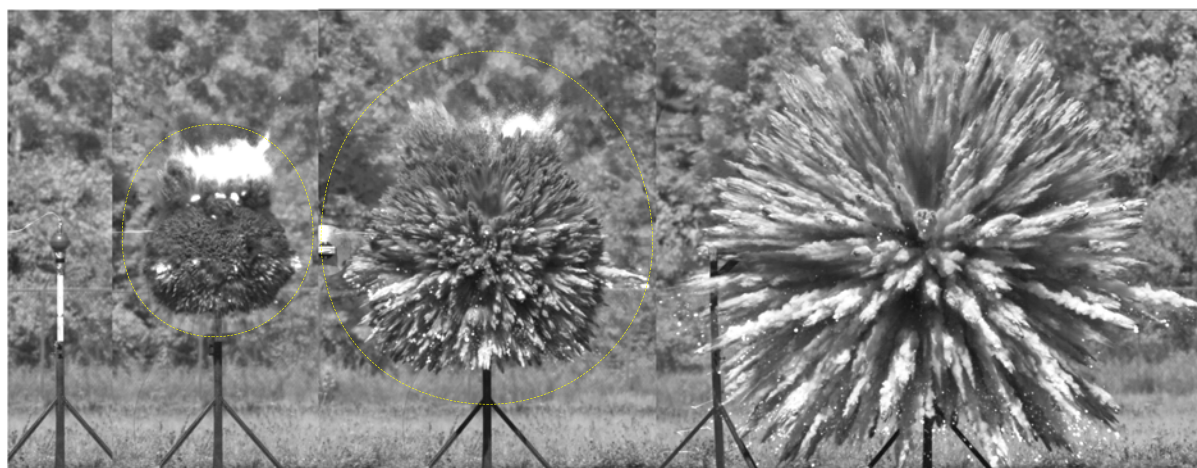


Figure 4.4: Single video frames taken during the explosive dispersal of SiC particles. Charge diameter is 12.7 cm dia, mass of SiC is 1512 g, mass of C-4 is 75 g, giving $M/C = 20.2$. Pictures shown were taken at times of 0, 1, 2, and 4 ms after detonation of the charge. The dashed yellow circles in the middle two images show the approximate location of the blast wave at these times.

is dispersed with a 75-g C-4 charge. At a time of 2 ms, the powder is concentrated in a thin shell that is expanding radially outwards. The shell of particles becomes more diffuse at later times. The picture taken at 4 ms shows that coherent linear strands of particles, elongated radially, form during the dispersal process. These radially strands are remarkably stable and gradually stretch radially as they move along radial trajectories. The origin of these particle strands is not known, but they may be a remnant of the force chains that form within shocked particle beds, which may lead to partial consolidation of a radial line of particles. When the M/C ratio is increased by reducing the charge mass, the formation of the particle strands is less prevalent.

Metal particles that are more ductile than hardened steel shot, such as Al, Mg, pure iron, or brass particles, lead to jet formation, in general, during explosive dispersal. An example of this is shown in Figure 4.6 for the dispersal of brass powder. A portion of the powder immediately adjacent to the explosive charge is consolidated to near-solid densities. For the case of aluminum powder, evidence for the powder consolidation is provided by the mm-scale fragments of compacted powder that are recovered after a trial.

Saturating a porous particle bed has an influence on the subsequent morphology of the particle dispersal. Figure 4.7 shows single video frames from the dispersal of a bed of S110 steel shot saturated with water. The steel shot forms a layer that is even more coherent than for the dispersal of dry powder. At later times, the formation of jets of water droplets within the shell of steel particles is evident.



Figure 4.5: Single video frames taken during the explosive dispersal of S110 steel shot particles. Charge diameter is 12.7 cm dia., mass of steel is 4130 g, mass of C-4 is 75 g, giving $M/C = 55.1$. Pictures shown were taken at times of 0, 2, 4, and 6 ms after detonation of the charge.

Saturating a porous bed of SiC particles with water eliminates the formation of the large coherent jets of SiC particles that occurs during the dispersal of a bed of dry SiC particles, as shown in Figure 4.8. At a time of 2 ms, the surface of the expanding SiC/water cloud has a fine structure, but no large coherent jets are present. As the material expands, it becomes evident that a large number of fine jets have been generated. The jets are likely comprised of a slurry of SiC/water droplets. Some of the jets evident in the photograph at 6 ms have a narrow diameter and project ahead of the cloud of SiC and water droplets.

4.7.2 Particle Dispersal Velocities

The initial/maximum terminal shell velocities for all liquid-containing and dry granular packed bed experiments are plotted in Figures 4.9 and 4.10. Figure 4.9 depicts the terminal velocities for all liquids, slurries/particle suspensions, and liquid-saturated packed particle beds. Figure 4.9 depicts the terminal velocities for all dry packed particle bed experiments. The data is plotted as two separate sets because they exhibit different scaling with the value of M/C . In both plots the black curve represents the spherical Gurney curve (4.4) using a Gurney velocity fitted to the liquid and wetted particle experiments. Since prominent but fine scale jetting was present in all liquid and wetted particle experiments, the reported velocity represents the maximum jet tip velocity obtained from high-speed video. For the dry materials the reported velocity represents either the jet tip velocity for jetting material, or the outermost extent of the perturbed shell for

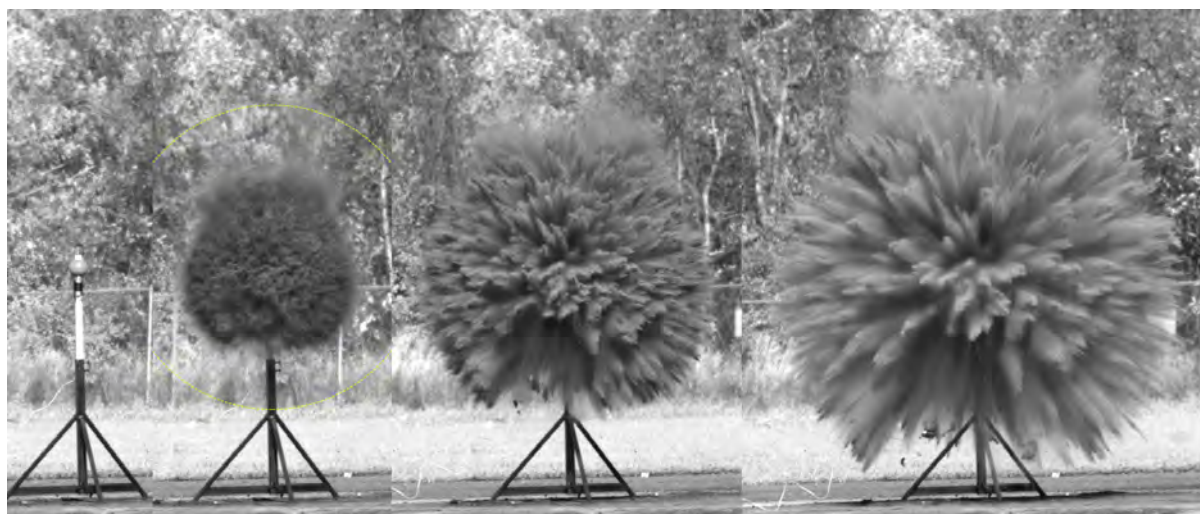


Figure 4.6: Single video frames taken during the explosive dispersal of brass particles. Charge diameter is 12.7 cm dia., mass of brass powder is 3490 g, mass of C-4 is 75 g, giving $M/C = 46.5$. Pictures shown were taken at times of 0, 2, 4, and 6 ms after detonation of the charge. The yellow circle surrounding the charge in the image taken at 2 ms shows the approximate location of the blast wave.

the non-jetting steel experiments. As noted, only the various steels dispersed as a perturbed shell while all other dry solids dispersed with prominent jetting.

Although there is considerable scatter of approximately $50 \text{ m} \cdot \text{s}^{-1}$ between neighbouring data points and for different liquid materials or wetted systems, the spherical Gurney model reasonably predicts a mean initial terminal velocity of the jet tips across the full range of M/C values and materials considered for the liquid/wetted subset. The Gurney curve depicted in Figure 4.9 was defined using a value of $2462 \text{ m} \cdot \text{s}^{-1}$ for the explosive Gurney velocity. This value was obtained by fitting Equation 4.4 to the data subset using the built-in Matlab fitting routine. With this Gurney velocity a maximum error of 15.6% and a mean error of 6.1% were obtained between the model and the experiments. The error was not biased with M/C .

In a previous study, the authors fitted a value of $2680 \text{ m} \cdot \text{s}^{-1}$ for the Gurney velocity of C-4 using open face sandwich flyer plate experiments. The present fitted value is thus 92% of the previously reported value and is slightly lower than other literature values [8]. This discrepancy is likely due to the geometry, the range of M/C values considered, and dynamics of the liquid/wetted shell breakup rather than dissipation through the shell. Since the Gurney velocity is principally an experimental fitting parameter that can be freely adjusted, this slight discrepancy poses no issue, particularly since there was some scatter in the data used to fit the

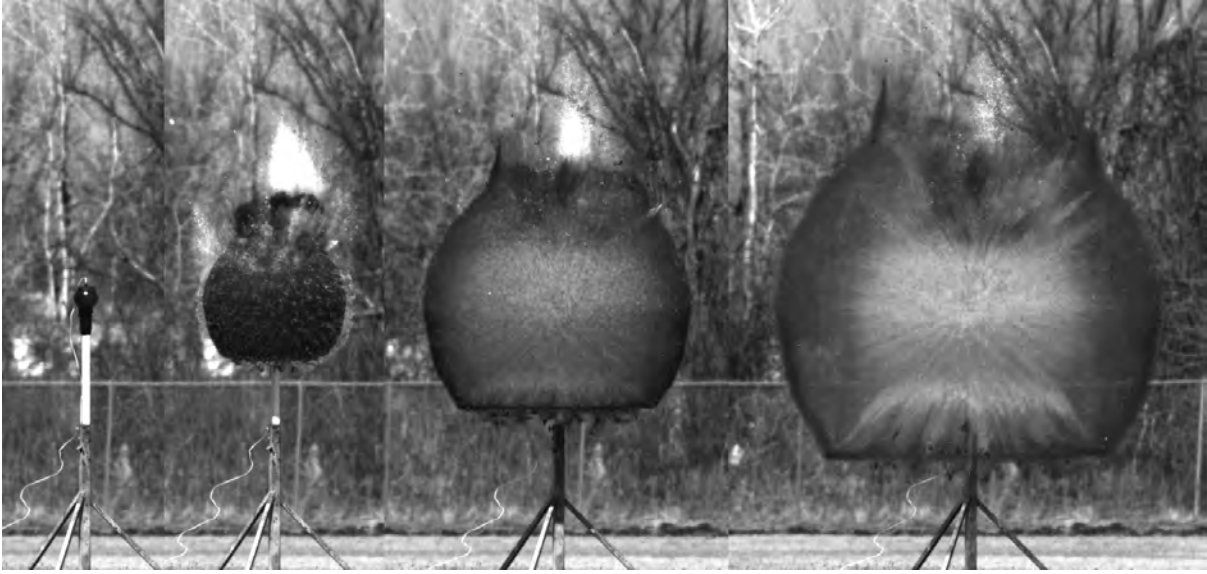


Figure 4.7: Single video frames taken during the explosive dispersal of a bed of S110 steel shot saturated with water. Charge diameter is 12.7 cm dia., mass of steel shot is 4410 g, mass of water is 338 g, mass of C-4 is 28.3 g, giving $M/C = 168$. Pictures shown were taken at times of 0, 2, 4, and 6 ms after detonation of the charge. In the second frame, the fine fragments of the glass casing are visible just outside the layer of steel particles. The shell of steel particles becomes thin enough at later times so that the formation of jets of water droplets is visible contained within the shell of steel particles in the last frame.

larger value for the Gurney velocity in the previous study. We note that a modified power law fit (e.g., Eq. 4.5), was not necessary for good agreement with the experimental data.

Overall good agreement between the spherical Gurney equation and the liquid/wetted particle experiments indicates that the Gurney model assumptions approximate the actual partition of explosive energy between the material shell and the detonation products. Close agreement between Gurney energies measured in disparate geometries and over wide ranges of M/C further indicates that liquids and wetted solids are accelerated similar to homogeneous solid shells despite prompt, cavitation-driven breakup of the liquid. Conceptually this breakup is quite different to the extended period of plastic flow and then fracture observed in ductile metal casings, but does not manifest as a large reduction in propulsive efficiency. Thus, liquid or wetted shells are non-dissipative and do not leak detonation product sufficiently to result in much lower terminal velocities.

In contrast, the experimental velocities for the dry granular materials departed from the classic Gurney Model both in magnitude and how velocity scales as a power law with M/C . Based on Figure 4.10 it is apparent that the terminal velocities are, at best 75% and at worst 40% of

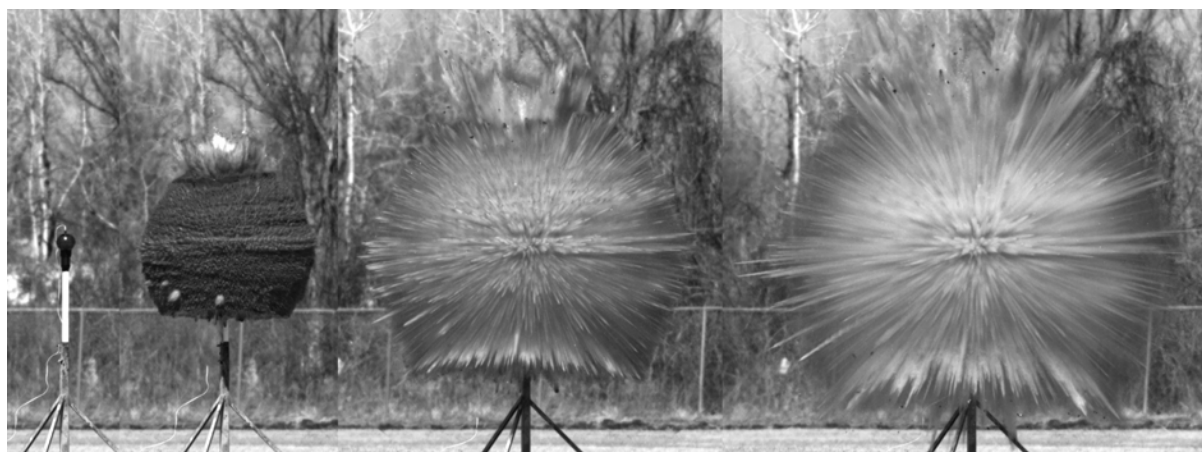


Figure 4.8: Single video frames taken during the explosive dispersal of a bed of SiC particles saturated with water. Charge diameter is 12.7 cm dia, mass of SiC 1511 g, mass of water is 338 g, mass of C-4 is 28.3 g, giving $M/C = 65.3$. Pictures shown were taken at times of 0, 2, 4, and 6 ms after detonation of the charge.

their Gurney-predicted values using the same Gurney velocity as before; suggesting substantial dissipation of energy by the dry granular shells as the relative amount of material increases. The solid black line in Figure 4.10 represents the spherical Gurney curve with a Gurney velocity of $2462 \text{ m} \cdot \text{s}^{-1}$ while the dashed black line represents an equivalent Gurney curve with the C-4 Gurney velocity scaled by a factor of 0.55 ($1354 \text{ m} \cdot \text{s}^{-1}$). The dashed curve effectively illustrates the departure of the experimental material velocities from the inverse square root scaling of the Gurney model: terminal velocities are slightly over-predicted for the largest values of M/C (>225), and then increasingly under-predicted for M/C values below 30. In all cases, the terminal velocity is lower than what is predicted by the spherical Gurney equation using the same Gurney energy as for the liquid/wetted cases. These discrepancies are characteristically different from disagreements typically observed at very low values of M/C in flyer plate and cylinder expansion experiments, which arises due to gasdynamic and wavedynamic departures from the assumption of linear velocity profile and no density gradient in the detonation products [5, 9, 53, 54]. This situation typically arises when large charges relative to the flyer mass are used, described by M/C ratios of around 0.1 or lower. On a mass-ratio basis, this regime was avoided in the present experiments.

The contrast between the velocity of dry granular materials and an equivalent scaled mass of the same material saturated with water is a clear indication of the role of pore collapse in dissipation of the explosive energy. As shown in Figure 4.11, when a packed bed of material

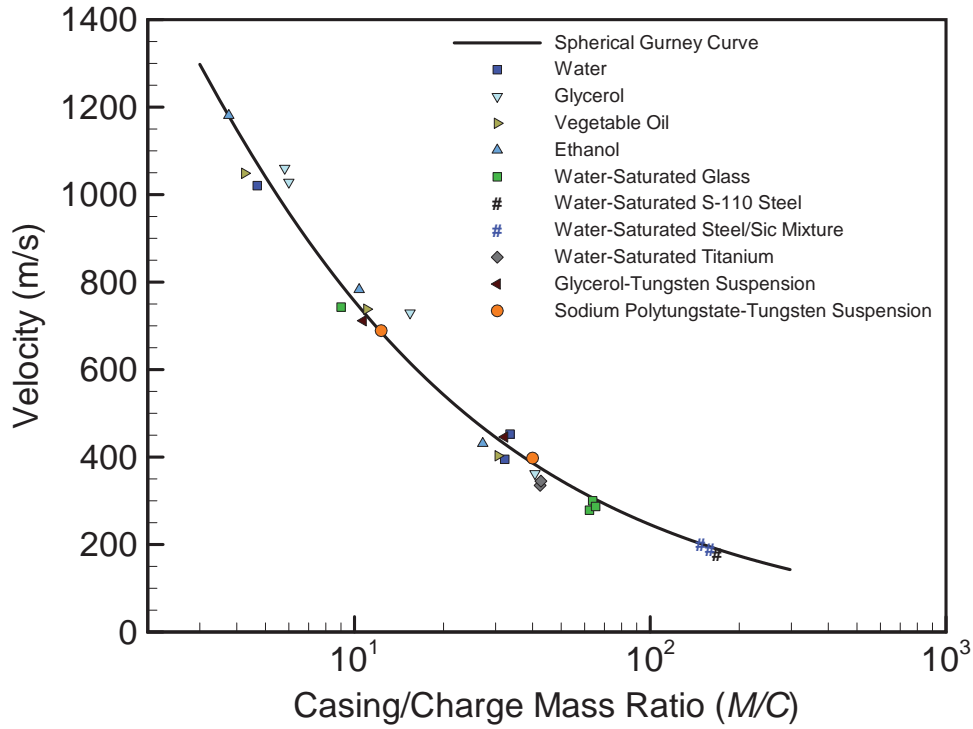


Figure 4.9: Experimental data for liquids, slurries and water-saturated granular materials versus the unmodified spherical Gurney equation (Eq. 4.4—solid black curve) using a Gurney velocity of $2462 \text{ m} \cdot \text{s}^{-1}$.

was saturated with water such that the interstitial spaces were replaced with a fluid, the total shell velocity increased despite the added mass of liquid. We postulate this occurred because the liquid is capable of supporting sufficient stress to entirely suppress material consolidation through pore collapse. Further evidence for this arises from the jetting behaviour of these wetted systems: breakup and jetting of the shell occurred with a fine scale associated with cavitation-driven failure of the liquid, rather than fragmentation of a consolidated solid. This implies that no consolidated material is fragmenting, but rather that the liquid is cavitated by nucleation sites at the particles upon wavedynamic release. The different jetting phenomenology have already been illustrated for 12.7 cm bulb experiments containing either dry (Figure 4.5) or water-saturated (Figure 4.7) S110 steel, dispersed by 75 g burster charges. Figure 4.7 clearly shows fine-scale liquid jetting within a smooth, mostly steel outer layer, while Figure 4.5 shows a diffuse expanding layer of particles with jetting only present at the detonation product/air interface.

While there is substantial scatter in velocities for given ratios of M/C and for both similar and dissimilar materials there is no evidence of a robust influence of material properties on shell

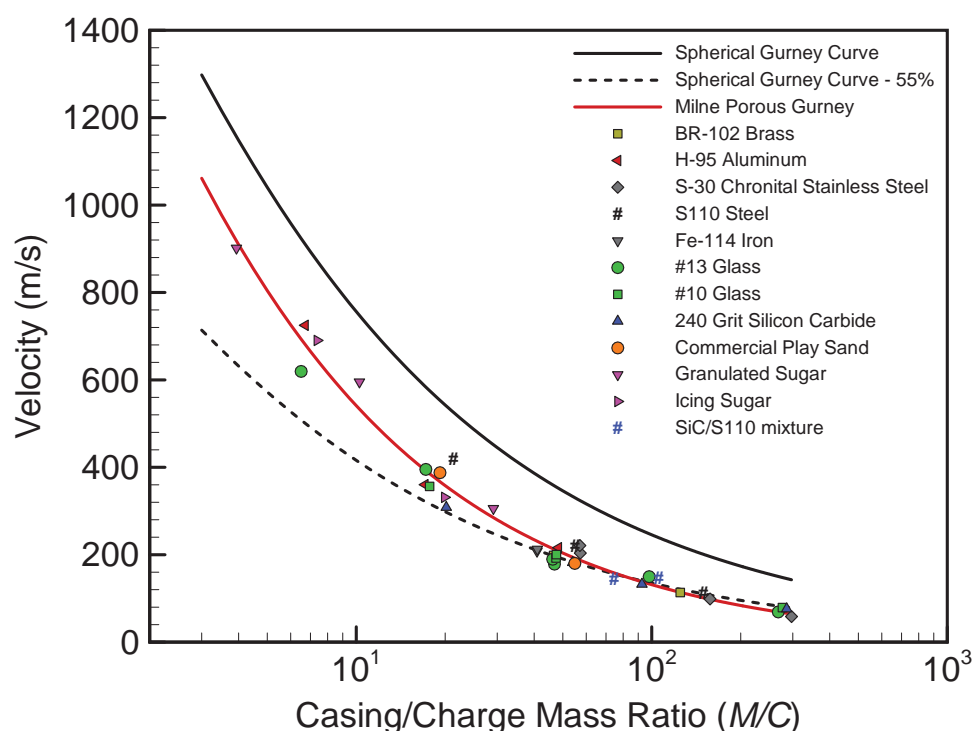


Figure 4.10: Experimental data for dry granular materials versus the unmodified spherical Gurney equation (Eq. 4.4—solid and dashed black curves) and the modified spherical Gurney equation (Eq. 4.7—red curve) using a Gurney velocity of $2462 \text{ m} \cdot \text{s}^{-1}$.

velocity. Similarly there is no significant difference in velocity caused by the extent of jetting or presence of jetting at similar mass ratios. On average the hard, non-jetting steels reached higher velocities, while the brittle and relatively weak glass particles, and the brittle but strong SiC particles, reached lower velocities. Ductile aluminium and sugar also reached higher velocities than the glass for small values of M/C . These trends, however, were not consistent across the full range of M/C values considered, and the relative discrepancy between points and materials diminished or disappeared as the value of M/C became large. A substantial and systematic effect from material solid density was not observed in the current data either: iron and brass showed similar terminal velocities compared to much less dense glass, and dispersed sugar had substantially higher velocity than glass at small M/C values. Several factors may explain this lack of consistent material effect: the degree of porosity was not constant throughout the different materials due to differences in particle morphology and size distribution. It is further challenging to ensure a consistent packing fraction across multiple fillings even with the same powder due to jamming and settling during filling. Finally, for the small values of M/C , relative placement errors of the burster charge may result in larger velocity anomalies.

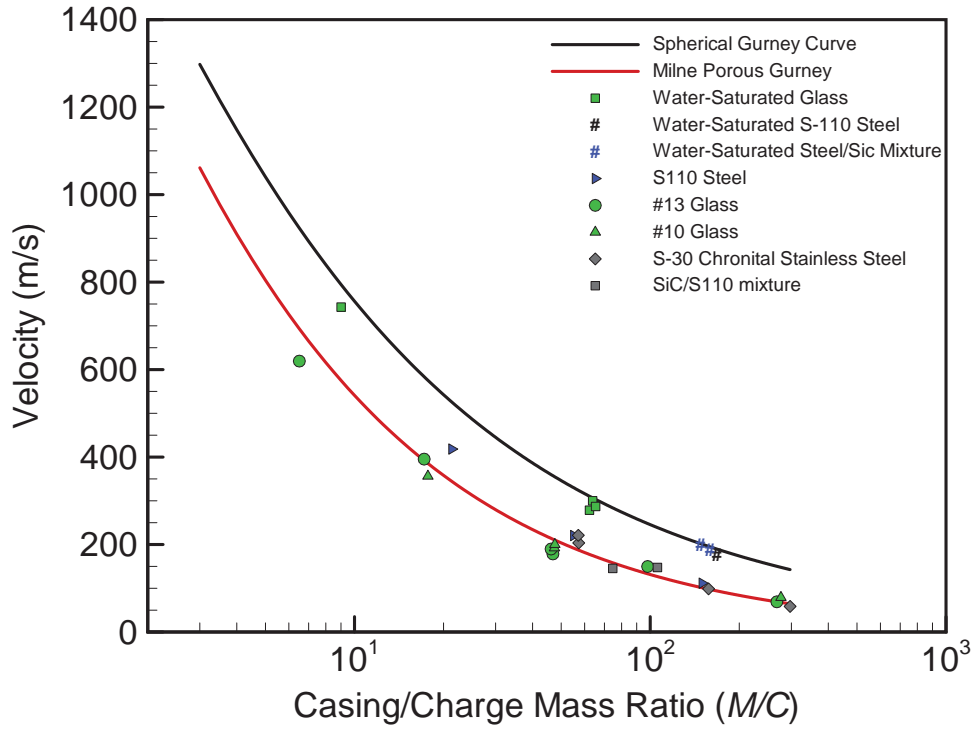


Figure 4.11: Comparison of terminal velocities for dry, and water saturated powders.

To further explore material dependencies, the sugar and high-density metal data was plotted separately in Figure 4.12 versus two corrected Gurney model curves. Solid densities of $1590 \text{ kg} \cdot \text{m}^{-3}$ for sugar and $7860 \text{ kg} \cdot \text{m}^{-3}$ for steel, and an average porosity of 0.5 were used to calculate the fitting parameters. The pink curve represents the sugar model, while the black curve represents the steel model. The model curves reasonably predict the scaling of velocity with M/C for both materials as well as the convergence of the terminal velocities for large values of M/C for all material densities. Notably, the experimental velocities for the iron and brass fell below the steel data, particularly at smaller values of M/C , despite similar densities. One possible explanation for this is that their irregular shape resulted in lower porosity than equivalent quantities of the nearly spherical steel. Alternatively their lower strength and higher ductility resulted in a greater degree of compaction and thus void collapse; the high strength steels are quite resistant to consolidation by comparison. This resistance to compaction is evidenced by the suppression of jet formation in the steel experiments, which we postulate arises due the steel shell not being compressed into a solid layer that subsequently fragments. By contrast, the brass and the iron readily jetted. However, as evidenced by this data, resistance to consolidation does not have a large impact on the dissipation of energy by the granular shell.

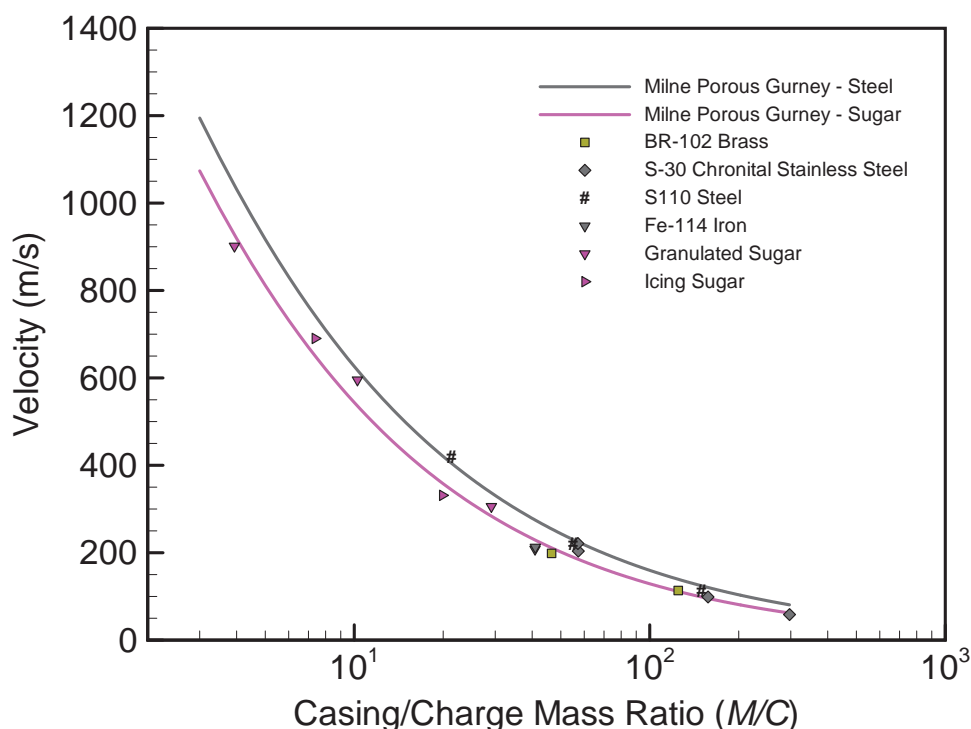


Figure 4.12: Experimental data for dry granular and icing sugar, S-110 and Vulkan S-30 steels, Fe-114 iron, and BR-102 brass versus material-specific curves constructed using the Milne model. The Gurney velocity was $2462 \text{ m} \cdot \text{s}^{-1}$.

Due to these factors and observations, and the fact that the effect of solid density on shell velocity is modest, it is attractive to attempt to fit the entire data set with a single model curve that is a function of only the explosive Gurney velocity and the charge mass ratio (M/C). Here K and α were taken to be free parameters and used to fit the form of eq. 4.7 to the full data using Matlab. Values of $K = -0.1985$ and $\alpha = 0.7870$ were determined, the fit is depicted as a solid red line in Figure 4.10. An average error of 8.7% and a maximum error of 18.9% was obtained with this fit; similar but slightly higher than what was obtained for the liquid/wet data. The largest errors are due to the wide scatter in the data, not a systematic bias.

The critical feature of the improved fit relative to the baseline Gurney equation is the logarithmic dependence of the Gurney velocity scaling parameter, F , on the M/C ratio. This supports the hydrocode-derived hypothesis that it is primarily the relative quantity of collapsing pores that controls the dissipation of explosive energy and thus the reduction in shell velocity. Larger relative quantities of granular material (large values of M/C) contain a greater quantity of pores and thus exhibit more energy dissipation. The functional form proposed by Milne is thus a representative scaling law to estimate shell terminal velocity when dissipation is present.

Deviation from the hydrocode-derived form of the Gurney correction are likely due to experimental factors such as variabilities in packing density between experiments, as well as the fact that the model was only corrected for solid density using simulations for a couple of materials. In the present experiments, a wide range of materials of different strengths, and with different compaction dynamics because of their morphology, were considered.

4.8 Conclusion

The explosive dispersal of spherical shells composed of a variety of dry granular materials, liquids, and wetted granular materials was conducted experimentally. The resulting dispersal was typically characterized by the formation of jet-like structures of varying numbers depending on the material and relative mass of the shell compared to the mass of the explosive burster charge (M/C). Only strong and hard steel particles were capable of suppressing this jetting behaviour.

For liquid shells, the terminal velocity of the jet tips closely followed predictions of the conventional Gurney model in spherical geometry. This implies that the acceleration of liquid or wetted shells is non-dissipative and thus analogous to the acceleration of a conventional homogeneous solid casing. Despite prompt, cavitation-driven breakup, the liquid jets reached the terminal velocity expected using a nearly-typical value of C-4 Gurney velocity.

For dry powders, the jet terminal velocity was substantially lower than that what was predicted by the Gurney model and the scaling of jet velocity with shell-mass to charge-mass did not follow the inverse-square-root dependence stipulated by Gurney. These departures were attributed to the highly dissipative nature of the collapse of voids during shock-loading of the dry granular materials. For liquid saturated granular materials, void collapse and inter-particle damage and consolidation was suppressed due to the stress-bearing capability of an interstitial fluid. Wetted particle systems thus followed the classic Gurney scaling observed with the liquid experiments.

To account for the dissipative nature of the porous particle beds an empirical correction was proposed based on Gurney model corrections developed by Milne [166]. Satisfactory, engineering-model agreement for the complete data set was obtained with a single set of fitting parameters. Robust dependencies of shell velocity on particle material properties were not

observed for the entire data set, and we explain this by variances in packing density due to particle morphology and variations in actualized packing during charge filling.

4.9 Acknowledgements

The authors thank Rick Guilbeault at the Canadian Explosive Research Laboratory for assistance with the experiments and the Defense Threat Reduction Agency for funding under the basic research grant HDTRA1-11-1-0014.

Chapter 5

Particle Segregation During Explosive Dispersal of Binary Granular Material Mixtures

David L. Frost, Jason Loiseau, Bradley J. Marr, and Samuel Goroshin

[AIP Conference Proceedings, SSCM-2015](#)

5.1 Abstract

The explosive dispersal of a layer of solid particles surrounding a spherical high explosive charge generates a turbulent, multiphase flow. The shock-compacted particle layer typically fractures into discrete fragments which move radially outwards on ballistic trajectories. The fragments shed particles in their wakes forming jet-like structures. The tendency to form jets depends on the mass-ratio of the particles to explosive and the type of particles. Brittle or soft, ductile particles are more susceptible to forming jets during compaction and dispersal, whereas particles that are comprised of material with moderate hardness, high compressive strength and high toughness are much less prone to forming jets. Experiments have been carried out to determine the degree of particle segregation that occurs during the explosive dispersal of a uniform, binary mixture containing both “jetting” (silicon carbide) and “non-jetting” (steel) particles with various mass fractions of each particle type. During the dispersal of mixtures that contain pre-

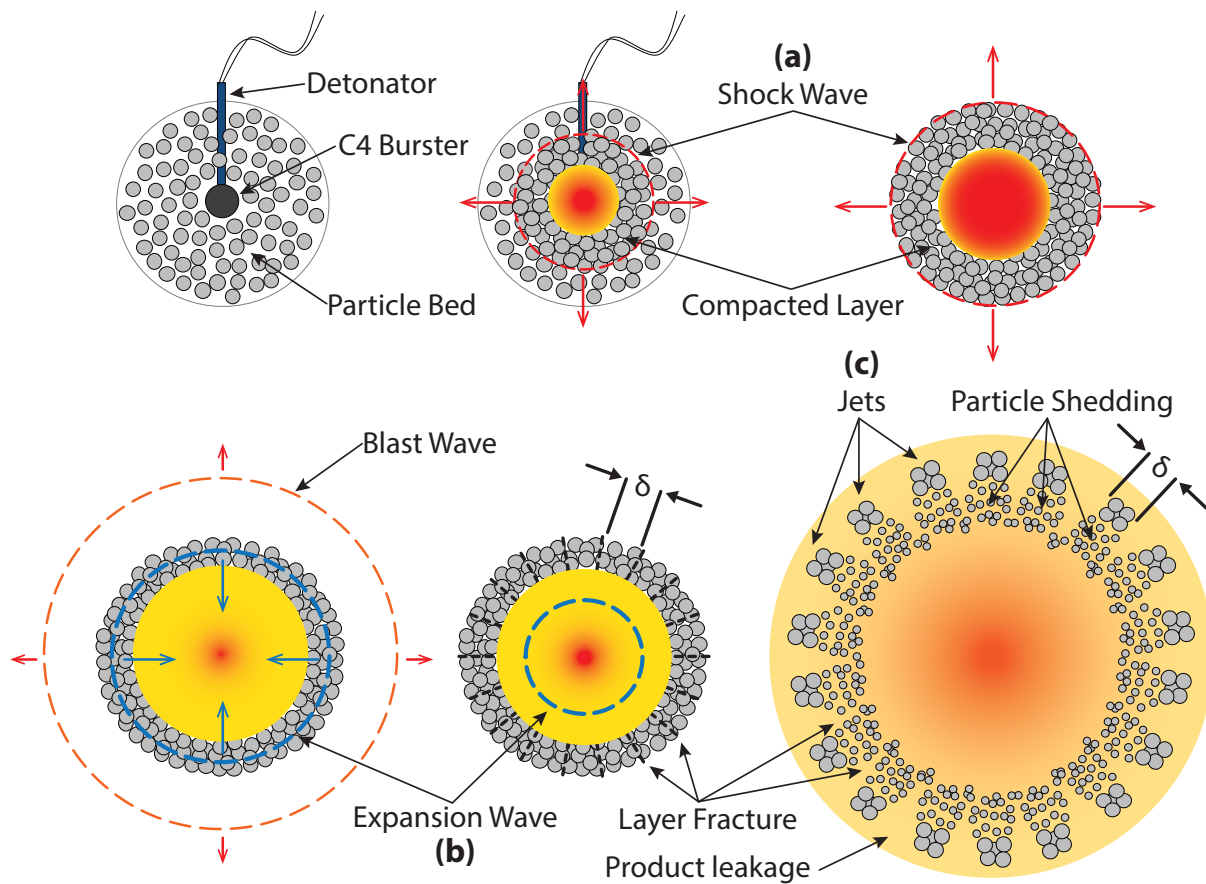


Figure 5.1: Schematic of particle jet formation during explosive dispersal. **(a)** Detonation of the burster drives a shock into the particle bed, which subsequently compacts. **(b)** When the shock reaches the outside of the charge it generates an air blast and a strong expansion wave returns into the compacted layer and expanding products. The compacted layer experiences hoop stress at this stage and begins to fracture. **(c)** These fragments form the jet tips and aerodynamically shed particles in their wake.

dominantly non-jetting (steel) particles, the steel particles form a stable layer whereas the jetting (silicon carbide) particles rapidly segregate and form jets which are confined within the shell of steel particles. As the fraction of silicon carbide particles increases, the jet structures dominate the particle motion and the steel particles are entrained into the jet structures.

5.2 Introduction

When a layer of solid particles is explosively dispersed by the detonation of a high explosive charge, the expanding particle cloud typically forms a non-uniform structure comprised of coherent jets [167]. A similar behavior occurs for the explosive dispersal of liquids [168] or liq-

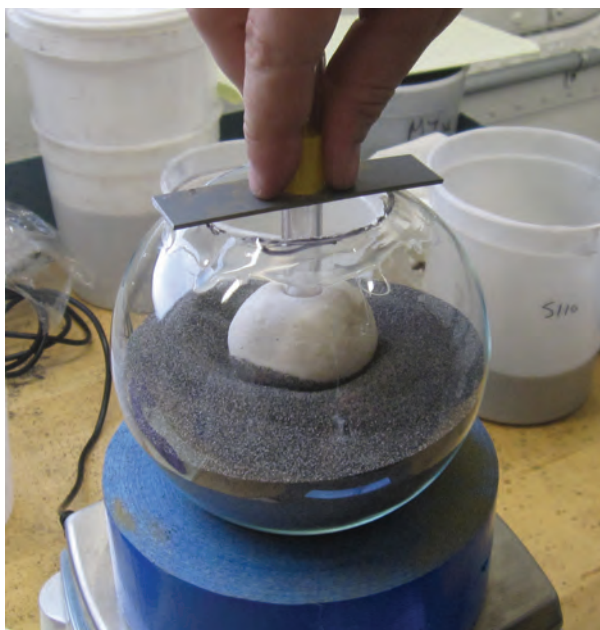


Figure 5.2: Photograph of experimental charge, partially filled with powder. The mass of the ball of C-4 visible in the center of the glass sphere in this case was 75 g.

uid/particle mixtures [170, 179]. A growing body of photographic and radiographic evidence suggests that the jets form early during the dispersal process, on the timescale of the propagation of the shock and release wave through the particle layer [169]. Figure 5.1 shows a schematic of our working hypothesis for the jet formation. After detonation of the charge, a shock wave propagates outwards, compacting all or a portion of the powder bed. When the shock reaches the outer surface of the powder, a blast wave is transmitted into the surroundings and an expansion or release wave moves back into the compacted bed, putting the bed under tension. About the time that the release wave reaches the inner surface of the particle bed, if the compacted layer has some material strength following the compaction process, the layer fractures into fragments that have a scale similar to the compacted thickness of the layer and much larger than the original particle size. Each fragment, consisting of a partially consolidated mass of particles, moves radially outwards, shedding finer fragments which form the billowing wakes visible in high-speed visualization of the particle dispersal.

For solid particles, the number of jets scales inversely with the ratio of the mass of the particles to that of the explosive (M/C), or fill/burster ratio [168]. Furthermore, the tendency to form coherent jets is dependent on the particle material properties and to a lesser extent on the F/B ratio. Particles that are brittle, such as sand, glass, or silicon carbide, or particles that are

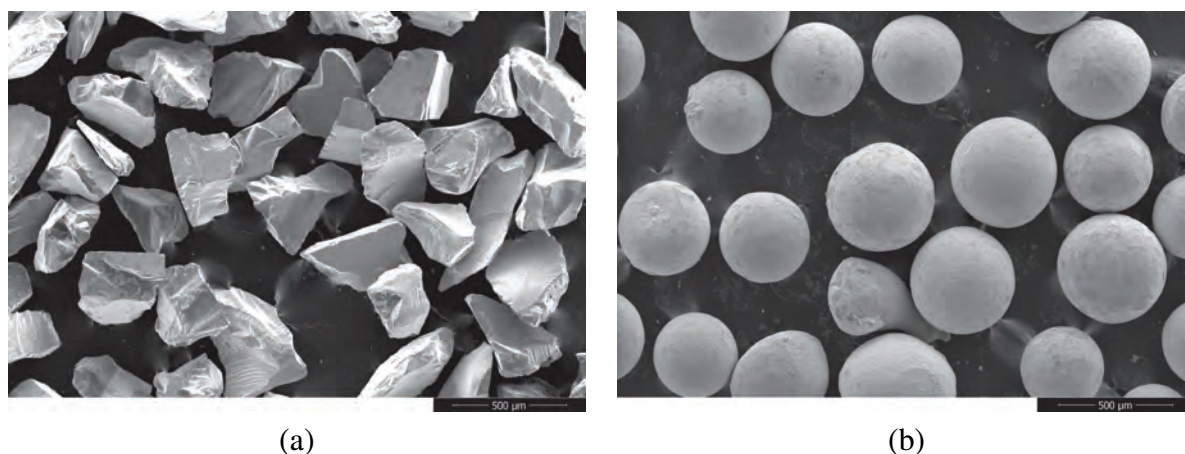


Figure 5.3: SEM micrographs of the two powders used in present investigation: **(a)** silicon carbide, and **(b)** S110 steel shot.

comprised of soft, ductile materials such as aluminum, magnesium, and brass are susceptible to forming jets. In contrast, particles made of materials with a combination of high compressive strength, high toughness, and moderate hardness, such as steel shot with Rockwell C hardness of 45–50, are less likely to form jets. In general, the state of the particle bed after compaction determines whether or not jets form. In particular, the greater the degree of consolidation of the powder during shock compaction, the greater the tendency for jet formation following expansion of the compacted layer.

A question naturally arises as to the tendency to form jets for binary mixtures of two types of powders. If “jetting” and “non-jetting” particles are mixed together uniformly and explosively dispersed, it is not clear, *a priori*, whether jetting will be suppressed and if this depends on the relative mass fractions of each type of particle. The present experiments were carried out to investigate this question. The powder mixtures considered had various volume fractions (ranging from 0% to 100%) of silicon carbide particles, which readily form jets, and hardened steel shot particles, which generate a relatively uniform particle layer during dispersal. The dispersal dynamics were visualized with high-speed videography and the particle velocities are inferred from the photographic records.

5.3 Experimental Details

The charges used in the present study consisted of thin-walled (1 mm thick) G40 globe light bulbs (12.3-cm diameter, 1 L volume) prepared by removing the filaments. A 28 g spherical

ball of C-4 high explosive was formed by hand and placed in the center of the glass sphere. A plastic tube was inserted into the top of the C-4, which allowed the detonator to be inserted into the charge prior to a test. Figure 5.2 shows the C-4 ball within the glass sphere with the charge partially filled with powder. Note that there was no casing on the C-4 to eliminate any interior casing effects on the subsequent particle motion.

The particles used in the present investigation included silicon carbide (240 grit size, bulk density 1.56 g/cm^3), and steel shot (SAE standard S110, bulk density 4.46 g/cm^3). SEM micrographs of the two powders are shown in Figure 5.3. Both particles had a nominal size of about $300 \mu\text{m}$, but had a very different morphology. The SiC particles had an angular shape whereas the steel particles were highly spherical with the exception of infrequent tear drop shaped particles.

5.4 Results

Visualization of the explosive dispersal was carried out with a Photron SA5 high-speed video camera operating at 10,000 fr/s. Figure 5.4 shows several individual frames from the high-speed video records from 4 trials, illustrating the effect of changing the amount of steel in the SiC/steel mixtures.

The first sequence shows a charge containing only SiC particles and shows that these particles form coherent jet structures with each jet consisting of a fragment of compacted powder which sheds fine fragments (likely with a size similar to the original powder) progressively until the mass of the initial large fragment is exhausted, at which point the jet stops moving outwards. The second sequence in Figure 5.4 shows a mixture containing 80% SiC by volume (or about 63% by mass) and 20% S110 steel by volume. The jet formation appears similar to the case with pure SiC, although the tips of the jets appear darker suggesting that the steel particles have become entrained into the jets. The thickness of the jets is also slightly reduced compared to the 100% SiC case.

Particle Segregation During Explosive Dispersal of Binary Granular Material Mixtures

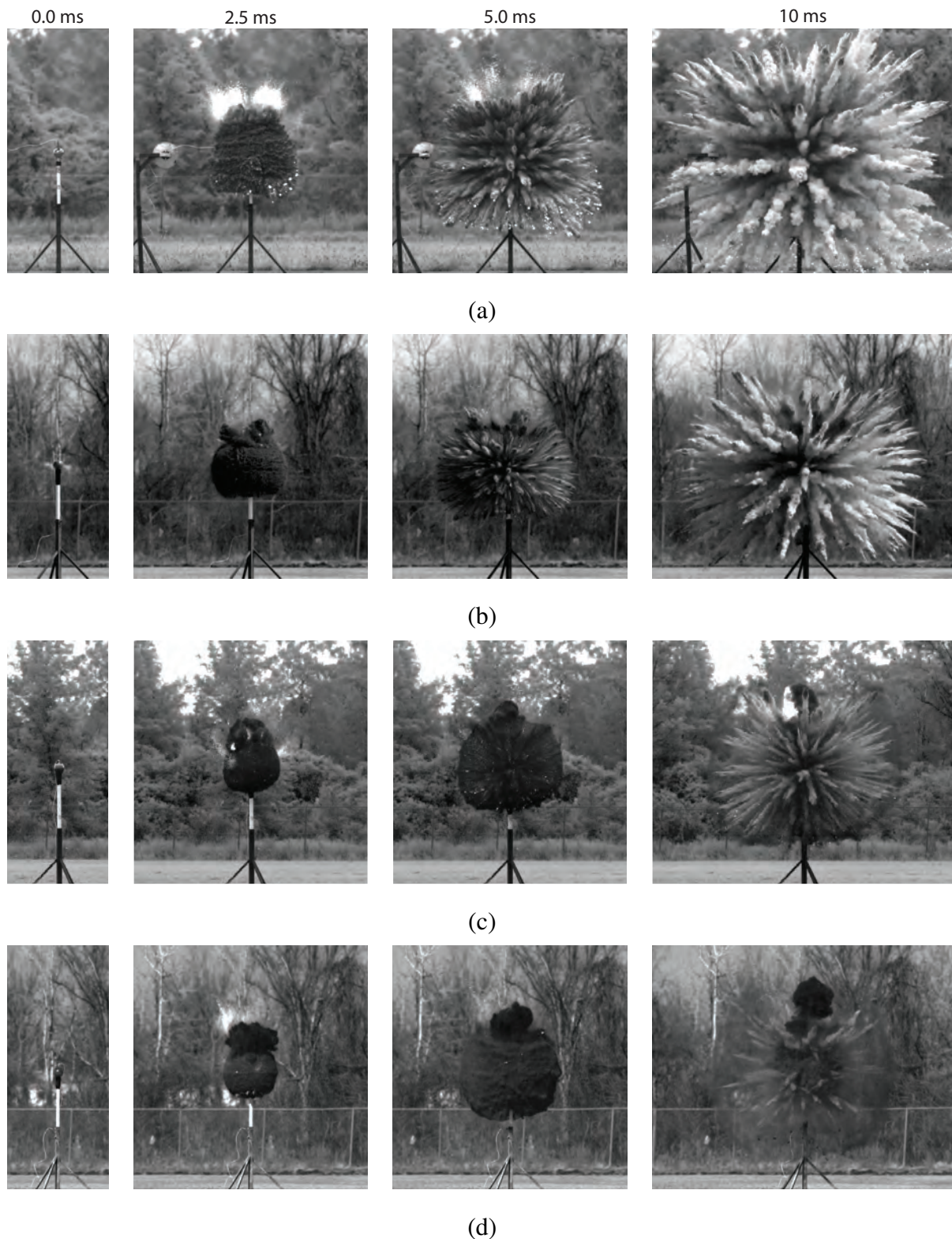


Figure 5.4: Single frames from high-speed video for trials with mixtures of SiC and steel shot containing: **(a)** 0% steel, **(b)** 20% vol. steel, **(c)** 65% vol. steel, and **(d)** 80% vol. steel. In each case the 4 photographs correspond to times of 2 ms, 2.5 ms, 5 ms and 10 ms after detonation of the charge.

When the SiC volume fraction is reduced to 35% (19% by mass), a shell of steel particles is clearly visible (see the third sequence in Figure 5.4 and the SiC jets do not penetrate the steel particle layer. By 10 ms, the jets have begun to slow down and lag behind the front of the steel particle layer. The jets are also substantially thinner compared to experiments with larger fractions of SiC. For the case of 20% SiC by volume (or 10% by mass), the SiC jets still form and appear to cause small perturbations to the steel particle layer (see photo at 5 ms in last sequence of Figure 5.4), before becoming visible as the steel layer becomes transparent. A similar behavior was observed for 10% SiC by volume (5% by mass).

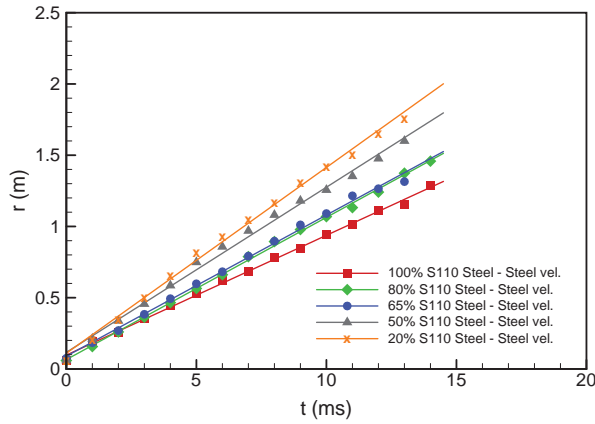
5.5 Discussion

The radial velocity of the outer surface of the explosively dispersed particles may be determined from the high-speed video images. Figure 5.5a shows the trajectories of the outer surface of the steel particle layer in a radius-time plot, while Figure 5.5b show the trajectories of the SiC jet tips in a radius-time plot. The radial velocity of the steel particles is essentially constant over this time period, whereas for the case of pure SiC, the SiC jets begin to slow down after about $10 \text{ m} \cdot \text{s}^{-1}$. Slowing of the jet tips can be observed in the mixture experiments as well. If a line is fit to the maximum extent of the steel particle shell or SiC jet radial position versus time for camera frames over the first $5 \text{ m} \cdot \text{s}^{-1}$, the average particle velocities may be determined, and range from $195 \text{ m} \cdot \text{s}^{-1}$ for the charge containing 100% SiC to $92 \text{ m} \cdot \text{s}^{-1}$ for the charge with 100% steel shot. The velocities are shown in Figure 5.5c, normalized by the Gurney velocity for a spherical charge of equivalent M/C ratio. The classic Gurney equation for a spherical cased charge is used [3]:

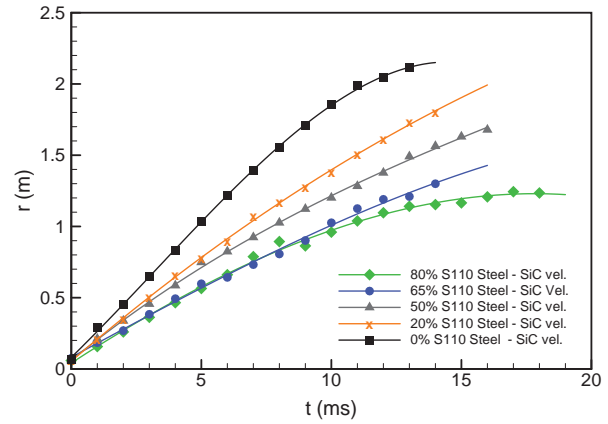
$$V_o = \sqrt{2E} \left(\frac{M}{C} + \frac{3}{5} \right)^{-\frac{1}{2}} \quad (5.1)$$

The value for the Gurney Energy for C-4 was taken to be $\sqrt{2E} = 2.59 \text{ km} \cdot \text{s}^{-1}$ for C-4 and M and C are the masses of the particles and explosive, respectively, using the notation introduced above. Note that the normalized velocity is constant, independent of M/C , and the experimental velocity values are about one half the Gurney velocity [113]. This is consistent with the observation by Ripley et al. who found for explosive dispersal of a dry particle layer in cylindrical geometry, that the Gurney velocity was about 3 times that of the experimental velocity value

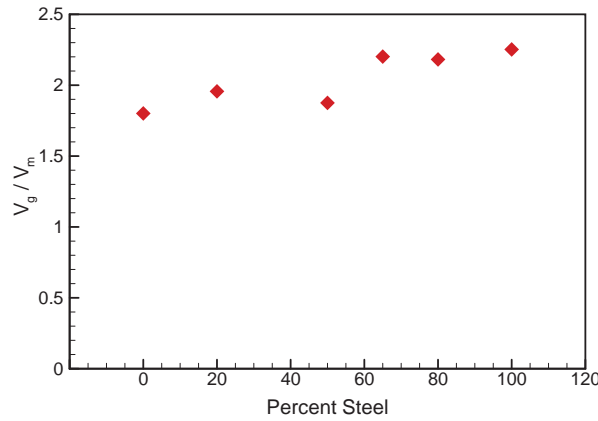
Particle Segregation During Explosive Dispersal of Binary Granular Material Mixtures



(a) Radial trajectories of the steel particles.



(b) Radial trajectories of the SiC jets for the different volume fractions of particles considered.



(c) The velocity of the outer extent of the dispersed particles normalized by the equivalent Gurney velocity as a function of mass fraction of steel particles.

obtained [170]. Factors that will contribute to the lower experimental values include energy losses during the compaction of the powder, and jetting of the detonation products around the compacted fragments, which will limit the time over which the particle fragments are accelerated.

5.6 Conclusion

The present experiments have demonstrated that during the explosive dispersal of binary particle mixtures, jet formation for the lighter particles is a robust phenomenon and occurs even if the mass fraction of the heavier component exceeds 95%. For the case considered, the particle densities differ by more than a factor of 2 ($3.21 \text{ g} \cdot \text{cm}^{-3}$ for SiC vs. about $7.5 \text{ g} \cdot \text{cm}^{-3}$ for the steel shot) and hence the differential acceleration of the lighter particle likely contributes

to the rapid segregation of the two particle components during explosive dispersal. In all of the mixtures considered, the particle velocities obtained are less than the predicted Gurney velocity by about a factor of 2, which indicates that the dynamics of the explosive dispersal of a porous particle bed differs considerably from that of a solid casing as investigated in the original ballistics analysis by Gurney.

Conclusion

In the present body of work, modified forms of the Gurney equations have been validated for both heterogeneous, non-conventional explosives and for conventional explosives driving shells of either granular material or liquid using a large number of experiments. Conclusively, Gurney's method of estimating the velocity of explosively accelerated material by considering a simple partition of explosive energy into the driven material and the expanding detonation products is a robust framework which can reasonably treat even heterogeneous systems.

For the study of heterogeneous explosives, the authors sequentially developed an experimental configuration to measure the acceleration ability of various explosive mixtures and then validated tilt-correction equations required to resolve the total flyer velocity based on interferometric measurements of flyer velocity. The charge configuration was then applied to measure the acceleration ability of a wide range of different heterogeneous mixtures. A second charge geometry was also developed to consider the acceleration of flyers by normally incident detonations. Flyer terminal velocity was shown to broadly follow predictions of the Gurney model. Notably, normally incident detonations propelled flyers to higher velocities than grazing detonations and this effect was amplified as the flyer was thinned. For the thinnest flyers, detonation-scale wave-dynamics increased flyer velocity anomalously. This has important implications for the design of small-scale, foil slapper initiators. The authors also demonstrated that explosives extremely loaded with dense materials do not follow flyer velocity scaling as predicted by the Gurney model. In contrast, the Gurney model was capable of accurately predicting flyer velocity for more typical heterogeneous explosives that contain smaller additive fractions. Consequently, the Gurney model can be used to estimate the relative exothermicity of reactive additives by quantifying the decrement in flyer velocity that would be associated with the additive behaving inertly. Following this conclusion, a number of experiments were conducted considering a range of reactive additives. The Gurney model was used to show that particle reactivity occurred

Conclusion

very fast, such that changing flyer acceleration timescale by using thicker or thinner flyers did not influence the acceleration ability of the metallized mixtures. It was also determined that prompt exothermicity is a robust phenomenon observable in many reactive metals and likely results from surface reaction on the particles as opposed to the particle being relatively slowly heated until ignition. The modest increases in accelerating ability obtained when reactive metals are added arises from the losses from having to accelerate the added particles in the flow. To increase accelerating ability, particle reaction must overcompensate for this loss. The degree of loss can be estimated by the Gurney equation, based on the inert additive experiments.

In the final two chapters, the Gurney model was applied to predicting the terminal velocity of heterogeneous material shells. It was demonstrated that liquids and wetted granular material shell velocities scaled consistently with the baseline Gurney model originally proposed in 1943. By contrast, dry granular materials were accelerated to velocities much lower than Gurney's model predicted. This was attributed to the dissipation of explosive energy when pores in the granular bed were collapsed during compaction. An empirically corrected form of the spherical Gurney equation was successfully fitted to the large experimental data set comprising materials of very disparate properties. These results have important implications for the design of blast mitigation systems that employ granular materials.

References

- [1] C. Rumchik. “An Investigation on the Effect of Aluminum Particle Size on Detonation, Metal Acceleration, and Airblast”. Thesis. University of Minnesota, Dec. 2015.
- [2] E. L. Lee, H. C. Hornig, and J. W. Kury. *Adiabatic Expansion of High Explosive Detonation Products*. Tech. Rep. UCRL-50422. Livermore, CA: Lawrence Radiation Laboratory, 1968.
- [3] R. W. Gurney. *The Initial Velocities of Fragments from Bombs, Shell and Grenades*. Tech. Rep. BRL-405. US Army Ballistic Research Laboratory, 1943.
- [4] P. W. Cooper. *Explosives Engineering*. New York: Wiley-VCH, 1996.
- [5] J. E. Kennedy. “The Gurney Model of Explosive Output for Driving Metal”. In: *Explosive Effects and Applications*. Ed. by J. A. Zukas and W. P. Walters. New York, NY: Springer New York, 1998, pp. 221–257. DOI: [10.1007/978-1-4612-0589-0_7](https://doi.org/10.1007/978-1-4612-0589-0_7).
- [6] J. Loiseau, J. Huneault, and A. J. Higgins. “Development of a Linear Implosion-driven Hypervelocity Launcher”. In: *Procedia Engineering* 58 (2013), pp. 77–87. DOI: [10.1016/j.proeng.2013.05.011](https://doi.org/10.1016/j.proeng.2013.05.011).
- [7] J. Huneault, J. Loiseau, M. Hildebrand, and A. Higgins. “Down-Bore Velocimetry of an Explosively Driven Light-Gas Gun”. In: *Procedia Engineering* 103 (2015), pp. 230–236. DOI: [10.1016/j.proeng.2015.04.031](https://doi.org/10.1016/j.proeng.2015.04.031).
- [8] W. P. Walters and J. A. Zukas. *Fundamentals of Shaped Charges*. New York, NY: Wiley-Interscience, 1989.
- [9] J. Loiseau, W. Georges, and A. J. Higgins. “Validation of the Gurney Model in Planar Geometry for a Conventional Explosive”. In: *Propellants, Explosives, Pyrotechnics* 41 (2016), pp. 655–664. DOI: [10.1002/prep.201500246](https://doi.org/10.1002/prep.201500246).
- [10] J. E. Kennedy. *Gurney Energy of Explosives: Estimation of the Velocity and Impulse Imparted to Driven Metal*. Tech. Rep. SC-RR-70-90. Sandia National Laboratories, 1970.
- [11] W. J. Flis. “Gurney Formulas for Explosive Charges Surrounding Rigid Cores”. In: *16th International Symposium on Ballistics*. San Francisco, CA, 23–28 September 1996.
- [12] C. L. Mader, J. D. Kershner, and G. H. Pimbley. “Three-Dimensional Modeling of Inert Metal-Loaded Explosives”. In: *Journal of Energetic Materials* 1.4 (1983), pp. 293–324. DOI: [10.1080/07370658308012323](https://doi.org/10.1080/07370658308012323).
- [13] O. Petel, D. Mack, A. Higgins, R. Turcotte, and S. Chan. “Minimum Propagation Diameter and Thickness of High Explosives”. In: *Journal of Loss Prevention in the Process Industries* 20.4–6 (2007), pp. 578–583. DOI: [10.1016/j.jlp.2007.05.007](https://doi.org/10.1016/j.jlp.2007.05.007).
- [14] L. L. Davis and L. G. Hill. “ANFO Cylinder Tests”. In: *AIP Conference Proceedings* 620.1 (24–29 June 2002), pp. 165–168. DOI: [10.1063/1.1483507](https://doi.org/10.1063/1.1483507).

References

- [15] J. Loiseau, J. Huneault, O. E. Petel, S. Goroshin, D. L. Frost, A. J. Higgins, and F. Zhang. “Development of Multi-component Explosive Lenses for Arbitrary Phase Velocity Generation”. In: *Journal of Physics: Conference Series* 500.19 (2014), p. 192010. DOI: [10.1088/1742-6596/500/19/192010](https://doi.org/10.1088/1742-6596/500/19/192010).
- [16] V. Nesterenko. *Dynamics of Heterogeneous Materials*. Shock Wave and High Pressure Phenomena. New York, NY: Springer-Verlag, 2001.
- [17] W. Georges, J. Loiseau, A. J. Higgins, and J. Zimmermann. “Effect of Scale, Material Strength, and Loading on Ejecta Formation from Explosively Driven Aluminum”. In: *Journal of Dynamic Behavior of Materials* (2017). DOI: [10.1007/s40870-017-0127-1](https://doi.org/10.1007/s40870-017-0127-1).
- [18] D. L. Frost, H. Kleine, M. Slanik, A. Higgins, S. McCahan, F. Zhang, and S. B. Murray. “Blast Waves from Heterogeneous Explosives”. In: *Proceedings of the 22nd International Symposium on Shock Waves*. Imperial College, London, UK, 18–23 July 1999.
- [19] D. L. Frost, C. Ornthanalai, Z. Zarei, V. Tanguay, and F. Zhang. “Particle Momentum Effects from the Detonation of Heterogeneous Explosives”. In: *Journal of Applied Physics* 101.11, 113529 (2007), p. 113529. DOI: [10.1063/1.2743912](https://doi.org/10.1063/1.2743912).
- [20] P. C. Souers and R. Minich. “Cylinder Test Correction for Copper Work Hardening and Spall”. In: *Propellants, Explosives, Pyrotechnics* 40.2 (2015), pp. 238–245. DOI: [10.1002/prop.201400135](https://doi.org/10.1002/prop.201400135).
- [21] G. I. Taylor. *Analysis of the Explosion of a Long Cylindrical Bomb Detonated at One End*. Vol. III. The Scientific Papers of Sir Geoffrey Ingram Taylor Volume III, paper 30. Cambridge University Press, 1963.
- [22] P. C. Souers, R. Garza, H. Hornig, L. Lauderbach, C. Owens, and P. Vitello. “Metal Angle Correction in the Cylinder Test”. In: *Propellants, Explosives, Pyrotechnics* 36.1 (2011), pp. 9–15. DOI: [10.1002/prop.201000006](https://doi.org/10.1002/prop.201000006).
- [23] P. C. Souers, L. Lauderbach, R. Garza, L. Ferranti, and P. Vitello. “Upgraded Analytical Model of the Cylinder Test”. In: *Propellants, Explosives, Pyrotechnics* 38.3 (2013), pp. 419–424. DOI: [10.1002/prop.201200192](https://doi.org/10.1002/prop.201200192).
- [24] J. E. Kennedy. “Explosive Output for Driving Metal”. In: *12th Annual Symposium on the Behavior and Utilization of Explosives in Engineering Design*. Albuquerque, NM: American Society of Mechanical Engineers, 2–3 March 1972.
- [25] B. M. Dobratz. *LNLL Explosives Handbook - Properties of Chemical Explosives and Explosive Simulants*. Tech. Rep. UCRL-52997. Lawrence Livermore National Lab, 1982.
- [26] W. P. Walters. *Explosive Loading of Metals and Related Topics*. Tech. Rep. BRL-SP-56. Aberdeen Proving Ground, MD: US Army Ballistic Research Laboratory, May 1986.
- [27] F. A. Baum, K. P. Stanyukovich, and B. I. Shekhter. *Physics of an Explosion (Translated from Russian: Fizmatgiz, Moscow)*. Arlington, VA.: Armed Services Technical Information Agency, Translated: 1963, Original: 1959.
- [28] G. E. Jones, J. E. Kennedy, and L. D. Bertholf. “Ballistics Calculations of Gurney, R. W.” In: *American Journal of Physics* 48.4 (1980), pp. 264–269. DOI: [10.1119/1.12135](https://doi.org/10.1119/1.12135).
- [29] J. T. Dehn. *Models of Explosively Driven Metal*. Tech. Rep. BRL-TR-2626. Aberdeen Proving Ground, MD: US Army Ballistic Research Laboratory, Dec. 1984.
- [30] J. T. Dehn. “Models of Explosively Driven Metal”. In: *8th International Symposium on Detonation*. Ed. by J. M. Short. Albuquerque, NM: Office of Naval Research, 15–19 July 1985, pp. 602–612.

-
- [31] L. H. Thomas. *Analysis of the Distribution in Mass, in Speed, and in Direction of Motion of the Fragments of the M71 (90mm) A. A. Shell, when Filled with TNT and when Filled with Ednatol*. Tech. Rep. BRL-434. US Army Ballistic Research Laboratory, 1943.
- [32] L. H. Thomas. *Theory of the Explosion of Cased Charges of Simple Shape*. Tech. Rep. BRL-475. US Army Ballistic Research Laboratory, 1944.
- [33] T. E. Stern. *A Note on the Initial Velocities of Fragments from Warheads*. Report BRL-646. US Army Ballistic Research Laboratory, 1947.
- [34] T. Stern. *The Fragment Velocity of a Spherical Shell Containing an Inert Core*. Report BRL-753. US Army Ballistic Research Laboratory, 1951.
- [35] I. G. Henry. *The Gurney Formula and Related Approximations for the High-Explosive Deployment of Fragments*. Tech. Rep. PUB-189. Hughes Aircraft Company, 1967.
- [36] Personal Communication. Nov. 2012.
- [37] M. Défourneaux. “Transferts d’Énergie dans les Combustions et Detonations avec Confinement”. In: *Astronautica Acta* 17 (1972), p. 609.
- [38] W. J. Flis. “A Lagrangian Approach to Modelling the Acceleration of Metal by Explosives”. In: *17th Southeastern Conference on Theoretical and Applied Mechanics*. Hot Springs, AK, Apr. 1994.
- [39] S. J. Jacobs. *The Gurney Formula: Variations on a Theme by Lagrange*. Tech. Rep. NOLTR 74-86. Naval Ordnance Laboratory, 1974.
- [40] N. E. Hoskin, J. W. S. Allan, A. Bailey, J. W. Lethaby, and I. C. Skidmore. “The Motion of Plates and Cylinders Driven by Detonation Waves at Tangential Incidence”. In: *4th International Symposium on Detonation*. White Oak, MD: Office of Naval Research, 12–15 October 1965, pp. 14–26.
- [41] D. J. Butz, J. E. Backofen, and J. A. Petrousky. “Fragment Terminal Velocities from Low Metal to Explosive Mass Ratio Symmetric Sandwich Charges”. In: *J. Ballistics* 6 (1982), pp. 1304–1322.
- [42] A. D. Solem and B. H. Singleton. *Rapid Expansion of Metal Cylinders Under Explosive Loading I: Studies of Initial Expansions with Rotating Mirror Camera*. Tech. Rep. NAVORD 2768. U.S Naval Ordnance Laboratory, 1953.
- [43] C. E. Weinland. *A Scaling Law for Fragmenting Cylindrical Warheads*. Tech. Rep. NWC-TP-4735. Naval Weapons Center, China Lake, 1969.
- [44] E. Hirsch. “Improved Gurney Formulas for Exploding Cylinders and Spheres using “Hard Core” Approximation”. In: *Propellants, Explosives, Pyrotechnics* 11.3 (1986), pp. 81–84. DOI: [10.1002/prop.19860110303](https://doi.org/10.1002/prop.19860110303).
- [45] E. Hirsch. “On the Inconsistency of the Asymmetric-Sandwich Gurney Formula When Used to Model Thin-Plate Propulsion”. In: *Propellants, Explosives, Pyrotechnics* 20.4 (1995), pp. 178–181. DOI: [10.1002/prop.19950200404](https://doi.org/10.1002/prop.19950200404).
- [46] W. Fücke, J. Bol, and S. Schumann. “Velocity of Sandwich Plates Driven by Thin H.E. Layers”. In: *10th International Symposium on Ballistics*. San Diego, CA, 1987.
- [47] C. P. Y. “An Analytical Model for Metal Acceleration by Grazing Detonation”. In: *7th International Symposium on Ballistics*. the Hague, Netherlands, 19–21 April 1983.
- [48] H. E. M. “Analytical Model of the Shaped Charge Liner Collapse”. In: *7th International Symposium on Ballistics*. the Hague, Netherlands, 19–21 April 1983.

References

- [49] E. Hirsch. “Simplified and Extended Gurney Formulas for Imploding Cylinders and Spheres”. In: *Propellants, Explosives, Pyrotechnics* 11.1 (1986), pp. 6–9. DOI: [10.1002/prop.19860110103](https://doi.org/10.1002/prop.19860110103).
- [50] P. C. Chou, J. Carleone, W. J. Flis, R. D. Ciccarelli, and E. Hirsch. “Improved Formulas for Velocity, Acceleration, and Projection Angle of Explosively Driven Liners”. In: *Propellants, Explosives, Pyrotechnics* 8.6 (1983), pp. 175–183. DOI: [10.1002/prop.830080602](https://doi.org/10.1002/prop.830080602).
- [51] J. E. Kennedy, C. R. Cherry, C. R. J. Cherry, R. H. Warnes, and S. H. Fischer. *Momentum Transfer in Indirect Explosive Drive*. Tech. Rep. LA-UR-96-1837. 1996.
- [52] G. E. Jones. “The Gurney equations for multilayered fragments”. In: *Journal of Applied Physics* 50.5 (1979), pp. 3746–3747. DOI: [10.1063/1.326282](https://doi.org/10.1063/1.326282).
- [53] F. E. Allison and R. W. Watson. “Explosively Loaded Metallic Cylinders - I”. In: *Journal of Applied Physics* 31.5 (1960), pp. 842–845. DOI: [10.1063/1.1735706](https://doi.org/10.1063/1.1735706).
- [54] F. E. Allison and J. T. Schriempf. “Explosively Loaded Metallic Cylinders - II”. In: *Journal of Applied Physics* 31.5 (1960), pp. 846–851. DOI: [10.1063/1.1735707](https://doi.org/10.1063/1.1735707).
- [55] R. R. Karpp and W. W. Predebon. “Calculation of Fragment Velocities from Fragmenting Munitions”. In: *1st International Symposium on Ballistics*. 1974.
- [56] R. R. Karpp and W. W. Predebon. *Calculation of Fragment Velocities from Naturally Fragmenting Munitions*. Tech. Rep. BRL-2509. Aberdeen Proving Ground, MD: US Army Ballistic Research Laboratory, Dec. 1975.
- [57] E. Hirsch, P. C. Chou, and R. D. Ciccarelli. “General Kinematical Solution to the Motion of an Explosively Driven Liner”. In: *Propellants, Explosives, Pyrotechnics* 11.2 (1986), pp. 53–64. DOI: [10.1002/prop.19860110205](https://doi.org/10.1002/prop.19860110205).
- [58] P. C. Chou, E. Hirsch, and R. D. Ciccarelli. *An Unsteady Taylor Angle Formula for Liner Collapse*. Tech. Rep. ARBRL-CR-00461. US Army Ballistic Research Laboratory, 1981.
- [59] G. Randers-Pehrson. “An Improved Equation for Calculating Fragment Projection Angle”. In: *2nd International Symposium on Ballistics*. 1976.
- [60] W. J. Flis. “The Effects of Finite Liner Acceleration on Shaped-Charge Jet Formation”. In: *19th International Symposium on Ballistics*. Interlaken, Switzerland, 7–11 May 2001, pp. 789–796.
- [61] L. G. Hill. “Detonation Product Equation of State Directly from the Cylinder Test”. In: *21st International Symposium on Shock Waves*. Great Keppel Island, AU, 20–25 July 1997.
- [62] S. I. Jackson. “An Analytic Method for Two-Dimensional Wall Motion and Product Isentrope from the Detonation Cylinder Test”. In: *Proceedings of the Combustion Institute* 35.2 (2015), pp. 1997–2004. DOI: [10.1016/j.proci.2014.07.071](https://doi.org/10.1016/j.proci.2014.07.071).
- [63] S. Jackson. “The Detonation Cylinder Test: Determination of Full Wall Velocity and Shape from a Single Velocimetry Probe with an Arbitrary Angle”. In: *AIP Conference Proceedings* 1793.1 (2017), p. 050017. DOI: [10.1063/1.4971551](https://doi.org/10.1063/1.4971551).
- [64] E. L. Baker, D. Murphy, C. Capellos, P. Anderson, E. Wrobel, and L. Stiel. *Recent Combined Effects Explosives Technology*. Report ARMET-TR-10004. ARDEC, Picatinny Arsenal, NJ, 2010.
- [65] A. E. H. Love and F. B. Pidduck. “Lagrange’s Ballistic Problem”. In: *Philosophical Transactions of the Royal Society of London A: Mathematical, Physical and Engineering Sciences* 222.594-604 (1922), pp. 167–226. DOI: [10.1098/rsta.1922.0006](https://doi.org/10.1098/rsta.1922.0006).

- [66] J. W. Kury, H. C. Hornig, E. L. Lee, J. McDonnell, and D. L. Ornellas. “Metal Acceleration by Chemical Explosives”. In: *4th International Symposium on Detonation*. White Oak, MD: Office of Naval Research, 12–15 October 1965.
- [67] M. J. Kamlet and J. M. Short. “The Chemistry of Detonations –VI: A “Rule for Gamma” as a Criterion for Choice Among Conflicting Detonation Pressure Measurements”. In: *Combustion and Flame* 38 (1980), pp. 221–230. DOI: [10.1016/0010-2180\(80\)90055-3](https://doi.org/10.1016/0010-2180(80)90055-3).
- [68] A. K. Aziz, H. Hurwitz, and H. M. Sternberg. “Energy Transfer to a Rigid Piston under Detonation Loading”. In: *Physics of Fluids* 4.3 (1961), pp. 380–384. DOI: [10.1063/1.1706337](https://doi.org/10.1063/1.1706337).
- [69] G. Rudinger. *Nonsteady Duct Flow: Wave-Diagram Analysis*. New York, NY: Dover Publications, Inc., 1969.
- [70] B. D. Lambourn and J. E. Hartley. “The Calculation of the Hydrodynamic Behaviour of Plane One Dimensional Explosive/Metal Systems”. In: *4th International Symposium on Detonation*. White Oak, MD: Office of Naval Research, 12–15 October 1965, pp. 538–552.
- [71] O. T. Strand, D. R. Goosman, C. Martinez, T. L. Whitworth, and W. W. Kuhlow. “Compact System for High-Speed Velocimetry Using Heterodyne Techniques”. In: *Review of Scientific Instruments* 77.8, 083108 (2006), p. 083108. DOI: [10.1063/1.2336749](https://doi.org/10.1063/1.2336749).
- [72] M. E. Briggs, L. M. Hull, and M. A. Shinas. “Fundamental Experiments in Velocimetry”. In: *AIP Conference Proceedings* 1195.1 (2009), pp. 577–580. DOI: [10.1063/1.3295203](https://doi.org/10.1063/1.3295203).
- [73] M. E. Briggs. “Velocities Measured Obliquely from Funny Shaped Bullets”. In: *Third Annual Photonic Doppler Velocimetry (PDV) Conference and Workshop*. Albuquerque, NM: Sandia National Laboratory, 3–4 September 2008.
- [74] D. H. Dolan. “What Does “Velocity” Interferometry Really Measure?” In: *AIP Conference Proceedings* 1195.1 (2009), pp. 589–594. DOI: [10.1063/1.3295207](https://doi.org/10.1063/1.3295207).
- [75] P. J. Miller and K. E. Alexander. “Determining JWL Equation of State Parameters Using the Gurney Equation Approximation”. In: *9th International Symposium on Detonation*. Portland, OR: Office of Naval Research, 28 August–1 September 1989, pp. 498–505.
- [76] J. E. Reaugh and P. C. Souers. “A Constant-Density Gurney Approach to the Cylinder Test”. In: *Propellants, Explosives, Pyrotechnics* 29.2 (2004), pp. 124–128. DOI: [10.1002/prop.200400031](https://doi.org/10.1002/prop.200400031).
- [77] J. A. Zukas and W. P. Walters. *Explosive Effects and Applications*. Shock Wave and High Pressure Phenomena. Springer-Verlag New York, 1998. DOI: [10.1007/978-1-4612-0589-0](https://doi.org/10.1007/978-1-4612-0589-0).
- [78] R. Catanach, L. Hill, H. Harry, E. Aragon, and D. Murk. *Cylinder Test Specification*. Tech. Rep. LA-13643-MS. Los Alamos, NM: Los Alamos National Laboratory, 1999.
- [79] D. L. Robbins, E. K. Anderson, M. U. Anderson, S. I. Jackson, and M. Short. “Cylinder Test Characterization of an Ammonium Nitrate and Aluminum Powder Explosive”. In: *15th International Symposium on Detonation*. Vol. 1. San Francisco, CA: Office of Naval Research, 13–18 July 2014, pp. 826–835.
- [80] M. Short and S. I. Jackson. “Dynamics of High Sound-Speed Metal Confiners Driven by Non-Ideal High-Explosive Detonation”. In: *Combustion and Flame* 162.5 (2015), pp. 1857–1867. DOI: [10.1016/j.combustflame.2014.12.007](https://doi.org/10.1016/j.combustflame.2014.12.007).

References

- [81] J. Souletis and J. Mala. “Influence of Test Conditions on the Ballistic Classification of Explosives”. In: *8th International Symposium on Detonation*. Ed. by J. M. Short. Albuquerque, NM: Office of Naval Research, 15–19 July 1985, pp. 625–631.
- [82] P. Gimenez, Y. de Longueville, and C. Saint-Martin. “EOS of Detonation Products Obtained from Symmetric Deflection of Liners Investigated by Laser Interferometry Techniques”. In: *8th International Symposium on Detonation*. Ed. by J. M. Short. Albuquerque, NM: Office of Naval Research, 15–19 July 1985, pp. 596–601.
- [83] L. G. Hill. “Development of the LANL Sandwich Test”. In: *AIP Conference Proceedings* 620.1 (2002), pp. 149–152. DOI: [10.1063/1.1483503](https://doi.org/10.1063/1.1483503).
- [84] J. M. Short, F. H. Helm, M. Finger, M. J. Kamlet, and M. J. Kamlet. “The Chemistry of Detonations –VII. A Simplified Method for Predicting Explosive Performance in the Cylinder Test”. In: *Combustion and Flame* 43 (1981), pp. 99–109. DOI: [10.1016/0010-2180\(81\)90009-2](https://doi.org/10.1016/0010-2180(81)90009-2).
- [85] M. J. Kamlet, J. M. Short, M. Finger, F. Helm, R. R. McGuire, and I. B. Akst. “The Chemistry of Detonations –VIII: Energetics Relationships on the Detonation Isentrope”. In: *Combustion and Flame* 51 (1983), pp. 325–333. DOI: [10.1016/0010-2180\(83\)90110-4](https://doi.org/10.1016/0010-2180(83)90110-4).
- [86] C. L. Mader. *Numerical Modeling of Explosives and Propellants*. CRC press, 2007.
- [87] H. N. Presles, J. Campos, O. Heuzè, and P. Bauer. “Effects of Microballoon Concentration on the Detonation Characteristics of Nitromethane-PMMA Mixtures”. In: *9th International Symposium on Detonation*. Portland, OR: Office of Naval Research, 28 August–1 September 1989, pp. 925–932.
- [88] B. A. Khasainov, B. S. Ermolaev, and H. N. Presles. “Effect of Glass Microballoons on Shock Wave Sensitivity and Detonation Critical Diameter of Condensed Explosives”. In: *10th International Symposium on Detonation*. Boston, MA: Office of Naval Research, 12–16 July 1993, pp. 749–757.
- [89] H. N. Prestes, P. Vidal, J. C. Gois, B. A. Khasainov, and B. S. Ermolaev. “Influence of Glass Microballoons Size on the Detonation of Nitromethane Based Mixtures”. In: *Shock Waves* 4.6 (1995), pp. 325–329. DOI: [10.1007/BF01413874](https://doi.org/10.1007/BF01413874).
- [90] J. J. Lee, D. L. Frost, J. H. S. Lee, and A. Dremin. “Propagation of Nitromethane Detonations in Porous Media”. In: *Shock Waves* 5.1 (1995), pp. 115–119. DOI: [10.1007/BF02425043](https://doi.org/10.1007/BF02425043).
- [91] J. J. Lee, M. Brouillette, D. L. Frost, and J. H. S. Lee. “Effect of Diethylenetriamine Sensitization on Detonation of Nitromethane in Porous Media”. In: *Combustion and Flame* 100.1–2 (1995), pp. 292–300. DOI: [10.1016/0010-2180\(94\)00124-B](https://doi.org/10.1016/0010-2180(94)00124-B).
- [92] O. E. Petel, D. Mack, A. J. Higgins, R. Turcotte, and S. K. Chan. “Comparison of the Detonation Failure Mechanism in Homogeneous and Heterogeneous Explosives”. In: *13th International Symposium on Detonation*. Norfolk, VA: Office of Naval Research, 23–28 July 2007, pp. 2–11.
- [93] A. J. Higgins. “Discrete Effects in Energetic Materials”. In: *Journal of Physics: Conference Series* 500.5 (2014), p. 052016. DOI: [10.1088/1742-6596/500/5/052016](https://doi.org/10.1088/1742-6596/500/5/052016).
- [94] J. E. Backofen and C. Weickert. “Initial Free-Surface Velocities Imparted by Grazing Detonation Waves”. In: *Shock Compression of Condensed Matter–1999*. Ed. by M. D. Furnish, L. C. Chhabildas, and R. S. Hixson. AIP Conference Proceedings 505. Snowbird, UT: American Institute of Physics, 2000, pp. 919–922. DOI: [10.1063/1.1303618](https://doi.org/10.1063/1.1303618).

- [95] J. E. Backofen. “Modeling a Material’s Instantaneous Velocity during Acceleration Driven by a Detonation’s Gas Push”. In: *Shock Compression of Condensed Matter–2005*. Ed. by M. D. Furnish, M. Elert, T. P. Russell, and C. T. White. AIP Conference Proceedings 845. Baltimore, MD: American Institute of Physics, 2006, pp. 936–939. DOI: [10.1063/1.2263475](https://doi.org/10.1063/1.2263475).
- [96] F. Findik. “Recent Developments in Explosive Welding”. In: *Materials & Design* 32.3 (2011), pp. 1081–1093. DOI: [10.1016/j.matdes.2010.10.017](https://doi.org/10.1016/j.matdes.2010.10.017).
- [97] J. R. Asay. *Effect of Shock Wave Risetime on Material Ejection from Aluminum Surfaces*. Tech. Rep. SAND 77-0731. Albuquerque, NM: Sandia National Laboratories, 1977.
- [98] M. B. Zellner, M. Grover, J. E. Hammerberg, R. S. Hixson, G. S. M. A. J. Iverson, K. B. Morley, A. W. Obst, R. T. Olson, J. R. Payton, P. A. Rigg, N. Routley, G. D. Stevens, W. D. Turley, L. Veaser, and W. T. Buttler. “Effects of Shock-Breakout Pressure on Ejection of Micron-Scale Material from Shocked Tin Surfaces”. In: *Journal of Applied Physics* 102.1 (2007), p. 013522. DOI: [10.1063/1.2752130](https://doi.org/10.1063/1.2752130).
- [99] J. L. Copp and A. R. Ubbelohde. “Physico-chemical Processes Occurring at High Pressures and Temperatures - Part II: The Effect of “Inert” Components on Detonation”. In: *Transactions of the Faraday Society* 44 (0 1948), pp. 658–669. DOI: [10.1039/TF9484400658](https://doi.org/10.1039/TF9484400658).
- [100] *Proceedings of the Detonation Wave Shaping Conference*. Picatinny Arsenal. Jet Propulsion Laboratory, Pasadena, CA: Department of the Army, 5–7 June 1956.
- [101] O. N. Davydova, N. M. Kuznetsov, V. V. Lavrov, and K. K. Shvedov. “On Under-driven Detonation of Condensed High Explosives with Inert Admixtures”. In: *Chemical Physics Reports C/C of Khimicheskaiia Fizika* 18.4 (1999), pp. 723–750.
- [102] N. A. Imkhovik. “Specifics of the Detonation of Mixtures of Powerful High Explosives with W and Pb High-Density Inert Additives”. In: *Russian Journal of Physical Chemistry B* 3.4 (2009), pp. 620–628. DOI: [10.1134/S1990793109040174](https://doi.org/10.1134/S1990793109040174).
- [103] N. A. Imkhovik. “Influence of Dense Inert Additives (W and Pb) on Detonation Conditions and Regime of Condensed Explosives”. In: *Journal of Energetic Materials* 28.sup1 (2010), pp. 216–230. DOI: [10.1080/07370652.2010.502921](https://doi.org/10.1080/07370652.2010.502921).
- [104] N. M. Kuznetsov and O. N. Davydova. “Detonation of Explosives Containing Heavy Inert Particles”. In: *Journal of Experimental and Theoretical Physics* 93.3 (2001), pp. 519–532. DOI: [10.1134/1.1410597](https://doi.org/10.1134/1.1410597).
- [105] F. Zhang, D. L. Frost, P. A. Thibault, and S. B. Murray. “Explosive Dispersal of Solid Particles”. In: *Shock Waves* 10.6 (2001), pp. 431–443. DOI: [10.1007/PL00004050](https://doi.org/10.1007/PL00004050).
- [106] F. Zhang, P. A. Thibault, and R. Link. “Shock Interaction with Solid Particles in Condensed Matter and Related Momentum Transfer”. In: *Proceedings of the Royal Society of London A: Mathematical, Physical and Engineering Sciences* 459.2031 (2003), pp. 705–726. DOI: [10.1098/rspa.2002.1045](https://doi.org/10.1098/rspa.2002.1045). eprint: <http://rspa.royalsocietypublishing.org/content/459/2031/705.full.pdf>.
- [107] R. C. Ripley, F. Zhang, and F.-S. Lien. “Acceleration and Heating of Metal Particles in Condensed Matter Detonation”. In: *Proceedings of the Royal Society of London A: Mathematical, Physical and Engineering Sciences* 468.2142 (2012), pp. 1564–1590. DOI: [10.1098/rspa.2011.0595](https://doi.org/10.1098/rspa.2011.0595). eprint: <http://rspa.royalsocietypublishing.org/content/468/2142/1564.full.pdf>.
- [108] I. M. Voskoboinikov, A. A. Kotomin, and N. F. Voskoboinikova. “Effects of Inert Additives on the Divergence Speed of Plates Driven by Mixed Explosives”. In: *Combustion, Explosion and Shock Waves* 18.6 (1982), pp. 706–708. DOI: [10.1007/BF00802301](https://doi.org/10.1007/BF00802301).

References

- [109] Y. Kato, H. Kato, K. Murata, T. Hamada, and S. Itoh. “Overdriven Detonation in High Density Explosives Containing Tungsten Powder”. In: *13th International Symposium on Detonation*. Norfolk, VA: Office of Naval Research, 23–28 July 2007, pp. 196–203.
- [110] H. Kato, K. Murata, S. Itoh, and Y. Kato. “Investigation of Jet Formation with Overdriven Detonation in High Density Explosive”. In: *Materials Science Forum* 566 (2008), pp. 327–332. DOI: [10.4028/www.scientific.net/MSF.566.327](https://doi.org/10.4028/www.scientific.net/MSF.566.327).
- [111] M. Finger, H. C. Hornig, E. L. Lee, and J. W. Kury. “Metal Acceleration by Composite Explosives”. In: *5th International Symposium on Detonation*. Pasadena, CA: Office of Naval Research, 18–21 August 1970, pp. 137–152.
- [112] J. Loiseau, O. E. Petel, J. Huneault, M. Serge, D. L. Frost, and A. J. Higgins. “Acceleration of Plates Using Non-Conventional Explosives Heavily-Loaded with Inert Materials”. In: *Journal of Physics: Conference Series* 500.18 (2014). Ed. by W. T. Buttler and W. J. Evans, p. 182027. DOI: [10.1088/1742-6596/500/18/182027](https://doi.org/10.1088/1742-6596/500/18/182027).
- [113] J. Loiseau, W. Georges, D. L. Frost, and A. J. Higgins. “Acceleration of Planar Flyers by Explosives Heavily Loaded with Inert Materials”. In: *15th International Symposium on Detonation*. Ed. by J. R. Carney and J. L. Maienschein. San Francisco, CA: Office of Naval Research, 13–18 July 2014, pp. 1381–1391.
- [114] J. Loiseau, W. Georges, and A. J. Higgins. “The Effect of Detonation Wave Incidence Angle on the Acceleration of Flyers by Explosives Heavily Laden with Inert Additives”. In: *Journal of Physics: Conference Series* (14–19 June 2015). Ed. by R. C. Chau, T. Germann, and T. Sewell, TBD.
- [115] J. E. Backofen and C. A. Weickert. “The Effects of Plate Thickness and Explosive Properties on Projection from the End of a Charge”. In: *16th International Symposium on Ballistics*. San Francisco, CA, 1996, pp. 641–650.
- [116] M. Short, J. J. Quirk, C. B. Kiyanda, S. I. Jackson, M. E. Briggs, and M. A. Shinas. “Simulation of Detonation of Ammonium Nitrate Fuel Oil Mixture Confined by Aluminum: Edge Angles for DSD”. In: *14th International Symposium on Detonation*. Coeur d’Alene, ID: Office of Naval Research, 11–16 April 2010, pp. 769–778.
- [117] A. G. Ivanov, M. V. Korotchenko, E. Z. Novitskii, V. A. Ogorodnikov, B. V. Pevnitskii, and S. Y. Pinchuk. “Accelerating Plates to Hypersonic Velocities: Apparatus”. In: *Journal of Applied Mechanics and Technical Physics* 23.2 (1982), pp. 238–241. DOI: [10.1007/BF00911005](https://doi.org/10.1007/BF00911005).
- [118] Y. V. Bat’kov, N. P. Kovalev, A. D. Kovtun, V. G. Kuropatkin, A. I. Lebedev, Y. M. Makarov, S. F. Manachkin, S. A. Novikov, V. A. Raevsky, and Y. M. Styazhkin. “Explosive Three-Stage Launcher to Accelerate Metal Plates to Velocities more than 10 km/s”. In: *International Journal of Impact Engineering* 20.1 (1997), pp. 89–92. DOI: [10.1016/S0734-743X\(97\)87482-9](https://doi.org/10.1016/S0734-743X(97)87482-9).
- [119] A. Geille. “Status of Development of Space-Debris Hypervelocity Explosive Multi-Stage Launcher”. In: *International Journal of Impact Engineering* 20.1 (1997), pp. 271–279. DOI: [10.1016/S0734-743X\(97\)87500-8](https://doi.org/10.1016/S0734-743X(97)87500-8).
- [120] S. Chengwei, Z. Feng, W. Shanggang, L. Qingzhong, and L. Cangli. “High Velocity Flyers Accelerated by Multi-Stage Explosive Slabs”. In: *AIP Conference Proceedings* 429.1 (1998), pp. 971–974. DOI: [10.1063/1.55626](https://doi.org/10.1063/1.55626).
- [121] Z.-Y. Liu, K. Shiro, and I. Shigeru. “Numerical Study on Hypervelocity Acceleration of Flyer Plates by Overdriven Detonation of High Explosive”. In: *International Journal of Impact Engineering* 26.1 (2001), pp. 443–452. DOI: [10.1016/S0734-743X\(01\)00094-X](https://doi.org/10.1016/S0734-743X(01)00094-X).

- [122] R. A. Patterson. “Fundamentals of Explosion Welding”. In: *ASM Handbook, Volume 6: Welding, Brazing, and Soldering*. Ed. by D. L. Olson, T. A. Siewert, S. Liu, and G. R. Edwards. ASM International, 1993, pp. 160–164.
- [123] S. A. Sheffield, R. Engelke, and R. R. Alcon. “In-Situ Study of the Chemically Driven Flow Fields in Initiating Homogeneous and Heterogeneous Nitromethane Explosives”. In: *9th International Symposium on Detonation*. Ed. by E. L. Lee and J. M. Short. Portland, OR: Office of Naval Research, pp. 39–49.
- [124] J. J. Lee, J. Jiang, K. H. Choong, and J. H. S. Lee. “Effect of Diethylenetriamine and Triethylamine Sensitization on the Critical Diameter of Nitromethane”. In: *AIP Conference Proceedings* 505.1 (2000), pp. 797–800. DOI: [10.1063/1.1303591](https://doi.org/10.1063/1.1303591).
- [125] Y. A. Gruzdkov and Y. M. Gupta. “Mechanism of Amine Sensitization in Shocked Nitromethane”. In: *The Journal of Physical Chemistry A* 102.13 (1998), pp. 2322–2331. DOI: [10.1021/jp9803236](https://doi.org/10.1021/jp9803236).
- [126] V. M. Mochalova, A. V. Utkin, and S. M. Lapin. “Effect of Small Additions of Diethylenetriamine on the Width of the Reaction Zone in Detonation Waves in Nitromethane”. In: *Combustion, Explosion, and Shock Waves* 52.3 (2016), pp. 329–334. DOI: [10.1134/S0010508216030126](https://doi.org/10.1134/S0010508216030126).
- [127] J. C. Gois, J. Campos, and R. Mendes. “Shock Initiation of Nitromethane-PMMA Mixtures with Glass Microballoons”. In: *10th International Symposium on Detonation*. Boston, MA: Office of Naval Research, 12-16 July 1993, pp. 758–765.
- [128] J. C. Gois, H. N. Presles, and P. Vidal. “Effect of Hollow Heterogeneities on Nitromethane Detonation”. In: *Progress in Astronautics and Aeronautics* 153 (1993), pp. 462–462. DOI: [10.2514/5.9781600866265.0462.0470](https://doi.org/10.2514/5.9781600866265.0462.0470).
- [129] J. C. Gois, J. Campos, and R. Mendes. “Extinction and Initiation of Detonation of NM-PMMA-GMB Mixtures”. In: *AIP Conference Proceedings* 370.1 (1996), pp. 827–830. DOI: [10.1063/1.50836](https://doi.org/10.1063/1.50836).
- [130] J. C. Gois, J. Campos, I. Plaksin, and R. Mendes. “Failure and Re-initiation Detonation Phenomena in NM/PMMA-GMB Mixtures”. In: *AIP Conference Proceedings* 429.1 (1998), pp. 691–694. DOI: [10.1063/1.55581](https://doi.org/10.1063/1.55581).
- [131] E. Bouton, B. A. Khasainov, H. N. Presles, P. Vidal, and B. S. Ermolaev. “Sensitization of Two-Dimensional Detonations in Nitromethane by Glass Microballoons”. In: *Shock Waves* 9.2 (1999), pp. 141–147. DOI: [10.1007/s001930050148](https://doi.org/10.1007/s001930050148).
- [132] J. C. Gois, J. Campos, and I. Plaksin. “Effect of GMB on Failure and Reaction Regime of NM/PMMA-GMB Mixtures”. In: *AIP Conference Proceedings* 620.1 (2002), pp. 898–901. DOI: [10.1063/1.1483682](https://doi.org/10.1063/1.1483682).
- [133] A. Higgins. “Measurement of Detonation Velocity for a Nonideal Heterogeneous Explosive in Axisymmetric and Two-Dimensional Geometries”. In: *AIP Conference Proceedings* 1195.1 (2009), pp. 193–196. DOI: [10.1063/1.3295101](https://doi.org/10.1063/1.3295101).
- [134] W. Haynes, ed. *CRC Handbook of Chemistry and Physics, 95th Edition*. CRC Press, 2014, pp. 6–182, 6–231.
- [135] P. J. Haskins, M. D. Cook, and R. I. Briggs. “The Effect of Additives on the Detonation Characteristics of a Liquid Explosive”. In: *AIP Conference Proceedings* 620.1 (2002), pp. 890–893. DOI: [10.1063/1.1483680](https://doi.org/10.1063/1.1483680).
- [136] A. Koch, N. Arnold, and M. Estermann. “A Simple Relation Between the Detonation Velocity of an Explosive and its Gurney Energy”. In: *Propellants, Explosives, Pyrotechnics* 27.6 (2002), pp. 365–368. DOI: [10.1002/prop.200290007](https://doi.org/10.1002/prop.200290007).

References

- [137] L. S. Wise. *Effect of Aluminum on the Rate of Detonation of TNT*. Tech. Rep. No. 1550. Dover, NJ: Picatinny Arsenal, 1945.
- [138] M. A. Cook, A. S. Filler, R. T. Keyes, W. S. Partridge, and W. Ursenbach. “Aluminized Explosives”. In: *The Journal of Physical Chemistry* 61.2 (1957), pp. 189–196. DOI: [10.1021/j150548a013](https://doi.org/10.1021/j150548a013).
- [139] D. Price. *Aluminized Organic Explosives*. Tech. Rep. NOLTR 72-62. White Oak, Silver Spring, MD: Naval Ordnance Laboratory, 1972.
- [140] W. A. Trzciński, S. Cudziło, and L. Szymańczyk. “Studies of Detonation Characteristics of Aluminum Enriched RDX Compositions”. In: *Propellants, Explosives, Pyrotechnics* 32.5 (2007), pp. 392–400. DOI: [10.1002/prop.200700201](https://doi.org/10.1002/prop.200700201).
- [141] W. A. Trzciński, S. Cudziło, J. Paszula, and J. Callaway. “Study of the Effect of Additive Particle Size on Non-ideal Explosive Performance”. In: *Propellants, Explosives, Pyrotechnics* 33.3 (2008), pp. 227–235. DOI: [10.1002/prop.200800005](https://doi.org/10.1002/prop.200800005).
- [142] P. Brousseau and C. J. Anderson. “Nanometric Al in Explosives”. In: *Propellants, Explosives, Pyrotechnics* 27 (2002), pp. 300–306. DOI: [10.1002/1521-4087\(200211\)27:5<300::AID-PREP300>3.0.CO;2-#](https://doi.org/10.1002/1521-4087(200211)27:5<300::AID-PREP300>3.0.CO;2-#).
- [143] G. Baudin, A. Lefrançois, D. Bergues, J. Bigot, and Y. Champion. “Combustion of Nanophase Aluminum in the Detonation Products of Nitromethane and TNT”. In: *11th International Symposium on Detonation*. Snowmass, CO: Office of Naval Research, 30 August–4 September 1998.
- [144] A. Lefrançois, G. Baudin, C. Le Gallic, P. Boyce, and J.-P. Coudoing. “Nanometric Aluminum Powder Influence on the Detonation Efficiency of Explosives”. In: *12th International Symposium on Detonation*. Ed. by J. R. Carney and J. L. Maienschein. San Diego, CA: Office of Naval Research, 11–16 July 2002, pp. 22–32.
- [145] M. F. Gogulya, M. N. Makhov, A. Y. Dolgoborodov, M. A. Brazhnikov, V. I. Arkhipov, and V. G. Shchetin. “Mechanical Sensitivity and Detonation Parameters of Aluminized Explosives”. In: *Combustion, Explosion and Shock Waves* 40.4 (2004), pp. 445–457. DOI: [10.1023/B:CESW.0000033568.39812.2c](https://doi.org/10.1023/B:CESW.0000033568.39812.2c).
- [146] V. Y. Davydov and A. S. Gubin. “Acceleration Ability of High Explosives and their Mixtures with Fuel Additives - 2: Activated and Ultrafine Aluminum Powders”. In: *Russian Journal of Physical Chemistry B* 5.4 (2011), pp. 610–615. DOI: [10.1134/S1990793111040051](https://doi.org/10.1134/S1990793111040051).
- [147] P. J. Miller, C. D. Bedford, and J. J. Davis. “Effect of Metal Particle Size on the Detonation Properties of Various Metallized Explosives”. In: *11th International Symposium on Detonation*. Snowmass, CO: Office of Naval Research, 30 August–4 September 1998, pp. 214–220.
- [148] M. N. Makhov, M. F. Gogulya, A. Y. Dolgoborodov, M. A. Brazhnikov, V. I. Arkhipov, and V. I. Pepekin. “Acceleration Ability and Heat of Explosive Decomposition of Aluminized Explosives”. In: *Combustion, Explosion and Shock Waves* 40.4 (2004), pp. 458–466. DOI: [10.1023/B:CESW.0000033569.77449.d9](https://doi.org/10.1023/B:CESW.0000033569.77449.d9).
- [149] V. Y. Davydov and A. S. Gubin. “Acceleration Ability of High Explosives and their Mixtures with Fuel Additives - 1: Assessment by the M-40 Method”. In: *Russian Journal of Physical Chemistry B* 5.3 (2011), pp. 491–498. DOI: [10.1134/S1990793111030183](https://doi.org/10.1134/S1990793111030183).

- [150] V. W. Manner, S. J. Pemberton, J. A. Gunderson, T. J. Herrera, J. M. Lloyd, P. J. Salazar, P. Rae, and B. C. Tappan. “The Role of Aluminum in the Detonation and Post-Detonation Expansion of Selected Cast HMX-Based Explosives”. In: *Propellants, Explosives, Pyrotechnics* 37.2 (2012), pp. 198–206. DOI: [10.1002/prop.201100138](https://doi.org/10.1002/prop.201100138).
- [151] P. E. Anderson, P. Cook, A. Davis, and K. Mychajlonka. “The Effect of Binder Systems on Early Aluminum Reaction in Detonations”. In: *Propellants, Explosives, Pyrotechnics* 38.4 (2013), pp. 486–494. DOI: [10.1002/prop.201200104](https://doi.org/10.1002/prop.201200104).
- [152] M. F. Gogulya, A. Y. Dolgoborodov, M. A. Brazhnikov, and G. Baudin. “Detonation Waves in HMX/AL Mixtures (Pressure and Temperature Measurements)”. In: *11th International Symposium on Detonation*. Snowmass, CO: Office of Naval Research, 30 August–4 September 1998, pp. 979–988.
- [153] S. N. Lubyatinsky and B. G. Loboiko. “Reaction Zone Measurements in Detonating Aluminized Explosives”. In: *AIP Conference Proceedings* 370.1 (1996), pp. 779–782. DOI: [10.1063/1.50857](https://doi.org/10.1063/1.50857).
- [154] A. Lefrancois, G. Baudin, C. Le Gallic, P. Boyce, and J.-P. Coudoing. “Temperature and Pressure Measurements Comparison of the Aluminized Emulsion Explosives Detonation Front and Products Expansion”. In: *12th International Symposium on Detonation*. Ed. by J. R. Carney and J. L. Maienschein. San Diego, CA: Office of Naval Research, 11–16 July 2002, pp. 432–439.
- [155] J. L. Sabourin, R. A. Yetter, B. W. Asay, J. M. Lloyd, V. E. Sanders, G. A. Risha, and S. F. Son. “Effect of Nano-Aluminum and Fumed Silica Particles on Deflagration and Detonation of Nitromethane”. In: *Propellants, Explosives, Pyrotechnics* 34.5 (2009), pp. 385–393. DOI: [10.1002/prop.200800106](https://doi.org/10.1002/prop.200800106).
- [156] A. M. Milne, A. W. Longbottom, D. J. Evans, P. J. Haskins, M. D. Cook, and R. I. Briggs. “The Burning Rate of Aluminium Particles in Nitromethane in Cylinder Tests”. In: (11–16 July 2002), pp. 895–900.
- [157] Y. Kato, K. Murata, and S. Itoh. “Detonation Characteristics of Packed Beds of Aluminum saturated with Nitromethane”. In: *13th International Symposium on Detonation*. Norfolk, VA: Office of Naval Research, 23–28 July 2006, pp. 187–195.
- [158] F. Zhang, A. Yoshinaka, D. L. Frost, R. C. Ripley, K. Kim, and W. Wilson. “Casing Influence on Ignition and Reaction of Aluminum Particles in an Explosive”. In: *13th International Symposium on Detonation*. Norfolk, VA: Office of Naval Research, 23–28 July 2006, pp. 233–244.
- [159] D. L. Frost, S. Goroshin, J. Levine, R. Ripley, and F. Zhang. “Critical Conditions for Ignition of Aluminum Particles in Cylindrical Explosive Charges”. In: *AIP Conference Proceedings* 845.1 (2006), pp. 972–975. DOI: [10.1063/1.2263484](https://doi.org/10.1063/1.2263484). eprint: <http://aip.scitation.org/doi/pdf/10.1063/1.2263484>.
- [160] B. C. Tappan, L. G. Hill, V. W. Manner, S. J. Pemberton, M. A. Lieber, C. Johnson, and V. E. Sanders. “Reactions of Powdered Aluminum with Explosives that Selectively Form Carbon Dioxide or Water as Oxidizers”. In: *International Journal of Energetic Materials and Chemical Propulsion* 15.4 (2016), pp. 339–350. DOI: [10.1615/IntJEnergeticMaterialsChemProp.2017011503](https://doi.org/10.1615/IntJEnergeticMaterialsChemProp.2017011503).
- [161] J. Loiseau, W. Georges, A. J. Higgins, and D. L. Frost. “The Propulsive Capability of Explosives Heavily Loaded with Inert Materials”. In: *Shock Waves* (Accepted August 2017).

References

- [162] K. A. Trowell, J. Wang, Y. Wang, Y. Yavor, S. Goroshin, J. M. Bergthorson, D. L. Frost, J. C. St-Charles, and C. Dubois. “Effect of particle coating on the thermal response of mixtures of micro- and nano-aluminum particles with water”. In: *Journal of Thermal Analysis and Calorimetry* 127.1 (2017), pp. 1027–1036. DOI: [10.1007/s10973-016-5775-1](https://doi.org/10.1007/s10973-016-5775-1).
- [163] J. Hershkowitz and B. M. Dobratz. *Compendium of Nitromethane Data Relevant to the Tactical Explosive System (TEXS) Program*. Tech. Rep. ARFSD-SP-89001. ARDEC, Picatinny Arsenal, 1989.
- [164] R. K. Kurbangalina. “Critical diameter of liquid explosives as a function of powder content”. In: *Journal of Applied Mechanics and Technical Physics* 10.4 (1969), pp. 656–659. DOI: [10.1007/BF00916230](https://doi.org/10.1007/BF00916230).
- [165] C. E. Johnson, S. Fallis, A. P. Chafin, T. J. Groshens, K. T. Higa, I. M. K. Ismail, and T. W. Hawkins. “Characterization of Nanometer- to Micron-Sized Aluminum Powders: Size Distribution from Thermogravimetric Analysis”. In: *Journal of Propulsion and Power* 23.4 (2007), pp. 669–682. DOI: [10.2514/1.25517](https://doi.org/10.2514/1.25517).
- [166] A. M. Milne. “Gurney Analysis of Porous Shells”. In: *Propellants, Explosives, Pyrotechnics* 41.4 (2016), pp. 665–671. DOI: [10.1002/prop.201600016](https://doi.org/10.1002/prop.201600016).
- [167] D. L. Frost, Y. Gregoire, O. E. Petel, S. Goroshin, and F. Zhang. “Particle jet formation during explosive dispersal of solid particles”. In: *Physics of Fluids* 24 (2012). DOI: [10.1063/1.4751876](https://doi.org/10.1063/1.4751876).
- [168] A. Milne, A. Longbottom, D. L. Frost, J. Loiseau, S. Goroshin, and O. Petel. “Explosive Fragmentation of Liquids in Spherical Geometry”. In: *Shock Waves* (2016), pp. 1–11. DOI: [10.1007/s00193-016-0671-y](https://doi.org/10.1007/s00193-016-0671-y).
- [169] A. M. Milne, E. Floyd, A. W. Longbottom, and P. Taylor. “Dynamic fragmentation of powders in spherical geometry”. In: *Shock Waves* 24 (2014), pp. 501–513. DOI: [10.1007/s00193-014-0511-x](https://doi.org/10.1007/s00193-014-0511-x).
- [170] R. C. Ripley and F. Zhang. “Jetting instability mechanisms of particles from explosive dispersal”. In: *Journal of Physics: Conference Series* 500.15 (2014), p. 152012. DOI: [10.1088/1742-6596/500/15/152012](https://doi.org/10.1088/1742-6596/500/15/152012).
- [171] A. M. Milne, C. Parrish, and I. Worland. “Dynamic Fragmentation of Blast Mitigants”. In: *Shock Waves* 20.1 (2010), pp. 41–51. DOI: [10.1007/s00193-009-0235-5](https://doi.org/10.1007/s00193-009-0235-5).
- [172] D. Frost, J. Loiseau, S. Goroshin, F. Zhang, A. Milne, and A. Longbottom. “Fracture of Explosively Compacted Aluminum Particles in a Cylinder”. In: *Journal of Physics: Conference Series* (14–19 June 2015). Ed. by R. C. Chau, T. Germann, and T. Sewell, TBD.
- [173] V. F. Nesterenko. “Shock (Blast) Mitigation by “Soft” Condensed Matter”. In: *MRS Symposium Proceedings*. Vol. 759. Pittsburg, PA: Materials Research Society, 2003, pp. MM4.3.1–4.3.12. DOI: [10.1557/PROC-759-MM4.3](https://doi.org/10.1557/PROC-759-MM4.3).
- [174] R. M. Allen, D. J. Kirkpatrick, A. W. Longbottom, A. M. Milne, and N. K. Bourne. “Experimental and Numerical Study of Free-Field Blast Mitigation”. In: *AIP Conference Proceedings* 706.1 (2004), pp. 823–826. DOI: [10.1063/1.1780363](https://doi.org/10.1063/1.1780363).
- [175] A. M. Milne, S. B. Cargill, and A. W. Longbottom. “Modelling of Complex Blast”. In: *International Journal of Protective Structures* (2016). DOI: [10.1177/2041419616661431](https://doi.org/10.1177/2041419616661431).
- [176] S. P. Medvedev, S. M. Frolov, and B. E. Gel’fand. “Attenuation of Shock Waves by Screens of Granular Material”. In: *Journal of Engineering Physics* 58.6 (1990), pp. 714–718. DOI: [10.1007/bf00872723](https://doi.org/10.1007/bf00872723).

- [177] J.-F. Danel and L. Kazandjian. “A Few Remarks About the Gurney Energy of Condensed Explosives”. In: *Propellants, Explosives, Pyrotechnics* 29.5 (2004), pp. 314–316. DOI: [10.1002/prop.200400060](https://doi.org/10.1002/prop.200400060).
- [178] M. D. Hutchinson and D. W. Price. “On the Continued Acceleration of Bomb Casing Fragments Following Casing Fracture”. In: *Defence Technology* 10.2 (2014), pp. 211–218. DOI: [10.1016/j.dt.2014.06.001](https://doi.org/10.1016/j.dt.2014.06.001).
- [179] F. Zhang, R. Ripley, A. Yoshinaka, J. A. C. R. Findlay, and B. von Rosen. “Large-scale spray detonation and related particle jetting instability phenomenon”. In: *Shock Waves* 25 (2015), pp. 239–254. DOI: [10.1007/s00193-014-0525-4](https://doi.org/10.1007/s00193-014-0525-4).

